Metallic Component Margins under High Seismic Loads (MECOS): Towards a New Approach for Seismic Design of Piping Systems

OECD

BETTER POLICIES FOR BETTER LIVES

NEA

NUCLEAR ENERGY AGENCY

![NEA - Nuclear Energy Agency]

NEA/CSNI/R(2021)12

Unclassified

English text only

11 December 2024

NUCLEAR ENERGY AGENCY
COMMITTEE ON THE SAFETY OF NUCLEAR INSTALLATIONS

Metallic Component Margins under High Seismic Loads (MECOS): Towards a New Approach for Seismic Design of Piping Systems

This document is available in PDF format only.

JT03557392

ORGANISATION FOR ECONOMIC CO-OPERATION AND DEVELOPMENT

The OECD is a unique forum where the governments of 38 democracies work together to address the economic, social and environmental challenges of globalisation. The OECD is also at the forefront of efforts to understand and to help governments respond to new developments and concerns, such as corporate governance, the information economy and the challenges of an ageing population. The Organisation provides a setting where governments can compare policy experiences, seek answers to common problems, identify good practice and work to co-ordinate domestic and international policies.

The OECD member countries are: Australia, Austria, Belgium, Canada, Chile, Colombia, Costa Rica, Czechia, Denmark, Estonia, Finland, France, Germany, Greece, Hungary, Iceland, Ireland, Israel, Italy, Japan, Korea, Latvia, Lithuania, Luxembourg, Mexico, the Netherlands, New Zealand, Norway, Poland, Portugal, the Slovak Republic, Slovenia, Spain, Sweden, Switzerland, Türkiye, the United Kingdom and the United States. The European Commission takes part in the work of the OECD.

OECD Publishing disseminates widely the results of the Organisation's statistics gathering and research on economic, social and environmental issues, as well as the conventions, guidelines and standards agreed by its members.

NUCLEAR ENERGY AGENCY

The OECD Nuclear Energy Agency (NEA) was established on 1 February 1958. Current NEA membership consists of 34 countries: Argentina, Australia, Austria, Belgium, Bulgaria, Canada, Czechia, Denmark, Finland, France, Germany, Greece, Hungary, Iceland, Ireland, Italy, Japan, Korea, Luxembourg, Mexico, the Netherlands, Norway, Poland, Portugal, Romania, Russia (suspended), the Slovak Republic, Slovenia, Spain, Sweden, Switzerland, Türkiye, the United Kingdom and the United States. The European Commission and the International Atomic Energy Agency also take part in the work of the Agency.

The mission of the NEA is:

- to assist its member countries in maintaining and further developing, through international co-operation, the scientific, technological and legal bases required for a safe, environmentally friendly and economical use of nuclear energy for peaceful purposes;

- to provide authoritative assessments and to forge common understandings on key issues, as input to government decisions on nuclear energy policy and to broader OECD policy analyses in areas such as energy and sustainable development.

Specific areas of competence of the NEA include the safety and regulation of nuclear activities, radioactive waste management and decommissioning, radiological protection, nuclear science, economic and technical analyses of the nuclear fuel cycle, nuclear law and liability, and public information. The NEA Data Bank provides nuclear data and computer program services for participating countries.

COMMITTEE ON THE SAFETY OF NUCLEAR INSTALLATIONS

The Committee on the Safety of Nuclear Installations (CSNI) addresses Nuclear Energy Agency (NEA) programmes and activities that support maintaining and advancing the scientific and technical knowledge base of the safety of nuclear installations.

The Committee constitutes a forum for the exchange of technical information and for collaboration between organisations, which can contribute, from their respective backgrounds in research, development and engineering, to its activities. It has regard to the exchange of information between member countries and safety R&D programmes of various sizes in order to keep all member countries involved in and abreast of developments in technical safety matters.

The Committee reviews the state of knowledge on important topics of nuclear safety science and techniques and of safety assessments, and ensures that operating experience is appropriately accounted for in its activities. It initiates and conducts programmes identified by these reviews and assessments in order to confirm safety, overcome discrepancies, develop improvements and reach consensus on technical issues of common interest. It promotes the co-ordination of work in different member countries that serve to maintain and enhance competence in nuclear safety matters, including the establishment of joint undertakings (e.g. joint research and data projects), and assists in the feedback of the results to participating organisations. The Committee ensures that valuable end-products of the technical reviews and analyses are provided to members in a timely manner, and made publicly available when appropriate, to support broader nuclear safety.

The Committee focuses primarily on the safety aspects of existing power reactors, other nuclear installations and new power reactors; it also considers the safety implications of scientific and technical developments of future reactor technologies and designs. Further, the scope for the Committee includes human and organisational research activities and technical developments that affect nuclear safety.

Acknowledgements

Table of contents

Tables

Figures

List of abbreviations and acronyms

AFCEN	Association française pour les règles de conception et de construction des matériels des chaudières électronucléaires (French society for design and construction rules for nuclear island components)
ANL	Argonne National Laboratory
ASME	American Society of Mechanical Engineers
ASTM	American Society for Testing and Materials
BARC	Bhabha Atomic Research Centre (India)
BDBE	Beyond design basis earthquake
BNL	Berkeley National Laboratory (United Kingdom)
BWR	Boiling water reactor
CANDU	Canada Deuterium Uranium
CAV	Cumulative absolute velocity
CQC	Complete quadratic combination
CS	Carbon steel
CSA	Canadian Standards Association
CEA	Commissariat à l'énergie atomique et aux énergies alternatives (French Alternative Energies and Atomic Energy Commission)
CEGB	Central Electricity Generating Board (United Kingdom)
CFR	Code of Federal Regulation
CPRI	Central Power Research Institute (India)
CSNI	Committee on the Safety of Nuclear Installations (NEA)
CUF	Cumulative usage factor
DBE	Design basis earthquake
DBSGM	Design basis seismic ground motion
DOE	Department of Energy (United States)
EC	Effect of the clearance
ECCS	European Convention for Construction Steelwork
EDF	Électricité de France
EPRI	Electric Power Research Institute (United States)
ETEC	Energy Technology Engineering Center (United States)
FBR	Fast breeder reactors
FE	Finite elements
FEA	Finite element analysis

FEM	Finite element methods
FR	Fatigue ratchet
FRS	Floor response spectra
GE	General Electric company (United States)
GEJE	Great Eastern Japan Earthquake (11 March 2011)
HCLPF	High confidence low probability of failure
IAEA	International Atomic Energy Agency
IIRS	Incremental iterative response spectrum
INDUSE	INDUstrial Seismic
IPIRG	International Piping Integrity Research Group
JAEA	Japan Atomic Energy Agency
JNES	Japan Nuclear Energy Safety Organisation
JSME	Japan Society of Mechanical Engineers
LBB	Leak-before-break
LWR	Light water reactor
MECOS	Metallic Component Margins under High Seismic Loads
NCO	Niigata-ken Chuetsu-oki
NIED	National Research Institute for Earth Science and Disaster Resilience
NRC	Nuclear Regulatory Commission (United States)
NUPEC	Nuclear Power Engineering Centre (Japan)
OBE	Operating basis earthquake
OD	Outer diameter
PGA	Peak ground accelerations
PSD	Power spectral density
PVP	Pressure vessels and piping
PWR	Pressurised water reactor
R&D	Research and development
SAR	Safety analysis report
SMA	Seismic margin assessment
SPRA	Seismic probabilistic risk analysis
SPSA	Seismic probabilistic safety assessment
SRSS	Square root of the sum of the squares
SSCs	System, structures, and components
SSE	Safe shutdown earthquake
SSPS	Stainless steel piping systems

SWs	Spectrum waves
TG	Task group
TRS	Test response spectra
TSO	Technical support organisation
UHS	Uniform hazard spectrum
WGIAGE	Working Group on Integrity and Ageing of Components and Structures (NEA)
WPS	Welding procedure specification
WRC	Welding Research Council (United States)
WWER/VVER	Water-water energy reactor
ZPA	Zero period acceleration

Executive summary

The seismic design rules for nuclear power plant piping systems that have been in practice since the 1960s have been applied to hundreds of piping supports and seismic restraints for nuclear power plants. This quantity of seismic hardware brings about design and operational difficulties at nuclear power plants that include:

- excessive plant congestion that limits access for inspection and maintenance;

- plant staff facing increased radiation exposure while accessing equipment for inspection or maintenance;

- an unnecessary constraint of the thermal expansion of the pipes during normal operation;

- a high cost for the plant's initial construction;

- a high inspection and maintenance cost during the plant's lifetime.

Most national nuclear codes currently consider seismic inertial load to be purely primary. As a result, the seismic design is governed by a stress equation of the following type:

$$B_1 \frac{P\,D}{2\,t} + B_2 \frac{M_A + M_B}{Z} \le k\,S_h$$

In the equation, the loading factors are internal pressure (P), weight (M_A) and seismic inertial moments (M_B). This approach has three significant shortcomings:

1. The above equation protects against the formation of plastic hinges and collapse, which are very unlikely in a multiply-supported piping system.

2. The equation does not explicitly tackle the true failure mode from seismic shaking, which is fatigue.

3. As a result, aseismic measures lead to a large number of seismic restraints.

At the same time, the good seismic performance of pressurised metallic piping was confirmed by the seismic experience gained from the study of the consequences of real strong motion earthquakes and by a number of system or component tests under static or dynamic excitation simulating seismic input. There were no instances of plastic collapse-type ruptures among the piping failures reported after strong earthquakes. The failures were instead due to large anchor motion, brittle materials, non-welded joints, corrosion, failures of piping supports or seismic interactions.

However, there have been numerous experimental research projects and post-earthquake investigations since the original seismic design rules for piping systems were first published in design codes. These projects and investigations have helped the engineering community to better understand the seismic-induced failure modes of piping systems.

Due to (a) the practical and safety difficulties caused by an excessive number of seismic restraints and (b) our improved understanding of seismic failure modes, an international group of subject matter experts was assembled under the Metallic Component Margins under High Seismic Loads (MECOS) programme to propose improved seismic design rules for piping systems.

The MECOS programme consisted of three parts:

1. design and experimental information gathering;

2. benchmark analyses;

3. the development of proposals for improved seismic design methods for nuclear power plant piping systems.

This report documents the third part of the MECOS programme, which was the development of proposals for improved seismic design methods for nuclear power plant piping systems. For this objective, the group proposed to consider the following tasks:

- revisiting past experimental data as well as the interpretations that were carried out and conclusions that were previously drawn;

- reanalysing the data in the light of recent developments;

- considering recent experimental programmes carried out in India and Japan on pressurised piping;

- proposing design criteria that address the fatigue-ratcheting failure mode and plastic instability.

The work conducted by the MECOS group of experts is documented in Chapters 1 to 6, as listed below, with Chapter 7 presenting the conclusions of the programme:

1. introduction;

2. conventional code approach to seismic design of piping systems;

3. review of international research and development (R&D) programmes;

4. history of code modifications in different countries;

5. technical background to proposed new criteria;

6. towards a new approach;

7. conclusions and recommendations.

In addition, 10 Annexes provide additional complementary information on specific topics addressed in the chapters.

Chapter 1 describes the objectives of the project and Chapter 2 briefly presents the current conventional approach to the seismic design of piping systems. Chapter 3 describes the R&D programmes concerning seismic behaviour until the collapse of pressurised piping systems or components conducted in several countries and organisations, in particular within the United Kingdom, United States, Japan, India and European countries.

Reviewing these previous R&D programmes leads to the following three conclusions:

1. The R&D programmes by different organisations revealed that the failure mode was fatigue (or fatigue-ratcheting when the pipes are pressurised to cause a large hoop stress), whereas the piping design codes generally consider that the failure mode under high-level earthquake loads is plastic instability. Plastic collapse has not been confirmed by the experiments, except for when it was purposefully brought about by a statically unstable pipe configuration that had a cantilever with a heavy weight on one of its free ends.

   - It is therefore necessary to create code design criteria for the prevention of failure by fatigue and fatigue-ratcheting.

2. The experimental research results showed that the seismic response of actual piping did not linearly increase but saturated due to a damping increase by plastic behaviour in the piping system. However, the code criteria are based on a linear seismic response analysis of piping systems. The inelastic response of piping systems under large seismic input should be adequately addressed in the new criteria.

3. The evaluation of the pipe components could be based on plastic analysis and strain-based criteria are preferable to best capture the fatigue-ratcheting effect caused by large seismic excitations. However, it may be practically difficult to adopt the strain-based criteria in the seismic design because of their complexity, the difficulty of applying the inelastic analysis to the large number of piping systems in a nuclear power plant and the variability of the profile and thicknesses of commercial piping fittings and components.

The purpose of Chapter 4 is to present a history of piping system standards' evolution and modifications in different countries, namely the United States, Japan, France, Russia and Canada. Stress criteria aimed at preventing different types of damage according to national practices are presented in the report.

Regarding the United States, there is a focus on the well-known equation for primary stresses, which in the current practice includes seismically induced inertial stresses. The current American Society of Mechanical Engineers (ASME) III stress equations focus on the prevention of plastic instability (sometimes referred to as collapse), which is a buckling-like failure. However, tests carried out in the United States from 1985 to1988 also indicated cases of fatigue-ratcheting that caused the pressurised pipe to balloon under repeated large and plastic seismic strains. This particular failure mode, fatigue-ratcheting, is not explicitly addressed by the current stress equations.

The early regulation in Japan was based on the ASME code. The design procedure is now based on the Japan Society of Mechanical Engineers (JSME) code. Yet the seismic design is conducted based on the code and guide published by the Japan Electric Association (JEAG4601), which is revised approximately every five years. The code and guide complement each other. It was experimentally observed that piping systems can undergo significant beyond-design seismic input motions, resulting in fatigue failure mode. A code case that is presented in the report (Section 5.2) was established to examine such inelastic behaviour in the seismic design of piping systems.

The French code was also first based on ASME code. The code later evolved to better account for French and European practices and also to incorporate fast breeder reactors. A specific feature of the code is that thermal stresses are not necessarily regarded as purely secondary. The simple classification of seismic loads as primary was recognised as inadequate from the 2000s due to extensive R&D programmes, the most representative of which are described in this report.

In Russia, the first standards, identified as PNAE codes, were issued in the late seventies. Russian criteria are similar to the ASME criteria, although they have a more complex form with some specificities. For example, the code equation does not depend on the piping safety class; there is no specific guidance for dealing with secondary stresses induced by seismic anchor movement. A new edition of norms is currently being developed and should be better harmonised with international practices.

In Canada, the seismic design of nuclear power plant systems, components and structures is carried out following the guidance of the Canadian Standards Association (CSA) relating to Canada Deuterium Uranium (CANDU) reactor types. Pressure-retaining components and their supports are designed for the applicable subsections of ASME Code. The use of

uniform hazard spectrum, seismic margin assessment and seismic probabilistic safety assessment has been accepted.

Chapter 5 presents some background on the proposed new approach and criteria. The chapter discusses the incremental iterative response spectrum (IIRS) method. This is a linearisation method for evaluating ratcheting strains in pressurised piping systems and a Japanese elastic-plastic code case, a strain-based criterion using detailed inelastic response analysis.

A stepwise procedure of the IIRS method, which is a simplified procedure for predicting the non-linear ratchet strain, is then presented. The report outlines details on the evaluating rotational and translational compliances of piping components (e.g. the elbow) based on ratchet behaviour. Case studies validating the IIRS procedure at the component and system level using experimental data are described in detail. Experiments reveal that the global free vibration characteristics will not alter, even at the stage of piping failures.

Japanese elastic-plastic code is a strain-based criterion and an evaluation procedure using detailed inelastic response analysis with the finite element methods' (FEM) model. The code proposes a fatigue evaluation procedure that considers equivalent strain amplitudes and uses a fatigue curve. Details are presented on estimating strain amplitudes from the inelastic response of piping systems. The estimation of ratchet strain is clearly demonstrated to not necessarily be required for the conservative strain-based fatigue evaluation of piping components. The code case contains a mandatory appendix for the non-linear analysis of piping systems. Guidelines for dynamic analysis and static analysis considering material and geometric non-linearities are provided. Full, hybrid and zoom-up models of piping systems are briefly discussed. The procedure for approximating bilinear material properties is also discussed.

Chapter 6 proposes a new methodology that can obtain the rational seismic response of piping and thereby be used to prevent their plastic collapse. The MECOS group of experts (GE) conducted a study aiming to obtain the fair seismic load by considering that the seismic load could be a mixture of force-controlled and displacement-controlled loads. The floor response spectra (FRS) as seismic input for a piping system should be modified based on the mixture condition in order to achieve a fair seismic load. The proposed methodology has suggested an appropriate modification of FRS, which could be used to obtain a rational primary part of the seismic load.

A negative influence on the fatigue life by ratchet strain or plastic pre-strain, which is called ductility exhaustion, has been examined and discussed based on the experimental low cycle fatigue data of pipe fittings. As a result, there could be less influence on the fatigue life of piping for sound piping without degradation (like wall thinning). The design fatigue curve can also still provide a conservative evaluation, even with ratcheting.

The conclusions of this report, which are presented in Chapter 7, can be summarised as follows:

1. Experience from post-earthquake investigations and seismic test programmes show that significant seismic margins are present and indicate that seismic failures of welded metallic pressurised pipes are primarily caused by low-cycle fatigue, compounded by plastic ratcheting at high pressure-induced hoop stress. However, the current design rules are instead focused on preventing plastic instability.

2. New approaches are proposed to better account for the contribution of seismically induced inertial stresses to the primary stresses for the prevention of plastic instability. These approaches also better account for the seismically induced fatigue that results from the cyclic effect of seismic loads.

3. New fatigue-based design criteria are proposed to replace plastic instability-based criteria, which reflect the knowledge that is documented in this report.

4. The report recognises the necessity for criteria or engineering practices to be established that guarantee that seismically induced accumulated plastic strains (ratchetting) will not exceed an acceptable limit. Three tracks are proposed, consisting of non-linear time-response analysis, post-elastic analysis processing and ratchet strain data.

5. The report recognises that the possible degradation of piping systems before an earthquake should be taken into account. The report accordingly points out that some experiments on the shake table were prolonged for an artificially long period of time (e.g. half an hour). Therefore, a long period of the experiment was carried out using a degraded system before a significant wall crack appeared. The corresponding data should be assessed as an attempt to find a valid approach for degraded piping systems.

6. The report recognises the need for additional experimental data to be obtained from quasi-static cyclic tests of standard piping components that are subjected to high pressure-induced hoop stress. The need for the benchmarking of these tests by cost-effective elastic analysis methods is also highlighted.

7. The report recognises the need for international benchmarking of the criteria proposed within it (including primary vs. secondary stress, Markl's fatigue life assessment, elastic vs. plastic analyses and accounting for pressure-induced ratcheting). Benchmarking would publicise the proposed approach, compare it with the current code approach and challenge the proposal with alternative analyses.

1. Introduction

1.1. Three-part programme

In the wake of the Fukushima Daiichi Nuclear Power Plant accident in 2011, the Nuclear Energy Agency (NEA) Committee for the Safety of Nuclear Installations (CSNI) took initiatives for the evaluation of margins encompassed in the nuclear power industry's design procedures.

As part of this effort, the Metallic Component Margins Under High Seismic Loads (MECOS) programme was launched in 2015. This report categorises MECOS activities into three parts.

- Part 1 of the MECOS programme consisted of gathering information on: i) current design practices; and ii) piping system seismic tests carried out around the world that could be suitable for benchmarking.

- Part 2 was the implementation of the benchmark analyses.

- Part 3 was the development of proposals for new and improved seismic design criteria.

The results of the MECOS programme parts 1 and 2 were published in 2018 in the resulting report (NEA, 2018). The present report addresses part 3, which was the development of new and improved seismic design criteria for nuclear power plant piping systems.

1.2. Part one: Data gathering

The international team of seismic experts for piping systems that assembled for the MECOS programme summarised the current piping seismic design practices, as given in international design codes.

The expert team also reviewed the piping seismic test in order to: (1) share the experimental evidence of seismic piping behaviour with the engineering community; (2) forge a common understanding on the subject; and (3) contribute to the evolution of piping system design and qualification criteria.

For the purpose of the benchmark exercise, a series of 114 reports on seismic tests and analyses of piping systems was compiled and reviewed. Among the series of tests carried out around the world, the most suitable for a benchmark exercise were:

- The piping and fitting dynamic reliability programme, which was carried out in the United States in the 1980s and funded by the US Nuclear Regulatory Commission (NRC), the US Department of Energy (DOE), General Electric and the Electric Power Research Institute (EPRI). In this programme, a series of cyclic load tests were carried out on nearly 40 piping components and shake table tests on piping systems (Ranganath, 1994; Chen et al., 1987).

- A large-scale piping systems test programme, which was carried out in Japan in the 2000s and funded by Japan's Nuclear Power Engineering Centre (NUPEC). The programme consisted of a full-scale shake table test of a pressurised piping system on the large Tadotsu shaking table (De Grassi et al., 2008).

- Piping system tests carried out by Bhabha Atomic Research Centre (BARC), along with the Central Power Research Institute (CPRI) of Bangalore and funded by the Department of Atomic Energy in India. The tests consisted of shake table tests

being carried out on two sets of stainless steel (SS304L) and two sets of carbon steel piping systems of the same configuration (Ravikiran et al., 2013). The BARC research team is still actively working on the subject.

The three test campaigns provide important data on margins encompassed in the current engineering practices and supporting possible evolutions of piping systems' design criteria. The specimen in the three test campaigns were pressurised piping systems and the observed failure mode was fatigue-ratcheting, instead of plastic instability, which is the basis of the current seismic design criteria. In summary, the purpose of the benchmark exercise was to identify a benchmark exercise, described in Section 1.3, that aims to forge a common understanding on the subject of seismic-induced fatigue and fatigue-ratcheting and to propose corresponding seismic design criteria.

1.3. Part two: Benchmark analysis

Part two of the MECOS programme, the benchmark, spanned the period of March 2015 to November 2016. Participants were asked to perform seismic analyses on pressurised piping systems in carbon and stainless steel and to compare their results with the experimental outputs provided by BARC. A fair agreement was achieved for global variables such as accelerations or displacements. However, local strain predictions in critical areas, and especially in elbows, exhibited a significant scattering. Difficulties encountered by scientists and engineers in predicting localised strains have led to the conclusion that a possible criterion on prevention against fatigue-ratcheting should not be based on the calculation of accumulated plastic strains for the foreseeable future.

Consequently, the CSNI working group on the Integrity and Ageing of Components and Structures (IAGE working group) decided in 2017 that such a criterion should be based on a more direct interpretation of experimental results. The working group also concluded that this interpretation should be carried out by an international group of experts in part three of the programme.

The main results of parts 1 and 2 of the MECOS programme are reported in another report, "Final Report of the Project on Metallic Component Margins Under High Seismic Loads (MECOS)" (NEA, 2018).

1.4. Part three: Improved seismic design criteria

The present report focuses on the third part of MECOS programme, the proposed improvements to the design of metallic pressurised piping systems in nuclear power plants.

1.4.1. The need for improved criteria

Piping systems in nuclear power plants are designed and qualified – in accordance with codes, standards and regulations – to withstand loads that occur or could occur during the plant's design life. The loads to be considered in the design encompass normal operating loads, such as weight, operating pressures and temperatures and anticipated hydraulic transients. The piping systems in nuclear power plants also have to be designed for postulated accidental loads such as earthquakes. The postulated seismic loads are large and, when considered alongside the existing design criteria, have necessitated a number of seismic restraints to brace the pipe. There are some disadvantages to having an excess of seismic restraints:

- The seismic restraints result in plant congestion, which limits access for inspection and maintenance purposes.

- The plant congestion causes the access to equipment to take longer and therefore could increase the plant staff's exposure to radiation exposure.

- The seismic restraints could also act as unnecessary constraints on the pipe, which could hinder its thermal expansion in normal operation.

- The seismic restraints increase the initial construction costs.

- The seismic restraints result in a significant inspection and maintenance cost during the plant's lifetime.

It is therefore essential for engineers to have the correct seismic design rules and criteria and avoid unnecessary restraints. This objective has led the MECOS group of experts (GE) to re-visit the current seismic design practices for pressurised piping systems in nuclear power plants. The MECOS GE has considered past and current experimental data, analytical and numerical studies and observations of damage from actual earthquakes in order to optimise the seismic design, analysis and qualification rules and criteria.

At Fukushima Daiichi, the good seismic performance of piping systems during the 2011 earthquake before the station blackout due to the tsunami and of piping systems at Onagawa during the same earthquake confirmed the seismic ruggedness of well-designed piping systems. This performance has triggered a renewed interest in seismic design margins and their application to predictions of the performance of piping systems in beyond design basis earthquakes.

1.4.2. Guiding principles

The MECOS GE is guided by the following key principles when developing the proposed improvements to the design of metallic piping systems in nuclear power plants:

- The design rules should protect against the observed failure mode of pressurised piping components in seismic tests, which occurs by the formation and propagation of a fatigue crack.

- The design rules should protect against plastic instability.

- The design rules should be based on elastic analysis, using standard elastic pipe stress analysis software with pipes and fittings as beam and flexibility elements.

- Since elastic stress analysis does not precisely reflect the plastic strain behaviour of pipe and fittings, the design rules should include safety factors on stress and cycles.

- The strain rate during a seismic event is quasi-static and therefore quasi-static fatigue principles can be applied.

In addition, the CSNI suggested that a training course be organised to share the findings of the MECOS programme. The group of experts has elaborated on the possible programme for such a course, which is presented in the Annex J of this report.

1.5. References

Chen, W.P., A.T. Onesto and V. DeVita (1987), "Seismic Fragility Test of a 6-inch Diameter Pipe System", NUREG/CR-4859.

DeGrassi, G., J. Nie and C. Hofmayer (2008), "Seismic Analysis of Large-Scale Piping Systems for the JNES/NUPEC Ultimate Strength Piping Test Program", NUREG/CR-6983, Brookhaven National Laboratory, Upton, New York.

NEA (2018), "Final Report of the Project on Metallic Component Margins Under High Seismic Loads (MECOS)", OECD Publishing, Paris, www.oecd-nea.org/jcms/pl_19848.

Ranganath, S. (1994), "Piping and Fitting Dynamic Reliability Program", Volumes 1-5, EPRI TR-102792.

Ravikiran A., P.N. Dubey, M.K. Agrawal, G.R. Reddy and K.K. Vaze (2013), "Evaluation of Inelastic Seismic Response of a Piping System Using a Modified Iterative Response Spectrum Method", *Journal of Pressure Vessel Technology*, 135(4).

2. Conventional code approach for the seismic design of piping systems

2.1. Current qualification approach description

2.1.1. Intended current design margins in piping design

Piping systems in industrial plants have their design margins designed against the various failure modes. The intended current design margins for nuclear power plant piping are here described using the American Society of Mechanical Engineers (ASME) boiler and pressure vessel code division 1 subsection NC/ND-3600 class two and class three piping systems (referred to as ASME code in this section). Except for class one reactor coolant system, class two and three comprise the balance of safety-related piping systems. This section will address the intended current design margins against the three failure modes: bursting from internal pressure, cracking from fatigue cycling and plastic instability.

Prevention against bursting from internal pressure

The design margin against bursting from internal pressure is reflected in the minimum wall thickness equation, in the following form:

$$t_{min} = \frac{P\,D}{2\,S + 0.4\,P} + A$$

Where t_{min} = minimum required wall thickness for a straight pipe (mm); P = design pressure (MPa); D = outside diameter of the pipe (mm); S = allowable stress for the pipe material at the design temperature (MPa); and A = wall thickness allowance for future corrosion and mechanical machining such as machining (mm).

The design margin against bursting from internal pressure is captured in the allowable stress, in the following form:

$$S = min.\{\frac{S_u}{3.5}; \frac{S_y}{1.5}\}$$

Where S_u = minimum specified ultimate strength of the material at design temperature (MPa); and S_y = minimum specified yield strength of the material at design temperature (MPa).

For stainless steel, owing to its strain hardening characteristics, the margin against yield is reduced to 90% of S_y.

Therefore, the minimum margin against bursting from internal pressure is at a minimum 3.5 against the minimum specified ultimate strength at temperature. In practice, the thickness of the pipe is rounded up to a nominal schedule thickness that is a multiple of t_{min} because the pipe wall thickness is procured to commercial sizes and therefore the actual design margin is well above 3.5.

For service level C (events with fewer than 25 cycles of loads and in this case fewer than 25 pressure cycles) ASME class two and three piping allows the pressure to reach 1.5 times the design pressure and therefore the minimum design margin would be 3.5/1.5 = 2.3.

For a service level D event (a one-time event such as a pressure transient following a postulated pipe break) ASME class two and three piping allows the pressure to reach two times the design pressure and therefore the minimum design margin would be 3.5/2 = 1.75.

Prevention of fatigue cracking from thermal expansion-contraction

The design margin against fatigue cracking from the movement caused by thermal expansion and contraction is reflected in the secondary stress equation in the form:

$$i \frac{M_C}{Z} \leq S_A$$

where i = stress intensification factor of the pipe fitting, which is an experimental fatigue penalty factor that is a function of the type and size of the fitting; M_C = moment range (N.mm); Z = section modulus (mm3); and S_A = allowable stress (MPa).

This equation was introduced first in ASME B31.1 1955 and has remained unchanged. The allowable stress equation is in the form:

$$S_A = (\frac{6}{N^{0.2}} \leq 1.0)(1.25\,S_c + 0.25\,S_h)$$

Where N = number of cycles of moment M_C; and S_c and S_h = allowable stress in hot and cold conditions (MPa).

The stress margin is 2 for when N ≥ 7 000 cycles. For cyclic events with fewer than 7 000 cycles, the margin becomes much larger. For example, the allowable stress with a margin of 2 for 100 cycles would be 2 x (6/N$^{0.2}$ = 6/100$^{0.2}$ = 2.3) = 4.6.

Prevention of plastic instability

The prevention of plastic instability, which is also referred to as collapse in the ASME code, is reflected in a primary stress equation in the form:

$$B_1 \frac{P\,D}{2\,t} + B_2 \frac{M_A + M_B}{Z} \leq k\,S_h$$

where B_1 and B_2 are primary stress indices; P = pressure concurrent with the applied moments M_A and M_B (MPa); M_A and M_B = moment amplitude from sustained loads (such as deadweight) and occasional loads (such as seismic) (N.mm); k = a factor that is a function of the service level; and S_h = allowable stress (MPa).

The margin against plastic instability is captured by the factor k (Table 2.1).

Table 2.1. Factor k value for different service level designs

Service level design	Description	k
A	Normal operating conditions	Min. {1.8S$_h$; 1.5S$_y$}
B	Upset conditions, including the postulation of five operating basis earthquakes.	Same as Service level A
C	Emergency conditions, with fewer than 25 cycles with a stress above a certain threshold.	Min. {2.25S$_h$; 1.8S$_y$}
D	Faulted condition, a one-time event after which the plant is shut down and subjected to extensive inspections as well as possible repairs and replacements.	Min. {3.0S$_h$; 2.0S$_y$}

This formulation of the primary stress limits, with the primary stress indices B1 and B2, was introduced in a 1981 addendum of the ASME code. The design margin introduced into this primary stress equation is not a single value. The margin depends on the service loading (A, B, C and D) and the type of pipe and fitting (straight, elbow, tee, reducer, etc.). The primary stress design margin is explained in the paper "Background for Changes in the 1981 Edition of the ASME Nuclear Power Plant Components Code for Controlling Primary

Loads in Piping Systems" (Moore and Rodabaugh, 1982). This important paper notes the following:

"In nuclear power plant piping, Levels B, C, and D Service conditions usually include dynamics loads-earthquakes, relief valve operation, water hammer and postulated pipe breaks. It is these kinds of loads that has made the Code primary load criteria important in nuclear piping design. These dynamic loads are of short duration and we believe that they are applied and removed so quickly that gross plastic deformation does not have time to occur. An additional consideration is that Levels C and D Service are associated with plant shutdown for examination and repair of any damage. In light of the foregoing, we believe that primary stress limits up to, but not more than $2S_y$ can be safely used for the most severe Level D Service conditions."

Keeping in mind Moore and Rodabaugh's conclusions, and in light of experience feedback presented in Chapter 3, a major purpose of this report is to discuss the part of seismically induced stresses that contributes to the primary stress in the sense of the criterion for the prevention of plastic instability.

2.1.2. General seismic qualification criteria

The current rules for the seismic design of pressurised piping systems in nuclear power plants rely on qualification by analysis. The piping system is typically modelled and seismically analysed by linear elastic modal analysis. The seismic loads are combined with other concurrent loads and results are evaluated against several qualification criteria, for example: (1) stress limits for the pipe, fittings and welded joints, (2) stress limits at the welded attachments to the pipe, (3) limits on equipment nozzle loads, (4) loads and movements for the design of supports, (5) acceleration limits on valve actuators, (6) load and movement limits on mechanical joints and flange joints, and (7) wall penetrations' load and movement limits. The Metallic Component Margins under High Seismic Loads (MECOS) group of experts' (GEs) interest here is with criterion (1): the stress limits for the pipe, the fittings and their welded joints.

2.1.3. Current seismic stress qualification criteria

Of the various limits listed, the pipe fittings' and welds' stress limits are explicitly specified in the design codes in the form of stress equations. For seismic design, the practice has been to consider the stresses caused by seismic inertia (shaking of the piping system) to be primary stresses, which refers to stresses that could challenge the structural stability of the piping system (by preventing the formation of a plastic hinge and collapse), or stresses that could cause the tearing of the metal from a single application. Therefore, the general form of the seismic primary piping stress equation is currently:

$$B_1 \frac{P\,D}{2\,t} + B_2 \frac{M_A + M_B}{Z} \le k\,S_h$$

where B_1 and B_2 are primary (collapse) stress indices that depend on the type, shape and size of the piping component or fitting (elbow, tee, etc.); P is the system pressure coincident with the earthquake; D and t are the pipe's outside diameter and nominal wall thickness; M_A is the resultant moment caused by the deadweight of the pipe; M_B is the resultant moment caused by the seismic inertial load; Z is the pipe section modulus; k is a multiplier that depends on the probability of the earthquake; and S_h is the code-defined allowable stress that is a fraction of the ultimate and yield strengths of the material at a hot (operating) temperature.

- The first term of the seismic primary stress equation (the term $B_1PD/2t$) is the uniform axial stress in the pipe wall caused by internal pressure.

- The second term of the seismic primary stress equation (the term $B_2 M/Z$) is the maximum axial stress in the pipe wall due to weight and earthquake inertia.

2.2. Shortcomings of the current qualification criteria

The current primary seismic stress equation and stress limit has three important shortcomings:

- The first shortcoming of the current seismic stress equation ($B_2 M/Z$) is that it protects against the formation of plastic hinges and collapse, which is very unlikely for a multiply supported piping system. The pipe would need to undergo large deformations that can cause a hinge to form in order to develop multiple hinges and cause the structural collapse of a piping system. This is not feasible in practice because the piping system, with a few exceptions, is multiply supported. Shake table tests of piping systems and thorough observation of the damage sustained by actual earthquakes has confirmed that this occurrence is almost impossible. The series of seismic shake table tests was designed to purposely produce a hinge, as shown in Figure 2.1. Forty-one pipe fittings (also labelled components) were mounted on a shake table, one at a time, with a weight cantilevered at the top of a vertical run. This cantilevered unstable arrangement, which does not reflect a plant's actual configuration, was designed to intentionally make the fitting hinge. Only one out of the 41 components exhibited a hinge-like behaviour, which is illustrated in Figure 2.1. It is therefore questionable whether limiting $B_2 M/Z$ is a valid approach for preventing the seismic induced failure of piping systems. Similar tests (Kiran et. al., 2018) were carried out in India and showed how failure occurred at the crown due to large ratcheting strains and hinge-like behaviour.

- The second shortcoming of the current seismic stress equation is that it does not explicitly tackle the true failure mode from seismic shaking, which is fatigue. A piping operating at high pressure testing indicates that fatigue cracking is accelerated by hoop ratcheting (ballooning), which is caused by the large hoop stress. This failure mode (fatigue and fatigue-ratcheting at high pressure) have proven to be the predominant failure modes in shake table tests. An example is illustrated in Figure 2.2.

- The third shortcoming of the current equation is that it in practice requires a large number of large seismic restraints and structural attachments to be made to the building walls, floors and ceilings. This quantity of hardware significantly increases congestion in the nuclear power plant's compartments, reduces visibility and complicates access for inspections and operator actions. As a result, reliability is reduced.

The MECOS GE have therefore undertaken this project to resolve these shortcomings. They aim to improve the seismic design rules for nuclear power plant piping systems, to address the true failure mode and to reduce congestion, with the intention of improving access and mechanical reliability.

Figure 2.1. Depiction of the elbow shake table test
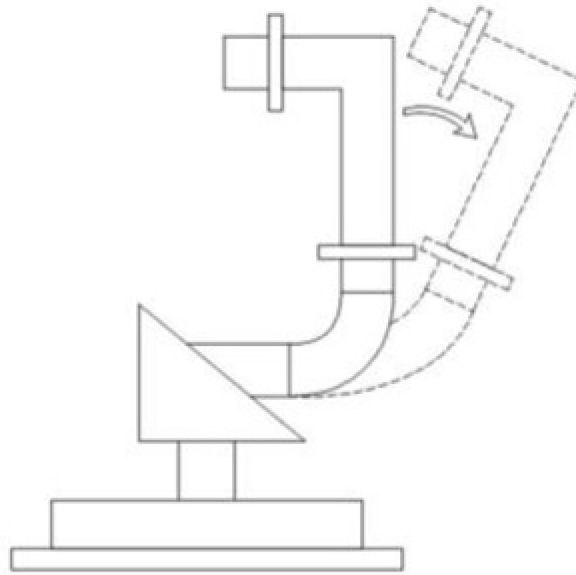
Note: This elbow test was designed as a cantilever, with a weight at the top, in order to purposely cause the elbow to hinge.
Source: Ranganath, 1994.

After several high amplitude seismic shake table tests, the elbow opened to the extent indicated in this figure (slightly less than a 45° angle). The test was completed when a fatigue crack failure occurred at the pipe-to-elbow weld, at the bottom.

Figure 2.2. Rupture of the pressure boundary during the shake table testing of a piping system
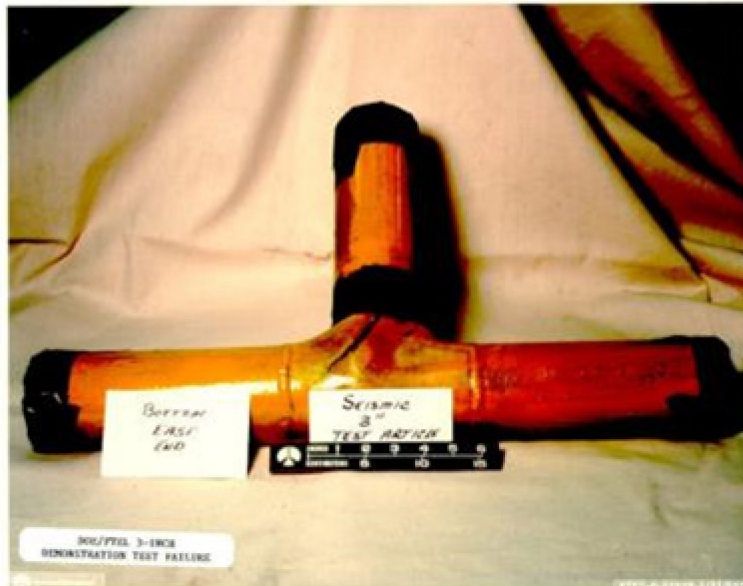
Note: Fatigue cracks were caused in fittings (such as the crack in the tee shown in this figure) by repeated shaking at seismic levels that exceeded the design basis earthquake.
Source: Ranganath, 1994.

2.3. Earthquake experience

The three sources of knowledge of the seismic performance of piping systems are:

1. The performance of piping systems in real strong motion earthquakes in industrial and commercial facilities, most of which are not seismically designed.

2. The performance of piping systems in system or component tests that are either static or dynamic shake table tests.

3. Analytical predictions using equations based on first principles and numerical simulations using elastic or plastic finite element analysis.

This section summarises the knowledge gained from the performance of piping systems in strong motion earthquakes at industrial and commercial facilities.

For several decades now, engineers have performed post-earthquake investigations on the performance (failures as well as non-failures) of buildings, structures, systems and components. Regarding the performance of piping systems, a selected bibliography of post-earthquake investigations is provided below. Several key lessons have been learnt from post-earthquake observations on the behaviour of non-seismically designed piping systems that have been subjected to actual strong motion earthquakes.

There is a differentiation in seismic behaviour between above-ground piping systems and buried piping and pipelines. There is also a differentiation in seismic performance between metallic and non-metallic piping. The matter of interest in this report, in the context of the piping in nuclear power plants, is above-ground metallic piping.

A lesson learnt regarding above-ground metallic piping systems in strong motion earthquakes is that the vast majority of them are highly robust. There are many cases where non-seismically designed above-ground metallic piping did not fail during strong motion earthquakes (shown in Figures B.1 to B.4).

The thermal power plants in the Tohoku area suffered during the Great East Japan Earthquake (GEJE) due to the earthquake, but there were no cases of damage to the large-diameter pipe connecting the boiler to the turbine. One of the instances of insignificant damage occurred to a broken lug used for the connection of the snubber and restraining a large-diameter pipe (see Annex B.2 for further details). There were also some cases where small-diameter pipes were damaged due to the forced displacement of large-diameter pipes connected to small pipes.

However, strong motion earthquakes can cause piping to fail and there is sufficient earthquake data to understand the causes of seismic induced failure of piping systems. A study of the failure data indicates that the causes of piping failure in strong motion earthquakes tend to result from a few common causes, which can be summarised as follows:

1. Large anchor motion

   – The failure of the piping is caused by the movement of the attached equipment. This is typically in the form of the rocking, sliding, or tipping of a pump, compressor, tank, or vessel, which causes the pipe to fail at its nozzle connection (shown in Figures B5 to B.9).

   – The failure of branch piping is caused by the swaying movement of a flexible header to which it is attached. This may be in the form of a rod-hung header that sways during the earthquake and connected branch line

that snaps because it is rigidly attached to the building structure and cannot accommodate the header's movement (see Figure B.10).

2. Brittle materials

   – Cast iron pipes, joints and components (such as valves) fracture in a brittle manner under seismic loads (shown in Figures B.11 and B.12).

3. Non-welded joints

   – Mechanical joints such as threaded joints, swaged couplings, clamped couplings, and in some cases expansion joints could leak or rupture due to the relative movement of the two sides of the pipe across the coupling (shown in Figures B.10 and B.13).

4. Corrosion

   – A corroded pipe has failed in badly damaged areas (see Figures B.14 and B.15).

5. Failure of pipe supports

   – The failure of under-sized, poorly designed or poorly maintained steel support members.

   – The failure of pipe supports at their attachment to the building structure, either by poor welding between steel members, or by poor anchorage to concrete.

   – The seismic-induced settlement of ground-mounted supports from ground failure (such as a liquefaction, landslide, or lateral spread) for ground-supported piping (shown in Figures B.16 to B.18).

6. Interaction

   – The failure of the piping by seismic interaction impact from a falling structural member or swing impact (see Figure B.19).

   – Swing impact damage to insulation, but without damage to the pipe itself (shown in Figures B.20 and B.21).

In addition to the data gathered from observations of earthquake damage, there is a large body of experimental data gathered from dynamic and static tests of piping systems and components, which is described in this report. The tests are often fragility tests, which are tests conducted to cause rupture under repeated seismic excitations of increasing magnitude. These fragility tests conducted at an artificially large amplitude and with a large number of repeated cycles, rather than during real earthquakes, enabled engineers to document fatigue and fatigue-ratcheting failures.

2.4. The CAV as a predictor of damage

The seismic design of piping systems – and of any system, structures, and components (SSC) – aims to provide margins against failure. The evaluation and quantification of margins depends on the function of the SSC and on the accident conditions defined for the plant. This subchapter presents some approaches on these subjects.

The seismic proof test of piping conducted by JNES (the Japan Nuclear Energy Safety Organisation) under repeated strong motion earthquakes resulted in fatigue-ratcheting. It was necessary to repeatedly apply seismic waves to the piping system to achieve these failures.

The failure was correlated to the cumulative absolute velocity (CAV) and the integral of the absolute value of the seismic acceleration $a(t)$ for the duration of the seismic excitation (0 to t_{max}).

$$CAV = \int_0^{tmax} |a(t)| dt$$

The CAV results are presented in Table 2.2. The table shows that the pipe was damaged when the CAV value was about 116 g-sec.

Table 2.2. Example of trial calculation of CAV from the ultimate strength test of piping system at JNES

Repetition	Cumulated time (sec)	ZPA(Gal)	Standardised CAV (g-sec)	Note
1	120	1 877	23.2	
2	240	1 877	46.5	
3	360	1 877	69.7	
4	480	1 877	92.9	
5	600	1 877	116.2	Crack penetrates the pipe wall

A similar study is shown for the results of calculating the CAV value from the seismic waves, which was measured at the reactor base mat of the Fukushima Daiichi nuclear power station. The measured CAV was about 4 g-sec for the emergency core cooling system piping installed at the base mat level and the piping system seems to have not been damaged at this level of seismic input.

The importance of the CAV has been recognised by the US Nuclear Regulatory Commission (NRC) in the regulatory guides 1.166, "Pre-earthquake planning, shutdown, and restart of a nuclear power plant following an earthquake".

Figure 2.3. CAV calculation example at Fukushima Daiichi nuclear power station
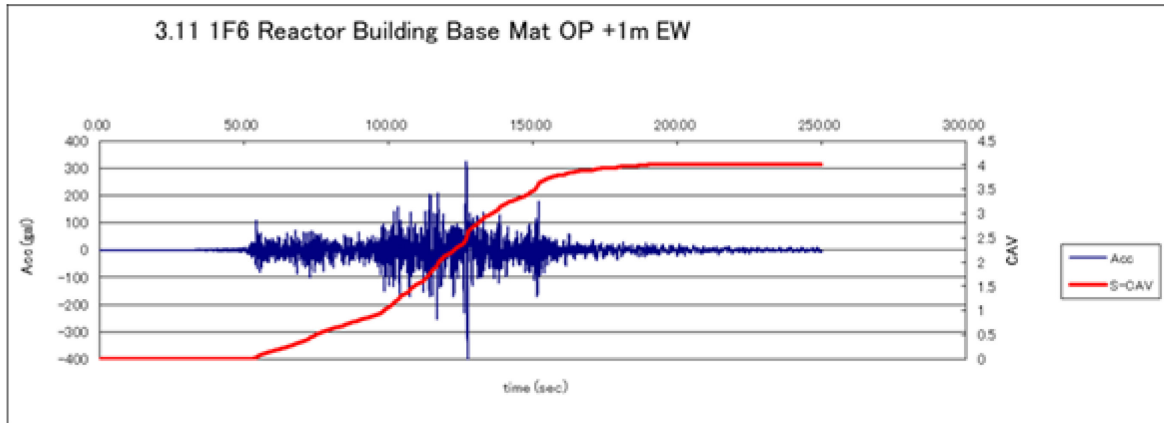
2.5. References

Comartin, C.D. (1995), "Guam Earthquake of August 8, 1993 Reconnaissance Report", National Emergency Training Center.

Earthquake Engineering Research Institute (1995), Earthquake Spectra, Supplement B to Volume 11, Guam Earthquake Reconnaissance Report, April 1995, Earthquake Engineering Research Institute, United States.

EQE International (1995), "The January 17, 1995 Kobe Earthquake: an EQE Summary Report", EQE International, United States.

EQE International (1994), "Performance of Piping During the January 17, 1994 Northridge Earthquake", EQE International, United States.

EQE International (1989a), "The October 17, 1989 Loma Prieta Earthquake, A Quick Look Report", EQE International, United States.

EQE International (1989b), "The December 7, 1988 Armenia, USSR Earthquake", EQE International, United States.

EQE International (1988a), "The Superstition Hills Earthquakes of November 23 and 24, 1987, An EQE Summary Report", EQE International, United States.

EQE International (1988b), "Summary of the June 12, 1988 Alum Rock Earthquake", EQE International, United States.

EQE International (1987a), "Summary of the 1987 Bay of Plenty, New Zealand Earthquake", EQE International, United States.

EQE International (1987b), "Piping Seismic Adequacy Criteria Recommendations Based on Performance During and After Earthquakes, Volume 1: Summary Document", NP-5617, EQE International, United States.

EQE International (1986a), "Summary of the May 2, 1983 Coalinga, California Earthquake", EQE International, United States.

EQE International (1986b), "Summary of the July 8, 1986 North Palm Springs, California Earthquake", EQE International, United States.

EQE International (1986c), "Summary of the May 7, 1986 Adak, Alaska Earthquake", EQE International, United States.

EQE International (1984), "Preliminary Report on the Effects of the April 24", 1984, Morgan Hill, California Earthquake", EQE International, United States.

Kiran, A.R., G.R. Reddy and M.K. Agrawal (2018), "Experimental and numerical studies of inelastic behaviour of thin-walled elbow and tee joint under seismic load", *Thin-Walled Structures*, *127*, pp.700-709.

Lawrence Livermore National Laboratory (1994), "1994 Northridge Earthquake Damage Investigation", Phenomenal News - Natural Phenomena Hazards Newsletter, Lawrence Livermore Laboratory, United States.

Murray, R.C. (1980), "Equipment Response at the El Centro Steam Plant During the October 15, 1979 Imperial Valley Earthquake", Lawrence Livermore Laboratory.

Newmark N.M. and W.J. Hall (1978), "Development of Criteria for Seismic Review of Selected Nuclear Power Plants", NUREG/CR-0098, US Nuclear Regulatory Commission, Washington, DC.

NRC (1985), "Report of the US Nuclear Regulatory Commission Piping Review Committee. Summary and evaluation of historical strong-motion earthquake seismic response and damage to aboveground industrial piping", No. NUREG--1061 (V. 2/ADD.), Nuclear Regulatory Commission.

Ranganath, S. (1994), "Piping and Fitting Dynamic Reliability Program", Volume 3, EPRI TR-102792.

Silver, M.M., G.S. Hardy, P.D. Smith, P.I. Yanev and S.P. Harris (1988), "Recommended piping seismic-adequacy criteria based on performance during and after earthquakes: Volume 1, Summary document", No. EPRI-NP-5617-Vol. 1, EQE, Inc., San Francisco.

Stevenson, J.D. (1993), "Survey of Strong Motion Earthquake Effects on Thermal Power Plants in California with Emphasis on Piping systems. Volume 1, Main report", Oak Ridge Laboratory, United States.

Stevenson, J.D. (1992), "Application of Bounding Spectra to Seismic Design of Piping Based on the Performance of Above Ground Piping in Power Plants Subjected to Strong Motion Earthquakes", Ohio National Laboratory, United States.

3. R&D programmes

This chapter will present and discuss the results of the main research and development (R&D) programmes concerning seismic behaviour until the point of collapse of pressurised piping systems or components.

Annex C details the results of experiments performed on piping elements (elbows, tees, etc.) by different teams mentioned in this chapter. The objective of Annex C is to compile a more complete picture of the results for components under fatigue ratchet loading, which enables an appreciation of the effect of different parameters such as the effect of ratchet strain on fatigue life. This chapter does nevertheless also provide a detailed description of the critical seismic test programmes.

3.1. CEGB tests (United Kingdom)

3.1.1. General

A series of tests were carried out in United Kingdom in the 1980s and 1990s at the Berkeley National Laboratories (BNL) of the Central Electric Generation Board (CEGB) on small size pipes (1" to 4" diameter) by Beaney (1985 to 1991b). Different geometries were considered (simple span or double span straight pipes, pipe segments with elbows or reducers, etc.). For the purpose of the present synthesis, only straight pipe tests will be focused on (Figure 3.1), as they are the easiest to interpret. When pipes were horizontal, they had some sagging, which is a ratcheting effect due to the combination of weight and cyclic plastic strains. This did not occur in the few tests where the pipe axis was vertical.

The straight pipes tested included ten carbon steel unpressurised specimens, 12 carbon steel pressurised, five stainless steel unpressurised and five stainless steel pressurised specimens. In this regard, it should be pointed out that experiments carried out on unpressurised piping systems are of very limited interest to considerations of the collapse modes of pressurised piping systems and related criteria. The natural frequencies of the pipes were five, seven and ten Hz.

Resonant displacement-controlled sinusoidal input motions were applied to the pipe supports, with a step by step increasing level. The piping system's effective frequency trends to decrease once it undergoes plastic deformation. The input frequency was adjusted so that a $\pi/2$ phase angle was kept between the end displacements and the central acceleration in order to keep the system at resonance. Information presented in the CEGB reports would be usable for an interpretation of effective damping versus ductile demand.

The CEGB reports how the author, Mr E.M. Beaney, introduced a theoretical prediction method of the test response, based on energy balance. This approach should be revisited when the establishment of appropriate criterion is discussed again.

Beaney (1985a): a presentation of the experimental concept, tests on an unpressurised straight pipe (outer diameter [OD]=25.4 mm, thickness [t]=2.64 mm) and a pipe with two elbows. The type of steel is not mentioned; the yield stress is 209 MN/m². The specimen frequency is five Hz; tests last three minutes. A 0.8% peak-to-peak cyclic strain was measured. There was no failure; the pipe sags due to the deadload.

Beaney (1985b): the same concept as described above. Five unpressurised straight pipes are tested with different OD/t ratios, from 3.0 to 26.8, which are made of steels of yield strains varying from 0.078-% to 0.144 %.

Figure 3.1. BNL straight pipe testing scheme
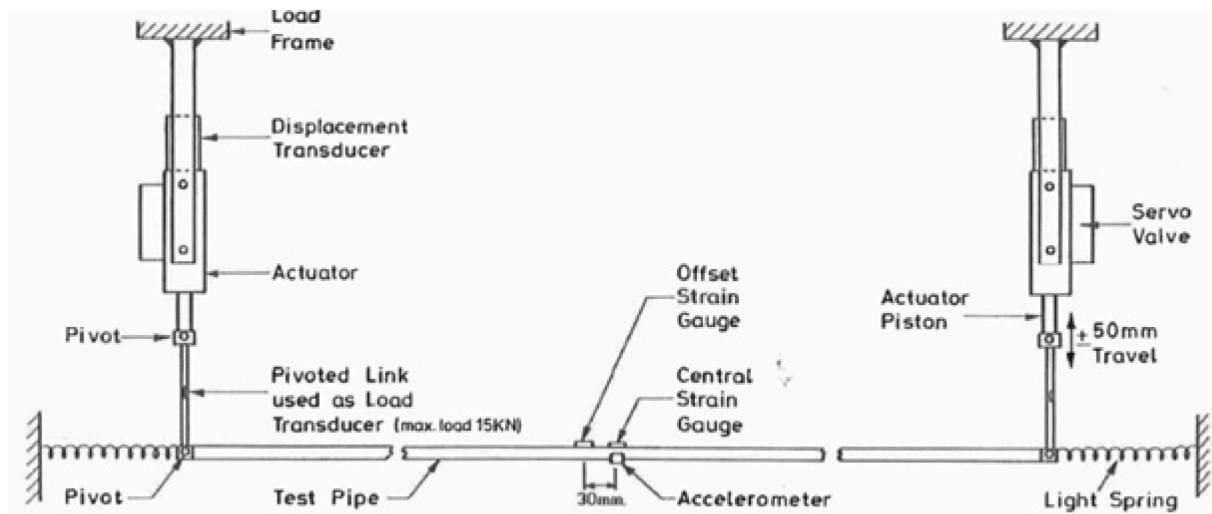
Source: Beaney, 1985b.

3.1.2. Unpressurised carbon steel straight pipes (Beaney 1985b)

The yield strain of the steel was at 0.06%. A preliminary test and series of five tests were carried out on unpressurised piping systems. The main observations and conclusions were as follows:

- Once in the plastic regime, a dramatic increase of the input motion (by a factor of 20 or 30) resulted only in a small increase of the central acceleration output, which looks "saturated" at around 25% above the acceleration at yield.

- The central strain increase is also very limited, for example by a factor of two, while the input multiplied by a factor of ten without displaying a "saturation" effect.

- The frequency shift was very small, for example varying from five Hz at 0.1 g (corresponding to the yield strain at the pipe mid span) to 4.6 Hz for a 2.36 g input.

- A sagging effect appeared, as mentioned above, which is illustrated in Figure 3.2.

Figure 3.2. Ratcheting effect in form of sagging of horizontal unpressurised pipe
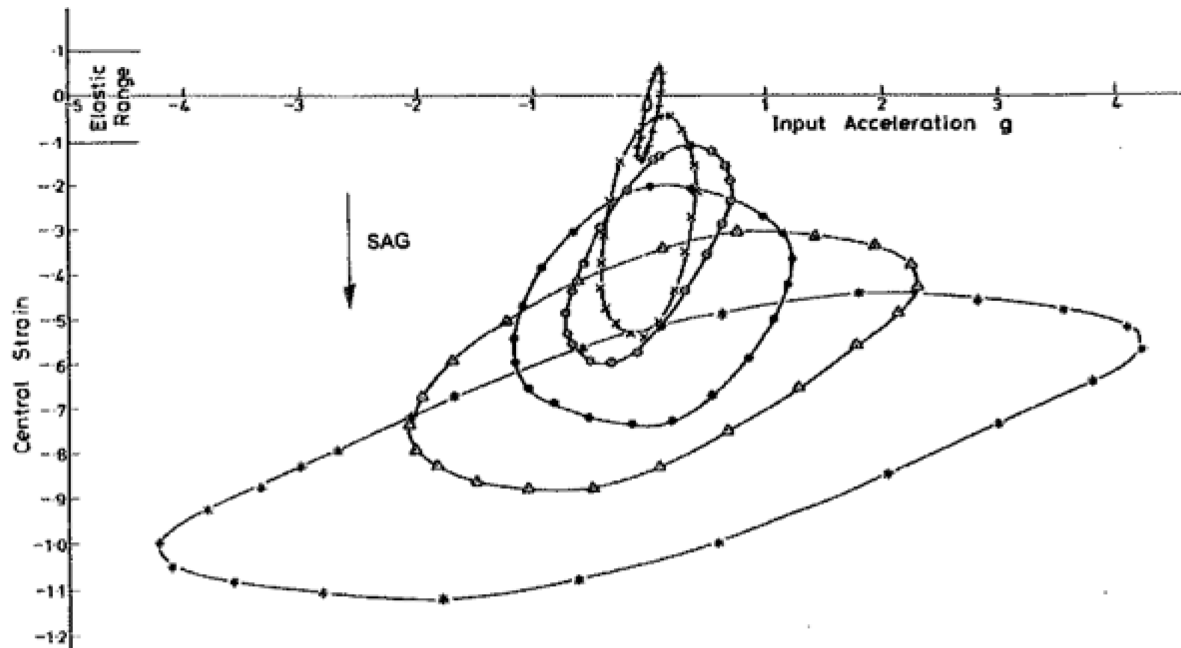
Source: Beaney, 1985a.

3.1.3. Pressurised carbon steel straight pipes

Eight tests were carried out at a pressure that caused the hoop strain to be equal to 2/3 S_y. Consequently, the pipes yielded at a lower input motion than for the similar unpressurised specimen. The pipes sagged as well as the unpressurised ones and a hoop ratcheting effect appeared due to the combination of the permanent pressure and cyclic plastic strain, which is illustrated in Figure 3.3. The strain analytical analysis was difficult to conduct due to the cumulative effect of the weight and pressure on the longitudinal strain. Large hoop strain increments appeared during the first cycles, but the rapidly decreased, which resulted in a hoop ratchet strain that did not exceed 4%. BNL did not report a pipe failure. Further analysis of the BNL documentation is necessary to identify the number of cycles that was experienced by the piping systems.

Figure 3.3. Hoop ratcheting effect
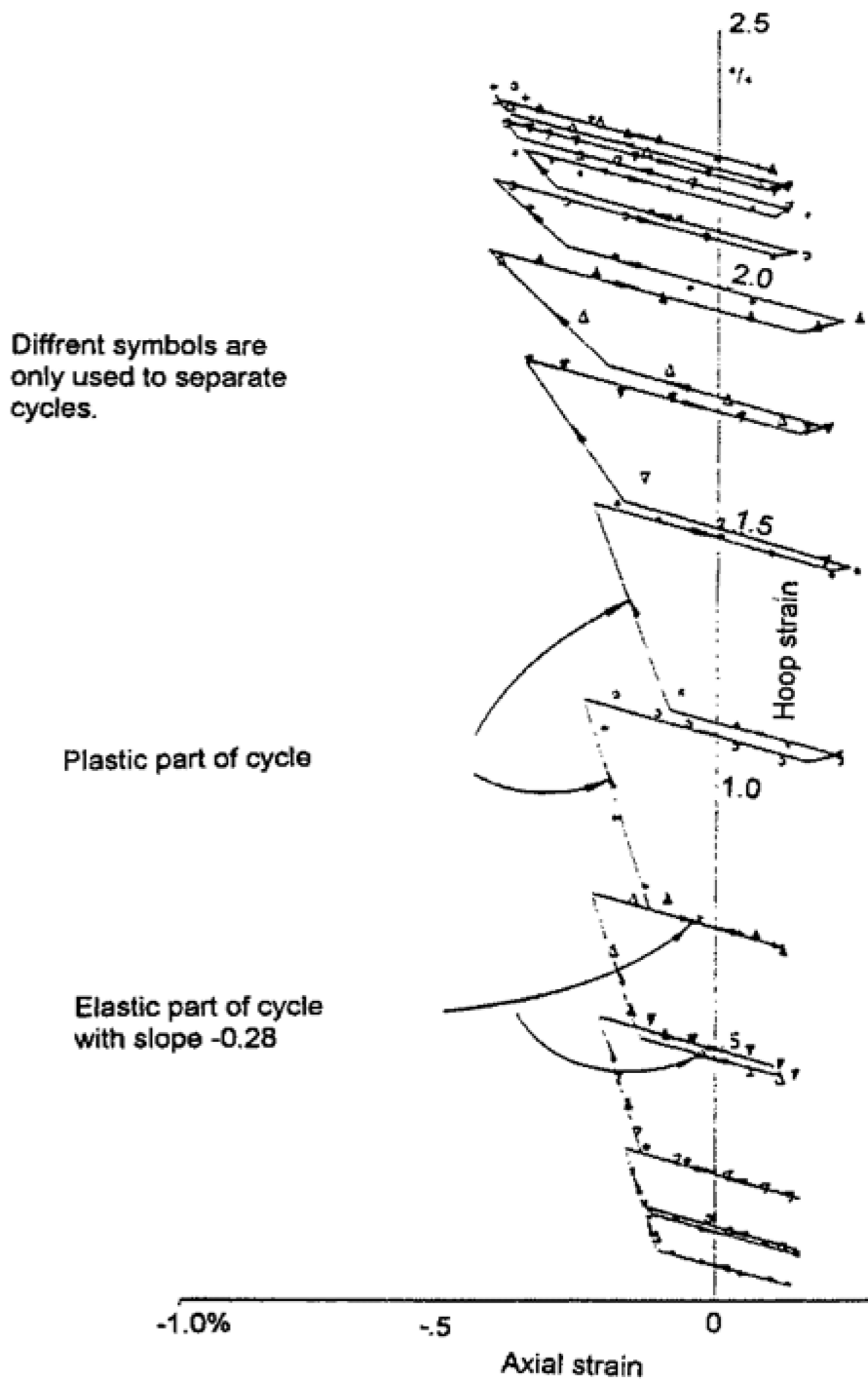
Hoop and Axial Strains on the Top of
the Pipe in Test 7

Source: Beaney, 1986.

Figure 3.4. Hoop ratcheting and hardening effects

FIG. 2. Hoop and Axial Strain on the Thinned Section of a Pressurised Pipe.
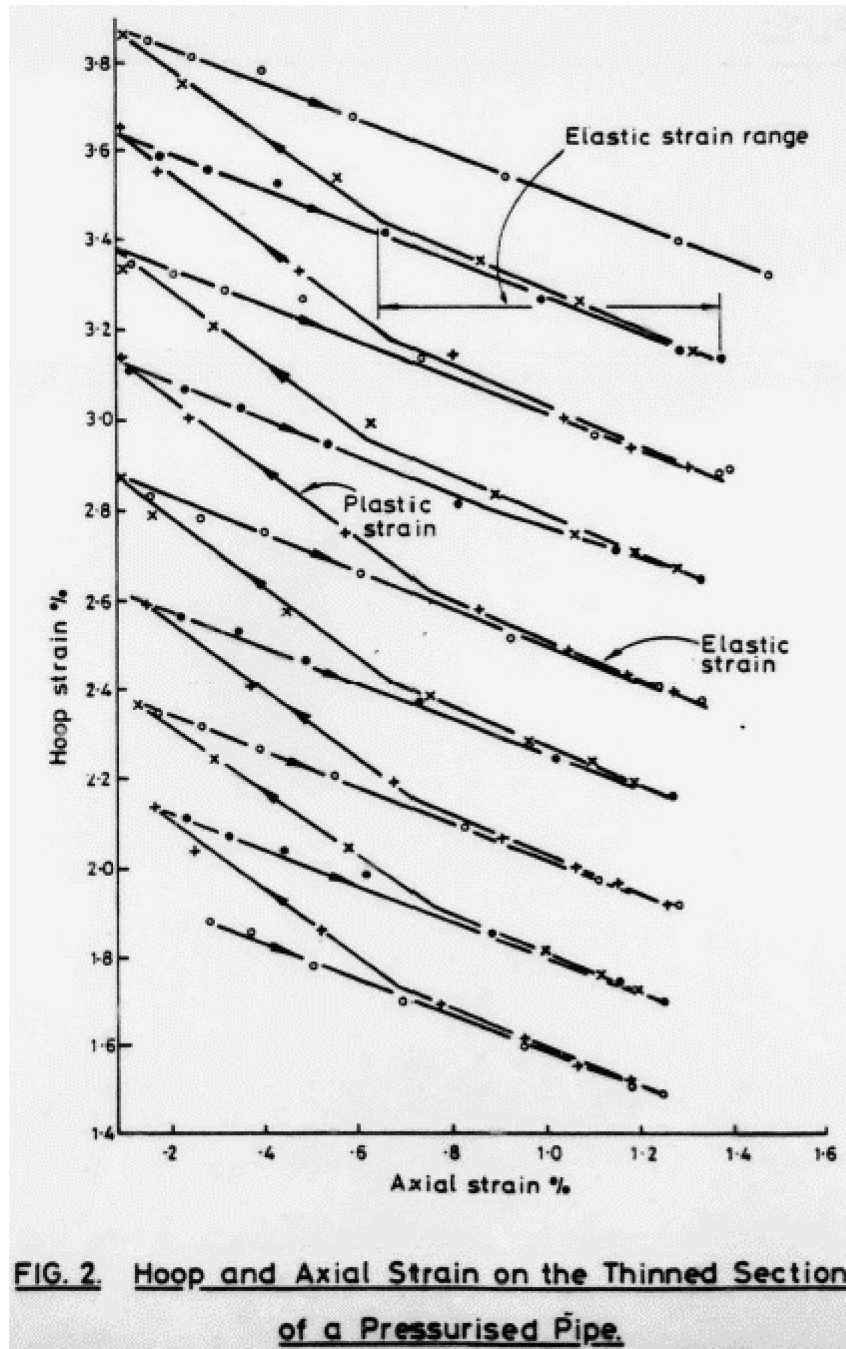
Source: Beaney, 1987.

3.1.4. Pressurised and unpressurised stainless steel straight pipes

An important observation is that stainless steel exhibits significant hardening capacity, unlike the carbon steel. One of the consequences of this capacity was that the output accelerations were significantly larger than for the carbon steel specimen, at around three times the acceleration at yield.

Unfortunately, the hoop strains were not reported. The BNL did not report a failure mode even though the pipes were put through over 1 000 cycles at the maximum loading possible.

3.1.5. Straight pipes with local thinned walls

Tests were carried out on straight pipes with local thinned wall (ten carbon steel and six stainless steel specimens). The wall thickness was reduced by 1/3 at the outer diameter on a length of 50 mm. The hoop stress was therefore larger than in the full section by a factor of 1.5, while the bending stress was larger by a factor of 1.59. The tests were run at either no pressure (four tests), or at a pressure corresponding to a hoop stress of 2/3 S_y, or S_y in the thinned section.

Hoop ratcheting was significant (see Figure 3.4) and concurrent with an isotropic hardening effect (an increase of the elastic domain size). Beaney (1985b) concluded from his analysis that most of the hardening can be obtained when the cumulative stain is less than 10%.

The BNL documentation reports large measured dynamic stresses (up to 1 000 MPa for a yield stress of 260 MPa) for around 5% accumulated strain in austenitic pipes. A similar phenomenon, albeit a less striking one, has been measured in ferritic specimen. The phenomenon observed in BNL documentation requires further investigation because it is hard to believe that such a large hardening effect is possible.

The tests were run to failure, which occurred for very large accumulated hoop strains (30-75%). A fatigue analysis was carried out by Beaney (1988b), which led to the conclusion that an S_y hoop strain in stainless steel specimens reduces the cycle life by a factor of 20 when compared with a non-pressurised specimen. This effect is even stronger for ferritic pipes.

3.1.6. References

Beaney, E.M. (1991a), "Failure of elbow under seismic loading", Central Electric Generating Board, Berkeley Nuclear Laboratories, Report TD/SID/REP/0134.

Beaney, E.M. (1991b), "Failure of socket welds in pipework under seismic loading", Central Electric Generating Board, Berkeley Nuclear Laboratories, Report TD/SID/REP/0183.

Beaney, E.M. (1989a), "The behaviour of discrete components in pipework subjected to seismic loading", Central Electric Generating Board, Berkeley Nuclear Laboratories, Report RD/B/6225, 89.

Beaney, E.M. (1989b), "Response of two spans of pipework to seismic excitation", Central Electric Generating Board, Berkeley Nuclear Laboratories, Report RD/B/6255, 89.

Beaney, E.M. (1989c), "Failure of pipework subjected to seismic loading", Central Electric Generating Board, Berkeley Nuclear Laboratories, Report RD/B/6315, 89.

Beaney, E.M. (1988a); "Response of stainless-steel pipes to seismic excitation", Central Electric Generating Board, Berkeley Nuclear Laboratories, Report TPRD/B/1051, 87.

Beaney, E.M. (1988b), "The response and failure of pipes with stress concentrations under seismic loading", Central Electric Generating Board, Berkeley Nuclear Laboratories, Report RD/B/6050, 88.

Beaney, E.M. (1987), "Response of pipes to seismic excitation, Theoretical response prediction", Central Electricity Generating Board, Berkeley Nuclear Laboratories, Report TPRD/B/0919, 87.

Beaney, E.M. (1986), "Response of pressurised straight pipes to seismic excitation", Central Electricity Generating Board, Berkeley NUC Labs, Berkeley Nuclear Laboratories, Report TPRD/B/0826, 86.

Beaney, E.M. (1985a), "Response of tubes to seismic loading", Central Electricity Generating Board, Berkeley Nuclear Laboratories, Report number not indicated, dated 23 November in PDF version.

Beaney, E.M. (1985b), "Response of pipes to seismic excitation - Effect of pipe diameter/ wall thickness ratio and material properties" Central Electricity Generating Board, Berkeley Nuclear Laboratories, Report TPRD/B/0605 N, 85.

3.2. US tests

3.2.1. EPRI/NRC component tests (United States)

Tests presentation and EPRI conclusions

A series of 41 components were tested in the "Piping and Fitting Dynamic Reliability Program", which was sponsored by the Electric Power Research Institute (EPRI) and the US Nuclear Regulatory Commission (NRC) and performed by ANCO Engineers. Components included elbows tees and reducers, most of them pressurised and six-inches large. A total of 32 tests are directly applicable to seismic situations, while the remaining tests are static or water hammer and relief valve loading tests. Most of the components were of schedule 40, some of them of schedules 80 and 10. Approximately half of them were made of carbon steel and the other half of stainless steel. Most of the tested components were pressurised (only five were not). The pressure followed the design pressure of the American Society of Mechanical Engineers' (ASME) code.

Figure 3.5. EPRI-NRC component test configuration
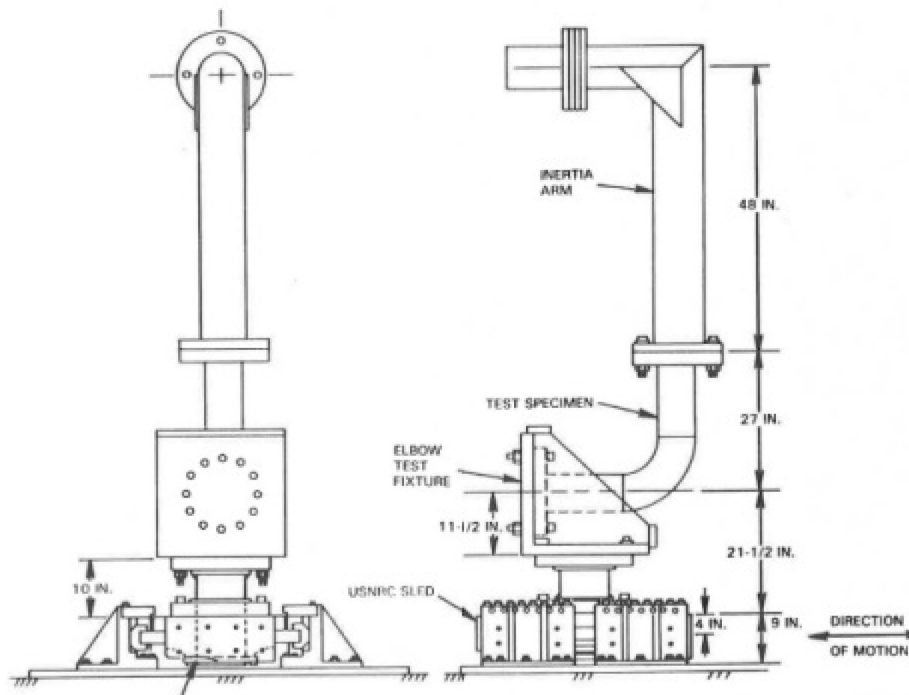
Source: EPRI, 1994b.

The typical test configuration for an in-plane elbow is presented in Figure 3.5. The seismic input motion was rather narrow-banded and taken as representative of a typical floor response. The motion had a peak at 6.3 Hz (and a duration of 22.76 s) for most of schedule 40 specimen, one between 7.0 and 7.5 Hz (20.48 s) for schedule 80 and one at 1.3 Hz (110.3 s) for two schedule 10 specimen. The natural frequency was tuned to be about 0.5 Hz larger than the central frequency of the input motion for several tests. As a result, the effective frequency of the component when softening under plastic regime corresponded to the central frequency of the input, maximising the response amplification.

The test's principle was to apply the full-scale capacity of the shaking table (above 20 g) and repeat the same run until failure occurred. The applied input motion was therefore far higher than the acceptable level D input motion, by between 9 times and 30 times according to EPRI reports, depending on the component. For schedule 80 components, no failure was obtained after five runs and therefore the pressure was increased to reach an Sm hoop stress at the sixth run.

All pressurised components exhibited ratcheting and failed by a through-wall fatigue crack. EPRI concluded that the failure mode was fatigue-ratcheting, as reported in Figure 3.6 that presents the main features of the EPRI-NRC component tests. Fatigue-ratcheting tests were carried out on different types of steel to evaluate the influence of ratchet strain on fatigue life. One conclusion was that accumulated ratchet strain has no effect on the material fatigue life when it does not exceed 10% of the material ductile capacity.

The key conclusion of EPRI-NRC tests is that, when dealing with seismic loads, the ASME code targets a failure mode (plastic instability) that does not occur. The ASME seismic design rules do not target the observed failure mode, which was fatigue-ratcheting or possibly conventional fatigue damage. However, the code encompasses enough margins for the piping system to be protected against this failure mode. The issue was raised that

the true failure mode should be explicitly addressed by the code and an appropriate criterion established.

Figure 3.6. EPRI-NRC component seismic tests

No	Type	Mtl/Sch	Residual Strain %	Press (PSI)	Load Direct	DYM M / LIM M	Load Type	Pk-to-Pk Cyclic Strain %	Input × Level D	Tests to Failure	Failure Mode
1	6"-ELBOW-LR	CS/80		1500	I-P	1.3	SSE	2.5	15	5-W/O	
	(RETEST)			2600	I-P	1.3	SSE	1.5	15	0.5	FR
2	6"-ELBOW-LR	CS/80		1500	O-P	1.4	SSE	1.4	15	5-W/O	
	(RETEST)			2600	O-P	1.4	SSE	1.4	15	4.5	FR
3	6"-ELBOW-LR	SS/10	3.5	400	I-P	3.1	SSE	2.4	21	3.5	FR
4	6"-ELBOW-LR	CS/40		1000	I-P	1.6	SSE	2.0	18	2.5	FR
5	6"-ELBOW-LR	CS/40	13.8	1700	I-P	1.9	SSE	2.0	21	3.5	FR
6	6"-ELBOW-LR	SS/40	16	1700	I-P	1.6	SSE	2.0	19	3.5	FR
7	6"-ELBOW-LR	SS/40	9	1000	I-P	1.5	SSE	2.0	23	4.5	FR
8	6"-ELBOW-LR	SS/40	1.5	0	I-P	1.5	SSE	2.0	24	5-W/O	
9	6"-TEE	SS/40	8	1700	O-P	2.6	SSE	2.2	21	1.5	FR
10	6"-TEE	SS/40	6.5	1000	O-P	2.3	SSE	2.2	21	2.5	FR
11	6"-TEE	SS/10	3	400	O-P	2.4	SSE	1.9	16	0.5	FR
12	6"-TEE	SS/40	11	1700	I-P	2.4	SSE	2.2	27	2.5	FR
13	6"-ELBOW-SR	CS/40	6	1000	I-P	2.1	SSE	1.9	22	2.5	FR
14	6"-TEE	CS/40	10	1700	O-P	2.7	SSE	—	18	1.5	FR
15	8" × 4"-REDUCER 4"-STR PIPE 4" × 6"-REDUCER	SS/40	18	1700		1.3	SSE	~13	13	5	FR
16	8" × 4"-REDUCER 4"-STR PIPE 4" × 6"-REDUCER	CS/40	2.5	1700		1.4	SSE	3.3	30	0.5	FR
17	6" ELBOW SR	CS/40	2.5	1000	TOR	N/A	SINE + SSE	2.5	20	3	FR
18	8" × 4"-FAB TEE REINFORCED	CS/40	0.6	1000	O-P	3.5	SSE	0.80	20	0.3	FR
19	6"-ELBOW-LR	SS/40	15	2500	I-P	1.6	SSE	1.8	22	3	FR
20	12" × 4"-NOZZLE	SS/40	6	1000	I-P	3.6	SSE	1.9	16	1.9	FR
21	8"-LUGS	CS/40	5	1700	TOR	N/A	SINE + SSE	1.5	19	0.4	FR
22	8"-LUGS	SS/40	5	1700	TOR	N/A	SINE + SSE	2.3	19	0.5	FR
30	6"-ELBOW-LR	SS/10	8.2	0	I-P	3.1	SSE	1.4	9	2	
				400	I-P	2.2	SSE	2.0	10	3	FR
31	6"-ELBOW-LR	SS/10	4	400	I-P	3.2	SINE + SSE	1.7	23	3.5	FR
34	6"-STR PIPE	CS/40	6.5	1000		1.2	SINE + SSE	2.2	12	4	FR
35	6"-ELBOW-LR	CS/40	13	1700	I-P	1.8	SSE	3.4	18	5	FR
36	6"-TEE	CS/40	3	1700	RUN	2.5	SINE + SSE	1.0	15	0.5	FR
37	6"-ELBOW-LR	SS/10	4	0	I-P	1.3	SSE	2.0	10	2	RB
38	6"-TEE	SS/40	20	1700	O-P	1.9	SSE	2.7	20	3.6	FR
39	6"-TEE	SS/40	10	0	O-P	1.5	SSE	3.4	21	4-W/O	
40	8" × 4"-REDUCER 4"-STR PIPE 4" × 6"-REDUCER	SS/40	9	0		1.4	SSE	3.3	22	2	RB
41	6"-ELBOW-LR	CS/40	10	1700	I-P	1.8	SINE + SSE	2.7	25	2	FR

Residual strain measured by 2-inch scratch marks
For elbows, the measured strain on the outside surface is lower than the strains expected at the inside surface
I-P is in-plane; O-P is out-of-plane; TOR is torsion.
SINE is for sine sweeps
W/O means without failure; FR is for fatigue ratcheting; RB is for ratchet buckling
DYM M + LIM M is the measured moment divided by the predicted static limit moment

Source: Slagis, 1997.

Some of the tests were monitored for structural dynamics effects. The effective frequency and effective damping were identified. The frequency shift towards lower frequency was observed and quantified versus the input level or the ductile demand. Two types of equivalent damping were considered, the "true" damping that better fits the observed transfer function and the "equivalent" damping that leads to the maximum observed response in bending moment. A schedule 10 elbow test was deeply investigated. The output was that a half peak-to-peak strain of 1% corresponded to 15% true damping and 30% equivalent damping. Damping was larger for larger schedules, for instance 30% damping corresponded to only 0.5% half peak-to-peak strain in a schedule 80 elbow.

Follow-up on EPRI-NRC elbows tests

Some of the values presented by EPRI (see Figure 3.5) were later discussed by Slagis (1997), who particularly focused on the input level and number of runs to failure.

Regarding the input level, Slagis objected to the fact that EPRI used the peak value of the response spectrum in place of the spectral acceleration at the natural frequency of the specimen when accounting for the anticipated frequency shift in the plastic regime. This issue necessitates further investigations.

Slagis concentrated on the level of input motion for tees, as compared to acceptable ASME level D. The failure did not occur in the tee itself but at its junction with the adjacent straight pipe, or even in the straight pipe. A discussion has therefore been raised on whether the code intensification factor for tees should be considered in interpretations of the test.

Nevertheless, EPRI evidently correctly (if not entirely exactly) calculated the acceptable input motion according to the code rule. The discussion mentioned above is therefore rather unnecessary. The information that should be retained is that in this situation, although the code again does not target the observed failure mode, it still encompasses the necessary margins to enable protection against this failure mode.

Regarding the number of runs to failure, special attention was paid to test three, which consisted of a series of increasing input motions that were applied to a schedule 10 long radius elbow, as presented in Figure 3.7. Slagis emphasised that the last two runs were the only strong motions and that it should consequently be concluded that failure occurred during the second run. However, it is possible to calculate the damage resulting from runs 6 to 11 on the basis of the Argonne National Laboratory (ANL) fatigue model for austenitic steels (see Figure 3.8). The output is that, in terms of fatigue damage, those runs were equivalent to 4.5 runs at 21 x level D, which confirms a prudent evaluation by EPRI.

The other number of runs to fail that Slagis discussed concerned test 37 of an unpressurised schedule 10 elbow, which was tuned at a low frequency by increasing the inertia arm length and inertia mass. This cantilevered configuration of the test resulted in a strong P-Δ effect under which the elbow buckled and as a result the test was not representative of actual piping systems.

Figure 3.7. Test three response data

	2% Peak Spectral Acc, g	Spectral Acc g @ 4 Hz	Sled Acc g	Top Acc g	Measured Moment in-kip
Run 5	1.49	0.9	0.14	1.5	31
elastic	[1]	[1]	[1]	[1]	[1]
Run 6	8.3	5.2	0.91	4.2	83
elastic x6	[5.6]	[5.8]	[6.5]	[2.8]	[2.7]
Run 7	12.3	7.6	1.39	4.9	101
elastic x9	[8.3]	[8.5]	[9.9]	[3.3]	[3.3]
Run 8	18.4	11.8	2.02	5.8	114
elastic x13.5	·[12]	[13]	[14]	[3.9]	[3.7]
Run 9	22.7	14.6	2.47	6.3	123
elastic x17	[15]	[16]	[18]	[4.2]	[4.0]
Run 10	43.7	27.6	6.65	8.3	153
elastic x28	[29]	[31]	[48]	[5.5]	[4.9]
Run 11	40.8	25	6.0	8.6	163
elastic x28	·[27]	[28]	[43]	[5.7]	[5.3]

Note: Numbers in brackets are the ratio of the reported parameter to the Run 5 value. "elastic x6" means that the programmed input is 6 times Run 5

Source: Slagis, 1997.

Figure 3.8. Fatigue life of austenitic steels (ANL)
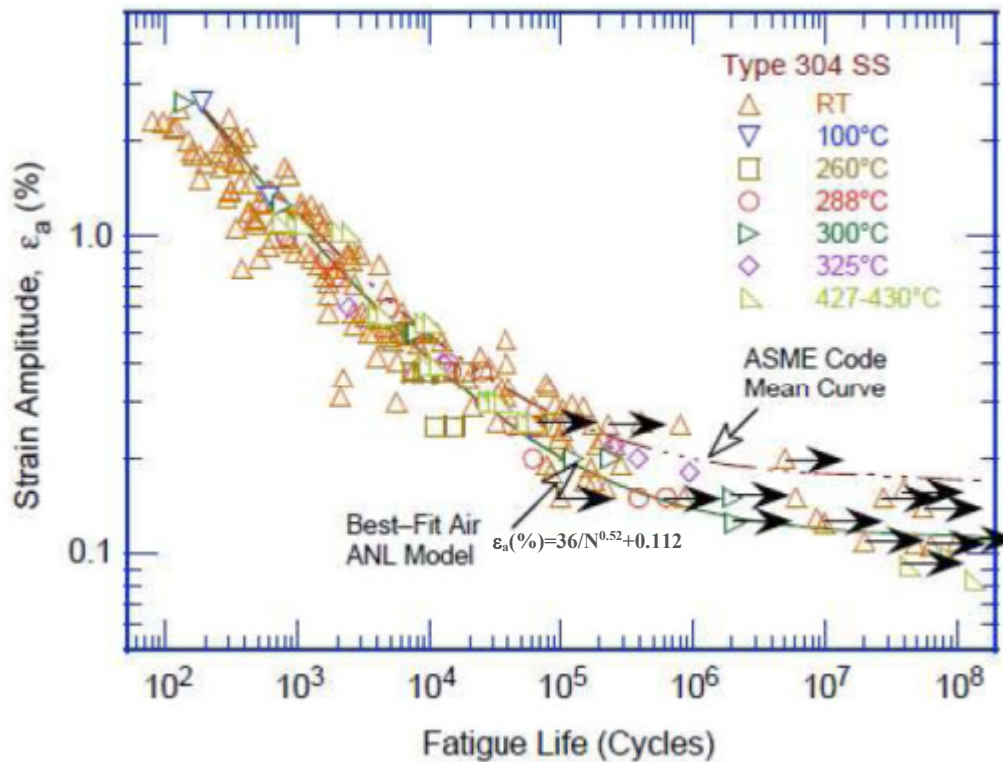
Source: US NRC, 2018.

3.2.2. EPRI-NRC-GE and ETEC system tests

Under the sponsorship of EPRI, NRC and the group of experts (GE), two seismic shake table tests were performed on piping systems at the Energy Technology Engineering Center (ETEC) (EPRI, 1994a). The system tests followed the component tests and had as objectives to:

1. compare the failure mode to the component test failure modes;

2. compare failure prediction stresses to the component tests;

3. evaluate design margins and compare them to component test margins;

4. evaluate the redistribution of loads that would follow large plastic deformation;

5. obtain baseline data to evaluate multi-input motions using different input at the shake table sleds;

6. evaluate the effects of mid-frequency spectra (such as that caused by boiling water reactor [BWR] hydrodynamic loads);

7. gather data on the performance of supports and operability of the in-line valve at high seismic accelerations.

Table 3.1. Piping system test at ETEC

System	Material	Sizes	Pressure	N[1]
1	Carbon steel	NPS 6 sch.40	1 000 psi	13
	ASTM A106 Gr.B	NPS 3 sch.40		
2	Stainless steel	NPS 6 sch.40	1 000 psi	17
	ASTM A312 TP.316L	NPS 3 sch.40		

Note: N is the number of shake table runs of increasing magnitude to reach failure.
Source: EPRI (1994a), "Reliability and Fitting Dynamic Reliability Program, Volume 3: System Tests",
Report EPRI TR-102792-V3.

The system 1 (carbon steel) tests consisted of operating basis earthquake (OBE), safe shutdown earthquake (SSE), sine sweeps, multiples of SSE, half sled capacity (10 g peak acceleration) and full sled capacity (17 g). The elastically calculated B_2 M/Z stresses at failure, which were based on a response spectral analysis at 2% damping with ±15% peak broadening, were reported to be $42 \times 3S_m$ (EPRI, 1994a: Table 2-1 and Table 5-6). The failure, a crack that appeared at a short radius elbow after 13 shake table runs, was described as follows: "fatigue ratcheting is the observed failure mode and not plastic collapse" in Sections 2.4 and 8.0 (EPRI, 1994a).

The system 2 (stainless steel) tests consisted of OBE, SSE, sine sweeps, multiples of SSE, half sled capacity and full sled capacity. The elastically calculated cumulative usage factor (CUF) at the failure location, which was based on a response spectral analysis at 2% damping with ±15% peak broadening, were reported to be 40 (EPRI, 1994a: Table 6-17). This CUF was 40 times larger than the ASME III NB-3600 design limit of CUF as 1.0. The failure, which was a crack that appeared at the nozzle of the vessel after 17 shake table runs, was described as fatigue-ratcheting, just as for system one.

Figure 3.9. Configuration of piping system models by EPRI-NRC-GE
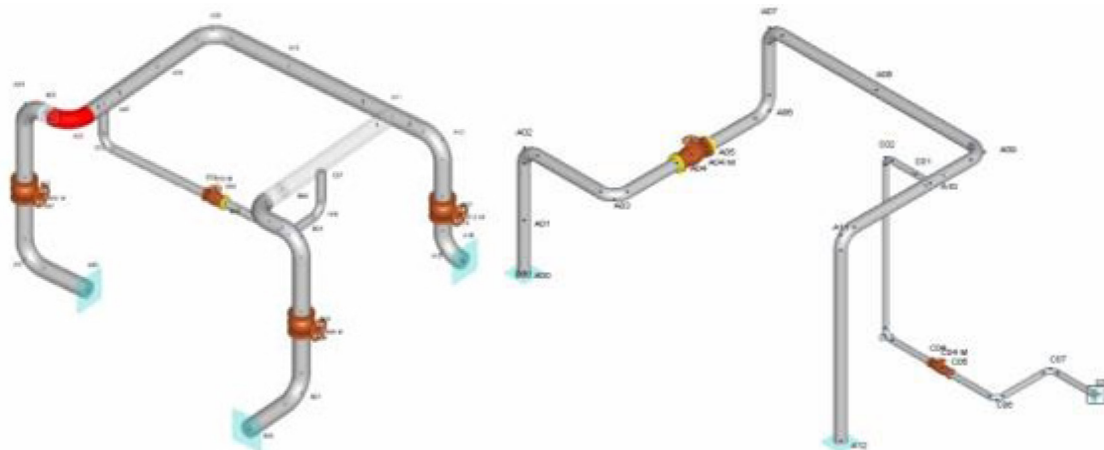
Note: System 1 Configuration   System 2 Configuration
Source: EPRI (1994a), "Reliability and Fitting Dynamic Reliability Program, Volume 3: System Tests",
Report EPRI TR-102792-V3.

3.2.3. References

EPRI (1994a), "Reliability and Fitting Dynamic Reliability Program, Volume 3: System Tests", Report EPRI TR-102792-V3.

EPRI (1994b), "Reliability and Fitting Dynamic Reliability Program, Volume 2: Component Tests", Report EPRI TR-102792-V2.

Slagis, G.C. (1997), "Evaluation of seismic response data for piping", *Welding Research Council Bulletin*, vol. 423, pp.1-162.

US NRC (2018), "Effect of LWR water Environments on the Fatigue Life of Reactor Materials", NUREG/CR-6909, Office of Nuclear Regulatory Research.

3.3. Japanese test

A large number of seismic performance experiments on nuclear piping systems have been conducted in Japan by public institutes, industry groups and universities. This section summarises the shake table tests on piping systems conducted by public institutes.

3.3.1. NUPEC/JNES

The Nuclear Power Engineering Corporation (NUPEC), which was reorganised and named the Japan Nuclear Energy Safety Organisation (JNES) in 2003, conducted a series of seismic safety verification campaign on the structures and components of nuclear power plants using a bi-axial shaking table in Tadotsu, Japan, from 1992 to 2002 (Suzuki et al., 2004a; Suzuki et al., 2004b). As for piping systems, experiments were conducted to confirm the ultimate strength of piping systems under seismic loads, which are referred to by "seismic proving tests". The tests consisted of confirmatory tests of the design rules, as well as fragility tests to explore ultimate strength and failure. The design method confirmation tests reflected the structural features and vibration characteristics of a nuclear power plant. The configuration consisted of three-dimensional piping routes with three fixed ends, five restraint supports, one weight, and ten pipe joints. For the ultimate strength test model, the piping system configuration was modified from the design method confirmation test model by the addition of a heavy mass and removal of horizontal support, which aimed to enable the shaking table test to obtain a larger response and the ultimate behaviour. The configuration of the test model used in the seismic proving test is shown in Figure 3.10. The shaking directions were horizontal and vertical. The pipe's material was carbon steel.

The experimental conditions and obtained results are summarised in Table 3.2. No evidence of piping failure was observed in the design method confirmation test, even though the input acceleration was up to 4.5 times the allowable primary stress limit of 3Sm, and elastic-plastic behaviour was confirmed in the strain time history. In the ultimate strength test, the failure mode was fatigue failure at an elbow after the fifth iteration of the maximum level input excitation. Ratcheting deformation was observed at Elbow one, Elbow two and the tee, but plastic collapse or buckling did not occur. Figure 3.11 shows the test situation in the ultimate strength test during which the pipe failure occurred.

Table 3.2. Basic conditions and results of the shaking table tests on a large-scale piping system model by NUPEC

Test name [a]	Pipe size [b]	Pressure	Natural frequency [c]	Input motion	Max. excitation level	Test results
DM	D= 216.3 mm t= '8.2 mm'	Hoop stress by internal pressure to be S_m level	6.3 Hz	Seismic wave	Primary stress to be 4.5 times $3S_m$	No evidence of piping failure
US			3.8 Hz		Primary stress to be 9 times $3S_m$	Fatigue failure at an elbow

Note:
a: DM: Design Method Confirmation Tests; US: Ultimate Strength Test
b: D: Outer diameter, t: wall thickness
c: From the test results, in the elastic region
Source: Nuclear Power Engineering Center, 2001.

Figure 3.10. Configuration of the test models
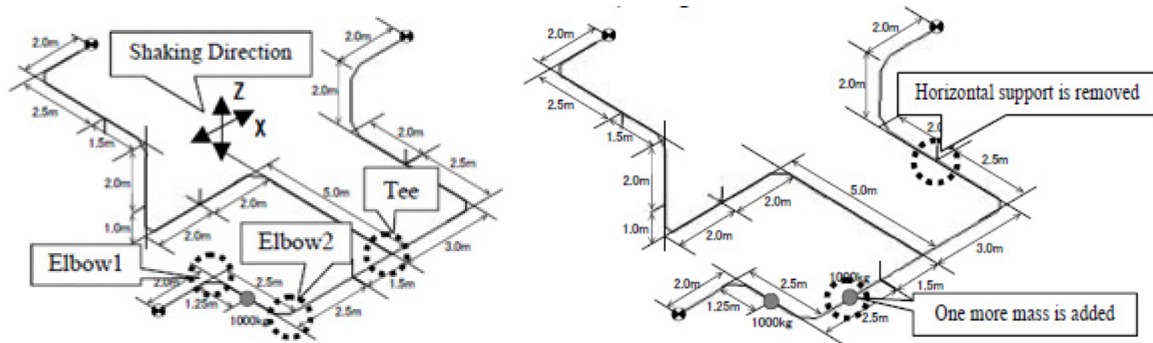
Source: Suzuki et al, 2004a.

Figure 3.11. Test situation when the pipe failure occurred in the ultimate strength test
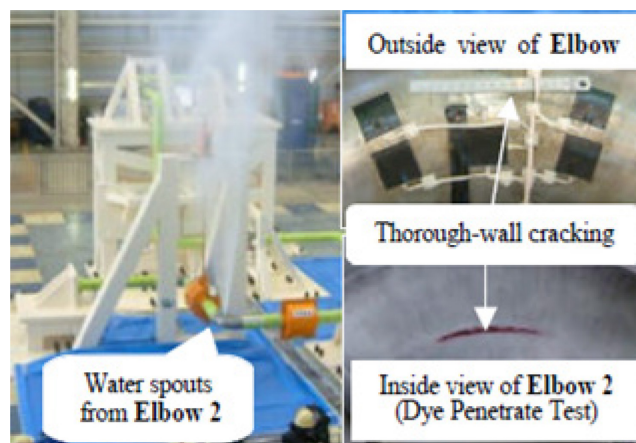
Source: Suzuki and Abe, 2005.

3.3.2. NIED

The National Research Institute for Earth Science and Disaster Resilience (NIED) conducted a series of loading tests on pipe components and a series of shaking table tests on piping systems with simulated defects due to the ageing effects. This was a joint research project with Yokohama National University and IHI corporation (Nakamura et al., 2004; Nakamura et al., 2010; Nakamura et al., 2011). The main defect considered in the experiment was wall thinning. Piping system models without defects were also used for the references in the series of the experiments. This section describes the three kinds of shaking table tests use in these experiments:

1. One-directional shaking table test on relatively simple piping system models. This experiment is hereafter referred to as "NIED-Test#01". (Nakamura et al., 2004)

2. Tri-axial shaking table test on piping system models with several elbows and a tee, which will be referred to as "NIED-Test#02". (Nakamura et al., 2010)

3. Tri-axial shaking table test on piping system models with several elbows and two tees. These are larger scale models than those used in NIED-Test#02 and will be referred to as "NIED-Test#03". (Nakamura et al., 2011)

Figure 3.12 shows the configuration of the test models used in those experiments. The material of the pipe was carbon steel for all piping system models.

The basic conditions and results are summarised in Table 3.3. The input acceleration levels for these shake table tests were several times higher than those for the design-based acceptable limit acceleration. The observed failure mode was the fatigue failure accompanied by ratchet deformation. Though the failure mode was considered to be the fatigue failure for the test models with wall thinning, a larger ratchet deformation was observed in these models due to the higher hoop stress at the wall thinning part. The failure position was different from that in the test models without wall thinning in some test cases due to the remarkable ratchet deformation. Figure 3.13 shows examples of the failure modes in the shaking table test. Unstable failure, such as progressive deformation or collapse, was not observed in the experiment.

Table 3.3. Basic conditions and results of the shaking table tests on piping system models conducted by NIED

Model name	Pipe size [a]	Defect condition	Pressure	Natural frequency [c]	Input motion	Max. applied acc. [b]	Test results
NIED-Test#01							
3D_A01	D= '114.3' mm t='8.6' mm	No defect	10 MPa	2.78 Hz	Narrow band random wave	18.5 m/s²	Fatigue failure at an elbow flank
3D_C01		Approx. 50% Wall thinning		2.42 Hz		18.5 m/s²	Fatigue failure at a wall thinning elbow flank
NIED-Test#02							
AP3_A31	D= '114.3' mm t='8.6' mm	No defect	3 MPa	5.30 Hz	High-pass filtered seismic wave	18 m/s²	Fatigue failure at an elbow flank
					Sinusoidal wave	9.8 m/s²	
AP3_C31		Approx. 50% Wall thinning		3.99 Hz	High-pass filtered seismic wave	17 m/s²	Fatigue failure at a wall thinning elbow, close to the pipe end
					Sinusoidal wave	9.8 m/s²	

Table 3.3. Basic conditions and results of the shaking table tests on piping system models conducted by NIED (Continued)

Model name	Pipe size [a]	Defect condition	Pressure	Natural frequency [c]	Input motion	Max. applied acc. [b]	Test results
NIED-Test#03							
AP3_EA01	D= '165.2' mm t='11.0' mm	No defect	10 MPa	3.23 Hz	High-pass filtered seismic wave	17 m/s^2	Fatigue failure at a tee
					Sinusoidal wave	14 m/s^2	
AP3_EC01		Approx. 50% Wall thinning		2.72 Hz	High-pass filtered seismic wave	17 m/s^2	Crack penetration at a wall thinning tee (fatigue or burst?)

Note:
a: D: Outer diameter; t: wall thickness (without defect)
b: Measured acceleration on the shaking table
c: From the test results, in the elastic region
Source: Nakamura et al, 2004; Nakamura et al, 2010; Nakamura et al, 2011.

Figure 3.12. Configuration of the test models (unit: mm)

(a)   NIED_Test#01
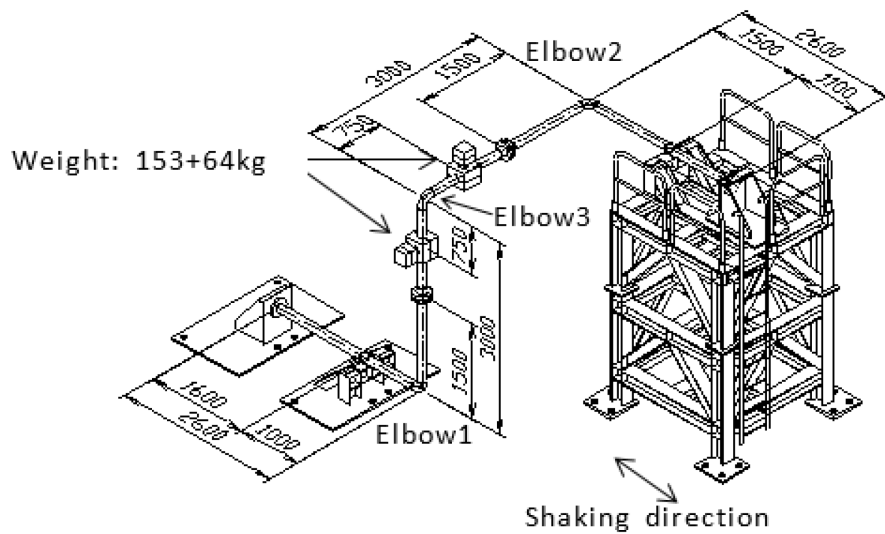
Figure 3.12. Configuration of the test models (unit: mm) (Continued)

(b) NIED_Test#02
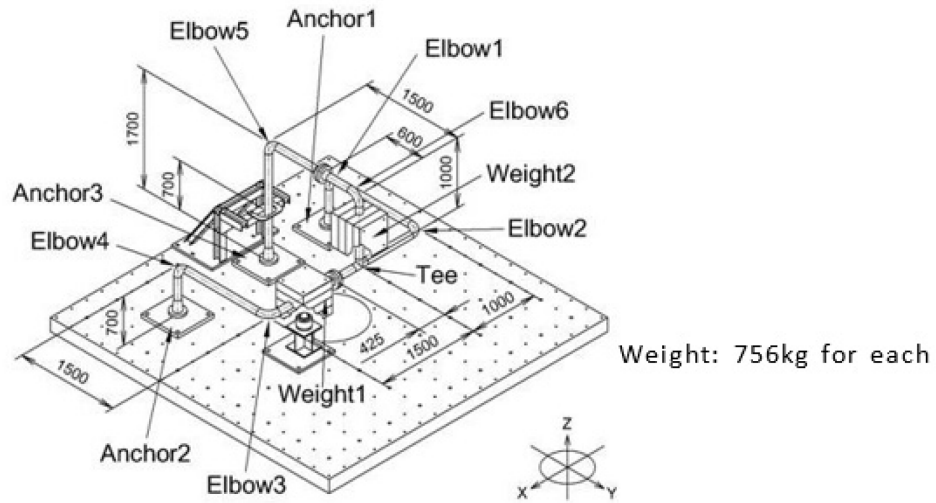
(c) NIED_Test#03
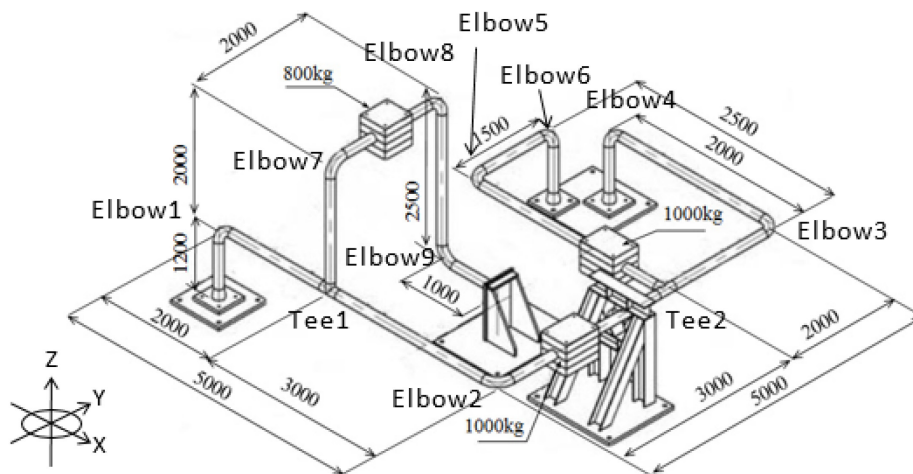
Note: Weight: 756 kg for each

Figure 3.13. Examples of the failure modes observed in the shaking table test
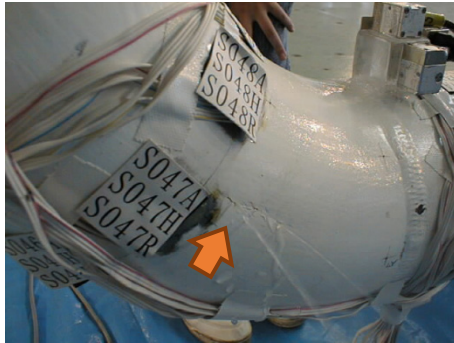
(a) Fatigue failure at an elbow flank
(Elbow1 of 3D_A01) NIED_Test#01)

(b) Fatigue failure at a wall thinning elbow,
close to the pipe end
(Elbow1 of AP3_C31, NIED_Test#02)
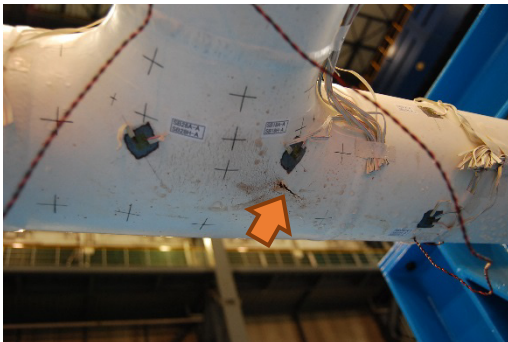
(c) Fatigue failure at a tee
(Tee2 of AP3_EA01, NIED_Test#03)

(d) Crack penetration at a wall thinning tee
(Tee2 of AP3_EC01, NIED_Test#03)

3.3.3. JAEA

The Japan Atomic Energy Agency (JAEA) has conducted shake table tests on piping components for fast breeder reactors (FBRs) (Watakabe et al., 2014; Watakabe et al., 2016). The purpose of the tests was to confirm the failure modes and ultimate strength of FBR pipes under large seismic load, which are relatively thin-wall pipes (diameter/thickness is 50-75) compared to pipes for light water reactors.

One-directional shaking table tests on elbow specimens (Watakabe et al., 2016) and tee specimens (Watakabe et al., 2014) were conducted. Figure 3.14 shows the configuration and setup of these experiments. The material of pipes was Type 304 SS.

The test conditions and results are summarised in Table 3.4. The shake table tests confirmed that the failure mode of thin-wall elbows and tees subjected to high-level seismic loads was low-cycle fatigue failure. The typical failure mode is shown in Figure 3.15. The maximum input acceleration was approximately 20 times higher than the primary stress limitation level for the elbow specimens, and approximately 13 times higher for the tee specimens. Although an extremely high input acceleration was applied, no structural instability such as collapse was observed for either the elbow specimens, or the tee specimens and the drastic decrease of the pipe section did not occur. The fatigue evaluation based on a finite element methods' (FEM) analysis showed that the current design procedure, which is based on the elastic response analysis and design fatigue curve, includes a large safety margin compared to the actual failure of the pipe.

Table 3.4. Basic conditions and results of the shaking table tests on FBR pipe components conducted by JAEA

(a) Elbow specimen

Model name	Pipe size [a]	Pressure	Natural frequency	Input motion	Max. applied acc.	Test results
LE1	D=165.2 mm	N/A	5.7 Hz	Seismic wave	11.7 G	Fatigue failure at the elbow flank
LE2	t=2.8 mm	20 kPa			10.3 G	
LE3		N/A			11.8 G	

Note: a: D: Outer diameter; t: wall thickness
Source: Wakatabe et al, 2016.

(b) Tee specimen

Model name	Type of tee joint	Pipe size [a]	Pressure	Natural frequency	Input motion	Loading direction	Max. applied acc.	Test results
TA1	Straight tee	D=165.2 mm t='5.0 mm' (Main pipe) t='3.8 mm' (Branch pipe)	20 kPa	8 Hz	Seismic wave	In-plane	8.90 G	Fatigue failure at the body of tee
TA2				8 Hz		Out-of-plane	7.78 G	

Note: a: D: Outer diameter; t: wall thickness
Source : Wakatabe et al, 2014.

Figure 3.14. Configuration of the test models and test

(c) Elbow specimen

Source: Wakatabe et al, 2016.

Figure 3.14. Configuration of the test models and test (Continued)
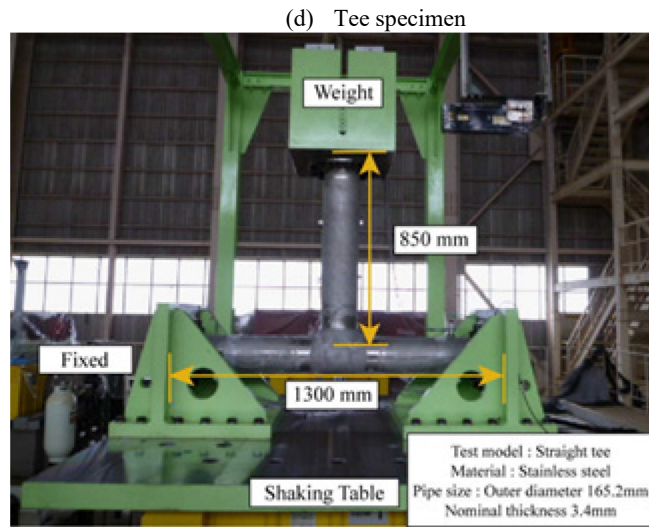
(d)   Tee specimen

Source : Wakatabe et al, 2014.

Figure 3.15. Examples of the failure modes

(e)   Elbow specimen
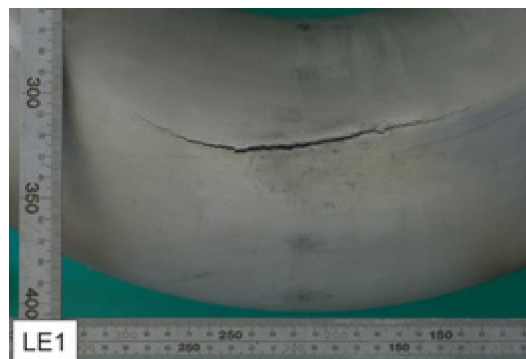
Source: Wakatabe et al, 2016.

(f)   Tee specimen
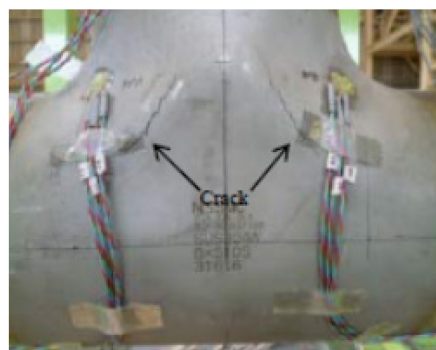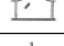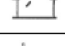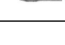
Source: Wakatabe et al, 2014.

3.3.4. *Fatigue test of pipe fittings – static and dynamic piping element tests*

The shake table tests showed the failure mode under sever seismic motion to be fatigue failure accompanied by ratchet phenomena (fatigue-ratcheting) without plastic collapse. Figures 3.16 and 3.17 summarise the experimental results of pipe elements under alternating static and dynamic load, which provide a more quantitative understanding of such failure mode and fatigue life. These experiments were conducted by a utility and maker group and NUPEC (Yoshino et al., 2000; NUPEC, 2001).

Figure 3.16. Piping element cyclic load test (statistic and dynamic)

	test case	static cyclic load test					dynamic load test			
		displacement (mm) ΔL	strain range (%) Δε	accumulated strain (%) εmax	cyclic number	crack penetration potion	load type	displacement (mm) ΔL	cyclic number	crack penetration potion
Test case A (Japanese Utilities research results)	Bend pipe C/S 100A sch 40 inner press equivalent Sm	±33	2.3	6.9	63		sin wave	±33	65	
	Bend pipe S/S 100A sch 40 inner press equivalent Sm	±33	2.4	31.3	169		sin wave	±33	121	
	Bend pipe C/S 100A sch 40 inner press equivalent Sm/2	±33	2.6	5.4	66		sin wave	±33	94	
	Bend pipe C/S 100A sch 40 inner press=0	±33	3.1	6.6	68		sin wave	±33	130	
	Bend pipe C/S 100A sch 40 inner press equivalent Sm	±9	0.6	1.7	1050		sin wave	±11	1300	
	Bend pipe C/S 100A sch 40 inner press equivalent Sm	±25	1.8	6.4	101		sin wave	±21	290	
	Tee C/S 100A sch 40 inner press equivalent Sm	±50	2.0	21.8	157		sin wave	±50	135	
	Straight pipe C/S 100A sch 40 inner press equivalent Sm	±55	2.3	34.1	164		sin wave	±56	146	

Pseudo dynamic test facility   Dynamic test facility
1002

Source : Yoshino et al, 2000.

Figure 3.17. Piping element cyclic load test (statistic and dynamic)

		static cyclic load test					dynamic load test			
	test case	displacement (mm)	strain range (%)	accumulated strain (%)	cyclic number	crack penetration potion	load type	displacement (mm)	cyclic number	crack penetration potion
		ΔL	Δε	ε max				ΔL		
Test case B (Nuclear Power Engineering Corporation test results)	Elbow S/S 200A sch. 40 inner press 10.7 MPa	±42.5	1.6	21.0	143		sin wave	range 78	75	
							seismic wave	range 79	3 times	
	Elbow C/S 65A sch. 40 inner press 19.8 MPa	±15.5	1.2	14.7	185		seismic wave	range 34	5 times	
	Elbow S/S 200A sch. 40 inner press 10.7 MPa	±42.5	1.6	21.0	143		sin wave	range 96	90	
							seismic wave	range 100	5times	
	Tee C/S 200A/200A sch. 40 inner press 10.7 MPa	±49.8	1.7	13.3	98		seismic wave	range 103	4times	
	Nozzle C/S 200A/250A sch. 40 inner press 10.7 MPa	±36.9	4.8	−1.6*1	71		seismic wave	range 74	5times	
	Reducer C/S 200A/150A sch. 40 inner press 10.7 MPa	±30.8	5.0	37.9	136		seismic wave	range 62	10times	

*1: effect by local deformation, compression cumulative strain was appeared
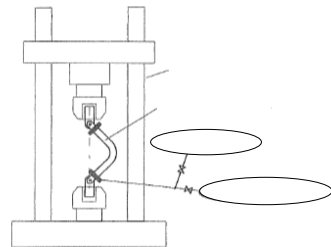
Pseudo dynamic test facility
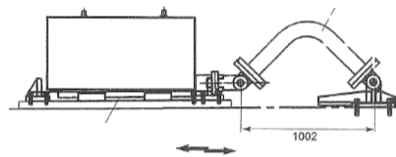
Dynamic test facility

Source: Nuclear Power Engineering Center, 2001.

3.3.5. References

Nakamura, I., A. Otani and M. Shiratori (2004), "Failure Behaviour of Piping Systems with Wall Thinning under Seismic Loading", *Journal of Pressure Vessel Technology*, Vol. 126(1), pp. 85-90.

Nakamura, I., A. Otani, Y. Sato, H. Takada and K. Takahashi (2010), "Tri-axial Shake Table Test on the Thinned Wall Piping Model and Damage Detection Before Failure", Proc. Of PVP2010, Report PVP2010-25839.

Nakamura, I., A. Otani, Y. Sato, H. Takada, K. Takahashi and T. Shibutani (2011), "Investigation of the Seismic Safety Capacity of Aged Piping System – Shake Table Test on Piping Systems with Wall Thinning by E-Defense", Proc. Of PVP2011, Report PVP2011-57560.

Nuclear Power Engineering Center (2001), "Report on Seismic Proving Test Program for Nuclear Power Plant: Seismic Proving Test of Ultimate Piping Strength – Part 2", Nuclear Power Engineering Centre, Japan.

Suzuki, K and H. Abe (2005), "Seismic Proving Test of Ultimate Piping Strength (Safety Margin of Seismic Design Code for Piping)", Proc. Of PVP2005, PVP2005-71005.

Suzuki, K., H. Abe and K. Suzuki (2004a), "Seismic Proving Test of Ultimate Piping Strength (Design Method Confirmation Test)", *ASME Pressure Vessels and Piping Conference*, Vol. 468-2, pp.187-194.

Suzuki, K., H. Abe and K. Suzuki (2004b), "Seismic Proving Test of Ultimate Piping Strength (Ultimate Strength Test)", *ASME Pressure Vessels and Piping Conference*, Vol. 486-2, pp.201-208.

Watakabe, T., K. Tsukimori, A. Otani, M. Moriizumi and N. Kaneko (2014), "Study on Strength of Thin-walled Tee Pipe for Fast Breeder Reactors under Seismic Loading", *Pressure Vessels and Piping Conference*, PVP2014-28619, V008T08A032, American Society of Mechanical Engineers.

Watakabe, Y., K. Tsukimori, S. Kitamura and M. Morishita (2016); "Ultimate Strength of a Thin Wall Elbow for Sodium Cooled Fast Reactors Under Seismic Loads", *Journal of Pressure Vessel Technology*, Vol. 138(2).

Yoshino, K., R. Endou, T. Sakaida, H. Yokota, T. Fujiwaka, Y. Asada and K. Suzuki (2000), "Study on Seismic Design of Nuclear Power Plant Piping in Japan Part 3: Component Test Results", *Proceedings of AMSE PVP*, 507, pp.131-137.

3.4. Indian BARC tests

3.4.1. Introduction

Several experimental and numerical studies were carried out at the Bhabha Atomic Research Centre (BARC) to examine the ratcheting phenomenon in piping systems and components under various loading conditions. These studies were carried out at specimen, component and system levels. The uniaxial experiments (Kulkarni et al., 2003) showed that some specimens exhibit an initial strain accumulation with subsequent material stabilisation, showing no further ratcheting when the number of cycles was increased. This behaviour, which is known as shakedown behaviour, was observed at low stress amplitudes following some strain accumulation. However, the specimens experienced continuous ratcheting with no shakedown before failure at higher stress amplitudes. Ratcheting behaviour under stress-controlled conditions has been studied (Gupta et al., 2005) at different stress ratios and stress rate combinations. The ratcheting experiments have shown that strain accumulation depends on the stress ratio. In the biaxial test on straight pipes (Kulkarni et al., 2004), ovalisation of the pipe cross section was observed when the pipe was subjected to constant internal pressure and a cyclic bending load. Local bulging was observed at higher cyclic bending load. The pipe did not exhibit any shakedown behaviour for the given cycles of loading and exhibited continuous ratcheting under the varying amplitude loading. Similar observations were made during a shake table test on a pressurised elbow (Ravikiran et al., 2006). A three-inch carbon steel piping system was tested by internal pressure and an increasing seismic load (Ravikiran et al., 2013) using a shake table. The test was continued until there was a pressure boundary rupture at the elbow's crown location. Ratcheting was observed at different locations of the piping system. Shake table tests were also carried out on two pressurised six-inch piping systems of stainless steel (SS304L) material (Ravikiran et al., 2015). The same configuration was chosen to check the repeatability of the two piping systems. The piping systems were pressurised with water and incremental base excitation was applied through the shake table until failure occurred. Shake table tests have also been carried out on two pressurised six-inch piping systems of carbon steel (SA333 Gr. 6) material.

A photograph of the test setup of the three-inch SS elbow is shown in Figure 3.18. The elbow is a long radius elbow made of stainless steel grade SS304L. It has an 89 mm outer diameter and thickness of 5.5 mm. The hoop strain time history at the elbow's crown is shown in Figure 3.19. Failure occurred during this test at the weld location between the elbow and pipe and strain accumulation was observed to increase by around 5% before failure.

Figure 3.18. Photograph of the test setup of a three-inch SS elbow

Source: Kiran et al., 2018b.

Figure 3.19. Hoop strain time history at crown of a three-inch SS elbow
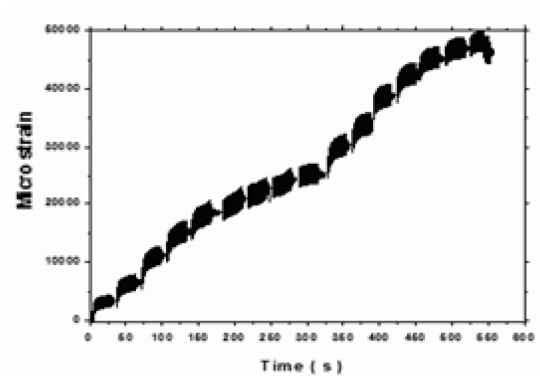
Source: Kiran et al., 2018b.

A photograph of the test setup of a three-inch carbon steel (CS) elbow is shown in Figure 3.20. The elbow is a short radius elbow made of carbon steel grade SA 106 GR B. It has an 89 mm outer diameter and thickness of 5.5 mm. The hoop strain time history at the elbow's crown is shown in Figure 3.21 (the gauge failed during the test). Fatigue-ratcheting failure has been observed during this test at the elbow's crown, as shown in Figure 3.22, and the elbow circumference was observed to increase by around 5%.

Figure 3.20. Photograph of the test setup of a three-inch CS elbow

Source: Kiran et al., 2018a.

Figure 3.21. Hoop strain time history at the crown of a three-inch CS elbow
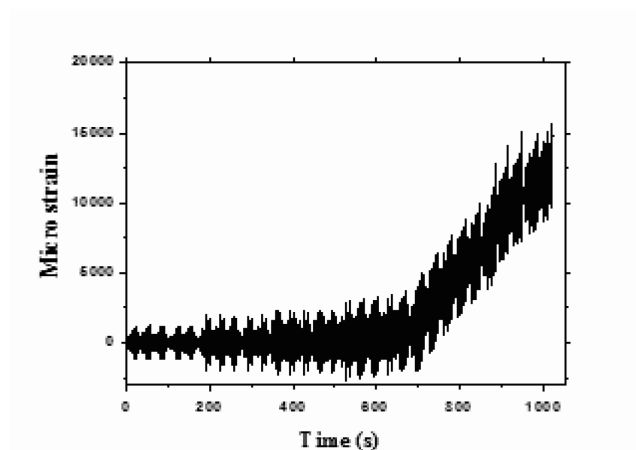
Source: Kiran et al., 2018a.

Figure 3.22. Photograph of fatigue-ratcheting failure at the crown location of a three-inch CS elbow

Source: Kiran et al., 2018a.

A photograph of the test setup of a three-inch CS tee joint is shown in Figure 3.23. The tee joint is made of carbon steel grade SA 106 GR B. It has an 89 mm outer diameter and thickness of 5.5 mm. The hoop strain time history at the joint is shown in Figure 3.24. Fatigue-ratcheting failure was observed during this test at the weld joint between the tee and pipe. The photograph of the water jet through a crack at the weld location of the tee and pipe is shown in Figure 3.25. Observations of this test noticed very little strain accumulation of 0.6% and how fatigue caused the failure of the tee joint.

Figure 3.23. Photograph of the test setup of a three-inch CS Tee joint

Source: Kiran et al., 2018a.

Figure 3.24. Hoop strain time history at a three-inch CS Tee joint
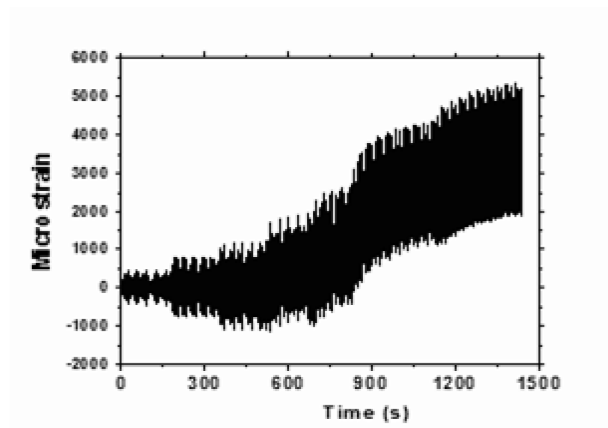
Source: Kiran et al., 2018a.

Figure 3.25. Photograph of a wall crack at the weld location of tee and pipe

Source: Kiran et al., 2018a.

A photograph of the test setup of a three-inch CS piping system (CSPS3-1) is shown in Figure 3.26. The piping system is made of carbon steel grade SA 106 GR B and has an 89 mm outer diameter and thickness of 5.5 mm. A damping of 0.6 to 2.2 % was observed to be obtained from a sine sweep test using a half power method. In this test, a dent was formed at the crown of elbow-1, as shown in Figure 3.28, and there was an increase in elbow circumference by around 5%. The hoop strain time history at the crown of elbow-1 is shown in Figure 3.27.

Figure 3.26. Photograph of the test setup of a three-inch CS piping system (CSPS3-1)

Source: Ravikiran et al., 2013.

Figure 3.27. Hoop strain time history at the crown of elbow-1
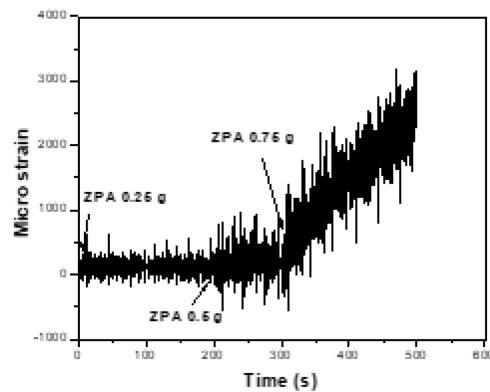
Source: Ravikiran et al., 2013.

Figure 3.28. Photograph of the dent at the crown location of elbow-1

Source: Ravikiran et al., 2013.

Shake table tests were conducted on two sets of six-inch stainless steel piping systems (SSPS-1&2) with same configuration, which is shown in Figure 3.29. The piping system was made of stainless steel grade SS304L and has a 168 mm outer diameter and thickness of 7 mm. The sine sweep test using a half power method was observed to produce a damping ranging from 1% to 2.7 %. There was around a 1.5% strain accumulation at the crown of elbow-1, as shown in Figure 3.30. Fatigue-ratcheting failure at the crown of elbow-1 in the first test (as shown in Figure 3.31) and weld failure of the anchor in the second test (as shown in Figure 3.32) was observed in these tests. Wavelet analysis has been carried out on the piping response signals. The analysis revealed how the natural frequencies of the piping systems were slightly reduced during the tests because plasticity in the piping system resulted in a slight reduction of stiffness.

Figure 3.29. Photograph of the test setup of a six-inch SS piping system (SSPS-1)

Source: Ravikiran, A., P.N. Dubey, M.K. Agrawal, G.R. Reddy, R.K. Singh and K.K. Vaze, 2015.

Figure 3.30. Hoop strain time history at the crown of elbow-1 of a six-inch SS piping system
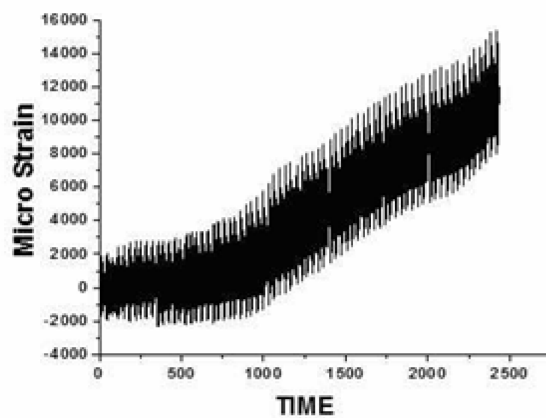
Source: Ravikiran, A., P.N. Dubey, M.K. Agrawal, G.R. Reddy, R.K. Singh and K.K. Vaze, 2015.

Figure 3.31. Photograph of a fatigue-ratcheting failure at the crown of elbow-1 in SSPS-1 test

Source: Ravikiran, A., P.N. Dubey, M.K. Agrawal, G.R. Reddy, R.K. Singh and K.K. Vaze, 2015.

Figure 3.32. Photograph of weld failure at the anchor location in the SSPS-2 test

Source: Ravikiran, A., P.N. Dubey, M.K. Agrawal, G.R. Reddy, R.K. Singh and K.K. Vaze, 2015.

Shake table tests were conducted on two sets of six-inch carbon steel piping systems (CSPS-1&2) with the same configuration, as shown in Figure 3.33. The piping system was made of carbon steel grade SA333 Gr 6 with a 168 mm outer diameter and thickness of 7 mm. The sine sweep test using a half power method was observed to produce a damping ranging from 1% to 3%. There was around 2.5% strain accumulation at the crown of elbow-1, as shown in Figure 3.34. Fatigue-ratcheting failure occurred in both tests at the crown of elbow-1 (as shown in Figures 3.35 and 3.36). Wavelet analysis has been carried out on the piping response signals. The analysis revealed how the natural frequencies of the piping systems were slightly reduced during the tests because plasticity in the piping system resulted in a slight reduction of stiffness.

Figure 3.33. Photograph of the test setup of a six-inch CS piping system
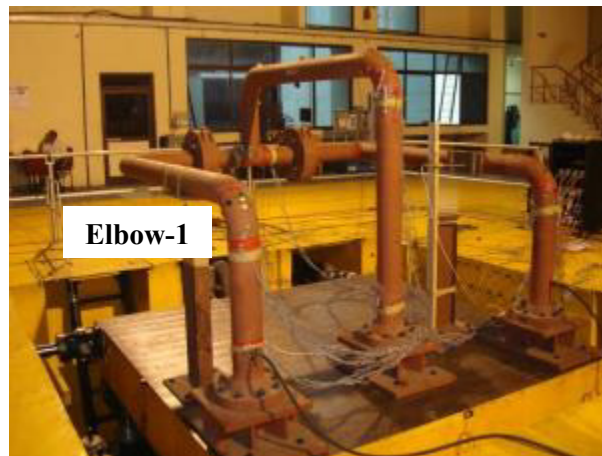
Source: Kiran et al., 2017.

Figure 3.34. Hoop strain time history at the crown of elbow-1 of a six-inch CS piping system
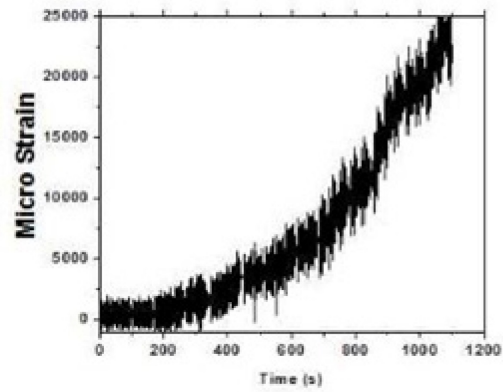
Source: Kiran et al., 2017.

Figure 3.35. Photograph of fatigue-ratcheting failure at the crown of elbow-1 in the CSPS-1 test

Source: Kiran et al., 2017.

Figure 3.36. Photograph of fatigue-ratcheting failure at the crown of elbow-1 in the CSPS-2 test

Source: Kiran et al., 2017.

A shake table test will be carried out on a six-inch carbon steel piping system shown in Figure 3.37 which will have a similar configuration to that shown in Figure 3.33.

Figure 3.37. Photograph of the test setup of a six-inch CS piping system (schedule 80)

Source: Kiran et al., 2019.

The damping values of the tested piping systems and components are summarised in Table 3.5. The damping of the tested piping systems and components were observed to range from 0.6 to 4%, with a mean value of 2%.

Table 3.5. Damping of the tested piping systems and components

S. No.	Description and size	Material	No. of test specimens	Damping (%)
1.	Large radius elbow (OD 89 mm and thickness 5.5 mm)	SS304L	1	4.1
2.	Short radius elbow (OD 89 mm and thickness 5.5 mm)	SA106 Gr B	1	1.1 - 2.3
3.	Tee joint (OD 89 mm and thickness 5.5 mm)	SA106 Gr B	1	2.1 - 2.7
4.	Three-dimensional piping system (OD 89 mm and thickness 5.5 mm)	SA106 Gr B	2	0.6 - 2.2
5.	Three-dimensional piping system (OD 168 mm and thickness 7 mm)	SS304L	2	1.0 - 2.7
6.	Three-dimensional piping system (OD 168 mm and thickness 7 mm)	SA 333 Gr 6	2	1.0 - 3.0

3.4.2. Conclusions from experimental and numerical studies at BARC

Experimental and numerical studies have been carried out on pressurised carbon steel and stainless steel piping systems and components under seismic load. Fatigue-ratcheting was observed to be the predominant failure mode of the pressurised piping systems and components. The maximum strain accumulation in elbows of the piping systems ranged from 1.5% to 5%. Shakedown behaviour was observed at the tee joint following initial strain accumulation in both the component and system level tests. Fatigue was observed to be the predominant failure mode for the tee joint. The wavelet analysis of piping response signals revealed that the natural frequencies of the piping systems were slightly reduced during the tests because plasticity in the piping system resulted in a slight reduction of stiffness. Damping of the tested piping systems and components was observed to range from 0.6% to 4%, with a mean value of 2%. Annex D describes some elements of the damping and reaction forces.

3.4.3. References

Gupta, C., J.K. Chakravartty, G.R. Reddy and S. Banerjee (2005), "Uniaxial cyclic deformation behaviour of SA 333 Gr 6 piping steel at room temperature", *International Journal of Pressure Vessels and Piping*, 82, pp.459-469.

Kiran, A.R., G.R. Reddy, M.K. Agrawal, M. Raj and S.D. Sajish (2019), "Ratcheting based seismic performance assessment of a pressurised piping system: Experiments and analysis", *International Journal of Pressure Vessels and Piping*, 177, p.103995.

Kiran, A.R., G.R. Reddy and M.K. Agrawal (2018a), "Experimental and numerical studies of inelastic behaviour of thin walled elbow and tee joint under seismic load", *Thin-Walled Structures*, 127, pp.700-709.

Kiran, A.R., G.R. Reddy and M.K. Agrawal (2018b), "Experimental and Numerical Studies on Inelastic Dynamic Behaviour of Stainless Steel Elbow under Harmonic Base Excitation", *ASME Journal of Pressure Vessel Technology*, 140(2), pp.1-9.

Kiran, A. Ravi, G.R. Reddy, P.N. Dubey and M.K. Agrawal (2017) "Fatigue-Ratcheting Behaviour of Six Inch Pressurized Carbon Steel Piping Systems under Seismic Load – Experiments and Analysis" 139 (2017) 061801:1-15., ASME Journal of Pressure Vessel Technology.

Kulkarni, S.C., Y.M. Desai, T. Kant, G.R. Reddy, P. Prasad, K.K. Vaze and C. Gupta (2004), "Uniaxial and biaxial ratchetting in piping materials—experiments and analysis", *International Journal of Pressure Vessels and Piping*, 81, pp.609-617.

Kulkarni, S.C., Y.M. Desai, T. Kant, G.R. Reddy, Y. Parulekar and K.K. Vaze (2003), "Uniaxial and biaxial ratchetting study of SA333 Gr.6 steel at room temperature", *International Journal of Pressure Vessels and Piping*, 80, pp.179-185.

Ravikiran, A., P.N. Dubey, M.K. Agrawal, G.R. Reddy, R.K. Singh and K.K. Vaze (2015), "Experimental and Numerical Studies of Ratcheting in a Pressurised Piping System under Seismic Load", *Journal of Pressure Vessel Technology*, 137(3), pp.1-7.

Ravikiran, A., P.N. Dubey, M.K. Agrawal, G.R. Reddy and K.K. Vaze (2013), "Evaluation of Inelastic Seismic Response of Piping System using Modified Iterative Response Spectrum Method", *Journal of Pressure Vessel Technology*, 135(4).

3.5. INDUSE project

3.5.1. Introduction

INDUstrial Seismic (INDUSE) was an interdisciplinary and multinational project that combined seismic engineering concepts with mechanical engineering practice and aimed to develop design guidelines/recommendations for the safeguarding of the structural integrity of industrial tanks, pressure vessels and piping under strong seismic action (www.mie.uth.gr/induse). The project was sponsored by the European Commission through the Research Fund for Coal and Steel. This project's activities included the following:

- A basic comparison was performed between the currently available seismic design provisions used for European and American standards, which considered specific design examples.

- The seismic actions of these industrial systems were determined, while accounting for the dynamic behaviour of each structural system.

- Critical piping components (nozzles, flanged connections, tees and elbows) were tested under strong cyclic loading. A pseudo-dynamic testing of a piping system was also performed.

- Extensive numerical studies were conducted on critical piping components, which were based on rigorous finite elements (FE) simulations and covered a wide range of geometric, material and loading parameters.

- Design guidelines/recommendations were developed that expand the EN 1998-4 provisions into an integrated seismic design of liquid storage tanks and extend the applicability of the Eurocode 8 (EN 1998) concepts to cases of industrial pressure vessels, attached equipment and piping systems (including their support systems).

The **INDUSE** project brought about an improved understanding of the structural behaviour of tanks, pressure vessels and piping under strong cyclic (seismic) loading. The project also produced a more reliable definition of the ultimate limit states for critical industrial components and significant improvements to the seismic design state-of-the-art. The results from **INDUSE** provided Code Drafting Committees with the necessary scientific background to develop a safer design of industrial power plants and chemical/petrochemical facilities. The final part of the project was an extensive presentation of the **INDUSE** results (Pappa et. al., 2013a).

The **INDUSE** partnership was composed of: [1] the University of Thessaly (Greece), coordinator; [2] Centro Sviluppo Materiali (Italy); [3] the Delft University of Technology (Netherlands); [4] the University of Trento (Italy); [5] the Aachen University of Technology (Germany); [6] EBETAM SA (Greece); and [7] TECHNIPETROL HELLAS SA (Greece).

The structural behaviour of industrial piping, and in particular its seismic behaviour, significantly differs to that of steel buildings. This structural behaviour is distinct in a number of ways and requires a combination civil and mechanical engineering expertise. The piping's particularities stem from their unique shape and geometry and the presence of high internal pressure, which can significantly affect their load and deformation capacity.

The **INDUSE** programme was an interdisciplinary research effort combining civil and mechanical engineering expertise, which aimed to develop guidelines that could be used for the seismic design of liquid storage tanks, pressure vessels and piping within the Eurocode's design framework. Extensive experimental, analytical and numerical work has

been conducted to this purpose within the **INDUSE** project thanks to the synergy of academic units, research centres and industrial partners.

3.5.2. Experimental testing

Extensive experimental testing was carried out on steel material, piping components and on a piping system.

The testing was carried out to examine the mechanical characterisations of both base and weld material. The base material characteristics have been evaluated for the following objects: elbows; tee fittings; plates for nozzles; and straight pipes connected to fittings in full-scale specimens. The base material characterisation consisted of (a) monotonic tensile testing; (b) cyclic loading with imposed strains to obtain hysteresis loops (cyclic hardening/softening) of elbows both longitudinally and transversely; (c) cyclic loading with imposed stresses to obtain ratcheting characteristics of elbows both longitudinally and transversely; (d) cyclic loading with imposed deformations to obtain cyclic hardening/ softening of straight pipes, which were connected to weld neck flanges in full-scale testing; and (e) ring crush testing to evaluate the possible material anisotropy of straight pipes, which were connected to flanges and elbows in full-scale testing. In addition, tests were carried out on butt welded specimens taken from eight-inch-diameter pipes, which aimed to check the validity of the welding procedure specification developed within the **INDUSE** project. Firstly, non-destructive tests were carried out. Then, destructive tests were performed, which consisted of: (a) a macroscopic examination of welds (EN1321); (b) hardness tests (EN1043-1); (c) a bend test on welds (EN910); (d) a transverse tensile test on welds (EN895, EN6892-1); and (e) a Charpy V-notch impact test on welds (EN875, EN10045-1).

A number of medium-scale experiments have since been carried out on key components of industrial structural systems under strong cyclic loading. These tests aimed to determine their mechanical behaviour and failure modes and obtain adequate measurements for the calibration of the numerical models. The components were six-inch and eight-inch pipes and the material of all specimens was P355N, which is equivalent to X52. In addition to these tests on specific components, a piping system containing three elbows, one tee junction and one flange was tested by pseudo-dynamic loading at four seismic levels. More specifically:

- Six tests were conducted on six-inch tank openings (nozzles). Three different shell nozzle reinforcement configurations were considered, namely an internal reinforcing plate (P_1), an external reinforcing plate (P_2) and a thickened nozzle reinforcement (P_3). The tests were carried out in the range of ultra-low-cycle fatigue considering longitudinal and transverse load directions for each nozzle reinforcement type. Amplitude loading was increasingly applied in accordance with the ECCS' No.45 protocol. Failure occurred in form of a fatigue crack on either side of the weld between the six-inch pipe and reinforced shell. All three types of reinforcement exhibited similar strengths in terms of loading cycles. Furthermore, transverse loading was observed as more severe than longitudinal loading (Wieschollek et al., 2013).

Figure 3.38. Mechanical behaviour of nozzles under strong repeated loading

Source: Wieschollek, M., B. Hoffmeister and M. Feldmann (2013), "Experimental and Numerical Investigation on Nozzle Reinforcements", *ASME 2013 Pressure Vessels & Piping Division Conference PVP2013*, 14-18 July, Paris.

- Six tests were conducted on full-scale PN_{40} and PN_{63} bolted (flanged) piping connections, as specified in EN 1092, and subjected to monotonic and cyclic bending load conditions in the presence of internal pressure (Ferino et al., 2013).

- A significant number of tests (13 tests) were performed on eight-inch (D=219.1 mm) long-radius (R/D=1.5) SCH_{40} (t= 8.2 mm) elbow specimens made from $P_{355}N$ material. The elbows were connected to straight pipes of the same dimensions on each side (L/D=5) and put under constant-amplitude in-plane loading. Eight non-pressurised specimens were tested at various loading amplitudes (covering the entire range from quasi-elastic to severely-plastic behaviour). In addition, five specimens were tested under pressure (at pressure levels of up to 42% of yield pressure) at strong cyclic loading, which caused severe plastic deformation. Failure occurred in all specimens in the form of a longitudinal crack at the elbow's central part, at the flank location. The number of cycles to failure was found to significantly depend on the loading amplitude, whereas the presence of internal pressure resulted in a small decrease of the number of loading cycles to failure (Varelis et al., 2013a; Varelis et al., 2013b; Varelis et al., 2015; Pappa et al., 2013).

Figure 3.39. Bolted (flanged) pipe connections subjected to severe cyclic loading

Source: Ferino et al., 2013.

Figure 3.40. Pipe elbows (bends) under severe cyclic loading actions

Source: Pappa et al., 2013a.

- Eight tests were performed on eight-inch to six-inch SCH$_{40}$ tee-branch pipe connections, which considered two configurations: (a) four specimens with tee fittings (TJF) and (b) four specimens with reinforcement plates at the connection of its two main parts (TJWR). The specimens were tested under monotonic loading (one test for each type) and cyclic out-of-plane bending loading (three tests for each type). The TJF specimen showed about 93% higher load capacity under monotonic loading conditions. The TJF specimen exhibited higher fatigue resistance of 7-8 times that of the TJWR specimen under cyclic loading conditions. The TJF specimen resisted 36% more loading cycles than the TJWR one during increasing amplitude loading. The TJWR specimens failed along the circumference of the branch-to-reinforcement plate weld-toe on either the branch side, or the welded reinforcement plate side of the connection. The TJF specimens failed in the region of the joint fitting, at a distance of 60 to 80 mm from the branch-to-fitting weld-toe (Papatheocharis et al., 2013).

Figure 3.41. Pipe tee branches subjected to out-of-plane cyclic loading

Source: Papatheocharis T., K. Diamanti, G.E. Varelis, P.C. Perdikaris and S.A. Karamanos (2013), "Experimental and numerical investigation of pipe Tee junctions under strong cyclic loading", *ASME 2013 Pressure Vessels & Piping Division Conference PVP2013*, 14-18 July, 2013, Paris.

Finally, in addition to testing individual components under strong cyclic loading, a piping system was tested through pseudo-dynamic loading at full scale (Reza et al., 2013). The piping system contained several critical components, which mainly consisted of elbows, as well as one flange and one tee. The test aimed to investigate the system's seismic performance at four seismic levels, thereby offering a good alternative to more expensive shaking table tests. The present testing employs a new hybrid testing technique, which enables the seismic testing of a structural system by using a limited number of actuators. Several pseudo-dynamic tests on the piping system were performed under different levels

of earthquake peak ground accelerations (PGAs) that corresponded to the serviceability and ultimate limit states suggested by standards. The experimental and numerical results correlated across all tests. Moreover, a good seismic performance of the piping system was observed during the experiments. Both the piping system and its critical components were found to not fail or yield, even when subjected to the collapse limit state level earthquake. It was therefore concluded that the present seismic design rules for piping systems and components are rather conservative and must be amended for this conservatism to be overcome.

Figure 3.42. Pseudo-dynamic test of a piping system
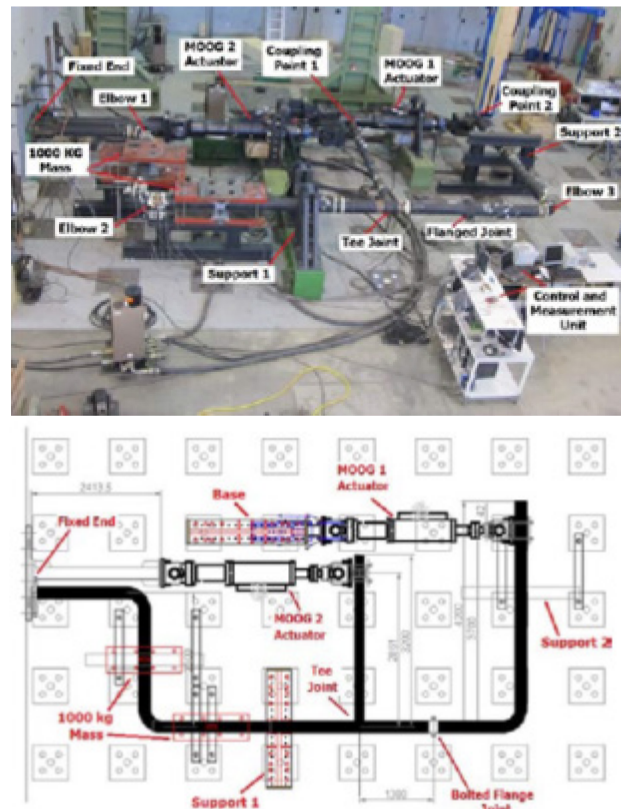
Source: Reza et al., 2013 (Top); Pappa et al., 2013a (Bottom).

3.5.3. Numerical simulation

The main purpose of the numerical part of the **INDUSE** work has been the development of an advanced numerical simulation procedure and its use for the prediction of the mechanical behaviour of critical structural components in a rigorous, efficient and accurate manner. The specific objectives have been:

- (a) The definition and calibration of an appropriate cyclic-loading constitutive material model to use for a realistic simulation of the elasto-plastic behaviour of tubular components. The constitutive material model should be able to simulate material degradation effects as well as low-cycle fatigue.

- (b) The development of a finite element modelling procedure that simulates accurately the behaviour of industrial components. The modelling procedure has been validated through the experimental data on critical components.

- (c) The performance of an extensive parametric study, using the finite element models, to examine the behaviour of structural components within a wide range of geometric and material parameters.

In particular, the work has focused on the implementation and calibration of a suitable material (constitutive) model for simulating the material behaviour of steel material. The non-linear kinematic hardening model, which is based on the classical Armstrong-Frederick (A-F) model, has been the one primarily used within the **INDUSE** project (Pappa et al., 2013a). The model adopts a von Mises description of the yield surface, and assumes a non-linear kinematic hardening rule for the evolution of the back stress (i.e. the centre of the yield surface). The calibration procedure of the model has been based on material test results, which originate from coupon specimens for the material testing that were extracted from the longitudinal and mainly from the hoop direction of elbow specimens. In addition, the Tseng-Lee model, which constitutes a simplified version of the bounding surface concept, has also been used and calibrated from the coupon tests. This type of model has not been incorporated into the commercial finite element codes (e.g. ABAQUS, MARC, etc.) and a special-purpose user subroutine has therefore been developed (Varelis et al., 2013b; Varelis et al., 2015).

The simulation of piping component experiments (nozzles, elbows, flanges and tees) aimed to develop and validate rigorous numerical tools. Non-linear finite element models have been used, which employ shell elements or solid elements, as well as the non-linear constitutive models for cyclic plasticity.

More recently, the **INDUSE** experiments on elbows have been used as a basis to develop novel numerical tools for the simulation of the cyclic response of piping components, with a focus on both cyclic strain ratcheting and low-cycle fatigue. Two particular elements of these experiments should be flagged:

1. The numerical implementation of a bounding-surface cyclic plasticity model, which can very efficiently describe the cyclic response of piping components. The main advantage of this model compared to the non-linear kinematic hardening models is its explicit definition of the hardening modulus, which allows for more efficient and accurate prediction of ratcheting (Chatziioannou and Karamanos, 2020; Chatziioannou and Karamanos, 2021).

2. The development of a plasticity-damage model and its numerical implementation within a finite element environment. Using this model, the progressive development of fatigue damage (crack propagation) is developed, and – upon proper calibration – the number of cycles to failure of a cyclic-loaded component can be predicted (Chatziioannou et al., 2021).

Figure 3.43. Numerical simulation of the elbow response under severe cyclic in-plane bending loading
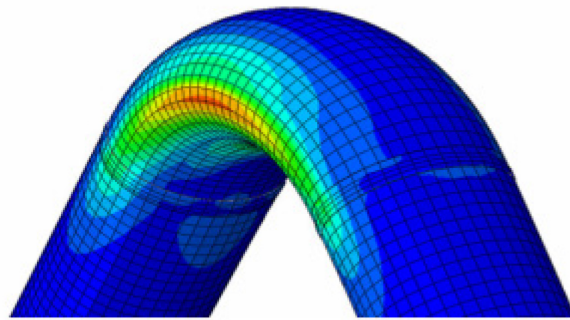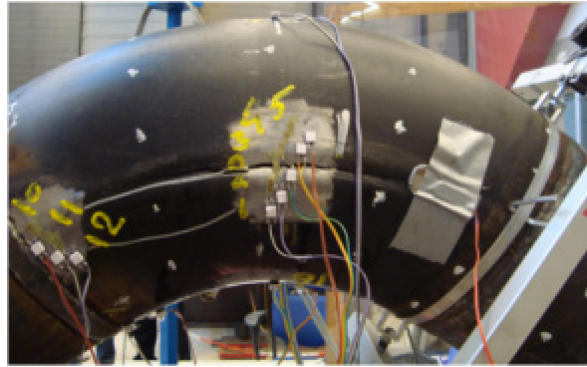
Source: Varelis et al., 2013b (Top); Varelis and Karamanos, 2015 (Bottom).

Figure 3.44. Damage distribution obtained from finite element simulation of low-cycle fatigue during the (a) 6th load cycle, (b) 8th load cycle and (c), 11th load cycle; (d) experimental shape of cracked specimen
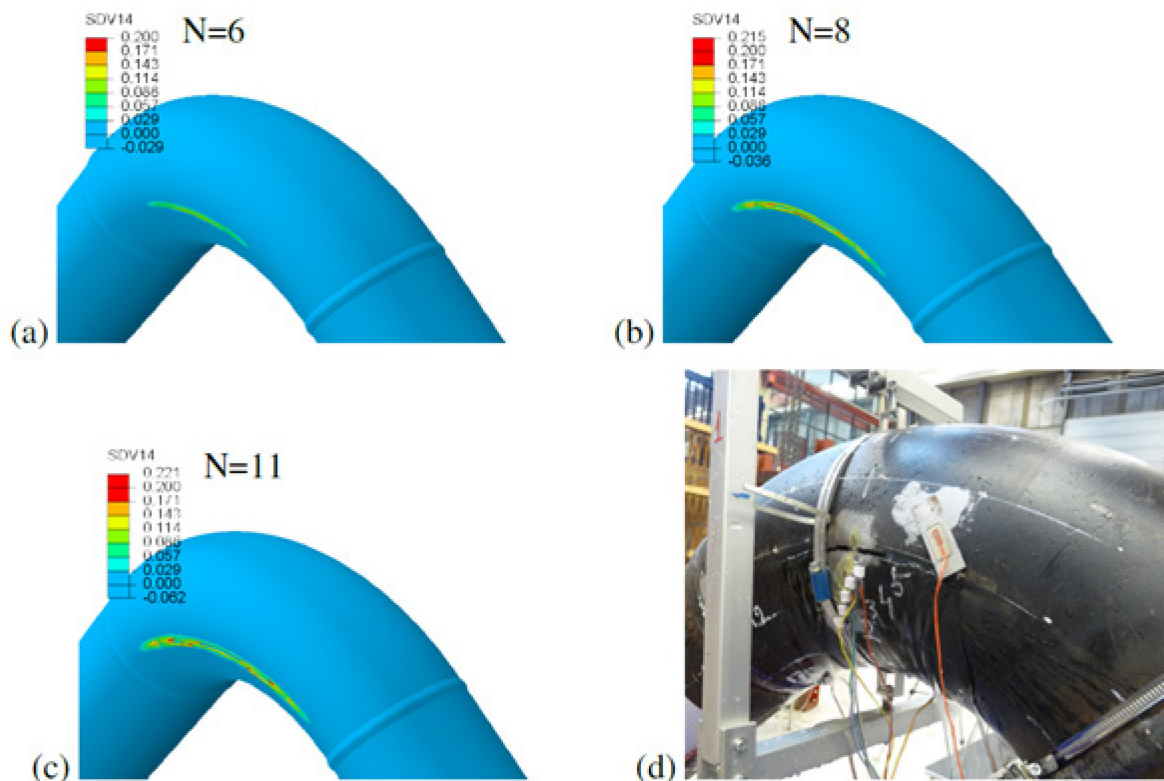
Source: Chatziioannou, K., S.A. Karamanos and Y. Huang (2021), "Coupled Numerical Simulation of Low-Cycle Fatigue Damage in Metal Components", *Engineering Structures,* Volume 229, p.111536.

3.5.4. References

Chatzopoulou, G. and S.A. Karamanos (2020), "Numerical Simulation of the Mechanical Behaviour of Steel Pipe Bends Under Strong Cyclic Loading", *International Journal of Pressure Vessels & Piping*, Volume 188.

Chatziioannou, K., S.A. Karamanos and Y. Huang (2021), "Coupled Numerical Simulation of Low-Cycle Fatigue Damage in Metal Components", *Engineering Structures*, Volume 229.

Chatzopoulou, G. and S.A. Karamanos (2021), "Numerical Implementation of Bounding-Surface Model for Simulating Cyclic Inelastic Response of Metal Piping Components", *Finite Elements in Analysis & Design*, Volume 185.

Ferino, J., A. Lucci and G. Demofonti (2013), "Pressurised Flanged Joints Subjected to Bending Cyclic Loading – Finite Element Analyses", *ASME 2013 Pressure Vessels & Piping Division Conference PVP2013*, 14-18 July, Paris.

Papatheocharis, T., K. Diamanti, G.E. Varelis, P.C. Perdikaris and S.A. Karamanos (2013), "Experimental and numerical investigation of pipe Tee junctions under strong cyclic loading", *ASME 2013 Pressure Vessels & Piping Division Conference PVP2013*, 14-18 July, 2013, Paris.

Pappa, P., et al. (2013a), "Structural safety of industrial steel tanks, pressure vessels and piping systems under seismic loading", INDUSERFCS project, Brussels.

Pappa, P., G.E. Varelis, S.A. Karamanos and A.M. Gresnigt (2013b), "Low cycle fatigue tests and simulations on steel elbows", *ASME 2013 Pressure Vessels & Piping Division Conference PVP2013*, 14-18 July, Paris.

Reza, M.S., O.S. Bursi, G. Abbiati and A. Bonelli (2013), "Pseudo-dynamic heterogeneous testing with dynamic substructuring of a piping system under earthquake loading", *ASME 2013 Pressure Vessels & Piping Division Conference PVP2013*, 14-18 July, Paris.

Varelis, G.E. and S. Karamanos (2015), "Low-Cycle Fatigue of Pressurised Steel Elbows Under In-Plane Bending", *Journal of Pressure Vessel Technology*, 137(1).

Varelis, G.E., J. Ferino, S.A. Karamanos, A. Lucci and G. Demofonti (2013a), "Experimental and Numerical Investigation of Pressurised Pipe Elbows under Strong Cyclic Loading Conditions", *ASME 2013 Pressure Vessels & Piping Division Conference PVP2013*, 14-18 July, Paris.

Varelis, G.E., S.A. Karamanos and A.M. Gresnigt (2013b), "Steel Elbow Response Under Strong Cyclic Loading.", *Journal of Pressure Vessel Technology,* 135(1).

Vathi, M., P. Pappa and S.A. Karamanos (2013), "Seismic Response of Unanchored Liquid Storage Tanks", *ASME 2013 Pressure Vessels & Piping Division Conference PVP2013*, 14-18 July, Paris.

Wieschollek, M., B. Hoffmeister and M. Feldmann (2013), "Experimental and Numerical Investigation on Nozzle Reinforcements", *ASME 2013 Pressure Vessels & Piping Division Conference PVP2013*, 14-18 July, Paris.

3.6. Conclusions

3.6.1. Plastic instability and fatigue-ratcheting

Piping design codes generally consider that the failure mode under high-level earthquake loads is plastic instability (sometimes referred to as plastic collapse) and the code's criteria have been written to prevent this plastic instability. However, as proven by this report, the experimental data indicate that the failure mode is instead fatigue as well as fatigue-ratcheting for pipes pressurised to a large hoop stress.

Ratcheting appears as an accumulated strain and a bulging of a pipe or pipe fittings. Bulging alone does not directly contribute to the loss of the piping's function, although it accelerates the formation and propagation of the fatigue cracking.

It is therefore necessary to derive code design criteria aiming to prevent failure by fatigue and fatigue-ratcheting to replace the current approach that focuses solely on plastic instability. The Japanese Codes rules moved in this direction in the recent past.

3.6.2. Linear and non-linear response

The code's criteria are based on the linear seismic response analysis of a piping system. The response of a piping system by linear analysis is proportional to the seismic input and increases as seismic input increases and plastic collapse can occur. However, the experiments described in this report show how the seismic response of actual piping did not linearly increase, but saturated due to a damping increase caused by plastic behaviour in the piping system. Plastic collapse has therefore not been confirmed by the experiments, except for a statically unstable pipe component such as a cantilever that has a heavy weight on one of its free ends.

Chapter 7 will address the response of piping systems to seismic excitation that is partially primary (which can lead to plastic instability) and partially secondary (which leads to the observed fatigue failures).

3.6.3. Strain-based criteria

The evaluation of the pipe components can be based on plastic analysis to best capture the fatigue-ratcheting effect caused by large seismic excitations, which is often larger than design basis earthquake input. There are nevertheless some difficulties involved when applying strain-based methods to a classic design of the hundreds of piping systems in nuclear power plants:

- Predicting strains requires a precise knowledge of the geometry of the component and its strain concentration features. This is not necessarily feasible in piping systems that are assemblies of standard commercial fittings (elbows, tees, flanges, etc.) whose exact profile is not necessarily controlled.

- Strain-based methods are non-linear and cannot be approached using the common linear modal analysis method for seismic design. If time history methods are applied, multiple time-histories may have to be analysed for each piping system in order to account for input and modelling uncertainties.

- The strain field can be complex: the amplitude or range can be greater on the inside surface of the pressurised component, while the ratchet strain can be greater on the outside surface.

4. History of codes' modifications in different countries

4.1. US- ASME III code seismic stress limits

4.1.1. Brief historical evolution

The American Society of Mechanical Engineers' (ASME) code's stress limits for the seismic design of piping systems were first introduced for class 1 (reactor coolant system piping) in the first edition of ASME B31.7 published in 1969. The current ASME III approach used to evaluate ratcheting and fatigue in piping systems is presented in Annex E of this report. The first class one seismic stress equation had the form:

$$B_1 \frac{P_{max} D_o}{2\,t} + B_2 \frac{D_o}{2\,I}\,M_i \leq k\,S_m$$

where B_1 and B_2 are primary stress indices; P_{max} is the maximum internal pressure concurrent with the moment M_i; D_o = pipe outer diameter; t = pipe wall thickness; I = cross-section moment of inertia; M_i = resultant moment amplitude caused by primary loads (weight, seismic and concurrent loads); k is a multiplier that is defined in each plant safety analysis report (SAR) and was typically 1.5 for service level B (upset) loads, which include operating basis earthquake (OBE), and 3.0 for service level D (faulted) loads, which include safe shutdown earthquake (SSE). The SSE load combination included pipe break loads. This equation, with the SSE stress limits, was intended to prevent plastic collapse (which is a structural instability and buckling-like failure) through a simple elastic stress method with a limit load approach. It was not a fatigue limit or a fatigue-ratcheting limit. Annex E summarises the current ASME III approach used to evaluate ratcheting and fatigue in piping systems.

The same equation was introduced for class two and three piping systems when piping was moved from B31.7 to ASME III in 1971. The class two and three stress equation used the stress intensification factor, in the form $0.75i$, instead of the stress index B_2, with the result that the class two and three stress equation was:

$$\frac{P_{max} D_o}{4\,t} + 0.75i\,\frac{D_o}{2\,I}\,M_i \leq k\,S_h$$

Where k was typically 1.2 for OBE load combinations and 2.4 for SSE load combinations. At that time, the reason for using $0.75i$ instead of B_2 was purely pragmatic and due to the fact that the stress indices B_1 and B_2 were not listed in the ASME III NC (class 2) and ND (class 3) code books. The stress intensification factor i was listed because it was used in the thermal expansion stress equation. The piping systems in most nuclear power plants that are currently in operation in the United States were designed according to this $0.75i$ stress equation. Then, in 1981, the class two and three stress equation was changed so as to be similar to the class one equation in the following ways. The B stress indices were used and the allowable stresses changed from using $0.75i$ stress indices to B and the allowable stresses were changed as follows:

- For class one, $k = 1.8$ (to not exceed 1.5Sy) for OBE and 3.0 for SSE (to not exceed 2S$_y$.

- For class two and three, $k = 1.8$ for OBE (to not exceed 1.5 S$_y$) and 3.0 (to not exceed 2S$_y$) for SSE.

The background to the 1981 changes is explained by S.E. Moore and E.C. Rodabaugh's 1982 publication (S.E. Moore and E.C. Rodabaugh, 1982).

4.1.2. Current ASME III stress equations

Starting in 1985 and throughout 1988, a series of shake table tests were conducted on pressurised steel piping systems and piping components, which aimed to bring about a better understanding of the seismic failure modes and margins. These tests were supported by the United States' Nuclear Regulatory Commission (NRC) and Electric Power Research Institute (EPRI) and conducted under the technical lead of the group of experts (GE). The tests are documented in a five-volume EPRI report entitled "Piping and Fitting Dynamic Reliability Program", which was published in 1994 as EPRI-TR-102792 Volumes 1 through 5 (EPRI, 1994). The results of this test programme were analysed by a task group on seismic stress limits of the ASME III working group piping design. The task group recommended a change to the seismic stress equations for classes one, two and three, to introduce higher allowable stresses and alternate rules for what has been labelled "reversing dynamic loads" (seismic) as opposed to non-reversing loads such as water hammer.

The changes proposed by the task group on seismic stress limits for the seismic stress equations were introduced into ASME III in 1994. However, the United States' NRC had several concerns about the new and larger allowable stresses and several studies and reviews were conducted, which have led to the current seismic stress equations that were approved by the United States' NRC in 2006. The current and approved equations are:

$$B_1 \frac{P_{max} D_o}{2\,t} + B_2 \left(\frac{M_A + M_B}{Z}\right) \leq k\,S$$

In these equations, M_B is the resultant moment loading due to occasional loads, such as seismic or water hammer loads. One slightly more liberal alternative is now provided for if the moment M_B is caused by seismic (reversing) loads and not by non-reversing dynamic loads such as water hammer, which is now labelled M_B':

$$B_1 \frac{P_{max} D_o}{2\,t} + B_2' \left(\frac{M_A + M_B'}{Z}\right) \leq k\,S$$

The reason for this slightly more liberal stress equation is that B_2' for a tee is about 2/3 B_2. The current allowable stresses are:

- For class one, k = 1.8 for OBE (to not exceed 1.5S_y) and 3.0 for SSE (to not exceed 2S_y), and

- For class two and three, k = 1.8 (to not exceed 1.5 S_y) for OBE and 3.0 (to not exceed 2S_y) for SSE

However, if the B_2' alternative is used for SSE, there are additional restrictions that have to be met. There is a limit on the internal pressure, limit on the seismic anchor motion bending and axial stresses, caution against strain concentrations and limits on pipe movements.

4.1.3. Change in allowable stresses

In 1999 the definition of allowable stresses in ASME II part D for ASME VIII Div.1 (pressure vessels) and ASME III class two and 3 (three nuclear piping systems) was revised to be based not on Su/4, where Su is the ultimate strength, but on $S_u/3.5$. This change was independently introduced in the form of the stress equations, with the result that the allowable stress, based on $S_u/3.5$, is slightly larger when applying the current seismic stress equations. The basis for the increased allowable stresses is addressed in (WRC Bulletin

435, 1998). This same increase in allowable stresses was introduced into ASME B31.1 in 2007.

4.1.4. Recent ASME III seismic design developments

Since the 2006 code changes that have been described above, there has been no activity in ASME III to change the seismic design equations. Some work was done in the years 2000- 2010 on seismic margins (fragilities) for piping systems, to be used in seismic probabilistic risk analysis (SPRA), following the Fukushima Daiichi accident. Some work had also been done over the years to refine the knowledge of fracture mechanics under seismic loads and partly to support leak-before-break. Finally, new regulation introduced in the late 1990s enabled a single SSE to be designed, accounted for only OBE in class one fatigue, shake table testing and in the threshold for plant shutdown. This new approach in the treatment of the OBE is addressed by the United States' NRC 10 CFR Part 50 Appendix S - Earthquake Engineering Criteria for Nuclear Power Plants.

4.1.5. Seismic fatigue-ratcheting

The current ASME III stress equations, which resulted from the analysis of the 1985-1988 system and component tests as well as previous knowledge, focus on the prevention of plastic instability (sometimes referred to as collapse), which is a buckling-like failure. This type of failure was observed in the elbow component test, where an elbow with a long cantilever weight added was opened during repeated seismic shake table tests. A long cantilever weight at the end of an elbow is not a typical configuration in a power plant, and was created for the test campaign to prompt a buckling-like failure. The current ASME stress equations protect against this rare failure mode. However, the 1985-1988 tests also indicated cases of fatigue-ratcheting that caused the pressurised pipe to balloon under repeated large and plastic seismic strains (Figure 4.1). The large pressure-induced hoop strains combined with the large seismic induced cyclic axial strains to cause a ratcheting fatigue failure. This particular failure mode fatigue-ratcheting under the combined effect of large pressure-induced hoop strains and large seismic axial strains is not explicitly addressed by the current ASME III NB/NC/ND-3600 stress equations.

Figure 4.1. Fatigue-ratcheting failure under combined large hoop (pressure) and axial (seismic) strains
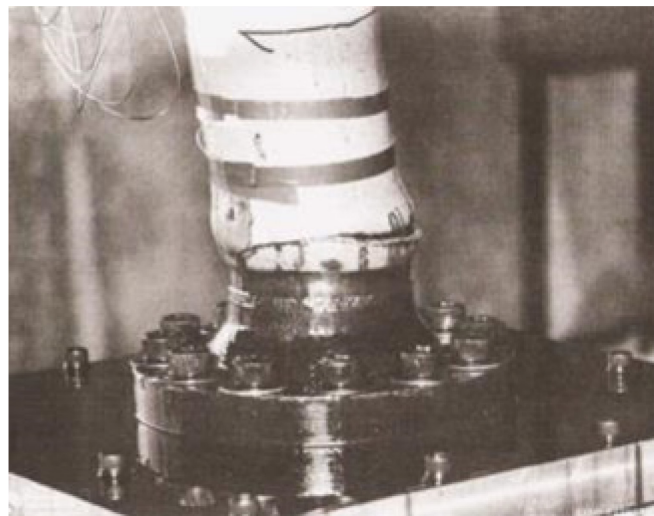
Source: Chen et al., 1987.

4.1.6. ASME III Appendix F methods

The classic method of seismic analysis of piping systems in accordance with ASME III NB/NC/ND-3600 using elastic piping analysis models, with limits on the intensified moment stresses M/Z, has been described above. However, ASME III Div.1 provides an alternative method for the analysis and qualification of the safe shutdown earthquake (SSE), the large and one-time faulted earthquake. The alternative method is described in ASME III non-mandatory Appendix F "Rules for Evaluation of Service Loadings with Level D Service Limits".

Appendix F provides five analysis methods and criteria. These Appendix F analysis methods date back to the 1960s, when strain-based plastic analysis was not as well developed as it is today. The following nomenclature applies: P_m = primary membrane stress intensity; P_b = primary bending stress intensity; P_L = primary local stress intensity; P_{max} = maximum primary stress intensity; τ_{avg} = average primary shear across the pipe wall; S_y = yield strength; S_u = ultimate strength; and S_m = ASME III Div.1 allowable stress intensity. The definition of these terms is given in ASME III Div.1 Appendix XIII, which was published in the 2017 edition.

Method 1 - elastic analysis. In this case, the finite element model is elastic ($\sigma = E\,\varepsilon$, no yielding) and the stresses are linearised through the pipe wall thickness along stress cut lines. The applicable stress limits depend on the stress classification, as follows:

$$P_m \leq min.\,(2.4S_m;\, 0.7S_u)$$
$$P_L \leq 1.5 \times min.\,(2.4S_m;\, 0.7S_u)$$
$$P_L + P_b \leq 1.5 \times min.\,(2.4S_m;\, 0.7S_u)$$
$$\tau_{avg} \leq 0.42S_u$$

(4.1-5)

Method 2 - collapse load analysis. In this case, the finite element model is elastic-perfectly plastic, with elastic behaviour ($\sigma = E\,\varepsilon$) when the stress is below the minimum ($2.3S_m$; $0.7S_u$), and perfectly plastic behaviour (σ = constant, no strain hardening) when the stress reaches the minimum point ($2.3S_m$; $0.7S_u$). The seismic load is then statically applied to this elastic-perfectly plastic model, in increments. As the static seismic load is increased, a first hinge forms, then as the load continues to increase a second hinge formed, until eventually, at a load $F_{collapse}$, the model becomes unstable or the deformations excessive. The allowable seismic equivalent static load is:

$$F_{allowable} = 0.90\,F_{collapse}$$

(4.1-6)

Method 3 - plastic analysis. In this case, the finite element model is plastic with strain hardening. The stress limits are:

$$P_m \leq 0.7S_u \; for \; ferritic \; steels$$
$$P_m \leq max.\,(S_y + (1/3)(S_u - S_y)\,;\, 0.7S_u)for \; austenitic \; steels$$
$$P_{max} \leq 0.90\,S_u$$
$$\tau_{avg} \leq 0.42S_u$$

(4.1-7)

Method 4 - plastic collapse analysis. As is the case for plastic analysis, the finite element model is plastic with strain hardening. The allowable load is the load for which the plastic stress intensity reaches the stress at which the plastic stress-strain curve intersects a straight line extending from (0,0) with a slope of $\Phi_2 = tan^{-1}\,(2\,tan\,\Phi_1)$, where Φ_1 is the angle of the

elastic portion of the stress-strain curve with respect to the stress axis, i.e. the angle established by the modulus of elasticity of the material.

Method 5 - plastic instability analysis. This is similar to Method 2, but the model is plastic instead of being elastic-perfectly plastic. In this case, the allowable load is

$$F_{allowable} = 0.70 \, F_{collapse} \tag{4.1-8}$$

4.1.7. ASME VIII Div.2 Part 5 plastic analysis method

The state-of-the-art condition of plastic analysis adopted by the ASME boiler and pressure vessel code is described in ASME VIII Division 2 Part 5, which is the code for the design and fabrication of non-nuclear pressure vessels. This state-of-the-art analysis has not yet been incorporated into ASME III, but plastic seismic analysis is permitted by the United States' NRC, if there is a review by the regulator on a case-by-case basis. The ASME VIII Division 2 Part 5 method was developed for pressure design but can also be applied for dynamic cyclic loads such as those caused by an earthquake, although explicit guidance for seismic analysis is not provided.

The ASME VIII Div.2 analysis approach is to provide stress, strain, or deformation limits to prevent the following four failure modes: (1) protection against plastic collapse; (2) protection against local failure; (3) protection against collapse from buckling; and (4) protection against failure from cyclic loading. More specifically, the protection against local failure by plastic analysis in particular is based on two key considerations:

When applied to seismic design, the seismic load is multiplied (increased) by a load factor of 1.7 and the time history strains must be accumulated over the earthquake cycles.

The resulting three-directional principal strains are combined with the cold forming (fabrication) strain and compared to the ultimate strain corrected for triaxiality, in the form:

$$\varepsilon_{peq} + \varepsilon_{cf} \leq \varepsilon_L = \varepsilon_{Lu} \times exp\left[\left(\frac{\alpha_{sl}}{1+m_2}\right)\left(\frac{\sigma_1 + \sigma_2 + \sigma_3}{3\,\sigma_e} - \frac{1}{3}\right)\right] \tag{4.1-9}$$

Where ε_{peq} = plastic equivalent (von Mises) strain; ε_{cf} = cold forming strain; ε_{Lu} = uniaxial strain limit; σ_i = principal stress components; σ_e = von Mises equivalent stress; and σ_{sl} and m_2 = material constants.

4.1.8. References

Chen, W.P., A.T. Onesto and V. DeVita (1987), "Seismic Fragility Test of a 6-inch Diameter Pipe System", NUREG/CR-4859.

EPRI (1994), EPRI-TR-102792, Piping and Fitting Dynamic Reliability Program, Vol. 1 – 5, Electric Power Research Institute, United States.

Moore, S.E. and E.C. Rodabaugh (1982), "Background for Changes in the 1981 Edition of the ASME Nuclear Power Plant Components Code for Controlling Primary Loads in Piping Systems", Transactions of the ASME (104), *Journal of Pressure Vessel Technology*, 104(4), pp. 351-361.

WRC Bulletin 435 (1998), "Evaluation of Design Margins for Section VIII, Div. 1 and 2 of The ASME Boiler and Pressure Vessel Code", WRC Welding Research Institute, United States.

4.2. Japanese code

4.2.1. General

The high seismicity in Japan means that the seismic design has been a crucial issue in the country from the beginning of the construction of nuclear power plants.

The first nuclear power plant for commercial use in Japan is the Tokai Power Station. Its constructed began in 1960 and its commercial operation in 1966. The reactor was based on the Calder-Hall type, a CO_2-gas cooled reactor. The static seismic intensity method was conducted.

For the following reactors, after the Tokai Power Station, the reactor type was either boiling water reactor (BWR) or pressurised water reactor (PWR). The first BWR plant was the Tsuruga Power Station, and the first PWR plant was the Mihama Nuclear Power Station. Both plants started their commercial operation in 1970. In the construction of light water reactor (LWR), the seismic design was mainly based on the static seismic intensity method, whereas the design based on the dynamic analysis were adopted for some important pieces of equipment.

Along with the construction of nuclear power plants, construction design procedures including seismic design were developed. At the beginning of the construction in Japan, the Ministry of International Trade and Industry promulgated Notification No. 501, which specified the structural design criteria for the nuclear power plants. Notification No. 501 was based on the ASME B&PV Code, Section III. Notification No. 501 was revised in 2006 to meet a performance-based requirement and merged with the Ministerial Ordinance No. 62. Since this revision became effective, the industrial standards have been used for specific design procedure.

In the current design procedure, the structural design of a nuclear power plant itself is based on the JSME Code (JSME, 2013), whereas the seismic design is conducted based on the code and guide published by the Japan Electric Association (JEAG, 1987). The code and guide complement each other.

JEAG4601, "Technical Guidelines for Aseismic Design of Nuclear Power Plants", was first published in 1970 (JEAG, 1987). This first version of the technical guide mainly described the basic concepts of seismic design, including the procedure of the determination of design seismic motion. The addendum to JEAC4601-1970 was published in 1984 to provide a seismic design classification and the allowable stress determination. JEAG4601 was significantly revised in 1987 (JEAG, 1987). The supplemental description for JEAG4601-1987 was published in 1991 (JEAG, 1991).

The regulatory guide for seismic design of nuclear power generation facilities was revised in 1995 after the large Kobe Earthquake in Japan.

In response to this revision of the regulatory guide, JEAG4601-1984, -1987, and -1991 were bound and revised as a seismic design code in the document "Technical Code for Seismic Design of Nuclear Power Plants" in 2008 (JEAC, 2008). The procedure to determine design seismic input was separated from the design code itself in this revision and issued as the relevant guide of the design code. Since then, the code has been revised approximately every five years. The latest version of JEAC4601 is JEAC4601-2015.

4.2.2. Stress evaluation in JEAG4601-1987

JEAG4601-1987 (JEAG, 1987) is the version of JEAG/JEAC4601 endorsed by the Japanese nuclear regulatory authority as of 2020. The English translation of JEAG4601-

1987 is available as a Nuclear Regulatory Commission (NUREG) report (Park & Hofmayer, 1994).

The allowable stresses of class one piping systems under the allowable stress level IVA S are provided as follows in JEAG4601-1987:

Primary stress (S_{prm})

For membrane stress:

$$S_{prm} \leq 2S_m \tag{4-2-2-1}$$

For membrane stress + bending stress:

$$S_{prm} \leq 3S_m \tag{4-2-2-2}$$

However, when the torsional stress is larger or equal to $0.55S_m$:

$$S_{prm} \leq 2.4S_m \tag{4-2-2-3}$$

Primary plus secondary stress range (S_n)

$$S_n \leq 3S_m \tag{4-2-2-4}$$

Fatigue evaluation

The primary + secondary + peak stress (S_p) and the repeatedly peak stress intensity (S_l) are calculated by the following equations:

$$S_p = \frac{K_2 C_2 M_{is}}{Z_i} \tag{4-2-2-5}$$

$$S_l = \frac{S_p}{2} \tag{4-2-2-6}$$

The fatigue evaluation is then conducted to confirm the cumulative fatigue damage is less or equal to 1.0.

4.2.3. Stress evaluation in JEAC4601-2008 or later

This version, or a later one, has not been endorsed by the Japanese nuclear regulatory authority. However, the utilities use the latest JEAC4601 for the seismic design /evaluation of their nuclear power plants to conform to the regulatory guide that was revised in 2006.

The allowable stresses of class one piping systems under the level Ds' service state are provided as follows in JEAC4601-2008 (JEAC, 2008):

Primary stress (S_{prm})

For membrane stress + bending stress:

When a short-duration mechanical load, such as a dynamic hydraulic load, exists with the seismic load:

$$S_{prm} \leq \min(3S_m, 2S_y) \tag{4-2-3-1}$$

Taking elbows as an example, S_{prm} is calculated by the following equation:

$$S_{prm} = \frac{B_1 P D_0}{2t} + \frac{B_2 M_{ip}}{Z_i} \tag{4-2-3-2}$$

where B_1, B_2: stress indices, P: pressure, D_0: outer diameter of pipe, t: wall thickness, M_{ip}: resultant moment by the mechanical loads, including the inertial force by seismic load, and Z_i: section modulus.

The primary stress must not necessarily be evaluated when there is no short-duration mechanical load. The reason for this provision is that the failure mode to be considered in the seismic design is fatigue instead of collapse, which is addressed by the primary stress limitation.

For torsional stress, or torsional stress + bending stress:

Primary stress by the torsional stress ($S_{prm,t}$):

$$S_{prm,t} \leq 0.73 S_m \tag{4-2-3-3}$$

where $S_{prm,t}$ is calculated by the following equation:

$$S_{prm,t} = \frac{B_2 T_{ip}}{Z_i} \tag{4-2-3-4}$$

where T_{ip}: torsional moment by the mechanical loads, including the inertial force by seismic load.

When $S_{prm,t}$ is over $0.73 S_m$, then the sum of torsional stress and bending stress ($S_{prm,tb}$) is to be satisfied by the following equation:

$$S_{prm,tb} \leq 2.4 S_m \tag{4-2-3-5}$$

where $S_{prm,tb}$ is calculated by the following equation:

$$S_{prm,tb} = \frac{B_2 M_{ip}}{Z_i} \tag{4-2-3-6}$$

Primary plus secondary stress range (Sn)

$$S_n \leq 3 S_m \tag{4-2-3-7}$$

Taking elbows as an example, Sn is calculated by the following equation:

$$S_n = \frac{C_2 M_{is}}{Z_i} \tag{4-2-3-8}$$

where C_2: stress index, and M_{is}: range of applied moment to a pipe caused by inertial force due to seismic load and relative displacement.

Fatigue evaluation

The primary + secondary + peak stress (S_p) and the repeatedly peak stress intensity (S_l) are calculated by the following equations:

$$S_p = \frac{K_2 C_2 M_{is}}{Z_i} \tag{4-2-3-9}$$

$$S_l = \frac{K_e S_p}{2} \tag{4-2-3-10}$$

where K_2: stress index, and K_e: the index provided by the JSME Code (JSME, 2013).

The fatigue evaluation is then conducted to prevent fatigue failure by limiting the cumulative fatigue damage to being less or equal to 1.0.

The number of seismic cycles is not explicitly designated by JEAC4601. Users must calculate this based on their plant's specific seismic input and the relevant response of piping systems. Generally, the number is in the dozens for a BWR and hundreds for PWR

plant. However, the numbers have increased in the past few years due to recent earthquakes like GEJE in 2011.

Activity to revise the torsional stress, or torsional stress + bending stress

Restrictions on the torsion and torsion + bending are described in the Japanese seismic design code.

This rule is described in the guideline of 1984 version and defined in addition to the provisions of Notification No. 501 of 1980.

The background to the addition of this rule is that the allowable value for the torsional moment of stainless steel was determined to be larger than that of carbon steel when comparing the yield moment of all members with the allowable moment, according to the regulations of the notification. This is because the allowable value was determined in anticipation of the strain hardening of stainless steel.

However, the standards committee at that time was concerned that a large twisting force would cause cracks in the entire circumference of the pipe and there was a concern that the guillotine breaks in the pipe. Consideration was therefore given to setting-out limits for twisting and twisting + bending for the piping system's soundness.

This provision has already been considered in the JSME construction standards and the 2Sy limit has been added to the JSME construction code.

It has been concluded that there is no need for restrictions on twisting and twisting + bending and therefore activities to eliminate the restriction of the Japan Electric Association are ongoing.

4.2.4. Design damping ratios for piping systems

Table 4.1 shows the design damping ratios for piping systems provided in JEAC4601-2008 or later.

Table 4.1. Design damping ratio for piping systems in Japanese seismic code (JEAC 2008)

	Type of piping system	Design damping ratio (%)	
		With a heat insulator	Without a heat insulator
I	Piping systems supported mainly by snubbers or frames; the number of supports is more or equal to 4.	3.0	2.0
II	Piping systems which have snubbers, frames, or hangers; the number of supports is more or equal to 4, and the piping system is not classified to Type I.	2.0	1.0
III	Piping systems using U bolts; the weight of the horizontal pipes is supported with 4 or more U bolts.	3.0	2.0
IV	Other than Type I, II or III	1.5	0.5

The design damping ratios in JEAG4601-1987 were slightly different to those shown in Table 4.1. In JEAG4601-1987, the design damping ratios ranged from 0.5% to 2.5% and the category Type III did not exist. In JEAG4601-1987, an additional damping ratio due to the existence of thermal insulation having the enough length along the piping was specified as 0.5%, but the additional damping ratio specified in JEAC4601-2008 is 1.0%.

4.2.5. New code case for advanced seismic design

According to JEAG/JEAC4601, piping systems are designed based on an elastic stress analysis, and a pseudo stress-based evaluation is conducted. Although the stress on the piping system may go over the yield point in some local areas, the effect of the inelastic

behaviour itself is not directly evaluated. However, a number of experimental studies on piping systems indicated that the piping systems exhibited significant plastic behaviour, which went beyond allowable stresses defined by conventional seismic design code. The failure mode confirmed in these experiments was fatigue failure.

A code case has been established in the framework of the JSME nuclear codes and standards (Morishita et al., 2020) to consider this type of inelastic behaviour in the seismic design of piping systems. The details of this code case will be described in Section 5.2 of this document.

4.2.6. References

JEAC (2008), "Technical Code for Seismic Design of Nuclear Power Plants", JEAC4601-2008.

JEAG (1987), "Technical Guidelines for Aseismic Design of Nuclear Power Plants", JEAG4601-1987.

JSME (2013), "Codes for Nuclear Power Generation Facilities – Rules on Materials for Nuclear Facilities", JSME S NJ1-2013.

Morishita, M., A. Otani, I. Nakamura, T. Watakabe, T. Shibutani and M. Shiratori (2020), "A JSME Code Case on Piping Seismic Design Based on Inelastic Response Analysis and Strain-Based Fatigue Criteria", *Transactions of the ASME Journal of Pressure Vessel Technology*, 142(2), 021203-1-021203-14.

Park, Y.J. and C.H. Hofmayer (1994), "Technical Guidelines for Aseismic Design of Nuclear Power Plants: Translation of JEAG 4601-1987", NUREG/CR-6241, US Nuclear Regulatory Commission, Washington, DC.

4.3. French nuclear codes for mechanical components - RCC-Ms

4.3.1. General

An important effort of codification was implemented in France from 1978 in order to assemble the French practice established during the construction and operation of nuclear power plant (Heng et al, 1987). At that time, 30 units were under construction or in operation and a specific practice was implemented. This practice was derived from the United States through the Westinghouse licence. This explains similarities with the ASME III code, whose basic structure was adopted. It was established by Électricité de France (EDF) and Framatome with the participation of the main manufacturers. The first published document was the RCC-M (Règles de Conception et de Construction) dealing with the mechanical components of PWR nuclear islands in 1981. One of the objectives was to include, as much as possible, French and later European community practices and standards and R&D results in the design, construction and inspection of nuclear projects.

Other documents were established in parallel concerning fuel elements (RCC-C), electrical equipment (RCC-E), process (RCC-P), civil works (RCC-CW) and rules for the design and construction of mechanical components for fast breeder reactors (RCC-MR). This latter document gathered the experience gained in the design and construction of PHENIX, SUPER-PHENIX and European fast breeder reactor.

The AFCEN ("French society for design and construction rules for nuclear island components") was created in 1980 and is in charge of drafting and developing the different RCCs at the national and international scale.

The French safety authority and TSO are informed of RCC developments; their experts participate in some meetings of the AFCEN's technical committees and they are consulted for the demonstration of the compatibility of the code with regulations.

There is one specific aspect of the code that deserves flagging. In current practice, thermal loads are considered as secondary and the inertial part of a seismic load as primary for almost all industrial piping codes. From the beginning of the 2000s, this simple classification for seismic loads was recognised to be incorrect, based on extensive research and development (R&D) programmes; the most representative of them are described in this document. The fact that a thermal load is not purely secondary was recognised early on because it depends on the relative flexibilities of different parts of the system (such as piping fixed to an equipment). This is known as elastic follow-up and has been explicitly considered in some high temperature piping systems. However, for "simplicity" reasons, thermal loads were considered as secondary. Yet in the RCC-M 2000 edition, the sentence mentioning that thermal stresses should be considered as secondary in every case was suppressed. This document also mentions that only a fraction of inertial dynamic loads can be taken into account for the verification of "primary loads'" damage.

4.3.2. RCC-M

Introduction

As explained above, RCC-M deals with the mechanical components of nuclear islands of a PWR, and more specifically, the pressure components, vessels, heat exchangers, pumps, valves, piping systems, reactor internals, low pressure storage tanks (atmospheric tanks) and supports (Rao, 2009: §49.7).

The document covers the design, materials, welding, inspection methods and manufacturing for the three safety classes defined in the safety analysis. The first edition was published in 1981, the second in 1983 and subsequent revisions of the document have been issued periodically.

Concerning the philosophy of seismic piping design, the content of the first editions is comparable with ASME III, paragraphs 36xx. At the end of the 1990s, many R&D programmes substantiated the existence of margins for seismic loadings (see Chapter 3 of this document). This introduced modifications into the code related to the seismic analysis of piping systems, which are briefly presented below.

Seismic analysis of piping systems - evolutions

The general form of the equation to prevent plastic collapse or excessive deformation (B 3652, Eq. 9 in RCC-M) is typically the following, for class one:

$$B_1 \frac{PD}{2t} + \frac{B_2 M}{Z_1} \leq k.S_m \qquad (4.3\text{-}1)$$

where *M* is the sum of the moment due to permanent and seismic loads. For faulted conditions $k=3$. In the 2000 revision, which was mentioned above, only a fraction of inertial dynamic loads can be taken into account for the verification of "primary loads" damage.

Different approaches were possible for considering the evidenced margins, as discussed by Le Breton et al. in a 2009 publication, such as increasing the *k* value in Equation 9, or verifying a progressive deformation condition.

It was eventually decided that the primary part of seismic moment must be considered in Equation 9. This primary part is considered to be the elastically computed moment when the damping ratio used for the analysis includes an additional damping due to elasto-plastic behaviour. This occurs when the total damping ratio is higher than 10%. This value is the result of interpretations of some of the tests performed in France or abroad (see Chapter 3 of this report). The conditions for the application of the rule are using a linear response

spectrum analysis with a broadened input response spectrum (of at least +/-15% in order to cover the frequency shift induced by global plastic deformation) and having the main piping frequencies below or in the amplification frequency zone of the input response spectrum. When the damping used for the (linear) analysis is taken between 2% and 5%, the primary part, M_E, of the seismic elastically calculated moment, M_s, can be determined by to the following formula:

$$M_E = \tau M_s \qquad \text{and} \qquad \tau = \sqrt{\frac{\xi}{10}} \qquad\qquad (4.3\text{-}2)$$

where ξ is the retained damping ratio (in %).

For a damping that is equal to 2%, the reduction factor is equal to 0.45 and 0.7 for 5% damping. The designer must provide a specific justification for other damping values, which are generally between 5% and 10%.

This reduction is not applicable to reaction loads or interface loads. The "normal" practice is to consider the total part of seismic loads for these cases and crack stability and leak-before-break (LBB) verifications, except for if specific justification, such as, for example, non-linear analyses) are provided. Similarly, displacements and accelerations obtained by elastic analysis must be used for subsequent treatments, such as, for example, interface conditions.

The validity of the proposed approach was demonstrated by a comparison of it to the seismic test results performed at the Commissariat à l'énergie atomique et aux énergies alternatives (CEA) on the TAMARIS shaking table in Saclay and the numerous static tests of elbows, which are summarised by Le Breton et al. in a 2009 publication. The comparison demonstrated that the new criteria guarantees margins larger than two for level D faulted conditions.

4.3.3. General considerations about RCC-MR, RCC-MX, RCC-MRx

This is a family of codes that have been specifically developed in France for fast breeder reactors, ITER vacuum vessels and research reactors.

RCC-MR is devoted to fast breeder reactors and was established at the end of the 1970s for the design and construction of the fast breeder SUPER-PHENIX plant. The code includes design rules for elevated temperatures (T>425°C). A tripartite committee was created in 1978 by CEA, EDF and NOVATOME in order to establish specific regulations for this reactor, which were based on the experience gained by the design of fast reactors, RAPSODIE, PHENIX and SUPER-PHENIX. The first edition of RCC-MR was issued in 1985. Its general structure is similar to the RCC-M code. The document was then enhanced to cover evolutionary project needs, such as the experimental reactor "Jules Horowicz" and ITER vacuum vessel, which were both under construction in CEA-Cadarache centre in south-east of France. These evolutions resulted in a new document, the RCC-MRx, the first edition of which was published in 2010. A new edition was then issued in 2013 and the latest edition in 2018. The general structure of the code is similar to the RCC-M and ASME Section III codes.

This report will only comment on points about RCC-MRx that specifically relate to the seismic design and analysis of piping systems. The parts relating to high temperatures and the resulting creep will not be mentioned.

The first important specific point to be made is the use of a method to derive non-linear "more realistic" stresses from linear results. This is the Roche method, which is presented in the Annex H. The second point is the use of specific criteria for piping components,

which have been derived from an important static test campaign on piping components. The effective implementation of these two points will now be further examined.

4.3.4. Seismic design for piping systems in RCC-MRx

The first main difference between RCC-MRx and codes used for pressurised reactors, such as ASME III Division 1 or RCC-M, is the formulation of maximum allowable stresses and a formulation giving stress intensification coefficient. It is important to mention that the thicknesses of fast breeder reactor pipelines are smaller compared to those of water reactors. As a consequence, pressure can have a more significant effect on the flexibility and, with temperature effects, on the stress distribution in elbows and tees. Plastic collapse and/or elastic buckling are possible failure modes for such elbows with applied forces and/or displacements. An important R&D programme that includes static tests on elbows and tees was conducted in France, aimed at characterising piping components' (straight pipes, elbows, tees, nozzles...) flexibility factors and stress intensity coefficients (Touboul, 1989; Berton, 1999). The results of these programmes were included in the code, which is explained below for class one piping. Class two piping design rules are identical to those of class one.

§ RB3643.2 presents the formulas for factors of flexibility for straight pipes, elbows, mitre bends, tees and nozzles.

§ RB3643.3 is devoted to the definition of elastic follow-up ratio as presented in Equation (C) in §4.3.3.2 Roche's method in this document. The reference stress formulation for application of either of Equation (C) has the following general form:

$$\sigma_{ref}^2 = [0.79 . B_2 . \frac{M_f}{Z}]^2 + [0.87 . \frac{M_{12}}{Z}]^2$$

(4.3-3)

Mf is the bending moment

M_{12} is the torsional moment.

The elastic follow-up ratio is determined separately for effects due to inertial and anchor movement of seismic loads.

§ RB3645.8 is dedicated to the classification of seismic moments and their combination with other moments. All loads other than seismic ones are classified as either force dependent or displacement dependent; seismic moments have to be classified in one of these categories in order to be cumulated with other moments. Two approaches are proposed:

- Calculation seismic model 1 (CMS1), in which:

  - The inertial part of seismic moments is classified as "force dependent" and is combined with other moments of force dependent loadings, which results in a moment of amplitude *M*.

  - Seismic moments due to anchor displacements are displacement dependent and combine with other moments of displacement dependent loadings, which results in a moment of amplitude *m*.

  - Ranges of seismic moments (double the amplitude) are also adequately combined for fatigue analyses.

- Stresses due to pressure P and moments due to forces are determined in the following classical formula:

$$p_m + p_b = B_1.\text{P } D/2t + B_2 M/Z \qquad (4.3\text{-}4)$$

  in the part related to moment effects of torsional and flexural moments that can be separated, leading to formulas that are comparable to the formula that gives σ_{ref} above. B_1 and B_2 are stress intensity factors similar to "classical" formula, with some modifications, especially when torsion and flexure are separated.

- Stresses due to pressure, force dependent moments and displacement dependent moments are calculated according to the following formulation:

$$s_m + s_b = \left[(D_1 P.D/2t)^2 + \langle \tfrac{D_2}{Z}, M + g.m \rangle^2 \right]^{0.5} \qquad (4.3\text{-}5)$$

- In this formula, the brackets ⟨⟩ represent either the product of two terms in them, or a linear or quadratic combination of products for each component of moments, torsional, flexural and different contribution of branch and run for a tee. D_i coefficients are specified for these different situations in RB3680. They result from the important R&D test and analysis programme that was mentioned above). g is the knock down coefficient. as defined in §4.3.3.2 c, which is calculated in each point of interest with the maximal follow-up coefficient r along the line and for maximal primary σ_p and allowable S stresses.

- Calculation seismic model 2 (CMS2), which differs from the first method by the classification of seismic moments:

  - A "quasi-static" inertial part of seismic moment is defined. In the 2013 edition, this is obtained by a response spectrum analysis with a damping of 10%. In the 2018 edition of the code, no method is mentioned. This moment is called M_{SI}.

  - The complement of this moment to the inertial seismic moment calculated with design damping values M_{S2} being considered displacement dependent. It is called m_{SI}. $m_{SI} = M_{S2} - M_{SI}$.

  - The seismic moment to be considered, as shown in Equation (4.3-2), is $M+g.m$

    $M+g.m+g_S.m_{SI}$, where g and m are similar to those in Equation (4.3-2), for the displacement part, and g_S has the same expression as g, but is calculated with the seismic moment M_{S2}. In addition, g can be taken equal to 1, which is a simplification.

Stresses in seismic conditions are compared to level D limits, according to the code practice, which is close to ASME and RCC-M practices.

4.3.5. References

Berton, M.-N., D. Plancq, B. Michel, P. Genette and N. Foucher (1999), "Piping System instability-margin on elastic analysis with local instability criterion", *SMIRT-15*, 15-20 August, Seoul.

Heng, C., J.M. Grandemange and A. Morel (1987), "RCC-M (Rules for design and construction of nuclear components)", *Nuclear Engineering and Design*, 98(3), pp. 265-277.

Le Breton F. and C. Petesch (2009), "Stress Criteria for Piping. RCC-M Rules and Validation", *SMIRT-20*, 9-14 August, Espoo, Finland.

Rao, K.R., editor (2009), "Companion Guide to the ASME Boiler and Pressure Vessel Code" Volume 3, 3rd edition, American Society of Mechanical Engineers Press, United States.

RCC-M (2009), "Règles de Conception et de Construction des Matériels Mécaniques des Ilots Nucléaires REP", AFCEN, France.

RCC-MRx (2012), "Design and Construction Rules for Mechanical Components of Nuclear Installations", AFCEN, France.

Roche, R.L. (1993), "Spring effect and primary stress", *SMIRT-12*, 15-20 August, Stuttgart, Germany.

4.4. Seismic design and stress analysis of nuclear power plant piping systems in Russia: Brief overview

4.4.1. Description

Russia has a long history in developing regulations for pressure equipment and piping. However, during considerations of a rather low seismicity of the Russian nuclear power plants' sites, seismic design was not in the focus of piping standards before the early eighties. Several documents were issued in a row at the time:

- 1979: VSN-15-78 "Temporary Norms for Design of Nuclear Installations for Seismically Active Zones";

- 1981: Norms for a Seismic Analysis of Equipment and Piping of VVER Nuclear Power Plants (Addendum to the Nuclear Norms of 1973);

- 1981-1985: RTM 108.020.37-81, Regulatory Guide for VVER NPPs Power Equipment and Piping. Seismic Analysis;

- 1987: PNAE G-7-002-87, Norms for Strength Analysis of Equipment and Piping of Nuclear Installations;

- 2001: NP-031-01, Norms for Seismic Design of NPPs.

The last two documents, PNAE Code and NP-031-01 Norms, are the Russian regulations currently being used for the seismic design of nuclear power plants' piping systems.

NP-031-01 prescribes seismic categorisation, the damping values used in analysis and loads' combination compatible with earthquakes, as well as the level of allowable stresses (see Tables 4.2 and 4.3).

PNAE G-7-002-87 provides formulas for the calculation of stresses in piping elements and fittings (see Table 4.4).

Nuclear power plants' piping and equipment are categorised on three seismic categories, depending on their safety relevance and designated functions:

Seismic category one includes:

- piping classified as safety classes one or two;

- piping belonging to the safety systems;

- piping whose failure under SSE can lead to a radioactive product release that exceeds permissible level.

Seismic category two covers plant systems and their elements (not ranked in the first category), the failure of them in operation, separately or together with other systems and elements, which can lead to an interruption in electric power and heat generation. Category two also covers safety class three systems and elements, which are not ranked in the first seismic category.

Finally, seismic category three is applicable for the rest of systems that are not included in categories one and two.

Table 4.2. Damping values used in analysis (in parts from critical damping)

Piping outside diameter	Level of calculated stresses comparing with "design strength" R	
	$\sigma = 0.67R$	$\sigma \geq 0.67R$
> 300 mm	0.02	0.03
≤ 300 mm	0.01	0.02

Table 4.3. Combination of loads and allowable stresses

Seismic Category	Combination of loads	Group of Stresses	Allowable stresses
I	NE+MRZ	$(\sigma_S)_1$	$1.4[\sigma]$
		$(\sigma_S)_2$	$1.8[\sigma]$
	NNE+MRZ	$(\sigma_S)_1$	$1.4[\sigma]$
		$(\sigma_S)_2$	$1.8[\sigma]$
	NE+PA+PZ (MRZ)	$(\sigma_S)_1$	$1.4[\sigma]$
		$(\sigma_S)_2$	$1.8[\sigma]$
	NE+PZ	$(\sigma_S)_1$	$1.2[\sigma]$
		$(\sigma_S)_2$	$1.6[\sigma]$
	NNE+PZ	$(\sigma_S)_1$	$1.2[\sigma]$
		$(\sigma_S)_2$	$1.6[\sigma]$
II	NE+PZ	$(\sigma_S)_1$	$1.5[\sigma]$
		$(\sigma_S)_2$	$1.9[\sigma]$
	NNE+PZ	$(\sigma_S)_1$	$1.5[\sigma]$
		$(\sigma_S)_2$	$1.9[\sigma]$

Notes:
NE: loads during normal operation (L1 per IAEA NS-G-1.6)
MRZ: earthquake-analogue of SSE or SL2 per IAEA NS-G-1.6
NNE: additional loads during anticipated operational occurrences (L2 per IAEA NS-G-1.6)
PZ: earthquake-analogue of OBE or SL1 per IAEA NS-G-1.6
PA: loads during accident conditions (L3 per IAEA NS-G-1.6)
[σ]: allowable nominal stresses;

R_m^T : minimum tensile strength at temperature;

$R_{p0.2}^T$: minimum yield strength at temperature;

$(\sigma_S)1$: equivalent membrane stresses;
$(\sigma_S)2$: equivalent membrane + bending stresses.

Table 4.4. PNAE code equations for (σ)2 stresses

Nomenclature:

Section loads: M_x, M_y – bending moments, M_z – torsional moment; N_z – axial force, P – internal pressure; c – mill tolerance; φ - weld's reduction factor; Do – outer piping diameter; s – wall thickness; W –section modulus of pipe; R – bend radii; r – mean radius of pipe; σ_1, σ_3 – principal stresses; σ_z – axial stress; σ_Ψ - tangent stress; σ_r – radial stress; τ - torsional stress

Straight pipes and curved pipes (bends):

$$\sigma_3 = \max \begin{cases} 0.5\left[\sigma_\psi + \sigma_z + \sqrt{(\sigma_\psi - \sigma_z)^2 + 4\tau^2}\right] \\ 0.5\left[\sigma_\psi + \sigma_z - \sqrt{(\sigma_\psi - \sigma_z)^2 + 4\tau^2}\right] \\ \sigma_r \end{cases} ; \quad \sigma_1 = \min \begin{cases} 0.5\left[\sigma_\psi + \sigma_z + \sqrt{(\sigma_\psi - \sigma_z)^2 + 4\tau^2}\right] \\ 0.5\left[\sigma_\psi + \sigma_z - \sqrt{(\sigma_\psi - \sigma_z)^2 + 4\tau^2}\right] \\ \sigma_r \end{cases}$$

$$\sigma_\psi = \sigma_{\psi p}; \quad \sigma_z = \sigma_{zp} \pm \frac{\sqrt{M_x^2 + M_y^2}}{W} + \frac{N_z}{A_s}; \quad \tau = \frac{M_z}{2W}; \qquad \sigma_r = -\frac{P}{2}; \quad \sigma_{\psi p} = \frac{P[D_o - 2(s-c)]}{2\varphi(s-c)};$$

$$\sigma_{zp} = \frac{P[D_o - 2(s-c)]^2}{4(D_o - s + c)(s-c)}; \quad (\sigma)_2 = \sigma_3 - \sigma_1$$

Curved pipe with λ parameter > 1.4 $\quad (\lambda = \dfrac{Rs}{r^2})$:

$$(\sigma)_2 = \frac{\Omega}{\Psi} \frac{\sqrt{M_x^2 + M_y^2 + M_z^2}}{W}; \quad ;$$

parameters Ω and Ψ used above are functions from the bend's geometrical properties and stress ratio, see Figures 4.2 and 4.3.

Figure 4.2. Parameter Ω
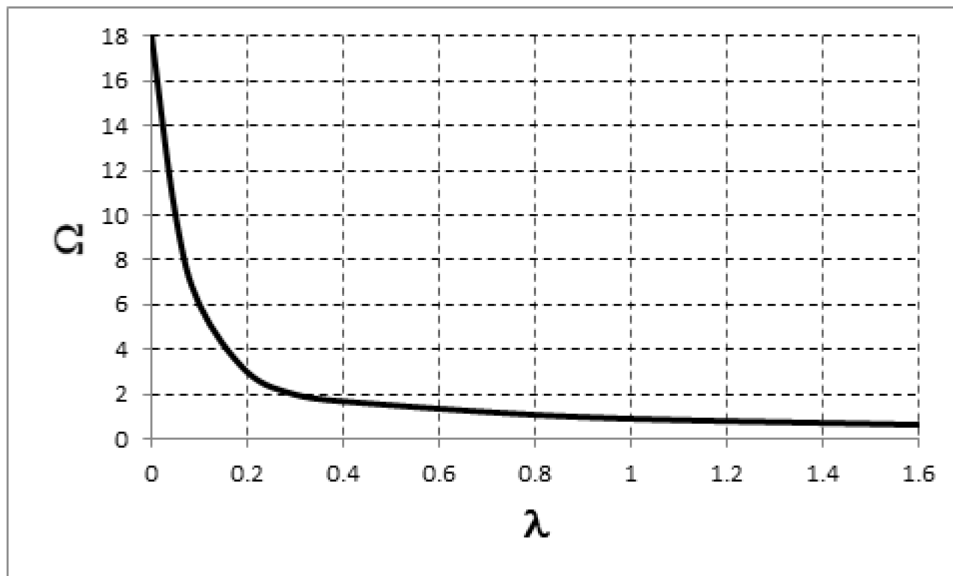
Figure 4.3. Parameter Ψ
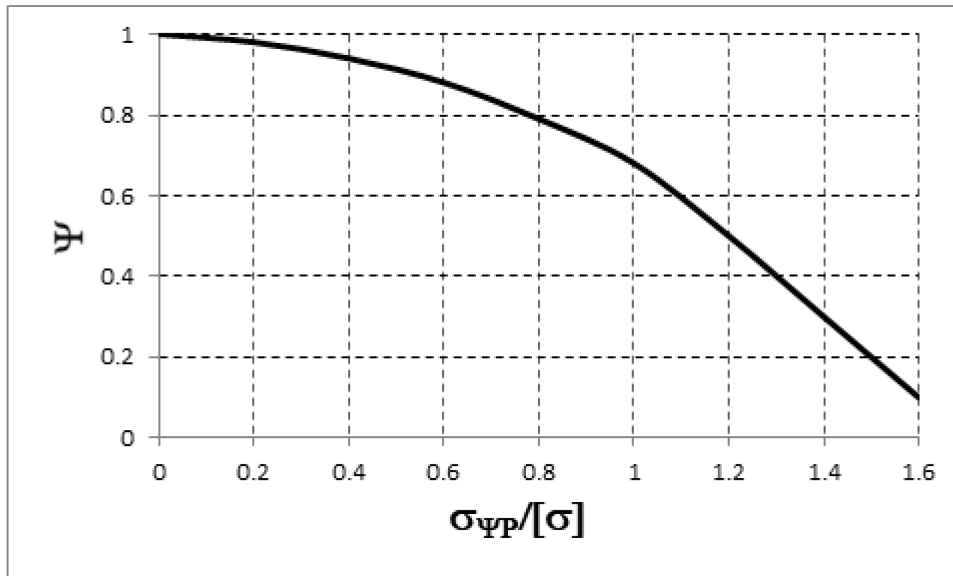
Table 4.5. PNAE code equations for tees and branch connections
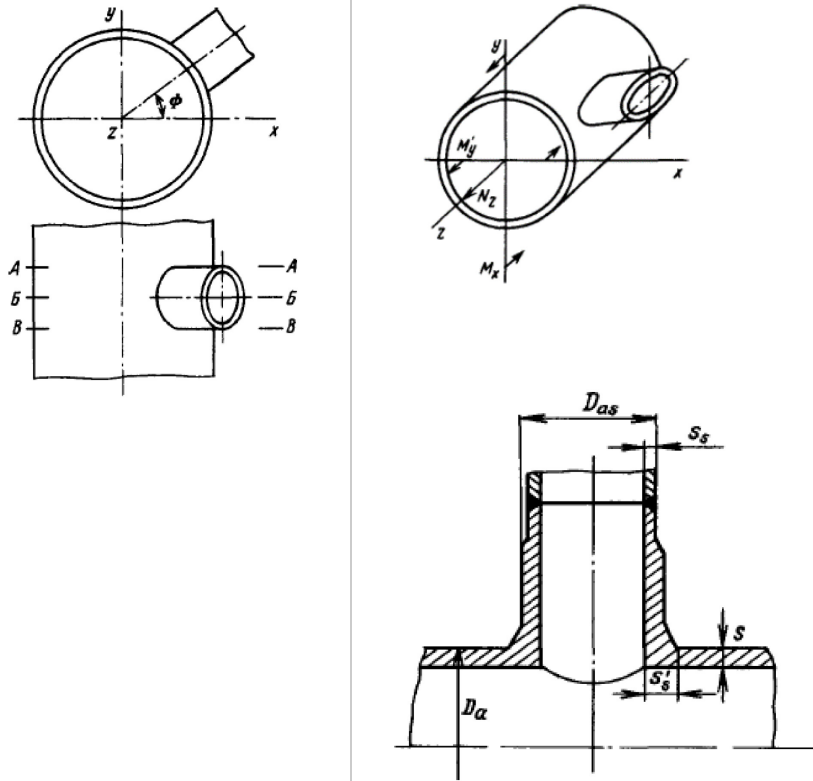
For cross-sections A-A and B-B: $\sigma_z = \sigma^O_{zMN} \pm 0.7 \sigma^O_{zMN(s)} K_{(s)} + \sigma_{zp}$;

For cross-section Б-Б: $\sigma_\psi = \sigma_{\psi p} \pm 0.7 \sigma^O_{zMN(s)} K_{(s)}$; $\sigma_z = \sigma^O_{zMN} + \sigma_{zp}$, where:

$$K_{(s)} = \max \left\{ \begin{array}{l} \frac{(D_{as}-s_s)s_s}{4(s-c)^2} \ln \frac{D_a - s}{s'_s}, if \ \frac{D_{as}-s_s}{2s} \leq 8 \\ \frac{6.2(D_{as}-s_s)s_s s}{(s-c)^2(D_{as}+10s-s_s)} \ln \frac{D_a-s}{s'_s}, if \ \frac{D_{as}-s_s}{2s} > 8 \end{array} ; 2 \right\}$$

$$\sigma^O_{zMN} = \frac{M_x \sin\Phi - M_y \cos\Phi}{W} + \frac{N_z}{A_s};$$

$$\sigma^O_{zMN(s)} = \frac{\sqrt{M_x^2 + M_y^2}}{W} + \frac{|N_z|}{A_s}$$

Both PNAE (for all classes) and ASME BPVC (for class one) must be subjected to a stress analysis that checks the primary stresses on the basis of the maximum shear stress theory of failure. These primary stresses consist of the general membrane stresses, local membrane stresses and bending stresses. The significant aspect of primary stresses is that they are not self-limited, but are caused by external loads such as internal pressure, inertial and weight loads, seismic inertial loads, etc.

Russian norms are essentially similar to ASME class one provisions, but have some specifications that make them different to ASME-type codes:

- code equations in PNAE do not depend on the piping safety class (they have the same requirements for primary loop piping and small drainage tubes);

- code equations in PNAE have a more complex form;

- norms do not recognise the variability of stress intensification factors and stress indexes for different types of tees and branch connections;

- there is no specific stress indexes for reducers and weld connections;

- there is no specific guidance on dealing with secondary stresses induced by seismic anchor movement.

A new edition of norms is currently under development in Russia. This edition should be much more harmonised with international codes, but also remain compatible with the PNAE document. The basic normative document, NP-031, governing seismic design, is expected to be revised and have some of its gaps and issues resolved over the next few years, including:

- a less conservative approach for using a system damping;

- the addressing of seismic anchor movement;

- the implementation of SMA-based approaches for existing plants;

- a consideration of beyond design basis earthquakes.

4.4.2. References

NP-031-01 (2001), "Norms for Seismic Design of NPPs", RUNORM, Russia.

PNAE (1981), "Norms for a Seismic Analysis of Equipment and Piping of VVER Nuclear Power Plants (Addendum to the Nuclear Norms of 1973)", PNAE, Russia.

PNAE (1987), "Norms for Strength Analysis of Equipment and Piping of Nuclear Installations", PNAE G-7-002-87, PNAE, Russia.

RUNORM (1985), RTM 108.020.37-81, "1981 – 1985: Regulatory Guide for VVER NPPs Power Equipment and Piping. Seismic Analysis", RUNORM, Russia.

Series, I.S.S. (2003), "Seismic Design and Qualification for Nuclear Power Plants", Safety Guide No. NS-G-1.6, Vienna, ISBN 92–0–110703–X.

VSN-15-78 (1979), "Temporary Norms for Design of Nuclear Installations for Seismically Active Zones".

4.5. Canada

4.5.1. Seismic design approach in Canada

The seismic design of nuclear power plant systems, components and structures in Canada is carried out under the guidance of the Canadian Standards Association (CSA) standard CSA-N289.3. CSA-N289.3 is part of the N289 series of standards, which provide the general requirements, a ground motion parameters estimation, design by analysis, design by testing and seismic instrumentation requirements. Standards in the N289 series were initiated in response to a recognition by utilities and industries concerned with nuclear structures in Canada of the need for the documentation and standardisation of the various

guides and procedures used for the seismic qualification of nuclear structures and components of a CANDU nuclear power plant.

The development of CSA-N289.3 (design procedures for the seismic qualification of CANDU nuclear power plants) standard began in 1976 under the sponsorship of the Canadian Nuclear Association's Codes, Standards, and Practice Committee. The decision was made in 1977 to promulgate the then available seismic design document as a CSA standard. The purpose of this standard was to provide requirements ensuring that nuclear structures, components and systems would be seismically qualified in a manner that utilised analytical techniques and met a quality and standard in line with the necessary safety principles, complying with the Canadian nuclear safety philosophy.

The Canadian seismic design approach is based on application of design basis earthquake (DBE). The DBE was defined as an engineering representation of design basis seismic ground motion (DBSGM) and expressed in the form of a response spectrum or time histories to be used for the purpose of the seismic qualification of systems, structures and components. The design basis seismic ground motion is the motion at site that represents the potentially severe effects of earthquakes in the region. The motion has a sufficiently low probability of being exceeded during the plant's lifetime.

According to Canadian seismic design philosophy, pressure-retaining components and the supports of such components are designed according to the applicable subsections of ASME code section III level C (emergency condition)'s service limits. The duration of the seismic ground motion that will be considered for analysis is a minimum of 15 seconds.

4.5.2. Main seismic design changes from "conventional" approach

Return period specified 1E-04 events/year

The return period for a DBE was not specified in the early CSA standard N289.3, but is explicitly stated in the newer/latest version. DBE is now defined as an engineering representation that has potentially severe effects at the site due to earthquake ground motions, with a selected probability of exceedance of 1×10^{-4} per year, or a probability level that is acceptable to the authority who has jurisdiction.

0.1 g minimum design horizontal response spectra for new design

No minimum design requirement was set in the earlier standard for low seismicity sites. It is now stated that the minimum design horizontal response spectra used in the design of new nuclear power plant SSCs should be a standard-shape ground response spectrum, which is anchored to a peak ground acceleration of 0.1 g on rock and modified to take the site's specific geological conditions into account.

Standard spectral shape FRS vs. site specific uniform hazard spectrum FRS

The use of uniform hazard spectrum (UHS) has been accepted as seismic design input. The standard-shape ground response spectra of nuclear power plants built in eastern North America (or a similar seismic region) have been observed to not reflect the expected high frequency content of the seismic ground motions and fall below the UHS. In such a case, additional evaluations should be performed to ensure that the high frequency-sensitive SSCs can perform their prescribed safety functions.

Seismic fatigue

The minimum number of seismic cycles should be 25 at the maximum peak response levels when determining the equivalent seismic fatigue effects from the applicable design fatigue curves. Conservatively, the number of cycles was only 200 in the early version of the standard.

Seismic evaluation beyond design basis to demonstrate seismic ruggedness

The application of both methodologies: a) seismic margin assessment (SMA), including EPRI SMA, NRC SMA., and PSA-based SMA, and b) seismic probabilistic safety assessment (SPSA), which use the checking/review level earthquake (RLE/CLE) have been accepted as valid tools for demonstrating that safety-related SSCs possess enough seismic ruggedness to withstand beyond design basis events.

4.5.3. References

CSA (2020), "Design procedures for seismic qualification of nuclear power plants", CSA N289.3:20, CSA group, United States.

CSA (2018), "General requirements for seismic design and qualification of nuclear power plants", CSA N289.1:18, CSA group, United States.

CSA (2010), "Ground motion determination for seismic qualification of nuclear power plants", CSA N289.2:10(R2020), CSA group, United States.

5. Background for evolution

5.1. Analysis methods

The linear and linearisation methods for a pressurised stainless steel piping system (SSPS), which was considered for phase-I of the Metallic Component Margins under High Seismic Loads (MECOS) benchmark exercise, are illustrated below.

5.1.1. Linear - models to be used

Response spectrum analysis is the most common method used by designers to analyse piping components under seismic load and carry out seismic design checks. Typical calculations are provided for SSPS under different levels of excitation, which are given in Table 5.1. A finite element model and the dimensions of the SSPS is shown in Figure 5.1. The test response spectra (TRS) in X, Y and Z directions for 2% damping are shown in Figures 5.2, 5.3 and 5.4 respectively. An evaluation of the elastic stresses for the piping system under seismic load (level D) was carried out, as per the procedure given in section-III, Division I, NB-3000 of the of the American Society of Mechanical Engineers (ASME) boiler and pressure vessel code. The Equation (9) of NB-3600 for level D service condition is given as:

$$B_1 \frac{PD_0}{2t} + B_2' \frac{M_i D_0}{2I} \leq 3S_m$$

(5.1-1)

For straight pipe, B_1= 0.5 and B_2= 1.0. For elbows, B_1= -0.1+0.4h, but not < 0 nor > 0.5

B_2= 0.87/h2/3 where, $h = \dfrac{tR}{r_m^2}$ D_0=0.168 m, t=0.0071 m, R=0.228 m and r_m = 0.08 m.

Figure 5.1. FE model of the piping system (SSPS)
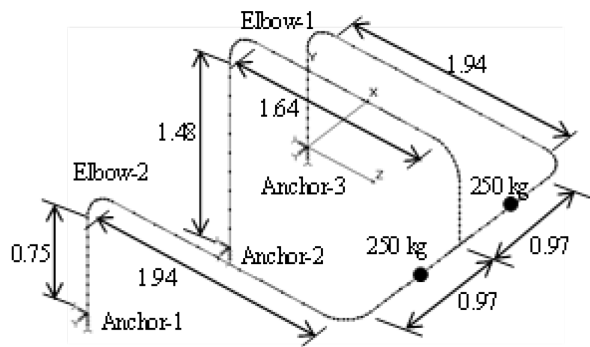
6" NB schedule 40 piping and long radius 90⁰ elbows are used

Source: Ravikiran, A., P.N. Dubey, M.K. Agrawal, G.R. Reddy, R.K. Singh and K.K. Vaze, 2015.

Figure 5.2. Test input spectrum in X-direction (horizontal) for 2% damping
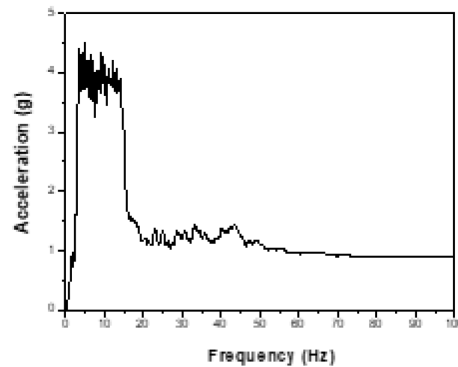
Source: Ravikiran, A., P.N. Dubey, M.K. Agrawal, G.R. Reddy, R.K. Singh and K.K. Vaze, 2015.

Figure 5.3. Test input spectrum in Z-direction (horizontal) for 2% damping
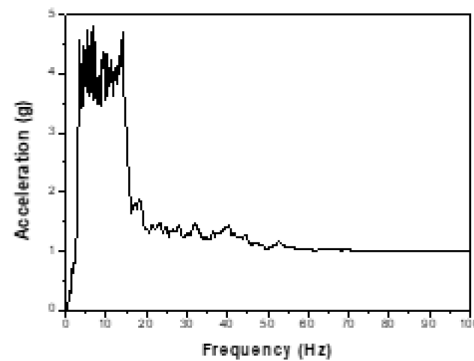
Source: Ravikiran, A., P.N. Dubey, M.K. Agrawal, G.R. Reddy, R.K. Singh and K.K. Vaze, 2015.

Figure 5.4. Test input spectrum in Y-direction (vertical) for 2% damping
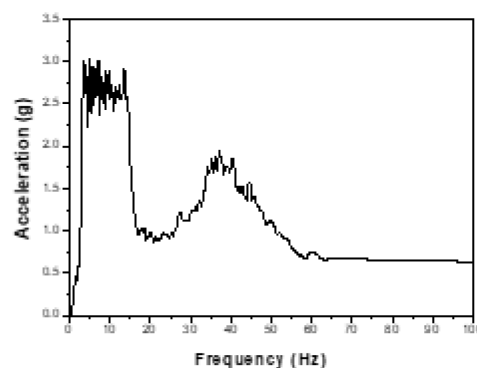
Source: Ravikiran, A., P.N. Dubey, M.K. Agrawal, G.R. Reddy, R.K. Singh and K.K. Vaze, 2015.

The TRS in three directions were applied to the piping model and a response spectrum analysis was carried out. The analysis revealed that elbow-1 was subjected to the maximum bending moment compared with other elbows. The primary stress in elbow-1 corresponded to various levels of excitation, which are shown in Table 5.1. One observation is that the

primary stress intensity exceeded the design limit of *3S~m~* at base excitation level corresponding to 1.75 g zero period acceleration (ZPA).

The limitation of this stress-based procedure is in obtaining strains and performance in terms of leakage in the piping systems.

Table 5.1. Details of various levels of base excitation for SSPS-1&2 tests

ZPA (g)	Internal pressure (MPa)	No. of base excitation time histories	Maximum primary stress Intensity (S_m)
1	12	5	1.72
1.25	12	5	2.15
1.5	12	5	2.58
1.75	12	5	3.02
2	12	5	3.45
2.25	12	5	3.88
2.5	12	5	4.31
2.5	14	30	4.31
2.5	16	8	4.31

5.1.2. Linearisation approach

The predominant failure mode for pressurised piping components under seismic load is fatigue-ratcheting (Kiran et al., 2018a; 2018b; 2017; 2015a; 2013), which is a strain-based phenomenon. This conclusion was drawn from earlier shake table tests on piping at the component level (Kiran et al., 2018a; 2018b), as well as system level (Kiran et al., 2017; 2015a; 2013; 2015b). There is therefore a need for a simplified numerical procedure that can be used by designers to predict ratcheting in piping components for a possible use of strain-based criterion. Carrying out detailed finite element analysis (FEA) for piping systems to predict ratcheting under seismic excitation is a cumbersome and expensive process, which requires advanced computing facilities. Detailed FEA is thus not a practical option for designers seeking to evaluate ratcheting in piping systems. A response spectrum analysis is a widely used procedure for performing the seismic design of piping systems. It would be useful for the designers if this analysis were to be extended/ modified so it can be used to predict ratcheting in piping systems. The extended method should still be validated by experimental results. The wavelet analysis of the test response of piping components (Kiran et al., 2018b) and systems (Kiran et al., 2015a; 2015b) led to the observations that natural frequencies reduce a little during the testing until failure occurs. This reduction suggests that the fatigue-ratcheting failure is local in nature and the global characteristics of the piping systems change slightly.

With this objective in mind, a linearisation technique known as the incremental iterative response spectrum (IIRS) method (Kiran et al., 2018a; 2018b; 2017; 2015a; 2013; 2015b) has been used to evaluate ratcheting strains in pressurised piping systems. The IIRS method has also been validated by experimental data at both the component level (Kiran et al., 2018a; 2018b) and the system level (Kiran et al., 2018a; 2018b; 2017; 2015a; 2013; 2015b). At the component level, the IIRS analysis was validated by the test results for a large radius stainless steel elbow with an outer diameter (OD) of 89mm and thickness (t) of 5.5 mm, which was subjected to internal pressure and incremental harmonic base excitation until failure occurred (Kiran et al., 2018a). The method was also validated by the test results of a short radius carbon steel elbow of same size subjected to internal pressure and incremental seismic excitation until failure occurred (Kiran et al., 2018b). In both cases, the strain accumulation from the IIRS method was observed to correlate reasonably well with the experimental results.

At the system level, the IIRS method was validated by shake table test results of six-inch carbon steel [3] and stainless steel (Kiran et al., 2018a; 2018b; 2017; 2015a; 2013; 2015b) piping systems of the same configuration, which were both subjected to the same internal pressure and incremental seismic load. This method was also validated by shake table test results of a three-inch carbon steel piping system (Kiran et al., 2013) subjected to internal pressure and incremental seismic load. The simulation of ratcheting by the IIRS method in these cases correlated reasonably well with the experimental results. The details of the IIRS method are provided below:

Description of the IIRS method

The IIRS method is based on an envelope moment-rotation curve that incorporates ratcheting. A flow chart for the IIRS method is given in Figure 5.5. This technique comprises two levels of analysis. In the first level, the envelope moment-rotation curves are generated for the elbow. These curves are generated from the ratcheting analysis of the pressurised components that are under incremental cyclic loading. In the second level of analysis, the whole piping system is modelled using pipe and elbow elements. A response spectrum analysis of the system is carried out to identify which components exceed yield limit, which are replaced with equivalent spring elements. Three translational and three rotational springs corresponding to each direction are used to represent the post-yield components. The spring constants are continuously modified from the envelope ratcheting moment-rotation curves by an increase in base excitation. The modification is carried out in an iterative way, which ensures that the resulting moment-rotation response of the component from response spectrum analysis matches the envelope characteristics obtained by the first level of analysis. The accumulated strain corresponding to each level of excitation is obtained from the cyclic moment-rotation-strain curves.

Figure 5.5. Flow chart of the incremental iterative response spectrum analysis of the piping system
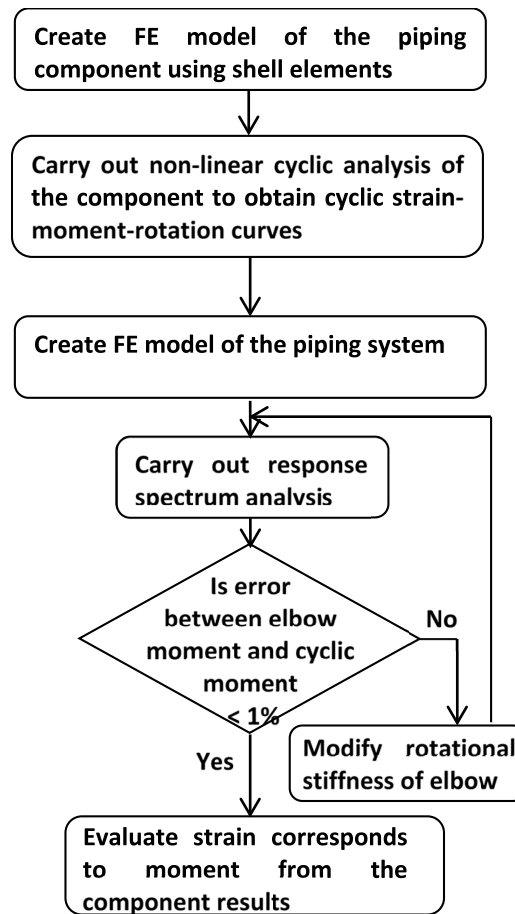
The details of the application of this method to the six-inch stainless steel piping system (SSPS) [4, 6] are provided below.

Level one: generation of envelope moment-rotation curve for the elbow:

Ratcheting analysis was carried out on 900 long radius elbows of the piping system. Figure 5.6 shows the finite element model of the elbow, which was modelled using shell elements. The ends were attached to straight pipes of a length of over three times diameter. A constant internal pressure of 12 Mpa, which corresponds to the design stress of $1S_{m,}$ was applied to the finite elements (FE) model. A cyclic non-linear static analysis was carried out to estimate the yield displacement, which forms the basis of ratcheting analysis. This analysis was carried out by incrementally applying a load to the tip of the elbow and the load displacement curve for the elbow is shown in Figure 5.7. The displacement corresponding to the yield was calculated by using the intersecting tangent method. The point of intersection of the two tangents to the elastic and plastic portion of curve was taken as the yield and the yield displacement (δy) was 30 mm. Based on this yield displacement, ratcheting analysis was carried out using the Chaboche model.

Figure 5.6. FE model of the elbow
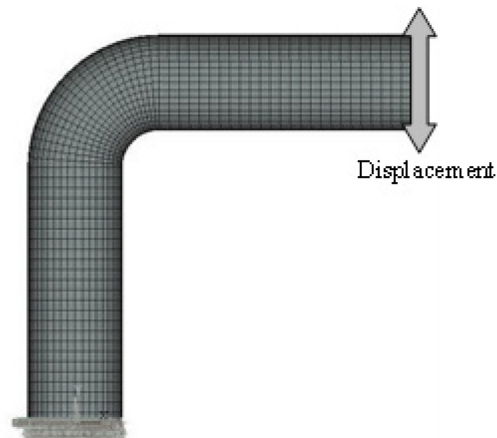
Source: Ravikiran, A., P.N. Dubey, M.K. Agrawal, G.R. Reddy, R.K. Singh and K.K. Vaze, 2015.

Figure 5.7. Determination of the yield displacement for elbow
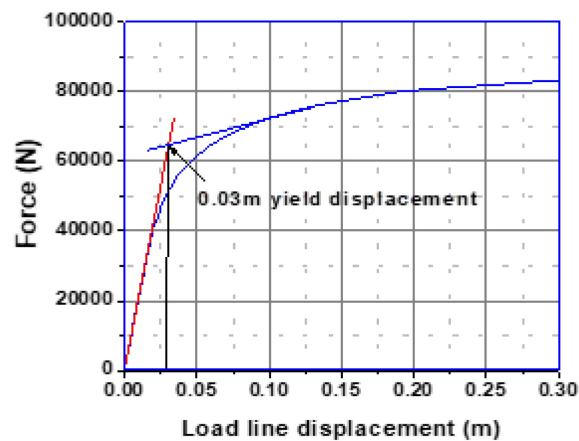
Source: Ravikiran, A., P.N. Dubey, M.K. Agrawal, G.R. Reddy, R.K. Singh and K.K. Vaze, 2015.

The Chaboche non-linear kinematic hardening model was used to simulate the ratcheting response. This model requires six parameters (Ci and γi, i=1, 2 and 3) for the three Armstrong-Frederick hardening rules. These parameters are determined from a uni-axial strain controlled stable hysteresis loop (Kulkarni, S.C., et al., 2004) generated from a strain controlled uni-axial strain cycling test. The equations used for the calculation of the three components of back stress (α_i) from the loading part of the hardening curves are given below.

$$\sum_{i=1}^{3} \alpha_i + \sigma_0 = \sigma_x$$

(5.1-2)

$$\alpha_i = \frac{C_i}{\gamma_i}\left[1 - 2\exp\left\{-\gamma_i\left(\varepsilon_x^p - \left(-\varepsilon_L^p\right)\right)\right\}\right]$$
, for i=1 and 2

(5.1-3)

$$\alpha_3 = C_3\varepsilon_L^p$$

(5.1-4)

C_1 should be a very large value to match the plastic modulus at the yielding and corresponding γ_1 also should be large enough to stabilise the hardening of α_1, which can be immediately calculated using Equation 5.1-3. C_3 is determined from the slope of the linear segment of the hysteresis curve at a high strain range. C_2 and γ_2 are evaluated by trial to produce a good representation of the experimental stable hysteresis curve, which also satisfies the relationship

$$\frac{C_i}{\gamma_i} + \frac{C_2}{\gamma_2} + \sigma_0 = \sigma_x - \frac{C_2}{2}\left\{\varepsilon_x^p - \left(-\varepsilon_L^p\right)\right\}$$

(5.1-5)

at or close to the plastic strain ε_L^p.

The Chaboche parameters C_1= 1 085 000, C_2=43 000, C_3=4 100, γ_1= 271 250, γ_2=300 and γ_3=9 are considered for the SS304L material. Figure 5.8 shows the comparison of the stable hysteresis loop by the Chaboche model with the experiment. Ratcheting analysis was carried out on the elbow subjected to internal pressure and a cyclic bending load. The loading details for the ratcheting analysis of the elbow are given in Table 5.2 and the applied load line displacement time history is shown in Figure 5.9.

Table 5.2. Loading details for the ratcheting analysis of the elbow

Displacement amplitude	No of cycles
0 to d_y	10 cycles
1.1 d_y	10 cycles
1.2 d_y	10 cycles
1.3 d_y	10 cycles
1.4 d_y	10 cycles
1.5 d_y	10 cycles

Figure 5.8. Comparison of the stable hysteresis loop by the Chaboche model with the experiment
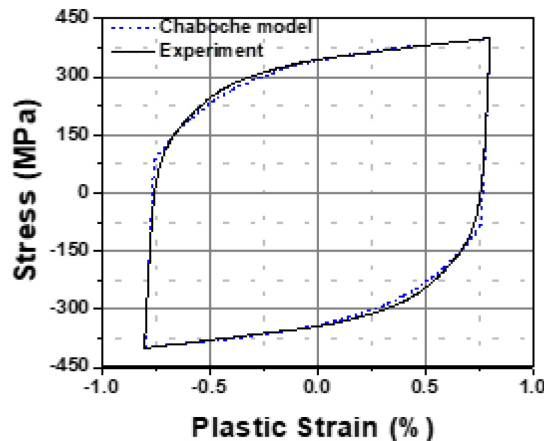
Source: Ravikiran, A., P.N. Dubey, M.K. Agrawal, G.R. Reddy, R.K. Singh and K.K. Vaze, 2015.

Figure 5.9. Load line displacement time history at the free end of the pipe
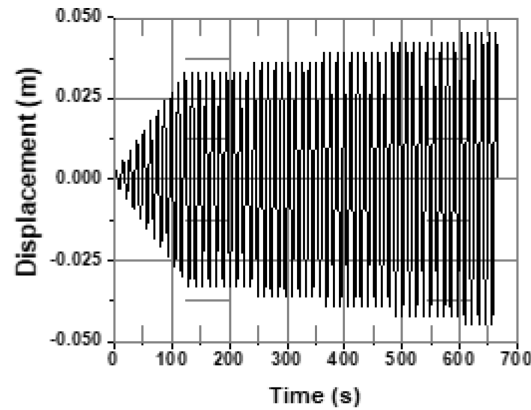
Source: Ravikiran, A., P.N. Dubey, M.K. Agrawal, G.R. Reddy, R.K. Singh and K.K. Vaze, 2015.

The variation of the moment with hoop strain at the crown of the elbow is shown in Figure 5.10. The moment rotation hysteresis loops for the elbow are shown in Figure 5.11. The cyclic strain-moment-rotation curve is obtained by joining the peak of each cycle in strain-moment to the moment-rotation plots, which is shown in Figure 5.12.

Figure 5.10. Variation of the moment with hoop strain at the crown of the elbow
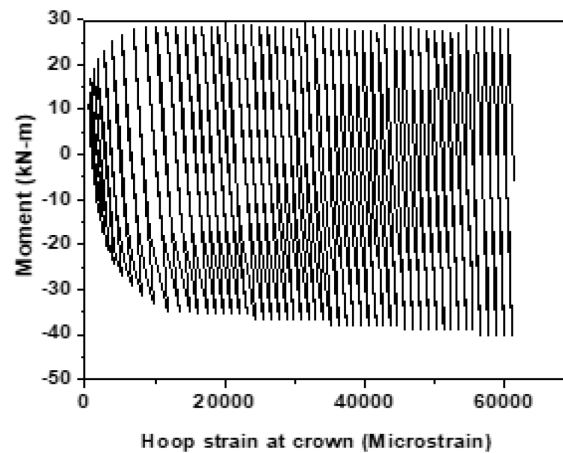
Source: Ravikiran, A., P.N. Dubey, M.K. Agrawal, G.R. Reddy, R.K. Singh and K.K. Vaze, 2015.

Figure 5.11. Moment-rotation hysteresis loops for the elbow
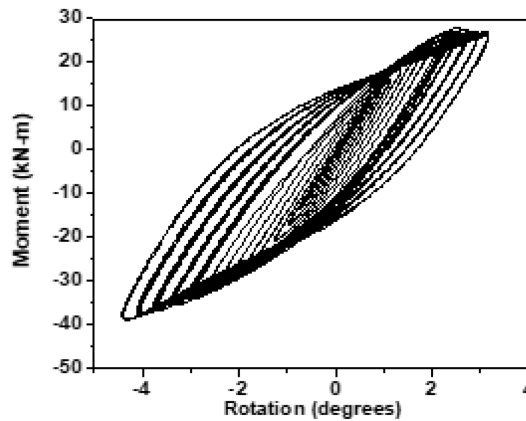
Source: Ravikiran, A., P.N. Dubey, M.K. Agrawal, G.R. Reddy, R.K. Singh and K.K. Vaze, 2015.

Figure 5.12. Cyclic strain-moment-rotation curves
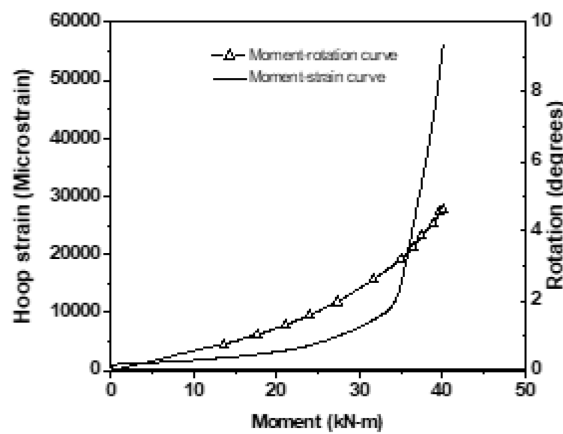
Source: Ravikiran, A., P.N. Dubey, M.K. Agrawal, G.R. Reddy, R.K. Singh and K.K. Vaze, 2015.

IIRS analysis for piping system

IIRS analysis is carried out on the piping system with the spring model shown in Figure 5.13. The figure also shows the details of the spring model in the elbow local co-ordinate system. The spring contains three translational and three rotational springs. The three translational springs in x_l, y_l and z_l directions are denoted as k_{Tx}, k_{Ty} and k_{Tz} respectively. Corresponding rotational springs in x_l, y_l and z_l directions are k_{Rx}, k_{Ry} and k_{Rz} respectively. The spring constants are evaluated numerically from the static analysis on the elbow. A comparison of the natural frequencies of the piping system is given in Table 5.3. An observation that can be made is that the frequencies of the analysis correspond well with experiment. The natural frequencies change slightly when the elbow is replaced by the spring model.

Table 5.3. Comparison of the natural frequencies of the piping system

Mode no	Natural frequency (Hz)		
	Sine sweep test SSPS-1	Analysis (model with pipe and elbow elements)	Analysis on piping model with springs replacing elbow
1	3.83	3.65	3.63
2	6.0	5.68	5.27
3	16	14.71	13.82

Figure 5.13. FE model of the piping system by replacing the elbow with springs
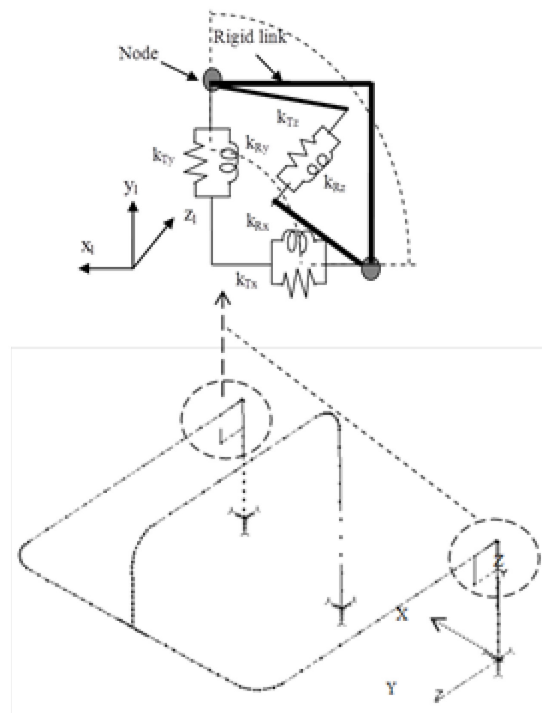
Source: Ravikiran et al., 2015.

IIRS analysis was carried out alongside constant internal pressure. The increasing excitation and cyclic characteristics of the elbow shown in Figure 5.12 were used. The analysis was started by applying a base excitation of 1 g ZPA to the piping model. As a result, there was plane moment (M_{elb}) and rotation (θ_{elb}) for Elbow-1, which were 15.52 kN-m and 0.85° respectively. The envelope moment corresponding to this rotation was 14.9 kN-m and the error 4.18%. The in-plane rotational stiffness of the elbow was modified to 0.96 MN-m/rad and second iteration of response spectrum analysis carried out with 1 g ZPA. The resulting moment and envelope moment were 15.34 and 15.03 kN-m respectively, which corresponded to a rotation of 0.87° and error of 2.04%. The in-plane rotational stiffness of the elbow was modified to 0.94 MN-m/rad and a third iteration of response spectrum analysis was carried out with 1 g ZPA. The resulting moment and envelope moment were 15.24 and 15.32 kN-m respectively, which corresponded to a rotation of 0.89° and error of -0.53%. The solution is thereby converged. The strain corresponding to this moment was 2 516 με, which is shown in Figure 5.12. Further iterative analysis was carried out for the excitation, which corresponded to a ZPA of 1.25 g

to 2.5 g with an interval of 0.25 g. The converged elbow moment was 33.29 kN-m, which corresponded to n excitation of 2.5 g. The strain corresponding to this moment was 9 224 με. Various levels of this analysis have been plotted on an envelope moment-rotation curve shown in Figure 5.14. A comparison of the predicted strain accumulation with the test results is shown in Figure 5.15. The results of the iterative response spectrum analysis are provided in Table 5.4. The ratcheting strain predicted by the iterative response spectrum method closely matches the experimental results.

Table 5.4. Results of IIRS analysis

ZPA (g)	Iter. no.	kRz (MN-m/rad)	M_{elb} (kN-m)	θ_{elb} (deg.)	M_{elbc} (kN-m)	Error (%)	ε_{elb}
1	1	1.0	15.52	0.85	14.9	4.18	2 516
	2	0.96	15.34	0.87	15.03	2.04	
	3	0.94	15.24	0.89	15.32	-0.53	
1.25	1	0.94	18.76	1.11	19.03	1.46	3 080
	2	0.93	18.9	1.12	18.95	0.28	
1.5	1	0.93	23.5	1.38	23.5	6.91	3 860
	2	0.87	23.01	1.45	23.01	1.96	
	3	0.85	22.87	1.47	22.87	0.73	
1.75	1	0.85	25.82	1.66	25.82	4.87	4 655
	2	0.81	25.41	1.71	25.41	0.85	
2	1	0.81	29.04	1.96	29.04	7.17	5 870
	2	0.76	28.36	2.05	28.36	1.89	
	3	0.74	28.18	2.07	28.18	0.68	
2.25	1	0.74	32.12	2.36	32.12	6.94	7 562
	2	0.7	31.36	2.47	31.35	1.90	
	3	0.68	31.14	2.5	31.14	0.70	
2.5	1	0.68	34.16	2.74	34.16	5.00	9 224
	2	0.65	33.52	2.82	33.52	1.67	
	3	0.64	33.29	2.85	33.3	0.45	

Figure 5.14. Various levels of the IIRS analysis on the cyclic moment-rotation curve
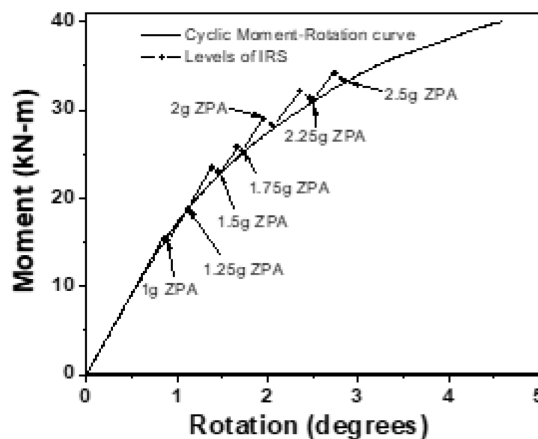
Source: Ravikiran, A., P.N. Dubey, M.K. Agrawal, G.R. Reddy, R.K. Singh and K.K. Vaze, 2015.

Figure 5.15. Comparison of the predicted strain accumulation with the test results
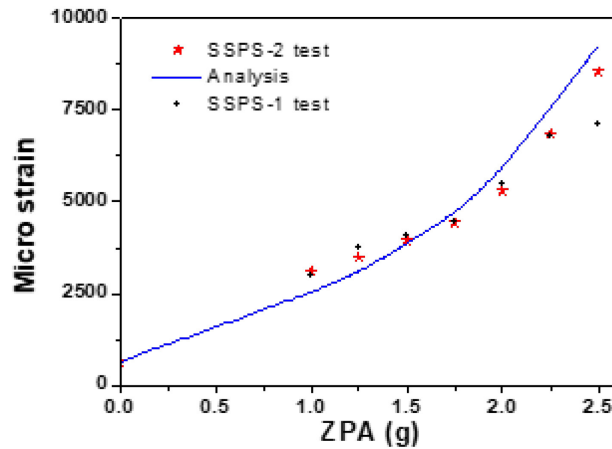
Source: Ravikiran, A., P.N. Dubey, M.K. Agrawal, G.R. Reddy, R.K. Singh and K.K. Vaze, 2015.

It can be concluded that the incremental iterative response spectrum method can be used to evaluate ratcheting strains in pressurised piping systems. The performance limits can also be fixed at a 5% strain limit, which is similar to the alternate strain-based criterion provided by an earlier version of the ASME code.

5.1.3. References

Kiran, A.R., G.R. Reddy and M.K. Agrawal (2018a), "Experimental and Numerical Studies on Inelastic Dynamic Behaviour of Stainless Steel Elbow under Harmonic Base Excitation", *Journal of Pressure Vessel Technology*, 140(2), pp.1-9.

Kiran, A.R., G.R. Reddy and M.K. Agrawal (2018b), "Experimental and numerical studies of inelastic behaviour of thin walled elbow and tee joint under seismic load", *Thin-Walled Structures*, Volume 127, pp.700-709.

Kiran, R.A, G.R. Reddy, P.N. Dubey and M.K. Agrawal (2017), "Fatigue-Ratcheting Behaviour of 6 in Pressurised Carbon Steel Piping Systems Under Seismic Load: Experiments and Analysis", *Journal of Pressure Vessel Technology*, 139(6), pp.1-15.

Kulkarni, S.C., Y.M. Desai, T.A.R.U.N. Kant, G.R. Reddy, P. Prasad, K.K. Vaze and C. Gupta (2004), "Uniaxial and biaxial ratchetting in piping materials—experiments and analysis", *International Journal of Pressure Vessels and Piping*, Volume 81, pp.609-617.

Ravikiran, A., P.N. Dubey, M.K. Agrawal and G.R. Reddy (2015), "Experimental and Numerical Studies of Ratcheting in Pressurised Stainless Steel Piping Systems under Seismic Load", BARC External Report No. SIRD/BARC/2015/E/018, Bhabha Atomic Research Centre, Mumbai, India.

Ravikiran, A., P.N. Dubey, M.K. Agrawal, G.R. Reddy, R.K. Singh and K.K. Vaze (2015), "Experimental and Numerical Studies of Ratcheting in a Pressurised Piping System under Seismic Load", *Journal of Pressure Vessel Technology*, 137(3), pp.1-7.

Ravikiran, A., P.N. Dubey, M.K. Agrawal, G.R. Reddy and K.K. Vaze (2013), "Evaluation of Inelastic Seismic Response of Piping System Using Modified Iterative Response Spectrum Method," *ASME Journal of Pressure Vessel Technology*, 135(4).

5.2. Proposed elastic-plastic code case in Japan

5.2.1. Background

Following the accident at the Fukushima Daiichi Nuclear Power Plant during the 2011 Great East Japan Earthquake disaster, the regulatory requirements on the design of seismic ground motion have tended to greatly increase in Japan. Piping systems used in the existing nuclear power plants have also been re-examined under the reassessed seismic motion. If they do not comply with the allowable stress level of the current seismic design code, which is essentially based on the elastic stress analysis, seismic retrofitting is required. However, there is also widespread recognition of the fact that piping systems have a large safety margin until boundary failure can occur, even when the input seismic load exceeds the design basis level. The reason for this protection is attributed to the large strength capacity of piping systems due to plastic deformation.

A task group (TG) activity under the Japan Society of Mechanical Engineers (JSME) has been conducted (Nakamura, et al., 2015) to establish an evaluation procedure that takes the elastic-plastic behaviour of piping systems into account in a rational way. A code case in the framework of the JSME nuclear codes and standards has been developed as a product of this activity. The code case provides strain-based criteria and evaluation procedure by a detailed inelastic response analysis with the finite element methods' (FEM) model.

A fatigue evaluation of piping systems is currently being conducted in Japan in accordance with JEAC4601-2015 (The Japan Electric Association, 2015), which is essentially based on an elastic response analysis and stress-based fatigue criteria. In contrast, the newly proposed code case gives fatigue evaluation procedures by a detailed inelastic response analysis and strain-based fatigue criteria. As for the primary stress, the code case must satisfy a stress limit that is the same as that in JEAC4601-2015, when mechanical loads other than the seismic load are considered.

The code case is entitled "An alternative rule on seismic qualification of seismic S class piping systems by detailed inelastic FE response analysis". Its content is as follows:

- main body of the code case (Morishita et al., 2017);

- mandatory Appendix SEGP-I: the guideline of a detailed inelastic response analysis methods for piping systems (analysis guideline) (Otani et al., 2017);

- non-mandatory Appendix SEGP-A: the method for the verification and validation;

- non-mandatory Appendix SEGP-B: the report of the benchmark analyses and the parametric analyses on piping systems.

The contents of the main body of the code case are described in 5.25.2-2. The contents of the mandatory Appendix SEGP-I are described in 5.25.2-3. The contents of non-mandatory appendix and some technical discussions about the code case and analysis guideline are discussed in the references (Nakamura et al., 2015; Nakamura et al., 2016; Morishita et al., 2017; Otani et al., 2017; Nakamura et al., 2017; Watakabe et al., 2017).

Note: the code case has been approved by the JSME Committee and published by the JSME in June 2019. The contents of the code case and the technical background are discussed in the references (Morishita et al., 2020; Nakamura et al., 2020).

5.2.2. Main body of the code case

Nomenclature

E	modulus of elasticity
N_{eq}	equivalent number of the load cycles of the earthquake
S_a	peak stress amplitude of the design fatigue curve
S_p	peak stress intensity
U_{AB}	fatigue usage factor of operation conditions A and B
U_{Ss}	fatigue usage factor by design earthquake load
U_f	total fatigue usage factor (UAB + USs)
$\varepsilon_x^p, \varepsilon_y^p, \varepsilon_z^p$	spatial components of the normal plastic strain
$\gamma_{xy}^p, \gamma_{yz}^p, \gamma_{zx}^p$	spatial components of the shear plastic strain
$\sigma_x^p, \sigma_y^p, \sigma_z^p$	spatial components of the normal stress
$\tau_{xy}^p, \tau_{yz}^p, \tau_{zx}^p$	spatial components of the shear stress

Fatigue evaluation procedure

In the route of fatigue evaluation by detailed inelastic response analysis, the equivalent strain amplitude is used as a measure and procedure for fatigue evaluation using the design fatigue curve given by the JSME Code (The Japan Society of Mechanical Engineers, 2012a). Using equivalent strain in the fatigue evaluation, instead of principal strain, is a similar approach to the one from ASME Section III, Division 5, Appendix HBB-T, HBB-T-1413. In design, there may be cases where the orientation of fatigue cracks is unknown and therefore the direction of the principal strain is also unknown. In consideration of these cases, the code case uses equivalent strain, which is independent of spatial directions.

The following two procedures are given as success criteria:

1. Limit to the maximum value of equivalent strain amplitude (half of the strain range);

2. Limit to the fatigue usage factor calculated from the series of the equivalent strain amplitude.

The code case does not allow fatigue evaluation by a detailed inelastic analysis and strain criteria to be applied to local strain concentrations such as weld joints because, material discontinuities, for example, are not accounted for in the detailed inelastic analysis.

The series of the equivalent strain amplitude can be calculated by the following six steps:

- Step 1: identify the component among each spatial component of plastic strain at the point of evaluation with maximum amplitude and treat it as the representative one.

- Step 2: extract peaks (both positive and negative) from the time history of the representative plastic strain component.

- Step 3: remove minor peaks from the extracted peaks that might be contained due to, for example, the contribution of higher frequency modes.

- Step 4: let the series of time of occurrence of the major peaks of the representative plastic strain time history be t_i (i=1, 2, 3, .., n).

- Step 5: let the spatial components of stress and plastic strain at time t_i be ($\sigma_{x,i}$, $\sigma_{y,i}$, $\sigma_{z,i}$, $\tau_{xy,i}$, $\tau_{yz,i}$, $\tau_{zx,i}$) and ($\varepsilon^p_{x,i}$, $\varepsilon^p_{y,i}$, $\varepsilon^p_{z,i}$, $\gamma^p_{xy,i}$, $\gamma^p_{yz,i}$, $\gamma^p_{zx,i}$) respectively.

- Step 6: successively calculate the equivalent strain range $\Delta\bar{\varepsilon}_i$ between the adjacent peaks i and i+1, using Equations from (5.2-1) to (5.2-4).

$$\Delta\bar{\varepsilon}_i = \Delta\bar{\varepsilon}_i^e + \Delta\bar{\varepsilon}_i^p , i = 1, 2, 3, ..., n-1 \tag{5.2-1}$$

The equivalent elastic strain range is here defined as

$$\Delta\bar{\varepsilon}_i^e = \Delta\bar{\sigma}_i / E \tag{5.2-2}$$

where

$$\Delta\bar{\sigma}_i = \sqrt{\frac{1}{2}} \left[\begin{array}{l} \left(\Delta\sigma_{x,i} - \Delta\sigma_{y,i}\right)^2 + \left(\Delta\sigma_{y,i} - \Delta\sigma_{z,i}\right)^2 + \left(\Delta\sigma_{z,i} - \Delta\sigma_{x,i}\right)^2 \\ +3\left\{ \left(\Delta\tau_{xy,i}\right)^2 + \left(\Delta\tau_{yz,i}\right)^2 + \left(\Delta\tau_{zx,i}\right)^2 \right\} \end{array} \right]^{\frac{1}{2}} \tag{5.2-3}$$

$$\Delta\sigma_{x,i} = \sigma_{x,i+1} - \sigma_{x,i}, \Delta\sigma_{y,i} = \sigma_{y,i+1} - \sigma_{y,i}, ..., etc$$

The equivalent plastic strain range is:

$$\Delta\bar{\varepsilon}_i^p = \frac{\sqrt{2}}{3} \left[\begin{array}{l} \left(\Delta\varepsilon^p_{x,i} - \Delta\varepsilon^p_{y,i}\right)^2 + \left(\Delta\varepsilon^p_{y,i} - \Delta\varepsilon^p_{z,i}\right)^2 + \left(\Delta\varepsilon^p_{z,i} - \Delta\varepsilon^p_{x,i}\right)^2 \\ +\frac{3}{2}\left\{ \left(\Delta\gamma^p_{xy,i}\right)^2 + \left(\Delta\gamma^p_{yz,i}\right)^2 + \left(\Delta\gamma^p_{zx,i}\right)^2 \right\} \end{array} \right]^{\frac{1}{2}} \tag{5.2-4}$$

$$\Delta\varepsilon^p_{x,i} = \varepsilon^p_{x,i+1} - \varepsilon^p_{x,i}, \Delta\varepsilon^p_{y,i} = \varepsilon^p_{y,i+1} - \varepsilon^p_{y,i}, ..., etc$$

The definition of the equivalent stress range and plastic strain range in Equations (5.2-3) and (5.2-4) are identical to that given in ASME Section III, division 5 in Appendix HBB-T, HBB-T-1413.

(a) Limit to the maximum value of the equivalent strain amplitude

In this route, the maximum value of equivalent strain amplitude is obtained by

$$\bar{\varepsilon}_{max} = \frac{1}{2}\max\left[\Delta\bar{\varepsilon}_i, i = 1, 2, 3, ..., n-1 \right] \tag{5.2-5}$$

This maximum value satisfies Equation (5.2-6):

$$\bar{\varepsilon}_{\max} < S_a\left(N_{eq}{}'\right)/E$$

(5.2-6)

where $S_a(N_{eq}{}')$ is the value of peak stress intensity determined from a reading made the design fatigue curve of the modified number of equivalent load cycles of the earthquake to be considered, as follows:

$$N_{eq}{}' = N_{eq}/\left(1-U_{AB}\right)$$

(5.2-7)

It should be noted that the modified number of equivalent earthquake loading $N_{eq}{}'$ has been introduced to limit the sum of the fatigue usage factors by the earthquake and operating conditions A and B to less than, or equal to, unity.

(b) Limit to the fatigue usage factor

The equivalent number of earthquake load cycles usually contains conservatism in the design practice in Japan (approximately 50~300 cycles, depending on each plant site's condition and the character of the design earthquake), the code case provides another procedure of fatigue evaluation that directly calculates a cumulative fatigue usage factor and strain time history in order to enable further rational fatigue evaluation.

In this route, a series of peak amplitude S_p^i is created by multiplying the series of equivalent strain range calculated in with steps 1 to 6 by $E/2$.

The cumulative fatigue usage factor by the design earthquake load can be calculated by Equation (5.2-8), which is provided below,

$$U_{S_z} = \sum_{1}^{n-1} \frac{1}{2N_i\left(S_p^i\right)}$$

(5.2-8)

$N_i(S_p^i)$ is the allowable number of load cycles in the design fatigue curve at the level with the peak stress amplitude. The factor of 2 is added into the denominator to account for the fact that $N_i(S_p^i)$ corresponds to a half cycle and not a full reversed cycle.

The sum of the fatigue usage factors by the operating conditions A and B and by the design earthquake satisfies Equation (5.2-9) provided below:

$$U_f = U_{AB} + U_{S_z} \leq 1$$

(5.2-9)

Inelastic response analysis is known to sometimes yield a fictitious ratcheting strain that is much larger than the test results. However, the code case does not require a consideration of ratchet strain in fatigue evaluation. The reasons for this is as follows:

- The results of piping component fatigue tests from previous studies are shown in Figure 6.7 (Arai et al., 2016). Most of the piping component fatigue test results in Figure 6.7 are with residual strain due to ratcheting, which ranges from about 5 to 30%. Nevertheless, this data shows that there is a significant amount of design margin in the design fatigue curve.

- According to the studies by Hasunuma et al. (2011) and Nakane et al. (2011), the low cycle fatigue lives with a large tensile pre-strain for up to 16%, or with a linearly increasing mean strain for up to 10%. These are within the range of usual fatigue data scatter. No apparent reduction of fatigue life was also observed.

- Considering that the equivalent number of earthquake load cycles ranges from around 50 cycles to 300 cycles, depending on the plant site's conditions, the design fatigue curve limits the strain amplitude to about 0.5~1%. No significant ratcheting is expected to occur within these design conditions (of the strain amplitude and number of cycles).

5.2.3. Analysis guideline

Contents of the analysis guideline

The mandatory Appendix SEGP-I is the analysis guideline for the seismic inelastic response time history analysis for piping (Otani et al., 2017). The guideline provides the elastic-plastic response analysis method used to take the seismic response reduction of piping by plastic deformation into consideration. The following are the contents of the analysis guideline.

- Mandatory Appendix SEGP-I
- SEGP-I-1000   General
- SEGP-I-1100   Analysis method
- SEGP-I-1200   Analysis type
- SEGP-I-1300   Analysis code
- SEGP-I-1200   The details of modelling condition
- SEGP-I-2100   Modelling of piping
- SEGP-I-2110   Element type
- SEGP-I-2120   Mesh size
- SEGP-I-2130   Material property
- SEGP-I-2140   Damping ratio
- SEGP-I-2200   Modelling of supports
- SEGP-I-2300   Seismic input
- SEGP-I-2400   Load applied with seismic input
- SEGP-I-3000   The post process for analysis output data
- SEGP-I-3100   Evaluation point and output data
- SEGP-I-3200   Calculation for evaluation

Some important items in the analysis guideline are explained in the following sections. For other items, see the reference by Otani et al. (2017).

Analysis type

The analysis guideline allows the following analysis types to be applied:

- An elastic-plastic seismic response analysis of the piping: a dynamic analysis using the time history analysis method with non-linear geometry and plastic material property.

- An elastic-plastic static analysis of the piping component: a static analysis of an individual piping component of interest with non-linear geometry and plastic material property.

The analytical guideline allows to use the following three kinds of modelling methods for the inelastic analysis of piping systems.

1. Full analysis model: the entire piping system is modelled by shell or solid elements.

2. Hybrid analysis model: the piping system is modelled mainly by beam elements. Some pipe components at which significant plastic strain is expected are modelled by shell elements.

3. Zoom-up analysis model: a combination of the dynamic analysis model, which has beam elements to obtain the dynamic behaviour of the piping system, and a static analysis model, which has shell elements to estimate the local strain behaviour.

Figure 5.16 shows examples of analysis model. The dynamic behaviour of the piping system and the local strain behaviour can be obtained simultaneously for the analytical model of a "full analysis model" and "hybrid analysis model". Concerning the "zoom-up analysis model", it is necessary to conduct the static analysis to obtain the inelastic strain, which is used in the fatigue estimation. The analysis type (a) elastic-plastic seismic response analysis of piping is used in all three analytical modelling methods to obtain the dynamic elastic-plastic response of piping system. The analysis type (b) elastic-plastic static analysis of piping component is used in the "zoom-up analysis model".

Figure 5.16. Analysis model types

(a) Full analysis model

(b) Hybrid analysis model

Beam element

Shell element

(c) Zoom-up analysis model

Beam element model for dynamic analysis

Shell element model for static analysis
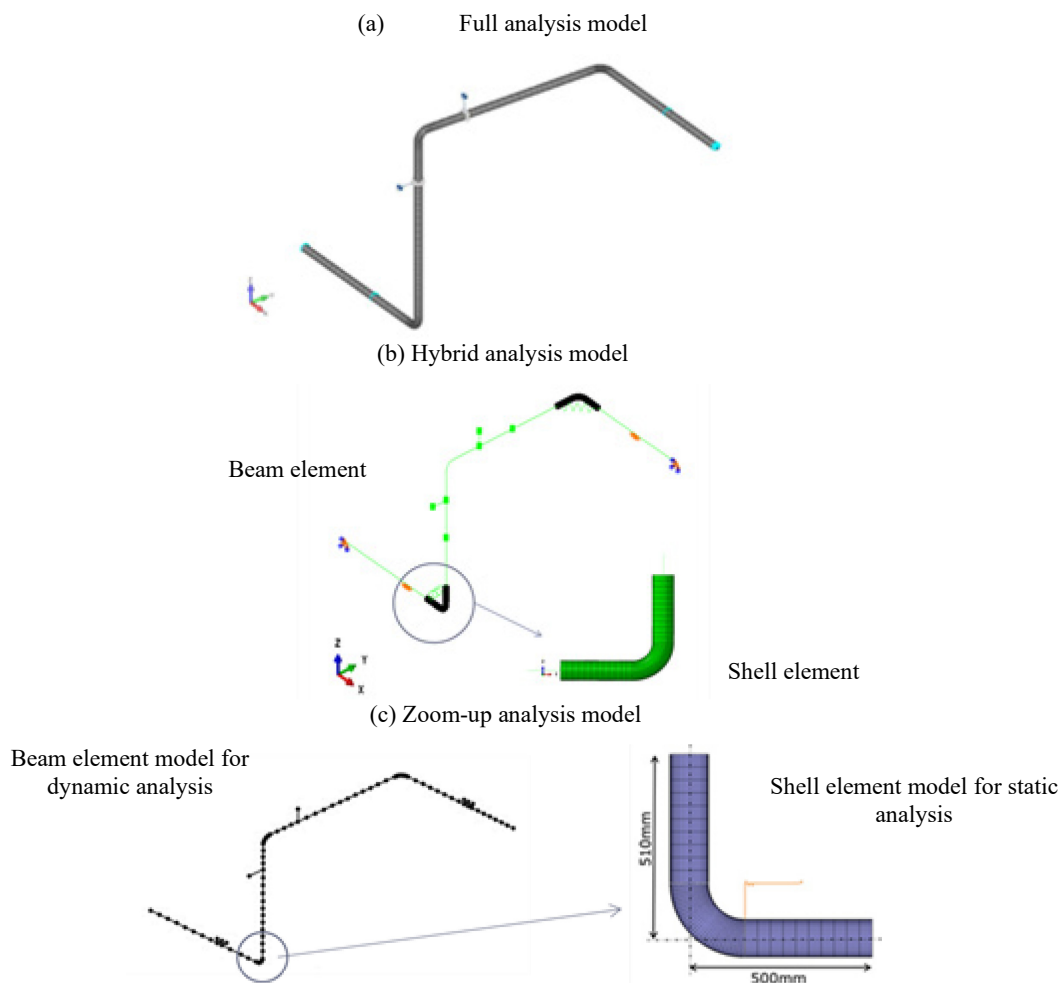
Material property

The analysis guideline recommends using the kinematic hardening rule with a bilinear stress-strain curve when the users model the material property. A more sophisticated constitutive law is acceptable if it is confirmed to be a reliable model.

Yield stress (σ_y) and work hardening modulus (E_2) for the bilinear approximation are determined as shown in the below equations:

$$\sigma_y = C_y \cdot S_y \tag{5.2-10}$$

$$E_2 = \frac{1}{C_E} E \tag{5.2-11}$$

where σ_y: yield stress of bilinear stress-strain curve [MPa]; C_y: coefficient of yield stress; S_y; the yield stress specified in design code [MPa]; E_2: work hardening modulus (the secondary slope of bilinear stress-strain curve); C_E: coefficient of the secondary slope; and E: Young's modules. S_y and E in these equations are specified in the JSME material code (The Japan Society of Mechanical Engineers, 2013).

The specific determination for C_y and C_E are as follows;

For carbon steel pipe: C_y=1.2, C_E=100

For stainless steel pipe:

SUS304 (Japanese Industrial Standards):

$$C_y = 2.29 \times 10^{-4} \cdot T + 1.24 \tag{5.2-12}$$

$$C_E = 69$$

SUS316 (Japanese Industrial Standards):

$$C_y = 2.16 \times 10^{-4} \cdot T + 1.28 \tag{5.2-13}$$

$$C_E = 75$$

where T: temperature (degrees Celsius, RT≤T≤425).

C_y and C_E for carbon steel pipe could be decided by referencing previous research (Watakabe et al., 2017; Nakamura et al., 2017; Nara et al., 2004). It is harder to determine a bilinear approximation for the stainless steel pipe. The equations for the stress-strain curve of stainless steel provided by the JSME design code for fast reactor power plant facilities (The Japan Society of Mechanical Engineers, 2012b) is applied in the analytical guideline in order to model the true stress-true strain curve, after which the bilinear approximation is conducted. C_y and C_E for stainless steel pipe is decided so that the energy of the original stress-strain curve and the energy of the bilinear approximation are equivalent, under the condition of the maximum strain being 3%. Figure 5.17 shows a schematic illustration of this procedure. It is also possible to use a result from an actual material test instead of the true stress-true strain curve that is determined by the code.

Figure 5.17. The bilinear approximation procedure for the stainless steel pipe's stress-strain curve
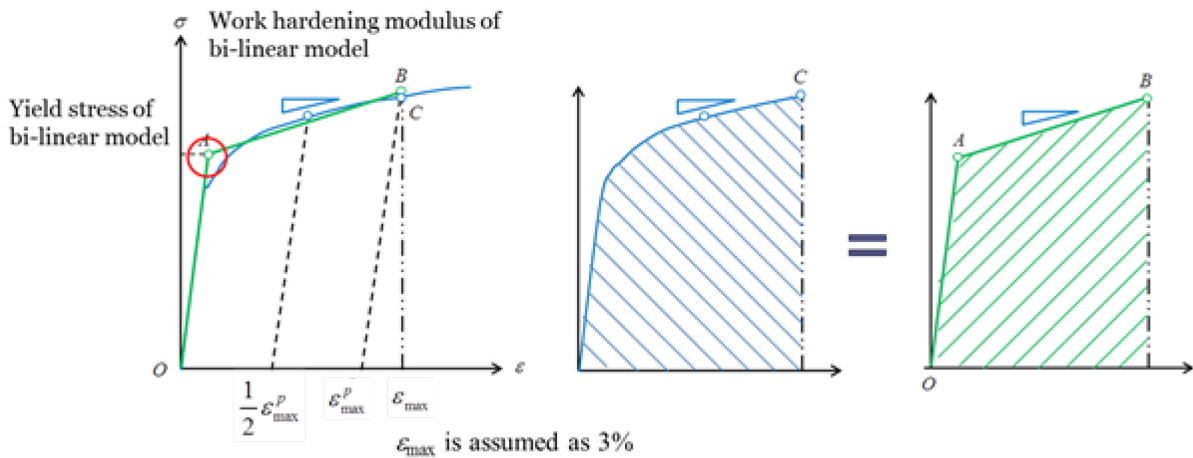
5.2.4. References

Arai, M., N. Kojima, T. Kabaya, S. Hirouchi and M. Bando (2016), "Investigation on Method of Elasto-Plastic Analysis for Piping System (Benchmark Analysis)", *Pressure Vessels and Piping Conference*, 50466, PVP2016-63186.

Hasunuma, S., Y. Miyata, T. Ogawa and K. Sakaue (2011), "Effect of Pre-Strain on Low Cycle Fatigue Strength of Austenitic Stainless Steel SUS316NG", *Transactions of the JSME, Series A,* 77(777), pp.843-851.

Morishita, M., A. Otani, I. Nakamura, T. Watakabe, T. Shibutani and M. Shiratori (2020), "A JSME Code Case on Piping Seismic Design Based on Inelastic Response Analysis and Strain-Based Fatigue Criteria", *Journal of Pressure Vessel Technology,* 142(2).

Morishita, M., A. Otani, T. Watakabe, I. Nakamura, T. Shibutani and M. Shiratori (2017), "Seismic Qualification of Piping Systems by Detailed Inelastic Response Analysis Part 1 - A Code Case for Piping Seismic Evaluation Based on Detailed Inelastic Response Analysis", *Pressure Vessels and Piping Conference, 58035*, PVP2017-65166.

Nakamura, I., A. Otani, M. Morishita, M. Shiratori, T. Watakabe and T. Shibutani (2017), "Seismic Qualification of Piping Systems by Detailed Inelastic Response Analysis Part 3 - Variation in Elastic-Plastic Analysis Results on Carbon Steel Pipes from the Benchmark Analysis and the Parametric Analysis", *ASME 2017 Pressure Vessels and Piping Conference*, ASME, United States, PVP2017-65316.

Nakamura, I., A. Otani, T. Shibutani, M. Morishita and M. Shiratori (2016), "Findings from the Benchmark Analyses on an Elbow In-Plane Bending Test and a Piping System Test", *Proceedings of the ASME 2016 Pressure Vessels and Piping Conference*, PVP2016-63419.

Nakamura, I., M. Shiratori, A. Otani, M. Morishita, T. Shibutani and H. Nakamura (2015), "A Research Activity on the Seismic Safety Evaluation of Nuclear Piping Systems Taking the Effect of Elastic-Plastic Behaviour into Account", *Proceedings of the ASME 2015 Pressure Vessels and Piping Conference*, PVP2015-45262.

Nakamura, I., T. Watakabe, A. Otani, T. Shibutani, M. Morishita and M. Shiratori (2020), "Benchmark Analyses on the Elastic–Plastic Behaviour of Carbon Steel Pipes Under Seismic Load", *Journal of Pressure Vessel Technology,* 142(2), pp.021901-1-021901-14.

Nakane, M., S. Kanno and Y. Takagi (2011), "Effect of Cyclic Pre-Strain on Low Cycle Fatigue Live at Middle High Temperature", *Transactions of the JSME, Series A,* 77(777), pp.694-697.

Nara, K., K. Nakamura, H. Yasunami, F. Kawabata and T. Shiwaku (2004), "Static Investigation for Thickness and Strength of Structural Steel Plate Used for Bridge", *Journal of Japan Society of Civil Engineers,* 752/*I-66*, pp.299-310.

Otani, A., T. Shibutani, M. Morishita, I. Nakamura, T. Watakabe and M. Shiratori (2017), "Seismic Qualification of Piping Systems by Detailed Inelastic Response Analysis Part 2 - A Guideline for Piping Seismic Inelastic Response Analysis", *Proceedings of the ASME 2017 Pressure Vessels and Piping Conference*, PVP2017-65190.

The Japan Electric Association (2008), Technical Code for Seismic Design of Nuclear Power Plants, JEAC4601.

The Japan Society of Mechanical Engineers (2012a), "Codes for Nuclear Power Generation Facilities - Rules on Design and Construction for Nuclear Power Plants", JSME S NC1-2012.

The Japan Society of Mechanical Engineers (2012b), "Codes for Nuclear Power Generation Facilities - Rules on Design and Construction for Nuclear Power Plants", JSME S NC2-2012.

The Japan Society of Mechanical Engineers (2013), "Codes for Nuclear Power Generation Facilities - Rules on Materials for Nuclear Facilities", JSME S NJI-2013.

Watakabe, T., I. Nakamura, A. Otani, M. Morishita, T. Shibutani and M. Shiratori (2017), "Seismic Qualification of Piping Systems by Detailed Inelastic Response Analysis Part 4 - Second Round Benchmark Analyses with Stainless Steel Piping Component Test", *Proceedings of the ASME 2017 Pressure Vessels and Piping Conference*, PVP2017-65324.

6. Towards a new approach

6.1. Technical background

6.1.1. Engineering practice of linear analyses

One of the main objectives of this report is to propose new engineering practices that better account for the actual behaviour of pressurised piping systems under seismic loads. This proposed new approach is not supposed to drastically change the current practice, but on the contrary is supposed to promote a reasonable evolution for the current practice that can be easily understood and accepted by the engineering community.

Related to this point, it should be kept in mind that categorising the seismic load and resulting stresses as either force-controlled or primary, or as displacement-controlled or secondary, is an operation that can only make sense once the analysis of the piping system response has been carried out in elasticity because this operation is the post-processing of the outputs of such an analysis. The preferred approach retained in this report is therefore that the analysis to be used remains elastic analysis.

However, this preferred approach is not exclusive. Engineering practices that rely on non-linear (and generally in time-response format) analyses are welcome, but face significant challenges if they are applied to the hundreds of piping systems in a nuclear power plant. The concept of stress categorisation does not operate in such analyses. Strains are the main outputs that must be examined and compared with acceptable strain values.

6.1.2. Findings

The proposed new approach is built on a series of findings, which can be summarised as follows:

1. Pressurised piping system under high seismic loads present ratchet and cyclic loading. The highly dominant failure mode is fatigue-ratcheting; plastic instability (plastic collapse) is not relevant because it occurs in a very limited number of cases associated with low pressure or specific, non-conventional configurations such as a cantilevered schedule ten pipe. This statement is based on a critical analysis of research tests and on post-seismic feedback of experiences.

2. The global behaviour of piping systems under seismic loads is well represented by linear models up to a certain level of ductility (to be specified) and with an increased damping, which represents plastic behaviour. It appears that the frequency shift is limited, except perhaps with sinus type excitation. This must be clearly documented.

3. Ratchet verification can be eliminated under some conditions that will be defined. They could be derived from some conventional code conditions (such as ASMEIII NB 3600).

4. Seismic (and some dynamic) loads can be eliminated for the verification of primary stress (Equation 9).

5. Seismic loads can be considered for low cycle fatigue verification. The adequate fatigue curve and specified number of cycles must be set according to the site's seismic conditions.

6. For higher excitations, non-linear models can be used with different degrees of sophistication according to the seismic level; their description should be specified.

7. Reaction loads on supports and equipment should be determined from a linear analysis for seismic loads, which ensures there is some conservatism. An interpretation of some tests with instrumented supports should be considered.

8. Degraded piping (wall thinning or cracking) should be considered for the operability evaluation of in-service inspection, leak-before-break (LBB) and the determination of break locations. A synthesis of International Piping Integrity Research Group (IPIRG) in the United States and of the results of Japanese tests should be included in this work.

9. A programme for the improvement of analytical non-linear computing models used to predict ratchet, hoop ratchet and strain range should be proposed, which has the objective (if feasible) of developing a practical tool that is not overly dependent on the shape and strain concentration features of standard and commercial pipe fittings.

The use of the cumulative absolute velocity (CAV) was reported as a predictor of damage. CAV is recognised by regulators in some countries and should be pursued.

6.2. Proposed new analysis of seismically induced stresses

6.2.1. Primary part

Principle of categorisation

Categorising the seismic load as either force-controlled or primary, or as displacement-controlled or secondary is crucial because the margins, and consequently the acceptance criteria, are significantly different depending on whether the load is categorised as primary or secondary. This crucial issue has been addressed in the past by some authors. For example, the inelastic response spectrum that was established by Newmark and Hall in 1978 for the Nuclear Regulatory Commission (NRC) can be considered as a classification of seismic load: secondary for flexible structures and primary for stiff ones.

Figure 6.1. Typical tensile curve
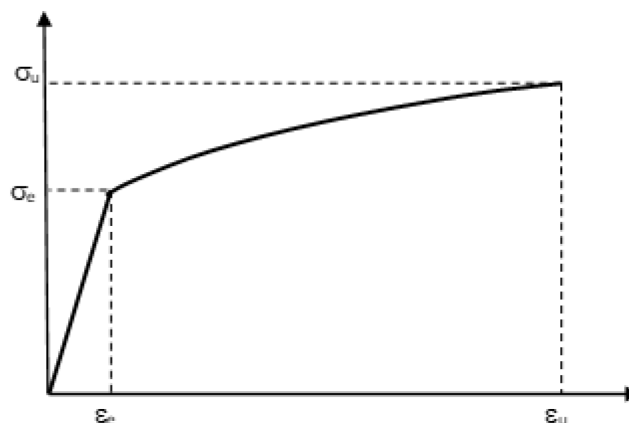
For this purpose, it is worth first recalling the basic background of load/ stress categorisation by considering a steel whose tensile curve, which is presented in Figure 6.1, is characterised by its elastic limit $(\varepsilon_e, \sigma_e)$ and ultimate capacity $(\varepsilon_u, \sigma_u)$. The steel's ductile

[hardening] capacity is $\mu_u = \varepsilon_u / \varepsilon_e$ [$\eta_u = \sigma_u / \sigma_e$]. Two identical simple rods made of this steel will now be considered. The first rod is subjected to a force-controlled load, with the result that F_e [F_u] is the force corresponding to the elastic [ultimate] capacity. The second rod is subjected to a displacement-controlled load, with the result that D_e [D_u] is the displacement corresponding to the elastic [ultimate] capacity. It is clear that $F_u / F_e = \eta_u$ and $D_u / D_e = \mu_u$. Put simply, η_u and μ_u can be regarded as the margin under the force-controlled load and displacement-controlled load of a beam that is designed at its elastic capacity.

Figure 6.2. The considered three rods
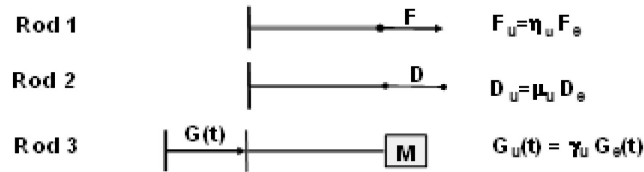
A third identical rod will now be considered, which is equipped at one end with a mass (it becomes an oscillator) and subjected at the other end to a seismic input motion G(t), as schemed in Figure 6.2. $G_e(t)$ and $G_u(t)$ can be identified on the basis of a linearisation technique, which is a method that was developed by Labbé in 2018, for which the elastic and ultimate capacity are reached in the oscillator. Therefore, it can be concluded that $\gamma_u = G_u(t)/G_e(t)$, which can be regarded as the margin under the seismic load of an oscillator that is designed at the elastic capacity. Two possible remarkable outputs are of special interest:

- If $\gamma_u = \eta_u$, the seismic load should be regarded as a force-controlled load.

- If $\gamma_u = \mu_u$, the seismic load should be regarded as a displacement-controlled load.

γ_u values that are different from η_u and μ_u are of course anticipated, meaning that a seismic load cannot be regarded as primary or secondary a priori.

Primary part definition

These three rods' acceptance criteria applicable to a stress, σ, will now be considered. The stress can be calculated under elasticity assumption, according to the engineering practice. These criteria are given by Formulas 6.2-1 for all three rods, where S is a possible security factor:

- Rod one: $\sigma < \eta_u \sigma_e / S$

- Rod two: $\sigma < \mu_u \sigma_e / S$ (6.2-1)

- Rod three: $\sigma < \gamma_u \sigma_e / S$

These three acceptance criteria can be turned into a common Formula 6.2-2.

$\sigma_P < \eta_u \sigma_e / S$, with: (6.2-2)

- Rod one: $\sigma_P = \sigma$

- Rod two: $\sigma_P = \eta_u / \mu_u \sigma$

- Rod three: $\sigma_P = \eta_u / \gamma_u \sigma$

Thanks to the observation that $\sigma_P = \sigma$ in the case of rod one, it is reasonable to conclude that σ_P can be regarded as the primary part of σ. As a result, the primary part of a seismically inertial stress can be calculated as:

$$\sigma_P = \eta_u / \gamma_u \sigma$$

Primary part calculation

According to the method established by Labbé in 2018 for calculating γu, it appears that two parameters play a key role in categorisation:

- p, the slope of the input motion response spectrum at the oscillator frequency;

- λ, a structural index comprised between zero and one, the value of which is mainly controlled by the effective stiffness of the oscillator when entered in the plastic regime.

Second order parameters are related to damping:

- q, which controls the damping dependence of the input spectrum;

- β, which controls the equivalent damping generated by energy dissipation in the plastic regime.

For practical reasons, a secondary index, m, is introduced according to Formula 6.2-4, so that m=0 for a primary load and m=1 for a secondary load. Eventually, the above introduced primary part of a seismically induced inertial stress simply reads as shown in Formula 6.2-5:

$$\gamma_u = \mu_u{}^m \eta_u{}^{1-m} \tag{6.2-4}$$

$$\sigma_P = (\eta_u / \mu_u)^m \sigma. \tag{6.2-5}$$

According to Labbé (2018), m can be calculated as per Formula 6.2-6. This formula can be put in the form of a diagram, as presented in Figure 6.3.

$$m = (1-\lambda) p/2 + \lambda (1+\beta q) \tag{6.2-6}$$

Figure 6.3. Diagram for seismic inertial stress categorisation, presenting the secondary index, m, as a function of p, q, p, q, λ, β
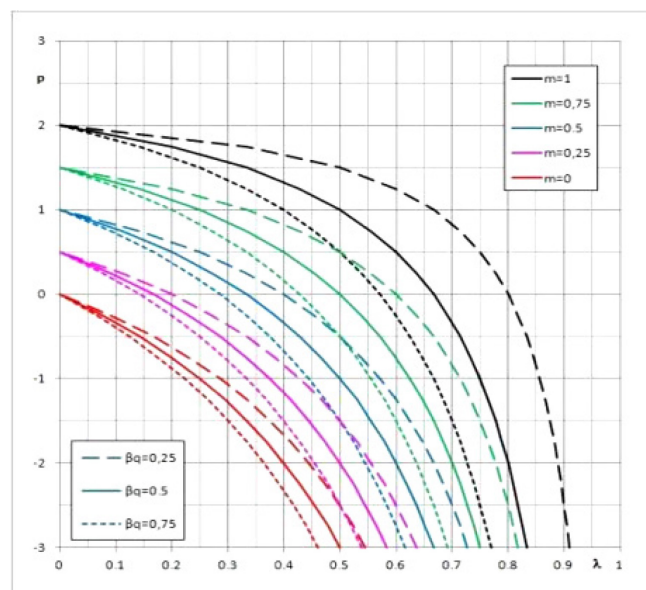
The possible values of these parameters will now be discussed, except for p values that will be discussed in the following section.

The outputs of two experimental campaigns, Japan's Nuclear Power Engineering Centre's (NUPEC's) campaign (DeGrassi et al., 2008) and the Bhabha Atomic Research Centre (BARC) campaign (Ravikiran et al., 2015) can be used to evaluate λ and β. It is worth noting that the first campaign led to a very large ductility demand (of the order of 20), while the second campaign led to a rather small ductility demand (of the order of 2). Detailed analyses of campaigns outputs are presented in the Annex G, which presents calculations of the λ and β values derived from both campaigns. In particular, λ values are 0.966 and 0.933, which means that the piping systems appear at the extreme right part of Figure 6.3. An earlier experimental campaign had also been carried out in the United States (Ranganath et al., 1994). Many interesting outputs of this campaign are considered elsewhere in this report. At this stage, attention must be drawn to the fact that experiments that were carried out on components overestimated the effective damping compared with experiments that were carried out on piping systems. The outputs of such campaigns on components were therefore not retained here. A system test campaign was carried out concurrently with this component test campaign (Ranganath et al., 1994), whose outputs have not yet been interpreted according to the process of primary part identification.

Multi modal piping systems

Concerning piping systems, the system response is frequently controlled by the first (fundamental) mode, which occurred during the tests mentioned in the previous paragraphs. The above developed oscillator approach is valid in situations like this. However, it is often the case that that several modes should be considered in practice when calculating the seismic response of a piping system, which leads to two additional issues:

The first issue is a practical one. When considering a typical floor response spectrum, such as the one presented in Annex G, it can be observed that its slope can greatly vary versus frequency. For example, the slope of the 5% spectrum jumps from -3 at 4 Hz to 0 at 5 Hz. Such variable slope values would result in a mode dependence of the primary part that would be complicated to handle and not make sense.

The second issue is a theoretical one. Numerical simulations (Labbé and Nguyen, 2019) provide evidence that the λ index (introduced above) and consequently the secondary index m are sensitive to the φ parameter, which can be defined by:

$$\varphi = f/f_c \qquad (6.2\text{-}7),$$

where

- f is the natural frequency of the oscillator;
- f_c is the central frequency of the input motion.

Essentially, m values that result from numerical simulations are larger than or equal to one when φ is lower than or equal to one and decreases towards zero for increasing φ values.[1]

---

1. This result concerning relative high frequency modes is consistent with the point made by Politopulos and Sollogoub (2005) that seismically isolated installations should be treated with care because the very low frequency filtering effect induced by the isolation system means that the transmitted seismic input motion should be regarded as a primary load.

For practical applications, m can be expressed as a function of φ in order to cope with both issues, which is presented in Figure 6.4 where:

- f_{peak} is the peak frequency of the input response spectrum. In case of a plateau, it is the high corner frequency of the plateau.

- f_{cut} is the cut-off frequency of the input response spectrum. f_{cut} can be defined as the frequency so that the spectrum value is equal to the spectrum asymptotic value plus 15%.

- $\varphi cut = f_{cut} / f_{peak}$.

An example of f_{peak} and f_{cut} determination is presented in Annex G.

Figure 6.4. Secondary index m(φ)
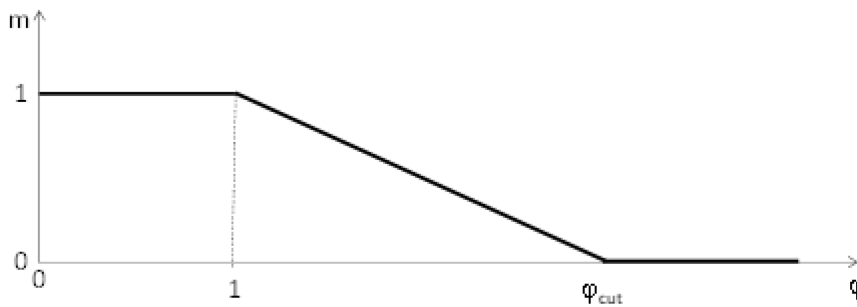
The obtained m(φ) function looks very simple. This simple form results from the fact that, by definition, p is positive or equal to zero for frequencies lower than the peak frequency and p is negative for larger frequencies.

Code implementation

Following the developments that have been outlined in the previous paragraphs, the criterion on primary stress seems usual, but the content of M evolves:

$$B_1 \frac{PD}{2t} + B_2 \frac{M}{Z_1} \leq k.S_{\square} \tag{6.2-8}$$

The primary part, M_S, of seismically induced moments should be incorporated into M in the form of $M_S = M_{SAM} + M_I$, where:

- M_{SAM} = is the primary part of the moment resulting from the non-cyclic part of differential seismic anchor motion;

- M_I is the primary part of the moment resulting from the inertial response of the piping system.

For M_{SAM} and M_I calculations, the non-linear constitutive relationship should be idealised as bilinear. This calculation is presented in Figure 6.5. Although the figure is plotted in terms of stresses and strain, alternative parameters such as moment and curvature can also be used. An acceptable ultimate ductility demand μ_u should be decided. η_u is then calculated by the Formula 6.2-9, where α is defined in Figure 6.5:

$$\eta_u = 1 + \alpha (\mu_u - 1) \tag{6.2-9}$$

Figure 6.5. Idealised constitutive relationship
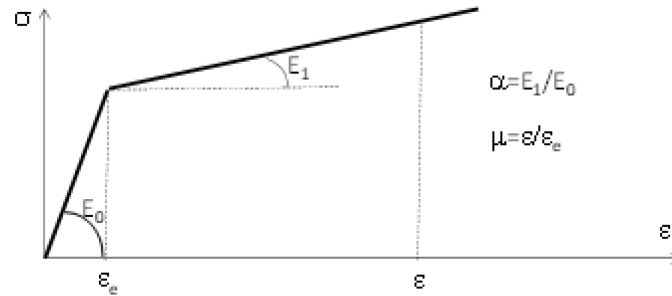
For every i mode, its non-dimensional frequency φ_i and its secondary index m_i should be calculated according to Formulas 6.2-9 and 6.2-10, whose $m(\varphi)$ function was introduced in Figure 6.4. The i mode primary ratio τ_{Pi} is then expressed as per Formula 6.2-11.

$$\varphi_i = f_i / f_{peak} \tag{6.2-9}$$

$$m_i = m(\varphi_i) \tag{6.2-10}$$

$$\tau_{Pi} = (\eta_u / \mu_u)^{m_i} \tag{6.2-11}$$

M_{SAM} and M_I can eventually be calculated as follows:

- $M_{SAM} = (\eta_u / \mu_u$ M_{SAM}^*, where M_{SAM}^* is the moment resulting from the non-cyclic part of differential displacements between supports in an elasticity-based analysis.

- M_I = combination (square root of the sum of the squares [SRSS] procedure or complete quadratic combination [CQC] method) of $\{M_{Ii}\}$;

- $M_{Ii} = \tau_{Pi}$ M_{Ii}^*, where M_{Ii}^* is the mode $_i$ contribution to the moment resulting from the inertial response of the piping system in an elasticity-based analysis.

Simplified code implementation

τ_{Pi} in the calculation of M_{Ii} can be regarded as a coefficient that applies to the floor response spectrum at the frequency of the mode $_i$. This interpretation is illustrated in Figure 6.14. As a result, the peak or the plateau of the spectrum, S_{peak}, is significantly reduced after being multiplied by the factor η_u / μ_u. The spectrum ordinate S_{ZPA} is unchanged for frequencies larger than f_{ZPA}. Consequently, a practical rule for the implementation of the approach is as follows:

$$S^*(f) = c^* \, S(f) \text{ for } f \leq f_{peak}, \text{ with } c^* = \eta_u / \mu_u \geq S_{ZPA} / \, _{Speak};$$

$$S^*(f) = S(f) \qquad \text{for } f \geq f_{ZPA}; \tag{6.2-12}$$

$$S^*(f) \text{ linear in log-log scale between } f_{peak} \text{ and } f_{ZPA}.$$

- Remark one: the role of c^* is to prevent $S^*(f_{peak})$ from being lower than $S(f_{ZPA})$.

- Remark two: it is not necessary in this simplified implementation for a cut-off frequency to be identified.

Comparison with other research work on stress categorisation

At this stage, it worth mentioning similar work carried out by Tamura et al. (2018; 2019) and the agreement in conclusions. This work was essentially a study of the response of elastic-plastic oscillators with a circular frequency ω_n to a sinusoidal excitation of the

support with a circular frequency ω_{wave}. The approach can be supplemented by studying the response to floor motions, which was recorded during the Western Tottori earthquake (6 October 2000) and Niigata-ken Chuetsu-oki earthquake (16 July 2007).

The authors reach the conclusion that the ratio ω_n/ω_{wave} plays a crucial role in the categorisation of the seismic load. The seismic load above an upper threshold (stiff oscillators) is of the force-controlled type, while it is of the displacement-controlled type under a lower threshold (flexible oscillators). The categorisation depends on the non-linear features of the oscillator.

The authors were also led to the conclusion that the primary part of the seismic load is controlled by the zero period acceleration (ZPA) of the input spectrum, which is consistent with the reduced spectrum that is presented in this report (albeit the modal combination is different).

References

DeGrassi, G., J. Nie and C. Hofmayer (2008), "Seismic Analysis of Large-Scale Piping Systems for the JNES/NUPEC Ultimate Strength Piping Test Program", NUREG/CR-6983, US Nuclear Regulatory Commission, Office of Nuclear Regulatory Research.

Labbé, P.B. (2018), "On categorization of seismic load as primary or secondary for piping systems with hardening capacity", *Pressure Vessels and Piping Conference*, Prague, Czechia, PVP2018-84608.

Labbé, P.B. and A. Nguyen (2019), "Frequency dependence of the ductility demand in a SDOF system", *SMIRT-25*, 4-9 August, Charlotte, United States.

Politopulos I. and P. Sollogoub (2005), "Vulnerability of elastomeric bearing isolated buildings and their equipment", *Journal of Earthquake Engineering*, 9(4), pp.525-546.

Ranganath S. (1994), "Piping and Fitting Dynamic Reliability Program", EPRI TR-102792, Volumes 1 to 5, Electric Power Research Inst., Palo Alto, CA (United States); General Electric Co., San Jose, CA (United States).

Ravikiran, A., P.N. Dubey, M.K. Agrawal, G.R. Reddy, R.K. Singh and K.K. Vaze (2015), "Experimental and Numerical Studies of Ratcheting in a Pressurised Piping System under Seismic Load", *Journal of Pressure Vessel Technology,* Volume 137, pp.031011:1-7.

Tamura I, S. Matsuura, R. Shimazu and K. Kimura (2019), "Categorization of seismic loadings for components and piping systems", *Journal of Pressure Vessel Technology*, PVT-19-1065.

Tamura, I., S. Matsuura, R. Shimazu and K. Kimura (2018), "Categorization of Dynamic Loading into Force-Controlled Loading and Displacement-Controlled Loading", American Society of Mechanical Engineers Paper No. PVP2018-85098.

6.2.2. Ratchet and fatigue-ratcheting

Introduction

Previous studies on uniaxial ratcheting have shown that strain accumulation under stress-controlled loading conditions depends on the applied stress range and stress ratio. The stress ratio is defined as the ratio of minimum stress to maximum stress and is related to the mean stress. Under small stress ratios, for example, those between 0.25 and 0, no ratcheting occurs. The ratcheting phenomenon is more pronounced in the presence of pressure.

Chen et al. (2006) have provided a ratcheting boundary for a combination of the internal pressure and bending load for elbows. For a bending load amplitude that is equal to ½ of that at which the straight pipe of same schedule yields, the maximum value of pressure that

does not cause ratcheting is equal to one-third of the pressure. This causes yielding of the straight pipe of the same schedule. For a bending load amplitude that is equal to ¼ of that which causes a straight pipe of the same schedule to yield, the maximum value of pressure that does not cause ratcheting is equal to approximately ½ of the pressure that causes yielding of the straight pipe of same schedule. The internal pressure corresponding to the ratcheting boundary can be considered as the limit pressure to be used to prevent ratcheting for any bending load.

Reference

Chen, X., B. Gao and G. Chen (2006), "Ratcheting Study of Pressurised Elbows Subjected to Reversed In-Plane Bending", *Journal of Pressure Vessel Technology,* Volume 128, pp.525-532.

Pre-strain and ratchet strain

A cumulative and residual plastic strain like pre-strain or ratchet strain is known to affect the fatigue life of the material. More specifically, the fatigue life would decrease as the plastic strain in the low cycle fatigue decreases. The effects of the pre-strain and ratcheting strain have been investigated because they concern the restarting of the Kashiwazaki-Kariwa Nuclear Power Plant, following the Niigata-ken Chuetsu-oki earthquake. A report was published by a committee called SANE. This committee claims in the report that there is less effect of the ratcheting strain up to about 10%.

A evaluation method of fatigue-ratcheting was proposed (Asada, 1985). The method took the ductility exhaustion factor D_d into consideration along with the fatigue damage factor D_f. Three kinds of criteria are proposed:

- *Coffin's expression:*

$$D_d + D_f \leq 1$$

- *Asada's expression, type I:*

$$\begin{cases} 3D_d + D_f \leq 1 \ (D_f \leq 0.25) \\ D_d + 3D_f \leq 1 \ (D_f > 0.25) \end{cases}$$

- *Asada's expression, type II:*

$$D_d + 2\sqrt{D_d D_f} + D_f \leq 1$$

where D_d and D_f can be calculated from the following equations.

$$D_d = \frac{\varepsilon_r}{\varepsilon_{f0}}, \ \varepsilon_{f0} = ln \frac{100}{100 - \phi(\%)}$$

$$D_f = \left(\sum_{i=1}^{n} \frac{N_i}{N_{fi}}\right)^m, m = 0.6 \text{ as recommended by Udoguchi and Asada}$$

D_d: factor of ductility exhaustion

D_f: factor of fatigue damage

ϕ: reduction of the area obtained from the tensile test using the round bar test piece

ε_r: ratchet strain

ε_{f0}: true fracture strain

An example of the evaluation is shown in Figure 6.6. A black diagonal straight line represents Coffin's expression, a red curve Asada's expression type I, and a purple quarter-circle Asada's expression type II. The allowable region for each expression is the left side of the curve. The curves of the series of Effect of the Clearance (EC) are the simulation results of the cyclic bending of pressurised pipes with wall thinning. The fatigue-ratcheting failure can be predicted by checking the cycles crossing the line.

The ductility exhaustion D_d might start to affect fatigue ratchet (FR) evaluation when D_d is more than about 0.05. This means that the ratcheting strain is more than about 5% because ε_{f0} could be more than 1.0. The ratcheting strain on a sound pipe subjected to seismic load could be estimated within several percent. As a result, the ductility exhaustion for the sound pipe would not be very large and it is not be necessary to consider the ductility exhaustion and D_d-D_f evaluation for the sound pipe without wall thinning.

Figure 6.6. Example of FR evaluation (D_d-D_f evaluation)
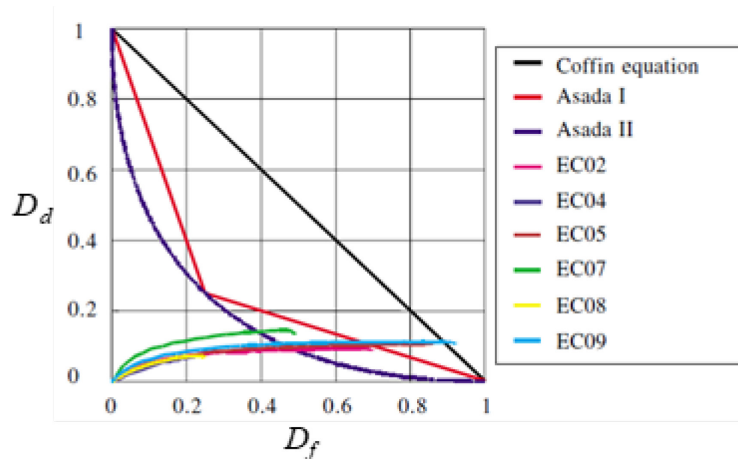
References

Asada, Y. (1985), "Fatigue Criterion on Low-Cycle Fatigue with Excessive Progressive Deformation", *Proceedings of 3rd German-Japanese Joint Seminar*, 2.2, pp.3-11.

JANTI (2012), "A report of Structure Integrity Assessment for Nuclear Power Components experienced Niigata Chuetsu-Oki Earthquake Committee (SANE)", Japan Nuclear Technology Institute, Japan.

Nakamura, I., A. Otani and M. Shiratori (2001), "Study on estimation method of seismic safety margin of aged piping system and equipment", *Technical note of the National Research Institute for Earth Science and Disaster Prevention*, pp.1-78.

Namaizawa, J., K. Ueno, A. Ishikawa and Y. Asada (1993), "Life Prediction Technique for Ratcheting Fatigue", ASME, United States, PVP-266, pp.3-11.

Experimental data of FR and availability of conventional fatigue evaluation

Japanese researchers have been acquiring experimental data of low cycle fatigue of pipe fittings. The data includes some results showing significant ratcheting strains. Figure 6.7 shows the low cycle fatigue data of pipe fittings, where the fatigue life of the data refers to the number of load cycles until crack penetration occurs, but not to the crack initiation. The crack penetration of piping means the loss of performance of the pressure boundary.

The strain amplitudes of the plotted data in the figure are largely obtained from the experiments, but with some analysis modifications. The analysis modifications are necessary because of the difficulty of measuring at the critical and very local point generating the maximum strain amplitude.

The strain amplitudes of the fatigue data of the elbows shown as E in the figure are the hoop and principal strains at the crown and inside surface of the elbow. The plotted data of the elbows therefore concerns single strain component, but not the equivalent strain considering the multi-axial strain condition, and the equivalent strains of the elbows must be plotted as the larger amplitudes. It was recently noted that this fatigue data can rise to the level of a best fit curve of the American Society of Mechanical Engineers (ASME) code if the strain amplitude is replaced by the Mises type of equivalent strain.

The percentage noted in the figure refers to the ratchet strain, which is a residual/ permanent hoop strain after cyclic loading at the maximum point and the outside surface, which is different from the maximum point of the amplitude or range of the strain. The significant reduction of the fatigue life by the ratcheting strain cannot be recognised. The design fatigue curve is considerably lower than the fatigue data as well as the data accompanied by a significant ratchet strain.

The SANE report mentioned in the previous paragraphs also expresses how the ratcheting strain up to about 10% has less influence on the fatigue life. A ratcheting strain of more than 10% could not appear in the actual pipes that were designed by current seismic design because the strain amplitude can be limited to a comparatively lower level by the design fatigue curve.

As a result, it can be concluded that the fatigue evaluation using the design fatigue curve still has enough margin against FR and it is not necessary to consider the influence of the ratcheting strain on the fatigue evaluation.

Figure 6.7. Low cycle fatigue data of pipe fittings
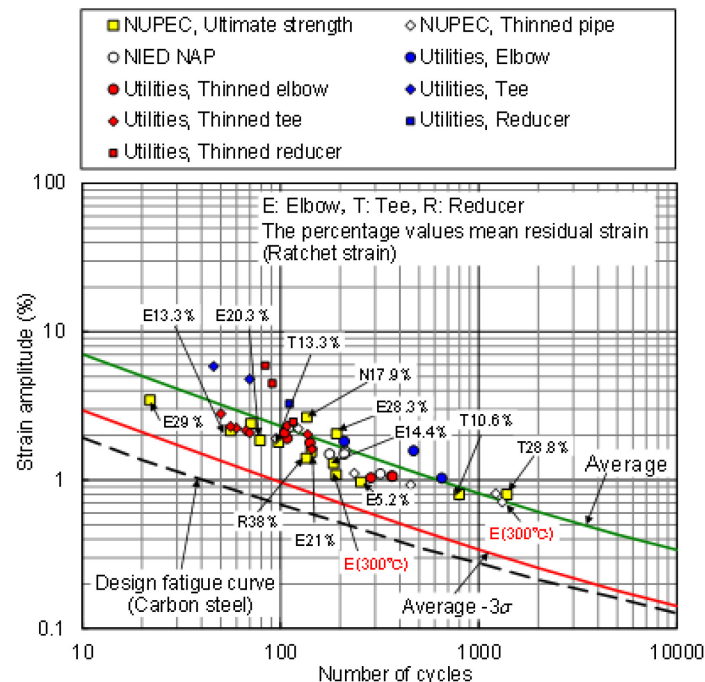
References

Arai, M., N. Kojima, T. Kabaya, S. Hirouchi and M. Bando (2016), "Investigation on method of elasto-plastic analysis for piping system (Benchmark analysis)", PVP2016-63186.

Nakamura, I., A. Ōtani and M. Shiratori (2007), "Study on fracture mechanics of eroded pipes under seismic loading", Technical Note of the National Research Institute for Earth Science and Disaster Prevention No.306, National Research Institute for Earth Science and Disaster Prevention, Japan.

Namita, Y., K. Suzuki, H. Abe, I. Ichihashi, M. Shiratori, K. Tai, K. Iwata and A. Nebu (2003), "Seismic proving test of eroded piping: Status of eroded piping component and system test", PVP2003-2097.

Otani, A., I. Nakamura, H. Takada and M. Shiratori (2011), "Consideration on seismic design margin of elbow in piping", PVP2011-57146.

Suzuki, K., Y. Namita, H. Abe, I. Ichihashi, K. Suzuki, M. Ishiwata, T. Fujiwaka and K. Tai (2003), "Seismic proving test of ultimate piping strength: Simulation analysis simplified piping system test", PVP2003-2098.

Uesaka, M., N. Kojima, I. Muroya, H. Nomura, J. Yamazaki and A. Otani (2014), "Investigation on fatigue curve against cyclic loads of an earthquake for piping components", PVP2014-28234.

Other consideration for the low cycle fatigue of pipe fittings

The fatigue life reduction of pipe fittings can be understood to depend on the multi-axial stress/strain condition rather than the influence of ratchet strain and ductility exhaustion (Ando and Takahashi). The low cycle fatigue data in the previous figure were obtained from the experiments that were also conducted under multi-axial stress/strain condition because the pressurised pipe fittings subjected to cyclic loading generated the multi-axial stress/strain condition.

Manson's universal slope can be modified by using the true stress and strain of the fracture under the multi-axial stress/strain condition (using the triaxiality factor proposed by Miyazaki). Figure 6.8 shows the comparison between the experimental data of elbows and the modified universal slope. The conclusion was that the influence of multi-axial stress/strain conditions might be important, instead of the influence of the ratchet strain and the ductility exhaustion.

$$\Delta\varepsilon = \frac{3.5\sigma_f}{E} \cdot N_f^{-0.12} + \varepsilon_{mf}^{0.6} \cdot N_f^{-0.6}$$

σ_f: true stress of the fracture

ε_{mf}: true strain of the fracture under multi-axial stress conditions (defined by the triaxiality factor)

$$\varepsilon_{mf} = \frac{\left(\frac{\omega m \sigma_{uf}}{\sigma_0}\right) + \lambda \left(\frac{\omega m \sigma_{uf}}{\sigma_0}\right)^n}{\left(\frac{\sigma_{uf}}{\sigma_0}\right) + \lambda \left(\frac{\sigma_{uf}}{\sigma_0}\right)^n} \cdot \varepsilon_{uf}$$

$$m = \sqrt{(1 + \alpha + \beta)^2 - 3(\alpha + \beta + \alpha\beta)}$$

$$\omega = \frac{1}{1 + \alpha + \beta} , \alpha = \sigma_2/\sigma_1 , \beta = \sigma_3/\sigma_1$$

σ_0: yield stress

$\sigma_1, \sigma_2, \sigma_3$: principal stresses

σ_{uf}: true stress of the fracture by a monotonic tensile test

ε_{uf}: true strain of the fracture by a monotonic tensile test

λ and n : indices of the Ramberg-Osgood stress-strain relation

$$\varepsilon = \frac{\sigma}{E} + \varepsilon_0 \lambda \left(\frac{\sigma}{\sigma_0}\right)^n$$

Figure 6.8. Revised universal slope for pipe fittings under multi-axial stress conditions
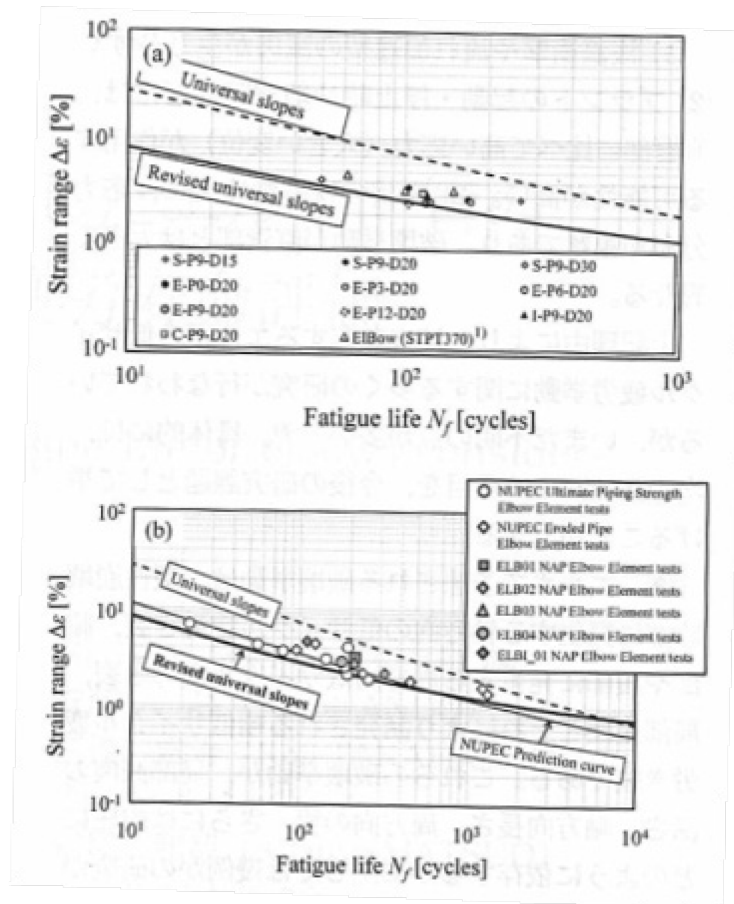
Source: Ando et al., 2012.

References

Ando, K., K. Takahashi, K. Matsuo and Y. Urabe (2012), "Estimation of low cycle fatigue life of elbows considering bi-axial stress effect", *Atsuryoku Gijutsu,* 50(4), pp.184-193.

Nakamura, I., A. Ōtani and M. Shiratori (2007), "Study on fracture mechanics of eroded pipes under seismic loading", Technical Note of the National Research Institute for Earth Science and Disaster Prevention No.306.

Takahashi, K., K. Ando, K. Matsuo and Y. Urabe (2014), "Estimation of Low-Cycle Fatigue Life of Elbow Pipes Considering the Multi-Axial Stress Effect", *Journal of Pressure Vessel Technology,* 136(4), 041405.

Urabe, Y., K. Takahashi and H. Abe (2015), "Low Cycle Fatigue Evaluation of Pipe Bends With Local Wall Thinning Considering Multi-Axial Stress State", *Journal of Pressure Vessel Technology,* 137(4), 041404.

Equivalent number of cycles

In common engineering practices the main output of a seismic response analysis is the maximum value, s_{max}, of the seismically induced stress at any location of interest in the piping system, in particular when the conventional spectral method is used. A question concerning seismically induced fatigue damage assessment must be answered: how many cycles of s_{max} amplitude generate the same fatigue damage as the entire seismic transient?

To reach an answer, the seismically induced damage must first be calculated. For this purpose,

- Many authors such as Vanmarke (1983) and Der Kiureghian (1980) have for decades typically considered the piping seismic response to be a sample of the narrow-banded stochastic process, characterised by its standard deviation σ_s.

- As suggested by Lin (1967), the conventional fatigue curve is replaced by its tangent at σ_s and takes the implicit form that is presented in Formula 6.2-13, where $N(s)$ is the number of cycles of amplitude s that corresponds to a fatigue usage deemed to be equal to one.

$$N(s)\, s^b = c \tag{6.2-13}$$

Following these assumptions, the seismically induced fatigue usage is given by Formula 6.2-14, which was established by Lin in 1967:

$$u = N_e \frac{(\sqrt{2}\,\sigma_s)^b}{c} \Gamma\left(\frac{b+2}{2}\right) \tag{6.2-14}$$

where

- $N_e = T/\tau$, where T is being the duration of the strong motion and τ the eigenperiod of the predominant mode. N_e represents the seismically induced number of cycles of various amplitudes.

- $\Gamma(\cdot)$ is the Gamma function.

For a given number of cycles, n, of amplitude s^{max}, the fatigue usage is given by Formula 6.2-15. The equivalent number of cycles, n_e, is required so that expressions of u in Formulas 6.2-14 and 6.2-15 are equal, which results in Formula 6.2-16. Formula 6.2-16 can be simplified by introducing the peak factor, p, which is defined by $p = s^{max}/\sigma_s$ and results in Formula 6.2-17.

$$u = \frac{n}{N(s^{max})} \tag{6.2-15}$$

$$n_e = N_e \left(\frac{\sqrt{2}\,\sigma_s}{s^{max}}\right)^b \Gamma\left(\frac{b+2}{2}\right) \tag{6.2-16}$$

$$n_e = N_e \left(\frac{\sqrt{2}}{p}\right)^b \Gamma\left(\frac{b+2}{2}\right) \tag{6.2-17}$$

The peak factors of seismic responses were extensively investigated by Der Kiureghian (1980), whose important results are reported in Annex F. It appears that p is a slowly increasing function of N_e. Therefore, it would not make sense to consider the ratio n_e/N_e, even though this is suggested by Formula 6.2-17.

Following the application of Formula 6.2-17, Table 6.1 has the equivalent number of cycles, n_e, as a function of N_e and b. For example, when there is a 20 s duration of strong motion and 2 Hz predominant eigen frequency, $N_e = 40$, resulting in an equivalent number of cycles between 7 and 13 depending on the b value. When there are very long input

motions, such as those considered nowadays in Japan, the equivalent number can be between 20 and 60.

Table 6.1. Equivalent number of cycles N_e as a function of N_e and b

N_e	b	3	4	5	6
10		6	5	5	6
25		9	7	6	6
50		14	10	8	7
100		22	15	11	9
250		43	26	17	12
500		71	40	25	17

b should be estimated for the tangent to the fatigue curve at σ_s, which means at s^{max}/p, where p is a function of N_e presented in Annex F.

The above n_e calculation is further simplified by considering a specific b value, namely $b=5$, which is regarded as appropriate according to the ASME (ASME B31J, 2017). In this case, a simple empirical formula can be established to derive n_e directly from N_e as follows:

$$n_e = 0.54\,(N_e^{0.6} + 5) \qquad\qquad (6.2\text{-}18)$$

Remark one: N_e is directly proportional to the strong motion duration. Because it may significantly vary from country to country in the post-Fukushima context, no assumption is made in this report on the duration, so that the proposed n_e calculation will be valid in any seismotectonic environment.

Remark two: the peak factors considered here are those of stationary random processes. Even the strong phase of a seismic input motion cannot be regarded as stationary. As a consequence, the realistic peak factors (ratio between s^{max} and σ_s calculated on the strong phase) are larger than the theoretical values considered in this report. Considering such realistic values would result in a lower equivalent number of cycles. In this regard, the values presented in Table 6.2-Y1 and those resulting from Formula 6.2-18 can be regarded as being on the safe side.

References

ASME (2017), "Stress Intensification Factors (I-Factors), Flexibility Factors (K-Factors), and Their Determination For Metallic Piping Components", American Society of Mechanical Engineers, United States.

Der Kiureghian, A. (1980), "A response spectrum method for random vibrations", Report No. UCB/EERC-80/15, Berkeley, California: University of California, Earthquake Engineering Research Center.

Lin, Y.K. (1967), "Probabilistic theory of structural dynamics", Mac Graw Hill.

Newmark, N.M. and W.J. Hall (1978), "Development of Criteria for Seismic Review of Selected Nuclear Power Plants", NUREG/CR-0098, US Nuclear Regulatory Commission, Washington, DC.

Vanmarke, E. (1983), "Random fields", MIT Press, Massachusetts Institute of Technology, Massachusetts.

6.3. Validation analyses

The proposed criteria should be checked for completeness, coherence and resulting margins on examples to be validated. A representative line was intentionally selected, which is presented in this section, as well as some associated results.

6.3.1. Description of the line

The water-water energy reactor (WWER) feedwater line was chosen as a prototype for the evaluation and verification of the new seismic criteria. The original seismic design of this line assumed additional horizontal restraining, but the line was removed from the model for the purposes of this analysis. The details of this line are presented in Figures 6.9 and 6.10 as well as in Table 6.2. Figure 6.11 provides data to be used as the seismic input: three-component floor response spectra. Figure 6.12 presents the first mode shapes and natural frequencies of the line.

Figure 6.9. Piping model general view
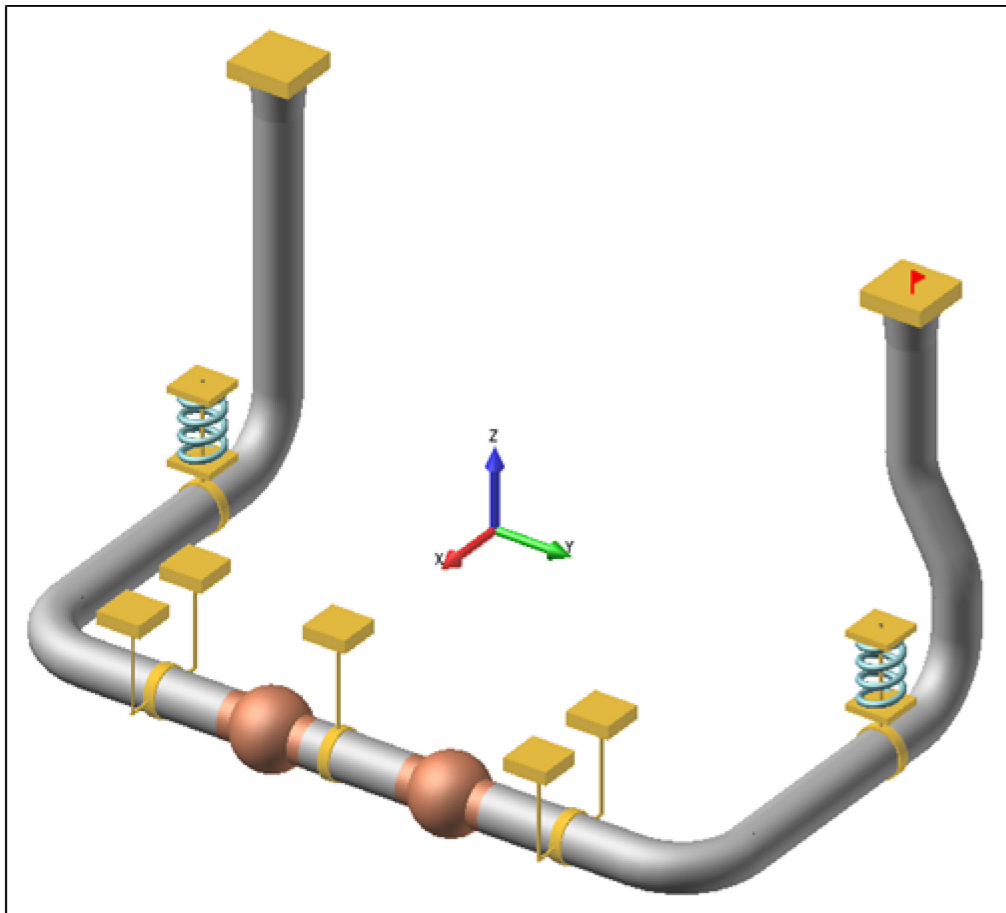
Figure 6.10. Piping model main dimensions
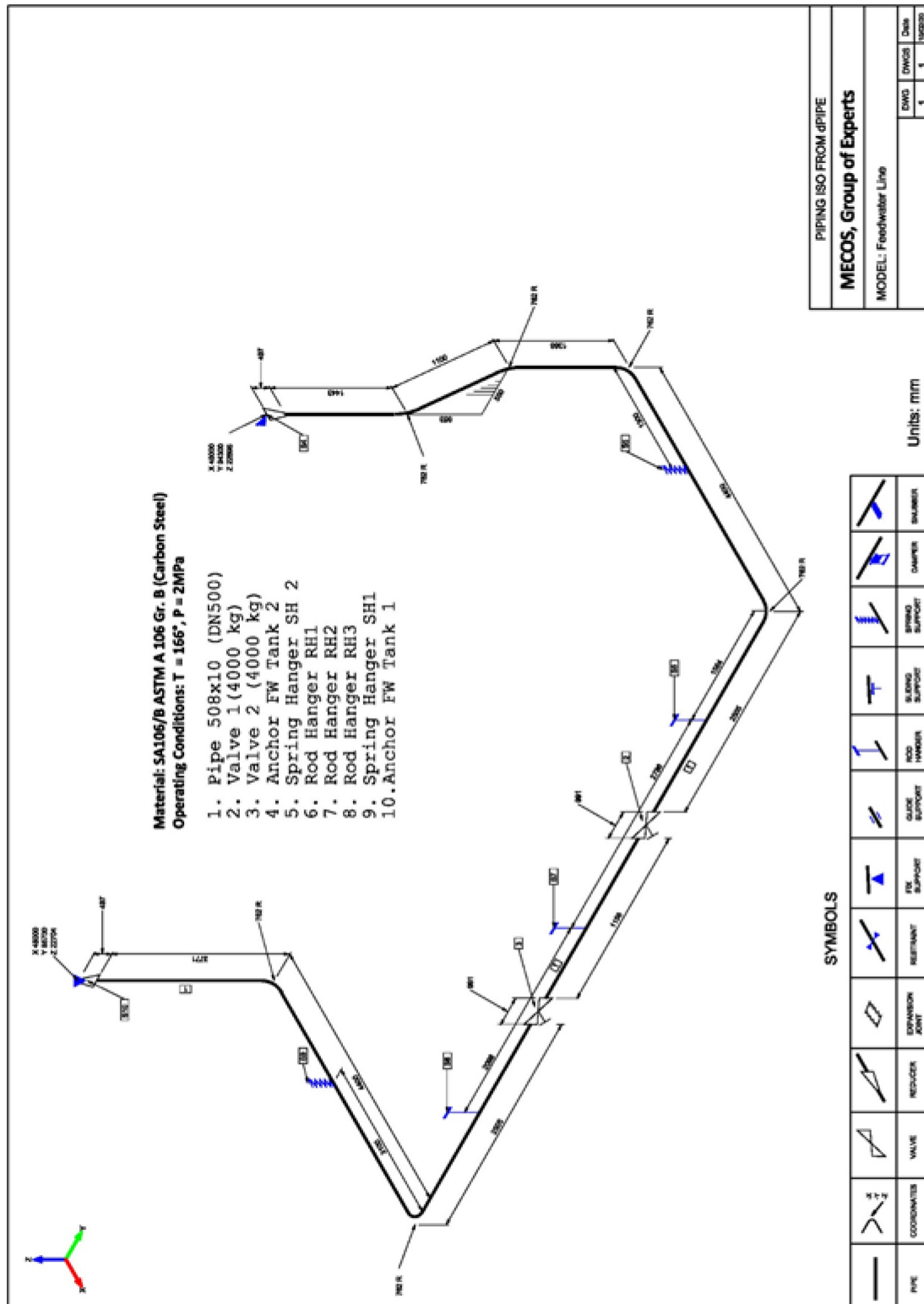
Figure 6.11. Input floor response spectra

FREQ	AX	FREQ	AY	FREQ	AZ
0.5	0.2324	0.5	0.2324	0.5	0.1672
1.27	0.9052	1.87	1.204	4.53	1.7768
1.44	0.9428	2.68	1.896	4.97	2.1664
2.38	1.5216	2.93	1.9232	9.82	2.1664
5.11	5.2368	3.57	2.2324	11.28	2.0176
8.29	5.2368	4.46	3.2008	11.9	2.0156
10.51	1.896	5.55	6.0376	12.98	2.3876
12.1	1.5248	8.19	6.0376	20.36	2.3876
14.87	1.6424	9.01	3.4252	23.55	1.2068
30.14	1.6428	11.01	1.9532	27.55	0.8236
35.92	1.0316	27.01	1.6108	36.7	0.7312
50	1.018	29.01	1.2884	50	0.6428
		50	1.0512		

Table 6.2. General data for the material and pipe's operation conditions

Parameters	Designation	Units	Expression	Value
outside diameter of pipe	D_o	mm	-	508
nominal wall thickness	t_n		-	9.53
inside diameter	D_i		$D_o - 2\,t_n$	488.94
mean radius of pipe	r		$(D_o - t_n)/2$	249.24
nominal bend radius of pipe bend	R		-	762
flexibility characteristic of the bend	h	-	$t_n R/r^2$	0.117
moment of inertia	I	mm⁴	$0.0491(D_o^4 - D_i^4)$	4.64E+08
reducer's cone angle	α	deg	-	15
section modulus of pipe	Z	mm³	$2*I/D_o$	1.83E+06
operating (hot) temperature	T_{hot}	°	-	166
cold temperature	T_{cold}		-	20
service Level D coincident internal pressure	P	MPa	-	0.77
material			**Carbon steel SA106B**	
basic material allowable stress at hot temperature, MPa	S_h	MPa		118
basic material allowable stress at cold temperature, MPa	S_c			118
material yield strength at a temperature consistent with the loading under consideration	S_y			212
service level D allowable stresses	*Sallw D*		$min.3Sh;2Sy$	354

Figure 6.12. First mode shapes and natural frequencies of the piping

Mode # 1

Mode # 2

Mode # 3

View EigenForms

Mode 0001: FREQ =   1.72 Hz
Mode 0002: FREQ =   3.35 Hz
Mode 0003: FREQ =   6.50 Hz
Mode 0004: FREQ =   9.96 Hz
Mode 0005: FREQ =   11.87 Hz
Mode 0006: FREQ =   15.21 Hz
Mode 0007: FREQ =   22.49 Hz
Mode 0008: FREQ =   25.42 Hz
Mode 0009: FREQ =   26.79 Hz
Mode 0010: FREQ =   30.72 Hz
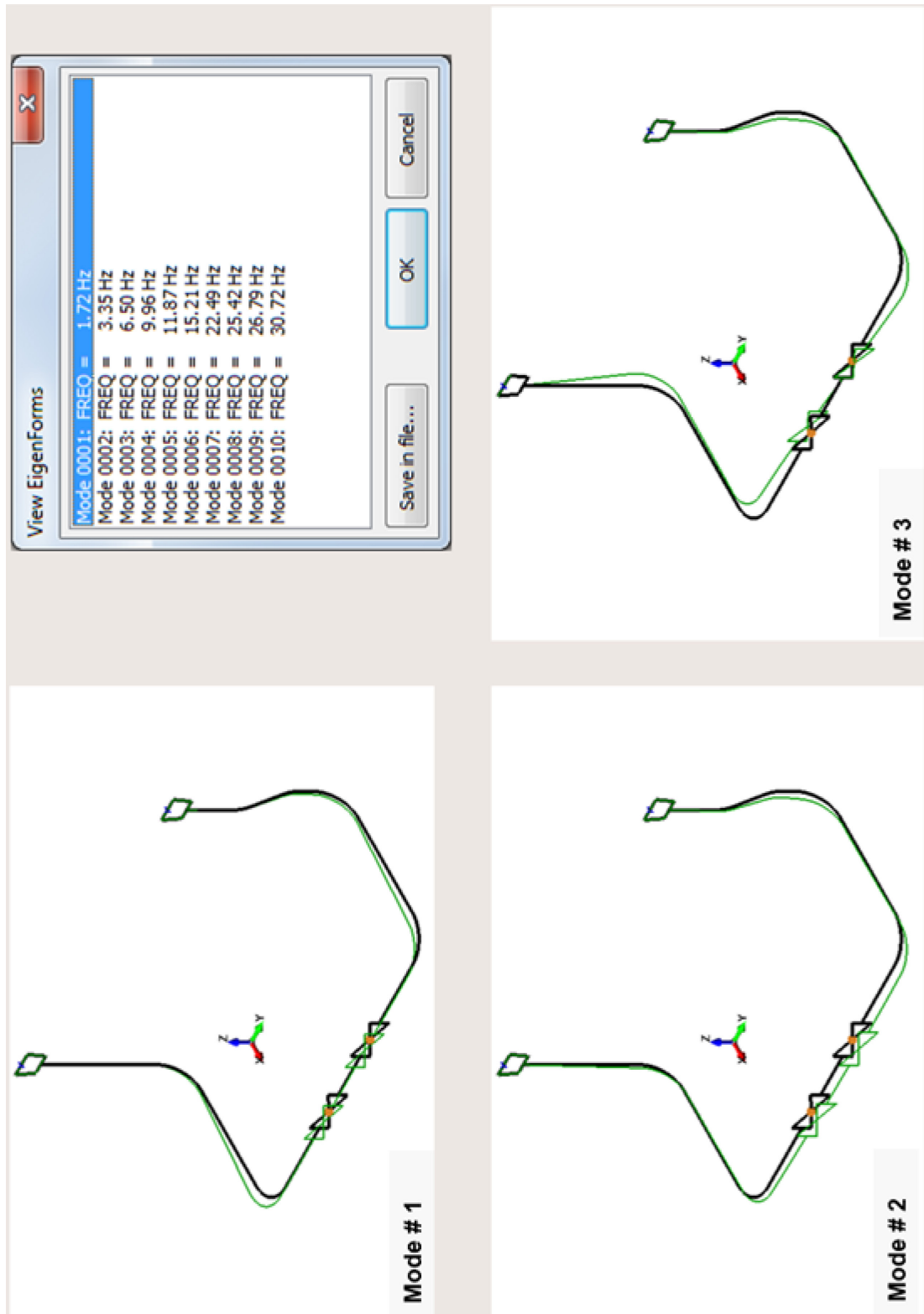
6.3.2. Analyses results

Conventional analysis in compliance with ASME BPVC NC-3600

The results of the conventional analyses with use of the response spectrum method are provided in the tables and figures below. Table 6.3 shows the calculated sectional moments. The resulting SRSS values are given in the column "M_A" for the weight and "M_B" for the seismic loads. Three different piping fittings with maximal seismic moments were selected for further processing, namely a straight pipe between nodes "250" and "260", bend element between nodes "30" and "40", and reducer between nodes "260" and "270". Figure 6.13 shows the nodes' numbering and the location of the mentioned elements.

Table 6.3. Section moments

Element	Nodes	M1	M2	M3	MA	M1	M2	M3	MB
		Weight loads, N*mm				Seismic loads, N*mm			
BEND	30	8.589E+04	-3.644E+05	-1.158E+06	**1.217E+06**	1.705E+08	2.841E+08	9.449E+07	**3.445E+08**
	40	-2.579E+05	2.777E+05	7.109E+05	8.056E+05	1.474E+08	2.193E+08	6.767E+07	2.727E+08
PIPE	250	-1.851E+05	-3.125E+05	-1.008E+05	3.769E+05	1.726E+08	1.498E+07	1.486E+07	1.738E+08
	260	1.851E+05	3.518E+05	-6.406E+04	**4.026E+05**	1.726E+08	5.667E+08	2.265E+08	**6.343E+08**
REDU	260	-1.851E+05	-3.518E+05	6.406E+04	4.026E+05	1.726E+08	5.667E+08	2.265E+08	6.343E+08
	270	1.851E+05	3.583E+05	-9.128E+04	**4.135E+05**	1.726E+08	6.583E+08	2.660E+08	**7.307E+08**

Figure 6.13. Piping FE model and nodes' numbering
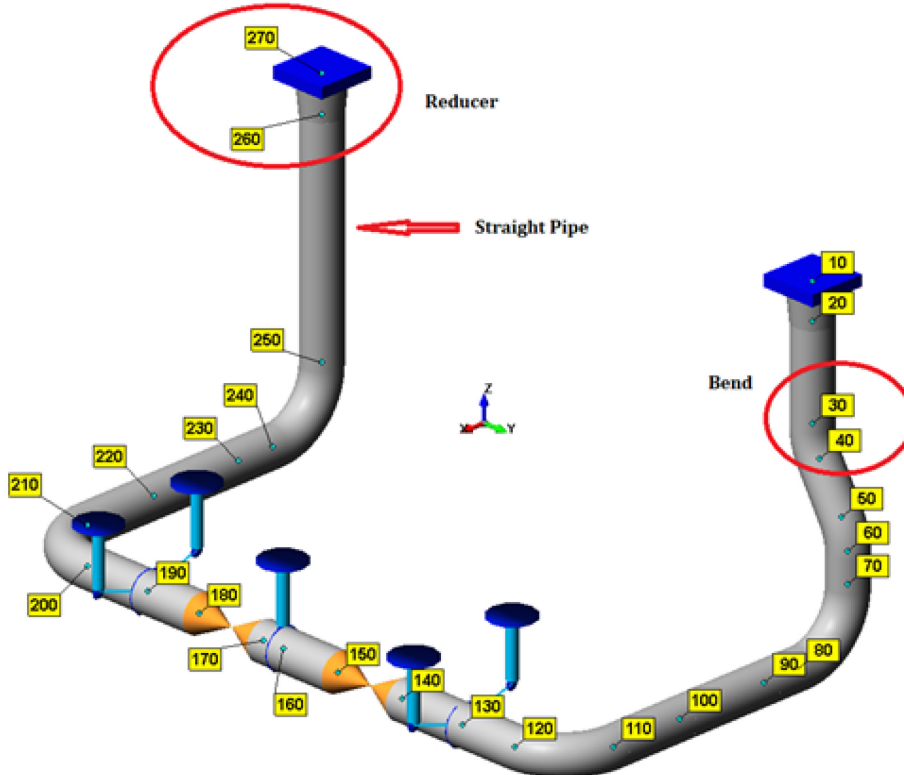
The Equation (9) for service level D, NC-3655, will be considered further:

$$B_1 \frac{P * D_0}{2t_n} + B_2 \frac{M_A + M_B}{Z} \leq S_{allw}^D = \min(3S_h; 2S_y)$$

A summary of calculations is given below in Table 6.4:

Table 6.4. Stress assessment of the pipes and fittings (conventional approach)

Parameters	Designation	Units	Expression	Value
primary stress indices				
straight pipe (nodes "250" – "260")	B_1		-	0.5
	B_2		-	1
bend (nodes "30" – "40")	B_1		$0.4*h-0.1 \leq 0.5$ and ≥ 0	0
	B_2	-	$1.30/h^{2/3}$	5.44
reducer (nodes "260" – "270")	B_1		-	0.5
	B_2		-	1
resultant moment loading on cross section due to weight loads				
straight pipe (nodes "250" – "260")		N*mm	-	4.026E+05
bend (nodes "30" – "40")	M_A			1.217E+06
reducer (nodes "260" – "270")				4.026E+05
resultant moment loading on cross section due to seismic loads				
straight pipe (nodes "250" – "260")		N*mm	-	6.343E+08
bend (nodes "30" – "40")	M_B			3.445E+08
reducer (nodes "260" – "270")				6.343E+08
Equation (9) resulting stresses				
straight pipe (nodes "250" – "260")		MPa		358
bend (nodes "30" – "40")	EQ9_D		$B_1 \frac{P * D_0}{2t_n} + B_2 \frac{M_A + M_B}{Z}$	1 030
reducer (nodes "260" – "270")				358
Demand to capacity ratio				
straight pipe (nodes "250" – "260")				1.01
bend (nodes "30" – "40")	FS$_{E9D}$	-	EQ9_D/S_{allw}^D	2.91
reducer (nodes "260" – "270")				1.01

Seismic analysis according to the proposed code case (see Annex I)

Prevention of fatigue failure

The assumption is set that the total equivalent number of cycles for all service level A and B thermal cycles is less than 1 000. Given that $S_h = S_c = 118$ MPa < 140 MPa, then the simplified form of the fatigue's prevention equation can be used:

$$S_{SD} = i \frac{M_{SD}}{Z} \leq \frac{1960}{N_{SD}^{0.2}}$$

where:

S_{SD} = stress range for service level D seismic loads, ksi (MPa);

i = stress intensification factor (NC-3673.2);

M_{SD} = range of resultant moments due to seismic loads specified for the level D service limits;

Z = section modulus of the pipe;

N_{SD} = equivalent number of maximum stress cycles for service level D seismic loads;

N_{SD} can be estimated according to Equation 6.2-18:

$$N_{SD} = n_e = 0.54 \, (N_e^{0.6} + 5)$$

where $N_e = T/\tau$. T is the duration of the strong motion and τ is the eigen period of the predominant mode.

According to NUREG/CR-5347, the strong motion duration can vary from 6 to 15 seconds. For the considered benchmark line, T can be assumed to be equal to 12 seconds. and the predominant mode to be the first eigen mode with a natural frequency of 1.72 Hz. Thus: $\tau = 1/1.72 = 0.58$ sec. The following calculations are summarised in Table 6.5.

Table 6.5. Stress assessment for the prevention of fatigue failure

Parameters	Designation	Units	Expression	Value
duration of the strong motion	T	sec	-	12
eigen period of the predominant mode	τ		-	0.58
seismically induced number of cycles of various amplitudes	N_e		T/τ	20.64
equivalent number of maximum stress cycles for service level D seismic loads	N_{SD}	-	$0.54 \, (N_e^{0.6} + 5)$	6.02
allowable stress for seismic fatigue evaluation	S_{allw}^{SF}	MPa	$\dfrac{1960}{N_{SD}^{0.2}}$	1 369
section modulus of pipe	Z	mm^3	$2*I/D_o$	1.83E+06
Range of resultant moments due to seismic loads:				
Straight pipe			$2*M_B$ from the Table 6.3.3	1.269E+09
Piping bend	M_{SD}	N*mm		6.890E+08
Reducer				1.269E+09
stress intensification factor				
Straight pipe			-	1.00
Piping Bend	i	-	$0.9/h^{2/3}$	3.76
Reducer			$0.5+0.01\alpha(D_2/t_2)^{0.5} = 2$	1.60
Straight pipe			$i\dfrac{M_{SD}}{Z}$	695
Piping bend	S_{SD}	MPa		1 419
Reducer				1 112
Demand to capacity ratio				
Straight pipe			$\dfrac{S_{SD}}{S_{allw}^{SF}}$	0.51
Piping bend	FS_{SF}	-		1.04
Reducer				0.81

<u>Prevention of plastic instability</u>

The same approach as for the conventional seismic analysis is used for the prevention of plastic instability, but for the seismic input a reduced floor response spectra (FRS) was used, as shown in Chapter 6 "Simplified code implementation". The initial spectra were reduced for the considered case, which is shown in Table 6.6 and Figure 6.14 below. The reduction coefficient c* was calculated as follows: c* = S_{peak}/S_{ZPA}.

Table 6.6. Reduction of the input seismic spectra to the primary part

	X-direction				*Y-direction*				*Z-direction*		
	f, Hz	S, g	S*, g		f, Hz	S, g	S*, g		f, Hz	S, g	S*, g
	0.50	0.23	0.05		0.50	0.23	0.04		0.50	0.17	0.04
	1.27	0.90	0.18		1.87	1.20	0.21		4.53	1.78	0.48
	1.44	0.94	0.18		2.68	1.90	0.33		4.97	2.17	0.58
	2.38	1.52	0.30		2.93	1.92	0.33		9.82	2.17	0.58
peak	**5.11**	**5.24**	1.02		3.57	2.23	0.39		11.28	2.02	0.54
	8.29	5.24	1.02		4.46	3.20	0.56		11.90	2.01	0.54
	10.51	1.90	1.02	peak	**5.55**	**6.04**	1.05	peak	**12.98**	**2.39**	0.64
	12.10	1.52	1.02		8.19	6.04	1.05		20.36	2.39	0.64
	14.87	1.64	1.02		9.01	3.42	1.05		23.55	1.21	0.64
	30.14	1.64	1.02		11.01	1.95	1.05		27.55	0.82	0.64
ZPA	**35.92**	**1.03**	1.02		27.01	1.61	1.05		36.70	0.73	0.64
	50.00	1.02	1.02		29.01	1.29	1.05	ZPA	**50.00**	**0.64**	0.64
				ZPA	**50.00**	**1.05**	1.05				
	c* = **0.19**				c* = **0.17**				c* = **0.27**		

Figure 6.14. Reduction of the input FRS to the primary part
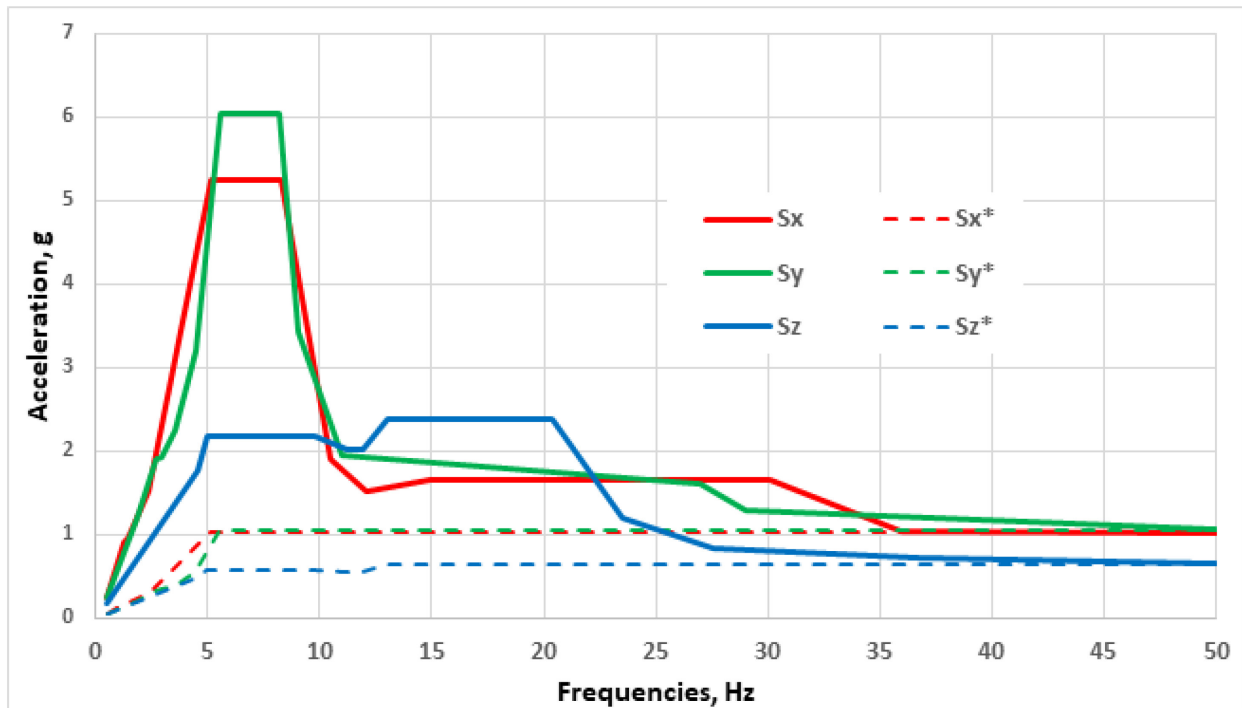
Table 6.7 shows the results of the seismic analysis for reduced FRS. The obtained results can be compared with the installed allowable stresses depending on the assigned levels of the service limits (B, C or D).

$$B_1 \frac{P * D_0}{2t_n} + B_2 \frac{M_A + M_B}{Z} \leq S_{allw}$$

Table 6.7. Stress assessment of the pipes and fittings based on the reduced FRS

Parameters	Designation	Units	Expression	Value
Service level D allowable stresses	S_{allw}^{D}	MPa	$\min(3.0S_h; 2.0S_y)$	354
resultant moment loading on cross section due to primary part of seismic loads				
straight pipe (nodes "250" – "260")				1.235E+08
bend (nodes "30" – "40")	M_B	N*mm	-	6.502E+07
reducer (nodes "260" – "270")				1.235E+08
Equation (9) resulting stresses				
straight pipe (nodes "250" – "260")				78
bend (nodes "30" – "40")	EQ9	MPa	$B_1\dfrac{P*D_0}{2t_n} + B_2\dfrac{M_A+M_B}{Z}$	197
reducer (nodes "260" – "270")				78
Demand to capacity ratio				
straight pipe (nodes "250" – "260")				0.22
bend (nodes "30" – "40")	FS$_{E9D}$	-	EQ9/S_{allw}^{D}	0.56
reducer (nodes "260" – "270")				0.22

Figure 6.15 demonstrates the benefits of the proposed procedure. The demand to capacity ratios for different piping elements are summarised in the above tables: conventional analysis (6.4) and new approach (6.5 and 6.7).

Figure 6.15. Comparison of margins when applying new approach
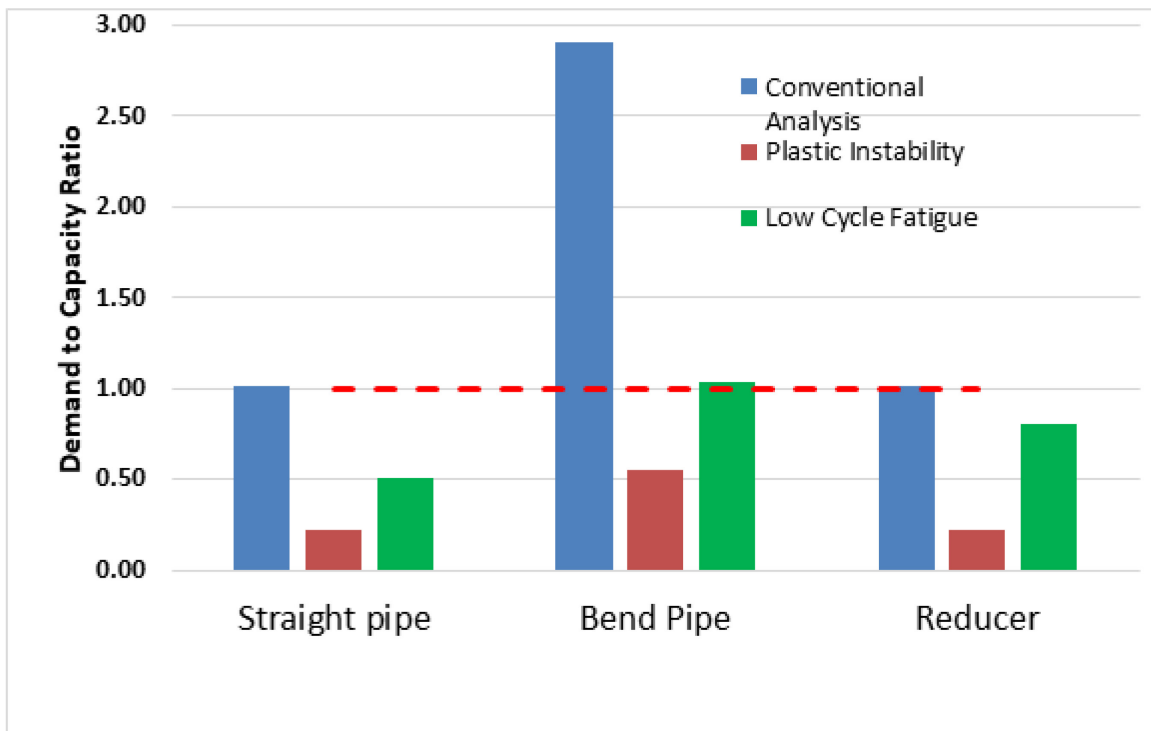
7. Conclusions and recommendations

7.1. Conclusions from earthquake experience

As presented in the references of Sections 2 and 3 of this report, it has been well established for some decades by post-earthquake reconnaissance that welded metallic piping systems exhibit strong ruggedness in strong motion earthquakes. However, there have also been cases where the piping did fail and there is sufficient data to suggest why such failures occur during real earthquakes. A study of the failure data indicates that the piping failures in strong motion earthquakes tend to result from a few common causes, including large anchor motions, brittle material, non-welded joints, corrosion, failure of supports and interaction.

7.2. Conclusions from seismic tests

Failures during fragility tests at seismic excitations well above the typical design input and under repetitive testing at a large number of seismic cycles tend to be due to fatigue, which is accentuated in some cases by ratcheting, such as when the pipe is under large hoop stress.

Experimental programmes were carried out in several countries to quantify the observed ruggedness, principally in Europe, India, Japan and the United States. Seismic testing of piping systems is still ongoing in India and Japan. The test programmes have confirmed that large margins are encompassed in the current design criteria of pressurised piping systems, in terms of a sustainable level of input motion as well as in terms of a duration of strong motion. These conclusions are reported in a previous Committee for the Safety of Nuclear Installations (CSNI) report (NEA, 2018).

In addition to confirming the large seismic margins, the test programmes have also indicated that the failure of pressurised piping components and systems occurred due to wall cracking that resulted from a combination of low cycle fatigue and accumulated plastic strain, which designated fatigue-ratcheting (NEA, 2018). This ratcheting effect is accentuated by internal pressure, which causes a bulging deformation of the pipe component that is superimposed to the seismic inertia-induced fatigue cycles.

In addition, the tests indicate that the effect of ratcheting on the cyclic life with relatively large residual strain is small, as explained in this report.

7.3. Conclusions about seismic design margins

As shown in the previous chapters, earthquake experience and numerous seismic tests have clearly demonstrated the significant margins that metallic pressurised piping has in resisting earthquake loads. However, this report's proposed approach for seismic design follows the general design principles that are described in Chapter 2.1.1:

1. This report does not propose any change to the design margin for internal pressure.

2. In Annex I, this report proposes to take a similar fatigue-based approach for evaluating the contribution of seismic inertia cyclic loads to fatigue damage. However, in contrast with the original Markl's approach that has a safety factor equal to two, the fatigue curve used for seismic fatigue is rebuilt with a reduced safety factor that is equal to 1.67, providing that the piping materials and contribution of non-seismic loads will correspond to the imposed limitations.

3. There is no proposal in this report to change the primary stress limit equation used for the prevention of plastic instability. Instead, there is a proposed approach that better segregates the part of the seismic response spectrum that contributes to primary stresses (plastic instability and the B stress indices).

7.4. Primary stress contribution

This report has established that the current code's categorisation of seismically induced stresses explains the ruggedness of a piping system, which has been recorded by testing and post-earthquake observations, when compared to the limited margins calculated on the basis of the code design's criteria. In current engineering practice, seismically induced inertial stresses are regarded as fully primary, causing plastic instability. However, according to Chapter 6 of this report, only a part of the seismic stress should be considered to be primary. The key parameter that controls this primary part is the non-dimensional frequency, φ, which can be calculated as the ratio of the mode frequency to the central frequency of the input motion.

An engineering approach has been presented in Section 6.2 that differentiates between the portion of the modal response as primary and that which can be considered secondary. This approach, which relies on a classic linear elastic modal analysis, should be pursued further because it could be of great practical benefit with regards to the seismic design of piping systems. Such a proposed stress re-categorisation would result in part of the seismic anchor motion stresses being regarded as primary (see Section 6.2.1.5).

7.5. Fatigue contribution

It should be recognised that seismically induced inertial stresses contribute to fatigue damage (regardless of whether they have a small or large primary part) because of their cyclic-like content. A related issue is that seismically induced stresses cannot be regarded as a series of cycles of constant amplitude, as is the case when running conventional fatigue analyses. A method presented in Section 6.2 of this report, which allows the designer to determine the equivalent number of cycles to be considered when calculating the seismic contribution to fatigue damage, could resolve this issue. This number is directly proportional to the duration of the strong motion, which can vary from country to country, and is an additional input to be provided to the designer. A draft procedure of a new design approach incorporating cyclic fatigue analysis and based on Markl's fatigue equation is presented in Annex I of this report. This approach does not require non-linear analysis. The approach consists of a processing of the outputs of a conventional linear elastic analysis. However, this classic fatigue approach faces the challenge of reflecting damage caused by ratcheting, which is addressed in the next section.

7.6. Seismically induced ratchet strain

7.6.1. Strain accumulation

Once it is accepted, as mentioned above, that conventional fatigue analysis, such as that presented in Annex I, is still valid as long as the accumulated plastic strain does not exceed a certain threshold (for example, 5% to be safe with respect to the 10% introduced in Section 6.2.2), it becomes necessary to estimate the strain to be compared against these limits (5% or 10%) that would still permit an equivalent linear analysis. The following methods can be used to estimate the seismic strain accumulation.

7.6.2. Non-linear time history analysis

Running systematic time history analyses could become an engineering practice, as indicated in Section 5.2.3, which describes the Japanese approach. However, as indicated by the large scatter of the Metallic Component Margins under High Seismic Loads (MECOS) benchmark analysis results (NEA, 2018), calculating the seismically accumulated plastic strain in a pressurised component by a time history analysis remains an issue. It is therefore recommended to improve the refinement of material modelling and local geometry modelling, which are necessary to develop predictive analyses of seismically induced ratcheting. In addition, the experimental results show that there is a significant random effect in the development of accumulated plastic strain and crack initiation/propagation. The corresponding uncertainties should therefore be properly taken into account. The finalisation of such research is expected to take some time.

Another important challenge for plastic analysis is the range of shapes and profiles of standard pipe fittings (elbows, tees, reducers, welded branch connections, socket welded fittings, etc.). Plastic analysis requires an accurate understanding of the fitting or component profile and therefore these would have to be controlled in a more rigorous manner than is the case in current practice by standard fitting manufacturers.

Finally, plastic analysis by time history input would probably require multiple time history inputs to capture the uncertainty of input and modelling. As a result, the plastic analysis method would be impractical on the large scale that would be needed to design hundreds of piping systems in a nuclear power plant.

7.6.3. Post-elastic analysis processing

A more pragmatic alternative for plastic strain analysis is the calculation of an upper bound of the seismic induced strain, instead of the precise accumulated strain. This could be done on the basis of i) equivalent linear analyses of the piping system under consideration through an appropriate methodology that should be calibrated against available experimental results, and ii) an assessment of an upper bound of the seismically induced ratchet through an appropriate post-treatment that incorporates the internal pressure and sustained loads effects.

The fittings would also have to be modelled to yield an upper bound strain solution, which represents a challenge because, as mentioned earlier, pipe fittings are standard commercial items with a broad range of shape tolerances.

7.6.4. Ratchet strain data

Regardless of the adopted approach, there is a recognised lack of experimental data from fatigue tests that have a small number of cycles under large hoop strains due to internal pressure. It is therefore recommended that further experimental campaigns be conducted on this subject. These tests do not have to be dynamic tests. A series of constant amplitude cyclic tests of components under high internal pressure would be sufficient, and even more appropriate for providing the needed data.

7.7. Degraded piping

An issue with the type of experiments that are presented in this report is that they were carried out on virgin piping systems, whereas an earthquake could affect a system with flaws.

Flaws in piping systems can be of four kinds: (1) wall thinning, (2) crack-like flaws, (3) embrittlement, and (4) mechanical damage such as surface dents and gouges.

The effect of wall thinning has been earlier mentioned to aggravate the pressure-induced ratcheting damage in the thinned section.

Cracking can be due to three causes: (1) a fabrication weld flaw, (2) a fatigue crack caused by a cyclic operation before the earthquake occurs, and (3) corrosion-induced cracking; or a combination of causes (1), (2) and (3). Regarding weld flaws, the construction codes require welds to be fabricated in accordance with qualified procedures and welds to be non-destructively examined to detect and correct crack-like flaws. In addition, the nuclear power industry implements an in-service inspection program, which includes the periodic volumetric inspection of welds to detect and correct operational-induced cracks. The likelihood of undetected crack-like flaws existing is therefore small. However, they cannot be fully excluded. The question of available margins in cracked piping systems should thus be addressed. The observed through-wall cracks appeared following a long series of seismic runs. This means that the crack appears after a certain period of time and the last runs are in fact performed on a cracked component. This situation should be carefully investigated so as to be able to account for possible cracks in fatigue analysis. Investigating this type of situation should not be solely analytical; it should be based on experimental data. For this reason, it is recommended that some elbows of the Bhabha Atomic Research Centre (BARC) campaigns that experienced through-wall cracks be subjected to metallographic examinations in order to precisely determine the crack initiation and propagation.

7.8. Loads on supports, restraints and equipment

The piping response forces that are transferred to the piping supports, restraints and equipment nozzles depend on the magnitude of the input excitations, piping frequencies and the actual damping present in the system. The prediction of accurate support, restrain and nozzle loads is an essential aspect required to achieve a safe design. While the welded metal pipe has significant ductility and can be used to justify the use of large damping, the damping to be used for the prediction of reaction loads needs to be carefully considered. Some results of studies in that domain are presented and discussed in Annex D.

The procedure and design methods concerning piping supports can be evolved in future tasks of research and development.

7.9. Needs for further experimental research

As presented in the report, many test campaigns have been implemented in many countries and by many organisations. Only some of the campaigns – those considered representative – are presented in the report. The detailed analysis of their results, as explained in §7-2, constitutes the basis for the development of the proposed approach.

However, a more systematic test campaign on components of piping systems (straight pipes, elbows and tees) seems necessary to improve the characterisation and quantification of the failure modes and paramount effect of internal pressure. Tests should be conducted under different pressure levels, inducing a wide range of circumferential stress values in conjunction with cyclically applied bending moments and under quasi-static loading conditions. Piping with different schedules (diameter-over-thickness ratio) should be considered.

As a complement to these component quasi-static tests, tests on complete piping systems with and without pressure, under seismic dynamic excitation and with appropriate

instrumentation could improve the understanding and predictability of the seismic behaviour of piping systems.

Some of the questions related to topics mentioned in previous paragraphs – such as plastic instability (§7.3), fatigue analysis (§7.4), ratchet strain (§7.5) and the presence of cracks (§7.6) – could be considered in these proposed tests. A review of planned tests, such as those in BARC or other organisations, should be made to optimise the programme.

7.10. Needs for future benchmarking

The MECOS initiative started with two benchmarks (NEA, 2018) that were analysed by different teams and brought about many exchanges between participants. It is recommended to organise international benchmark cases with the objective of having different teams that work on the same object and apply the criteria proposed here (primary vs. secondary stress, Markl's fatigue life assessment, elastic vs. plastic analyses and accounting for pressure-induced ratcheting). These additional cases would publicise the proposed approach, compare the approach to the current code approach and challenge the proposal by alternative analyses. Margin evaluation exercises could also be included. The important initial step in this benchmark would be to find one or a few candidate piping systems for the exercise. The tested system mentioned in §7.7 could be considered.

7.11. Other follow-up considerations

Some questions related to the seismic design and analysis of piping systems have deliberately not been considered in this report. The following actions would improve and optimise engineering practices:

- a design analysis of pipe supports and an analysis of piping-to-equipment nozzle loads, which is mentioned in §7-7;
- the drafting of a design and analysis approach for class-1 piping.

7.11.1. References

NEA (2018), "Final Report of the Project on Metallic Component Margins Under High Seismic Loads (MECOS)", OECD Publishing, Paris, www.oecd-nea.org/jcms/pl_19848.

Annex A. Contributors to the report

Table A.1. Contributors to the report

Name	Given name	Country	Organisation
BLAHOIANU	Andrei	Canada	CSNC (R)
CHAUDHRY	Khalid	Canada	CSNC (R)
AUDEBERT	Sylvie	France	EDF
BERGER	Julien	France	EDF
LABBE	Pierre	France	ESTP
MATHON	Cedric	France	EDF
MOREAU	François	France	GDS
NGUYEN	Thuong Anh	France	GDS
RAMBACH	Jean-Mathieu	France	GDS
SOLLOGOUB	Pierre	France	Consultant
KARAMANOS	Spyros	Greece	U. Thessaly
RAVI KIRAN	Akella	India	BARC
REDDY	G. R.	India	BARC
NAKAMURA	Izumi	Japan	NIED
OTANI	Akihito	Japan	IHI Corporation
YAMAZAKI	Tatsuhiro	Japan	JANSI
BERKOVSKY	Alexey	Russia	CVS
ANTAKI	George	United States	BECHT
NEVANDER	Olli	NEA	NEA

Annex B. Feedback of experience about piping seismic behaviour

B.1. Examples illustrating the general seismic behaviour of piping systems

Figure B.1. View of detailed piping system in Coalinga oil field
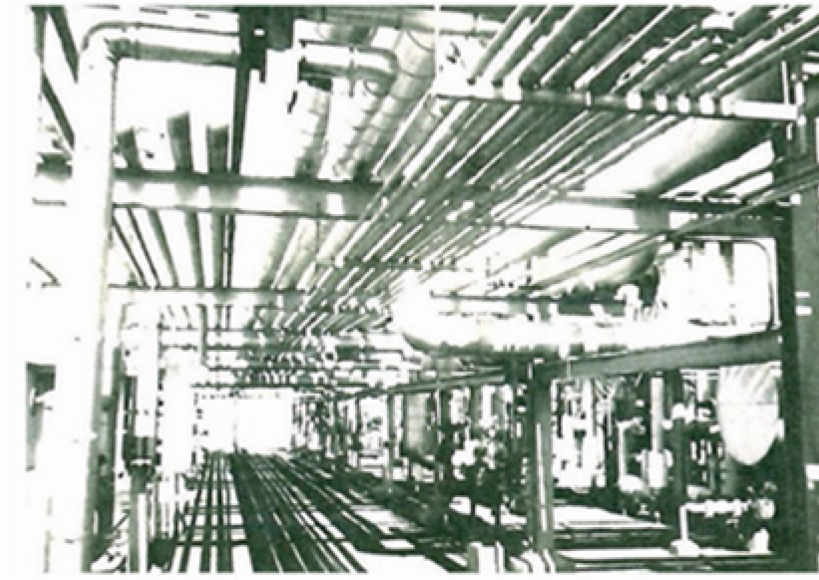
Note: In most cases, non-seismically designed, above-ground, welded and un-corroded welded steel pipes did not fail in strong motion earthquakes.
Source: EQE, 1983, Coalinga earthquake.

Figure B.2. View of detailed piping system in Coalinga oil field
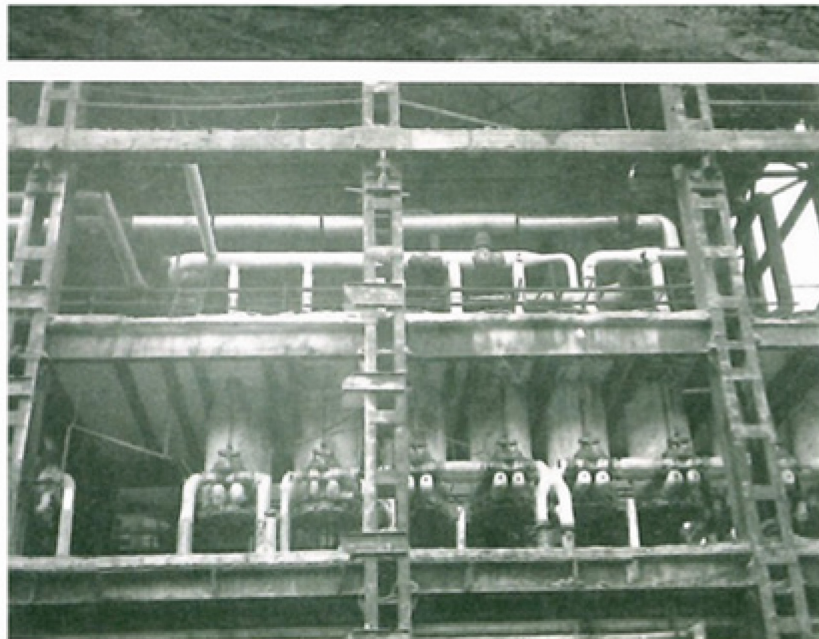
Note: In most cases, non-seismically designed, above-ground, welded and un-corroded welded steel pipes did not fail in strong motion earthquakes.
Source: EQE, 1983, Coalinga earthquake.

Figure B.3. View of general piping system at Las Ventanas coal-fired power plant
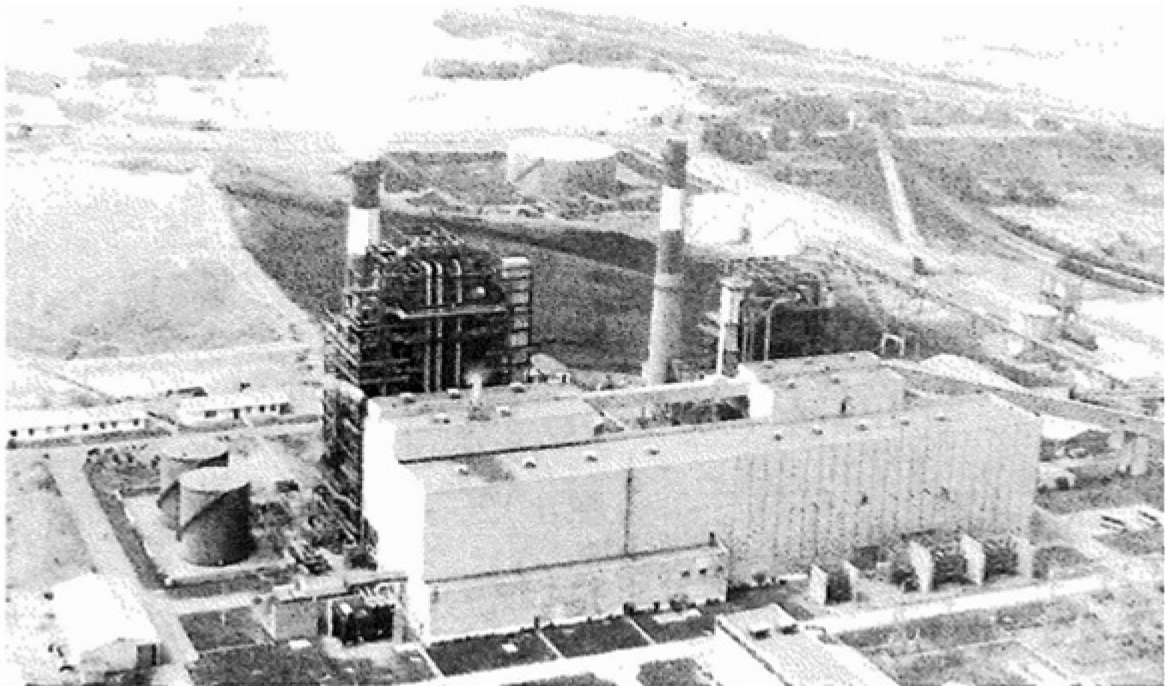
Note: There were no reported piping failures at the Las Ventanas coal-fired power plant.
Source: EQE, 1985, Chile earthquake.

Figure B.4. View of general piping system at ConCon refinery
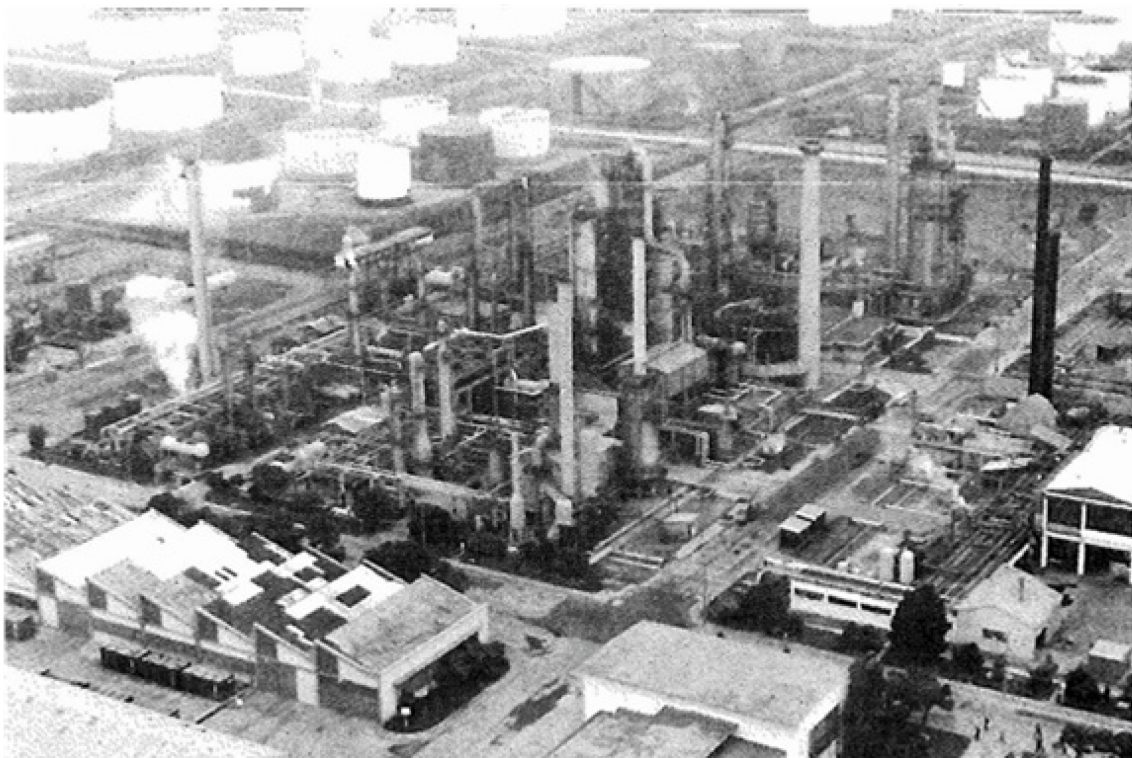
Note: There were no reported piping failures at the ConCon refinery.
Source: EQE, 1985, Chile earthquake.

Figure B.5. Detailed view of a pipe failure at a steam plant near Kobe
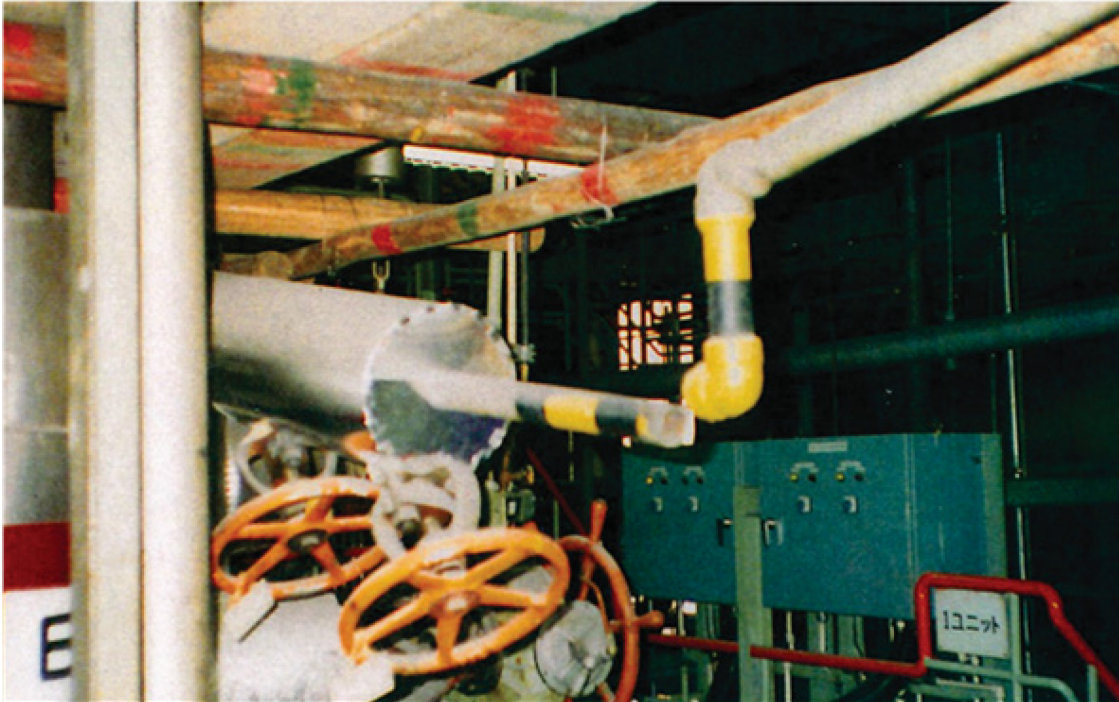
Note: Pipe failure caused by steam drum displacement at a steam plant.
Source: EQE, 1995, Kobe earthquake.

Figure B.6. Butane storage tanks affected by Coalinga earthquake
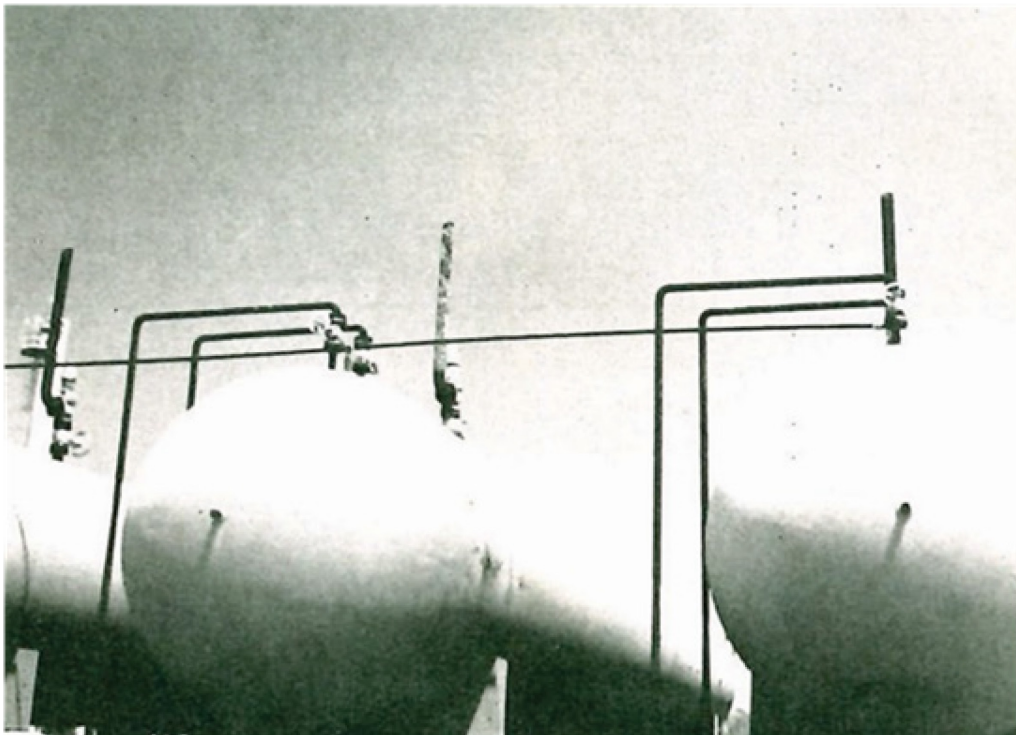
Note: The vent is reported to have ruptured as the butane storage tanks settled.
Source: EQE, 1983, Coalinga earthquake.

Figure B.7. View of a tank and attached piping affected by Loma Prieta earthquake
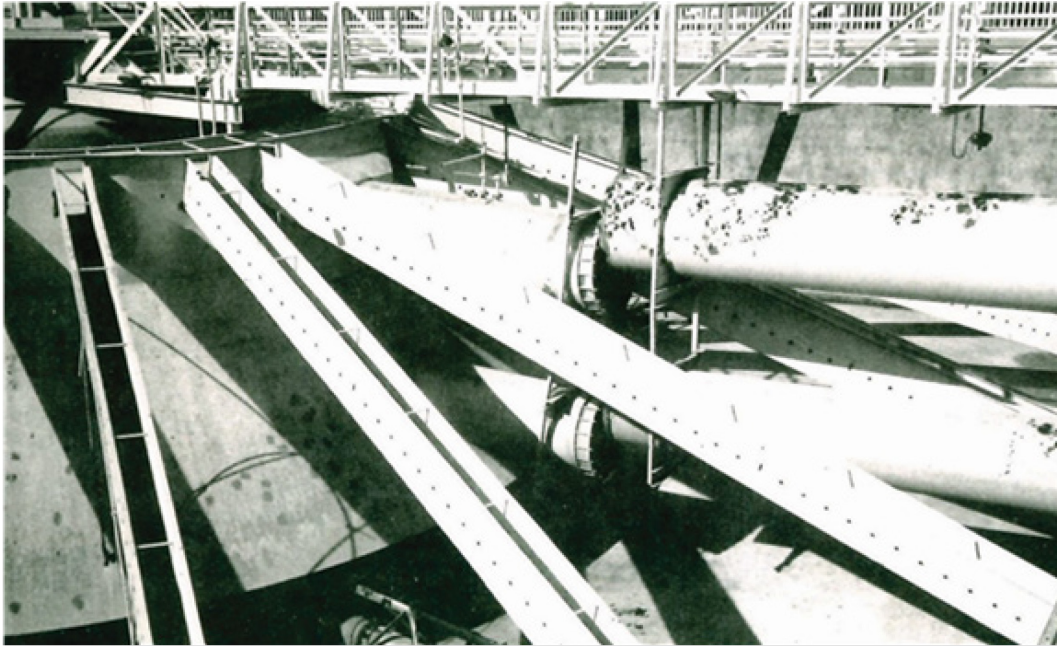
Note: Sloshing caused the tank to rock and pulled open a mechanical joint on the attached piping.
Source: EQE, 1989, Loma Prieta earthquake.

Figure B.8. Detail of the rupture of a pipe by the attached tank sliding in an oil field near Coalinga

Note: Rupture of a pipe caused by the attached tank sliding.
Source: EQE, 1983, Coalinga earthquake.

Figure B.9. Detailed view of pipe support failure at the industrial facility caused by the Northridge earthquake

Note: Pipe support failure caused by movement of the attached chiller.
Source: EQE, 1994, Northridge earthquake.

Figure B.10. Detailed view of pipe failure at the industrial facility caused by the Northridge earthquake

Note: Failure of ¾ in. (20 mm) threaded nipple caused by header movement
Source: EQE, 1994, Northridge earthquake.

Figure B.11. View of the fracture of a cast iron valve at the tank nozzle caused by the Northridge earthquake
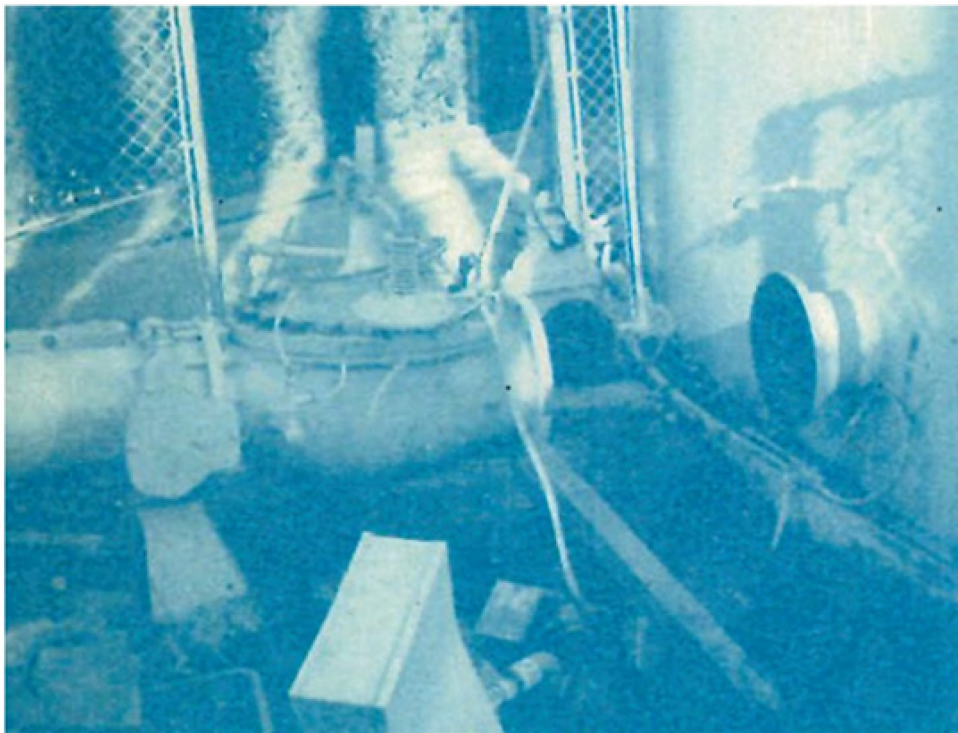
Note: Fracture of cast iron valve at tank nozzle.
Source: DOE/EH, 1994, Northridge earthquake.

Figure B.12. View of a broken cast iron valve caused by the Northridge earthquake

Note: Broken cast iron valve.
Source: EQE, 1994, Northridge earthquake.

Figure B.13. Fire protection pipes affected by the Northridge earthquake

Note: Damaged fire protection mechanical couplings.
Source: EQE, 1994, Northridge earthquake.

Figure B.14. View of the leaking corroded inlet riser to the cooling tower at ground level due to the Northridge earthquake

Source: EQE, 1994, Northridge earthquake.

Figure B.15. View of the leaking corroded elbow in a condensate line as a consequence of the Northridge earthquake

Source: EQE, 1994, Northridge earthquake.

Figure B.16. Pipe support failure from ground failure produced by the Northridge earthquake

Source: EQE, 1994, Northridge earthquake.

Figure B.17. Soil liquefaction caused the support saddle to drop nearly 12 in. (25 mm) in the Loma Prieta earthquake

Note: Wood blocks were added to support the pipe that was not damaged.
Source: EQE, 1989, Loma Prieta Earthquake.

Figure B.18. Pipes affected by the Adak Alaska earthquake
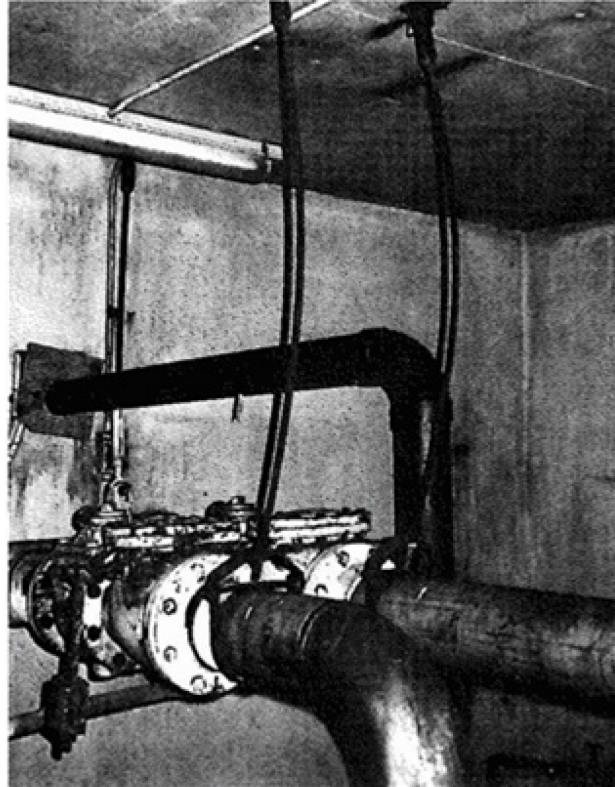
Note: Ceiling settlement buckles the strut supports.
Source: EQE, 1986, Adak Alaska earthquake.

Figure B.19. View of a pipe system affected by the Northridge earthquake
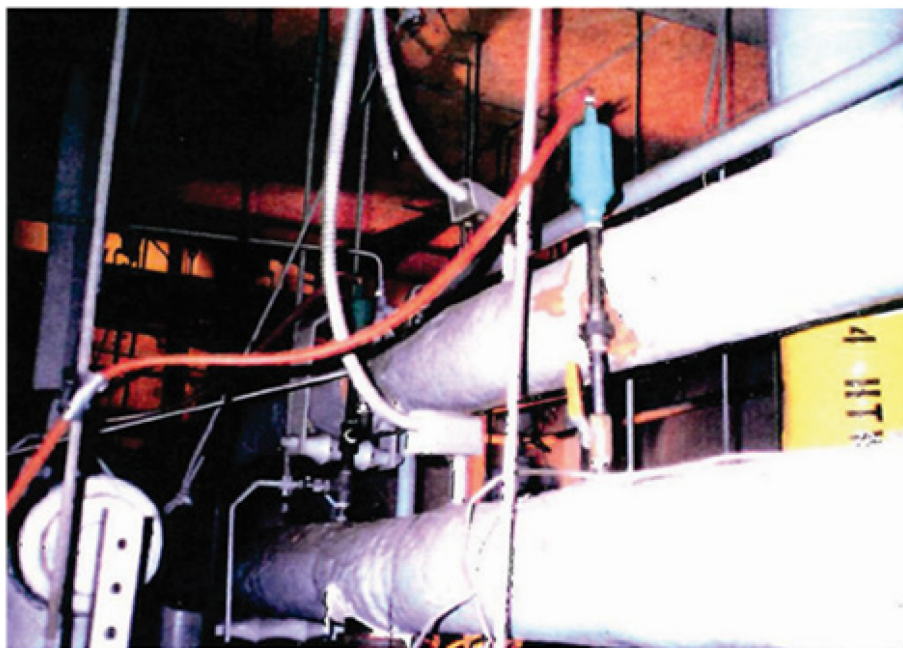
Note: ½ in. (12 mm) vent pipe failure caused by impact from the adjacent pipe header.
Source: EQE, 1994, Northridge earthquake.

Figure B.20. Picture of two pipes after impact due to the Superstition Hills earthquake
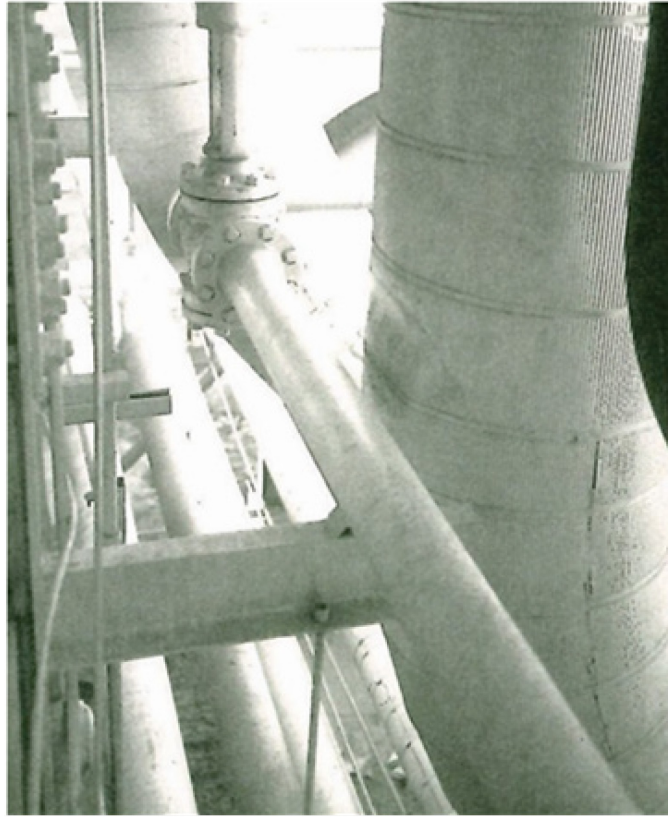
Note: Dented pipe insulation caused by pipe-to-pipe impact.
Source: EQE, 1987, Superstition Hills earthquake.

Figure B.21. View of pipe damages caused by the Chile earthquake
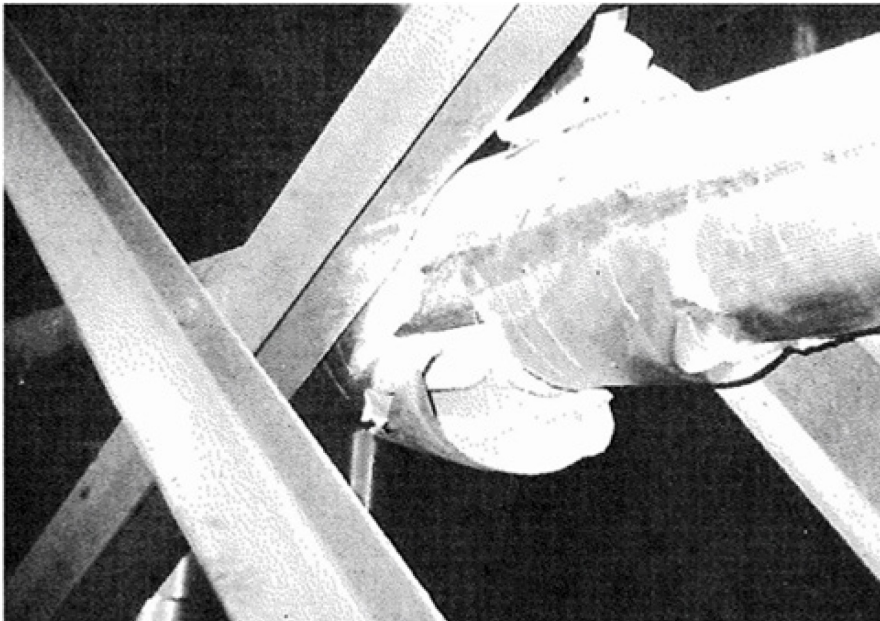
Note: Piping insulation damaged from impact with a nearby structure, but the pipe was not damaged.
Source: EQE, 1985, Chile earthquake.

B.2. Some specific examples from Japan

B.2.1. General

Although there have been many cases of Japanese nuclear power plants experiencing earthquakes, the safety of nuclear power plants has never been threatened by earthquakes.

The Niigata ken Chuetsu-oki (NCO) earthquake that occurred in 2007 caused a fire in the in-house transformer due to the ground subsidence of the Kashiwazaki-Kariwa Nuclear Power Station's Unit 3 of the Tokyo Electric Power Company. However, fire extinguishing efforts were not very successful because the fire extinguishing piping was also damaged by the deformation of the ground due to the earthquake. The buried fire extinguishing piping joint had been damaged by the forced deformation.

The Great East Japan Earthquake (GEJE) occurred on 11 March 2011. The tsunami that followed the earthquake caused power loss in the Fukushima Daiichi Nuclear Power Plant. The reactor core could not be cooled and there was core damage. The Tohoku Electric Power Co. Onagawa Nuclear Power Station closest to the epicentre survived damage from the tsunami because of the site height. An earthquake damage survey was conducted at the Onagawa Nuclear Power Station and concluded that there was minor damage but there was no problem in nuclear reactor safety and no damage done to piping systems.

In addition, an earthquake damage survey was carried out of the Sendai Thermal Power Plant and Shin Sendai Thermal Power Station near the Onagawa Nuclear Power Station. These thermal power plants are installed on the Japan Pacific coast. As a result, there was no damage to the piping systems, but there was damage to the mounting part of the hydraulic snubber, as well as deformation and damage to the vibration isolator.

Thermal power plants' seismic design is based on JEAC 3605 at about 0.3 g in Japan. It was found that the seismic acceleration recorded at the thermal power plant had more than about twice the specified acceleration value. Even when there were over twice the design accelerations, the piping system was not damaged by an earthquake.

In the survey of piping damage cases thus far, cases can be found where the small diameter piping attached to the large-diameter piping systems suffered damage due to the forced displacement of the large-diameter piping during the earthquake. A photo showing typical damage at the Fukushima Daiichi Nuclear Power Plant #5 during GEJE is listed below.

B.2.2. Examples of damage to the piping support section in a thermal power plant

Figure B.22. View of damage to the piping support section in a thermal power plant

Shinn-Sendai thermal power station oil snubber connecting the rod fix was partly damaged
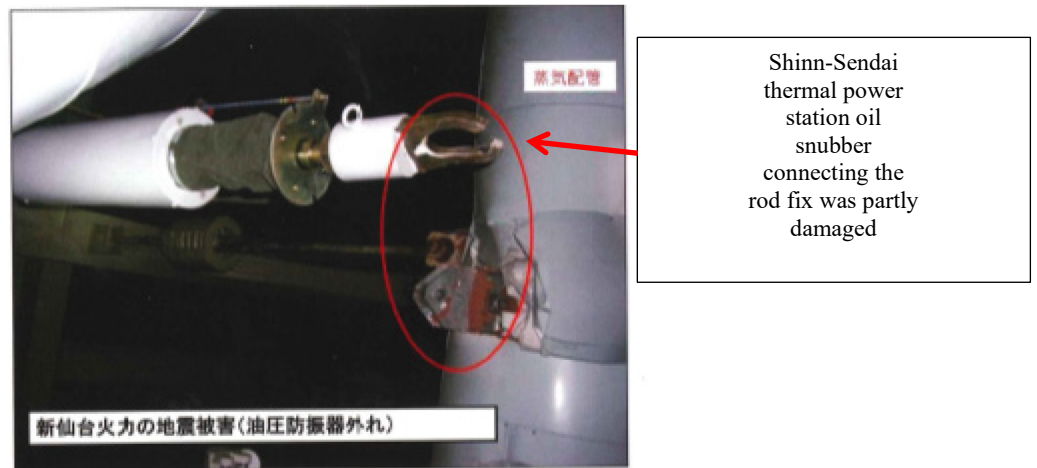
Source: Thermal and Nuclear Power Association, 2012.

Figure B.23. View of damage to the piping support section in a thermal power plant

Broken Sendai thermal power plant oil snubber rod
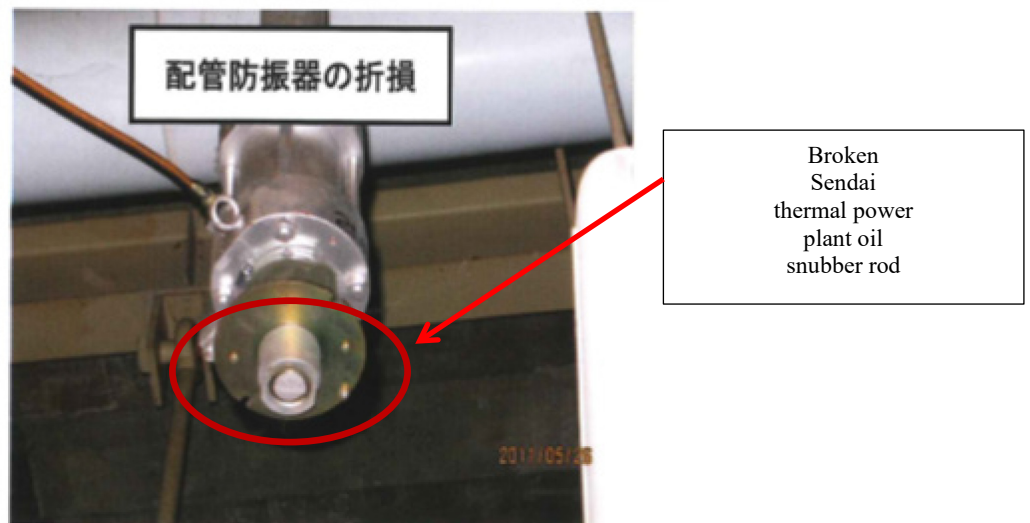
Source: Source: Thermal and Nuclear Power Association, 2012.

Figure B.24. View of damage to the piping support section in a thermal power plant

Fukushima Daiichi #5: turbine moisture separator drain piping line drain with a broken blow line during GEJE

Source: Tokyo Electric Power Company, 2021.

B.2.3. Detail of buried pipe damage by the NCO earthquake at Kashiwazaki-Kariwa Nuclear Power Plant

This earthquake caused a fire at the in-house transformer 3B of Unit 3. Fire extinguishing activities were attempted using outdoor fire hydrants, but the fire extinguisher piping was damaged by the earthquake and it was not possible to secure the water necessary for firefighting.

Analysis of the background of the fire extinguishing piping damage showed that mechanical joints such as coupling and threaded joints were used in the joints for the fire extinguishing piping.

Fire extinguishing piping damage:

- Large displacement occurred locally due to ground subsidence, etc.;

- Mechanical joints were completely broken and welded joints were damaged, but leakage was very small.

Figure B.25. View of buried pipe damage by the NCO earthquake at Kashiwazaki-Kariwa Nuclear Power Plant
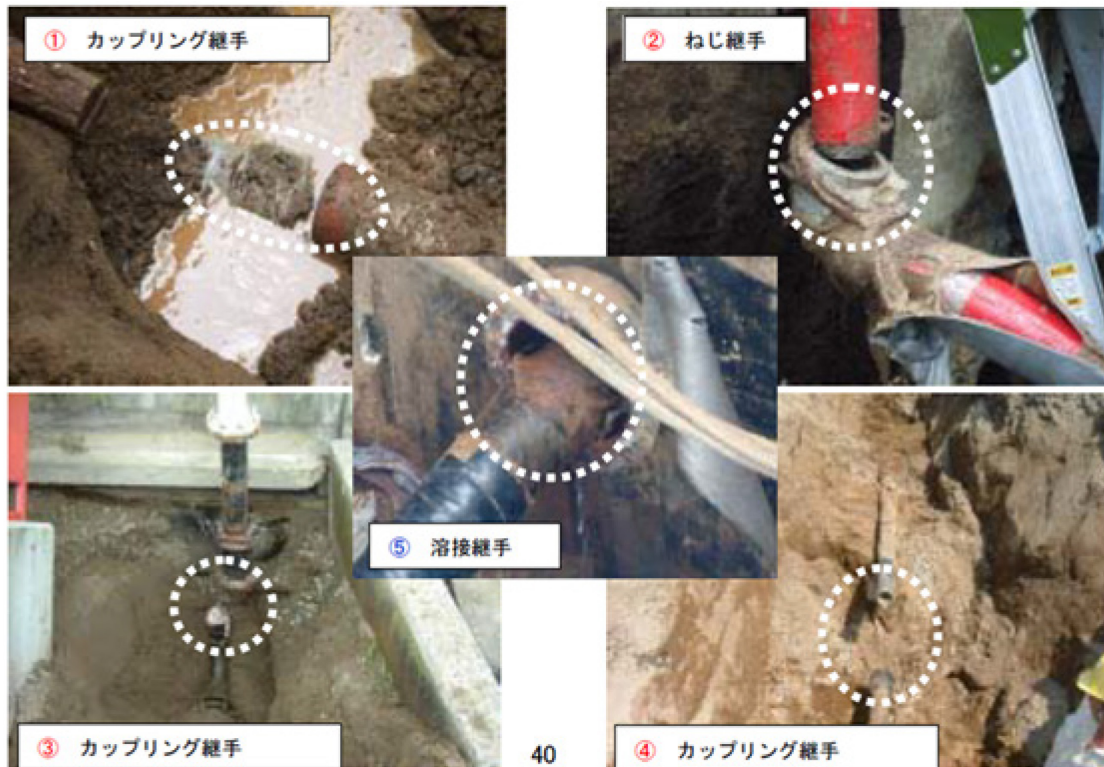
Source: Tokyo Electric Power Company, 2021.
Note: 1, 3, 4 - coupling joint; 2 - thread joint; 5 - weld joint.

B.3. Specific examples of support behaviour

Past earthquakes and shake table tests reveal that piping supports fail long before the actual piping system fails. This is attributed to the piping systems' high ductility. A shake table test was conducted on a three-inch pressurised carbon steel piping system with U-clamp support, as shown in Figure B.1. During the test, the support was observed to fail (at 1.2 g zero period acceleration [ZPA]) long before the failure of the piping system (at 2 g ZPA).

Figure B.26. Failure of the U-clamp support during a shake table test on a piping system

Source: Ravikiran et al., 2013.

Failure of piping supports was observed during the Bhuj earthquake of 2001 (Mw 7.7), as shown in Figure B.2. It is also observed that the piping systems were intact due to inherent ductility.

Figure B.27. Failure of piping supports during the Bhuj earthquake, India, 2001 (Mw 7.7)

During the Kobe Earthquake in Japan 1995 (Mw 7.0), the piping supports were also observed to fail, as shown in Figure B.3. Significant deformations of the piping systems were later observed after support failure.

Figure B.28. Failure of piping supports during the Kobe earthquake, Japan 1995 (Mw 7.0)

Some considerations about evaluation of reaction forces on supports are proposed in Annex D.

B. 3.1. References

Thermal and Nuclear Power Association (2012), GEJE Thermal Power Plant Damage Investigation Report.

Tokyo Electric Power Company (2021), TEPCO Homepage, www.tepco.co.jp/en/hd/index-e.html, accessed 2021.

Annex C. Failure modes observed in the test results

This Annex compiles the experimental results about fatigue life collected from tests conducted in multiple countries. The experimental results show the fatigue lives of pipe fittings under alternating cyclic loads. The strain ranges and cycles are provided. It is recognised that the values reported here have been developed over the years in different countries and are not always reported in a consistent manner. The variety of conditions generates a scattering of results in the figures and the different conditions must be recognised as causing the scattering.

The experimental results in this Annex are scattered but nevertheless essential. Continued efforts must be made to collect, accumulate and analyse this type of data.

Figure C.1. Annex C. Failure modes observed in the test results

		Input Data					Test Results								
Test n°	Type of Specimen	Material/ Schedule	Pressure P (MPa)	Reduced pressure[5]	Load application	Number of Cycles	Test Duration, (s)	Test Wave form[1]	Equiv Number of cycles[2]	Amplitude of input[3]	Max ratchet Strain, %	Peak to peak cyclic strain	Failure Mode[4]	Crack location	Notes
CEGB 1986-1	Straight	D/t=8.4	29.2	2/3 (hoop)	NA			SW		≈50					
CEGB 1986-2	Straight	D/t=8.4	29.2	2/3 (hoop)	NA			SW		≈50	2				
CEGB 1986-3	Straight	D/t=8.4	29.2	2/3 (hoop)	NA			SW		≈50	3.1				
CEGB 1986-4	Straight	D/t=27.9	14.3	2/3 (hoop)	NA			SW		≈50	3.1				
CEGB 1986-5	Straight	D/t=8.4	29.2	2/3 (hoop)	NA			SW		≈50	1				
CEGB 1986-6	Straight	D/t=27.9	14.3	2/3 (hoop)	NA		90	SW	810	≈50	2				
CEGB 1986-7	Straight	D/t=27.9	14.3	2/3 (hoop)	NA		40	SW	360	≈50	3.5				
CEGB 1986-8	Straight	D/t=8.4	29.2	2/3 (hoop)	NA		40	SW	360	≈50					
CEGB 1991-1	Straight with 2 elbows	CS Sch 20 D/t=14,8	16.69	[6]	IPB	750	115	SW	NA	[7]	[8]		F	Flank	
CEGB 1991-2	Straight with 2 elbows	CS Sch 20 D/t=14,8	16.69	[6]	IPB	1400	215	SW	NA	[7]	[8]		F	Flank	
J1-1	Bend pipe	CS	Eq. Sm	2/3	IPB	63				±33mm	6.9%	2.3%	F		Test case A
J1-3	Bend pipe	SS	Eq. Sm	2/3	IPB	169				±33mm	31.3%	2.4%	F		

Test n°	Input Data					Test Results									
	Type of Specimen	Material/ Schedule	Pressure P (MPa)	Reduced pressure[5]	Load application	Number of Cycles	Test Duration, (s)	Test Wave form[1]	Equiv Number of cycles[2]	Amplitude of input[3]	Max ratchet Strain, %	Peak to peak cyclic strain	Failure Mode[4]	Crack location	Notes
J1-5	Bend pipe	CS	Eq. 1/2*Sm	1/3	IPB	66				±33mm	5.4%	2.6%	F		
J1-7	Bend pipe	CS	0	0	IPB	68				±33mm	6.6%	3.1%	F		
J1-9	Bend pipe	CS	Eq. Sm	2/3	IPB	1050				±9 mm	0.6%	1.7%	F		
J1-11	Bend pipe	CS	Eq. Sm	2/3	IPB	101				±25 mm	6.4%	1.8%	F		
J1-15	Straight pipe	CS	Eq. Sm	2/3		164		sin	146	±55 mm	34.1%	2.3%	F		Test case B
J1-16	Elbow	SS	10.7	2/3 2/3	IPB	143		sin	75	±42.5 mm	21.0%	1.6%	F		
J1-17	Elbow	CS	19.8	2/3	IPB	185		seismic	5 times	±15.5 mm	14.7%	1.2%	F		
J1-18	Elbow	SS	10.7	2/3 2/3	IPB	143		sin	90	±42.5 mm	21.0%	1.6%	F		
BARC1	Straight pipe	CS, SA333 Gr 6, sch 80	18		3-point and 4-point bending	560	-	Cyclic		180 kN to 380 kN	9.5%	0.2%	FR		[9]
BARC2	Elbow	SS, SS304	18		IPB		550	Harm. base excitation	940	0.2g to 1g	5%	0.3%	FR		[10]
BARC3	Elbow	CS, SA106 Gr B, sch 40	21.3	-	IPB+OPB		35 each	Seismic	460 (46 TH)	0.25g to 2.25g	10.3 % (extrapolated)	0.45 %	FR	Crown	[11]
BARC4	Tee	CS, SA106 Gr B, sch 40	21.3	-	IPB+OPB		35 each	Seismic	440 (44 TH)	0.25g to 2.25g	0.7%	0.35 %	F		[12]

Test n°	Input Data					Test Results									
	Type of Specimen	Material / Schedule	Pressure P (MPa)	Reduced pressure[3]	Load application	Number of Cycles	Test Duration, (s)	Test Wave form[1]	Equiv Number of cycles[2]	Amplitude of input[3]	Max ratchet Strain, %	Peak to peak cyclic strain	Failure Mode[4]	Crack location	Notes
BARC5		CS, SA106 Gr B, sch 40	21.3	-	IPB+OPB		35 each	Seismic	600 (60 TH)	0.25g to 2.0g	5% (extrapolated)	0.3%	FR	Dent at crown	(13)
BARC6		CS, SA333 Gr 6, sch 40	18	-	IPB+OPB		35 each	Seismic	730 (73 TH)	1.0g to 2.5g	2.8%	0.6%	FR	Crown	(14)
BARC7		SCS, SS316L, sch 40	18	-	IPB+OPB		35 each	Seismic	730 (73 TH)	1.0g to 2.5g	1.6%	0.6%	FR	Crown	(15)
BARC8		CS, SA106 Gr B, sch 80	20		IPB+OPB		32 each	Seismic	290 (29 TH)	0.35g to 1.25g	8.3% (extrapolated)	0.5%	FR	Crown	
Ind-1	Elbow	P355N (X52)	0	0	IPB	13,160		Sin	13,160	$\pm25mm$		0.33	F	flank	
Ind-2	Elbow	P355N (X52)	0	0	IPB	444	12824	Sin	444	$\pm70mm$	2.8	1.23	F	flank	
Ind-3	Elbow	P355N (X52)	0	0	IPB	171	6617	Sin	171	$\pm100mm$	2.67 extr.		F	flank	
Ind-4	Elbow	P355N (X52)	0	0	IPB	61	3973	Sin	61	$\pm150mm$	4.79 extr.	2.61	F	flank	
Ind-5	Elbow	P355N (X52)	0	0	IPB	28	1589	Sin	28	$\pm20mm$	31.14 extr.		F	flank	
Ind-6	Elbow	P355N (X52)	0	0	IPB	17	950	Sin	17	$\pm250mm$	32.97 extr.	3.84	F	flank	
Ind-7	Elbow	P355N (X52)	0	0	IPB	10	698	Sin	10	$\pm300mm$	26.83 extr.	4.02	F	flank	
Ind-8	Elbow	P355N (X52)	0	0	IPB	16	9049	sin		Increasing amplitude	32.2 extr.	0.18 to 14.4	F	flank	~8.8 8%

			Input Data						Test Results						
Test n°	Type of Specimen	Material/ Schedule	Pressure P (MPa)	Reduced pressure[5]	Load application	Number of Cycles	Test Duration, (s)	Test Wave form[1]	Equiv Number of cycles[2]	Amplitude of input[3]	Max ratchet Strain, %	Peak to peak cyclic strain	Failure Mode[4]	Crack location	Notes
Ind-9	Elbow	P355N (X52)	3.2	0.12	IPB	26	20000	Sin	26	±200mm	5.04 extr.	3.01	F	flank	
Ind-10	Elbow	P355N (X52)	3.2	0.12	IPB	10	24800	Sin	10	±300mm	4.55 extr.		F	flank	
Ind-11	Elbow	P355N (X52)	7	0.26	IPB	27	12000	Sin	27	±200mm		2.45	F	flank	
Ind-12	Elbow	P355N (X52)	7	0.26	IPB	10	12200	Sin	10	±300mm		1.94	F	flank	
Ind-13	Elbow	P355N (X52)	12	0.45	IPB	22	19000	Sin	22	±200mm		2.28	F	flank	

C.1. Notes

1. Wave form: seismic (indicate the response spectrum used), spectrum waves (SWs), white noise ... The relation between the signal frequency content and eigen frequencies of the dynamic test rig should be indicated in a note attached to the corresponding test;

2. Indicate how the number of cycles was determined:

   - Using the formula (§7.2.4.1 of the MECOS GE report)

   - Other approach - precise

3. Amplitude of input:

   It could be defined as the maximum moment calculated on the specimen using a conventional linear analysis approach.

4. Failure mode

   - NF: No Failure

   - FR: Fatigue ratchet

   - F: Fatigue

   - PC: Plastic collapse

   - RB: Ratchet Buckling

5. Reduced pressure: p/p_y where p_y is the pressure inducing circonferential yield stress in a straight pipe. $p_y = 2*t*SIG_y/D$, where t is pipe wall thickness, D diameter, SIG_y is the yield stress

6. $PD/2t = 120$ MPa; $S_m = 138$ MPa $= S_y/2$

7. $C_2 \sigma_M = 6S_m$ with $C_2 = 3.85$

8. <1% for 10 cycles

9. Large amount of bulging is noticed, see: Ravi Kiran, A., M.K. Agrawal, G.R. Reddy, R.K. Singh, K.K. Vaze, A.K. Ghosh and H.S. Kushwaha (2006), "Ratcheting study in pressurised piping components under cyclic loading at room temperature", Report No. BARC--2006/E/013, Bhabha Atomic Research Centre.

10. Weld failure observed, see: Ravi Kiran, A., G.R. Reddy and M.K. Agrawal (2018), "Experimental and Numerical Studies on Inelastic Dynamic Behaviour of Stainless Steel Elbow under Harmonic Base Excitation", *Journal of Pressure Vessel Technology*, 140(2), pp.1–9 (021204).

11. Wall thinning with a rupture occurring at the crown, see: Ravi Kiran, A., G.R. Reddy and M.K. Agrawal (2018), "Experimental and numerical studies of inelastic behaviour of thin walled elbow and tee joint under seismic load", *Thin-Walled Structures*, Volume 127, pp.700-709.

12. Ravi Kiran, A., G.R. Reddy and M.K. Agrawal (2018), "Experimental and numerical studies of inelastic behaviour of thin walled elbow and tee joint under seismic load", *Thin-Walled Structures*, Volume 127, pp.700-709.

13. Wall thinning with a dent occurring at the crown, see: Ravikiran, A. P.N. Dubey, M.K. Agrawal, G.R. Reddy and K.K. Vaze (2013), "Evaluation of Inelastic Seismic Response of a Piping System Using a Modified Iterative Response Spectrum Method", *International Journal of Pressure Vessel Technology*, 135(4).

14. Wall thinning with a rupture occurring at the crown, see: Ravi Kiran, A., G.R. Reddy, P.N. Dubey and M.K. Agrawal (2017), "Fatigue-Ratcheting Behaviour of 6 in Pressurised Carbon Steel Piping Systems Under Seismic Load: Experiments and Analysis", *Journal of Pressure Vessel Technology*, Volume 139, pp.1-15.

15. Wall thinning with a rupture occurring at the crown, see: Ravi Kiran, A., P.N. Dubey, M.K. Agrawal, G.R. Reddy, R.K. Singh and K.K. Vaze (2014), "Experimental and Numerical Studies of Ratcheting in a Pressurised Piping System Under Seismic Load", *International Journal of Pressure Vessel Technology*, Volume 137, pp.1-7.

16. Wall thinning with a rupture occurring at the crown.

Abbreviations:

- CS: carbon steel
- SS: stainless steel
- D: diameter of the pipe
- t: thickness of the wall
- R: elbow radius
- IPB: in-plane bending
- OPB: out of plane bending
- SW: sinusoidal wave
- TH: time history

C.2. Remarks

C.2.1. Remarks concerning Japanese results, by Akihito Otani

The first impression of the figure regarding the fatigue lives in the experiments is that the strain ranges of the two group are separated.

The reason for the separation is supposed to be the evaluation point.

The strain ranges of the Japanese experiments were obtained at the point where the maximum strain range would be generated. It is of course difficult to measure the strain range at the maximum point because the point would be at the inside surface in pressurised water. It is also difficult to set up a strain gauge on the exact maximum point (see Ref. [1]).

FEA was therefore used to obtain the maximum strain range:

- Firstly, the strain ranges at the measurement point were compared by analysis and experiment and the validity of the analysis was confirmed.

- Then, the strain range at the maximum point was simulated and obtained by analysis.

C.2.2. Remarks concerning the Indian BARC results, by Ravi Kiran

Indian BARC provided the peak-to-peak cyclic strain values. The "range" values were thus provided. It is also to be noted that the maximum ratcheting strains provided in the table are from the actual measurements taken during shake table tests. In addition, the strain range in the (BARC) data is from the experimentally-measured data.

The high stressed elbow crown (flank) is the failure location in all these tests. Strain gauges were therefore installed at two crown locations of the elbow and the ratcheting strains provided in the table correspond to the maximum of the two, which corresponds to the failure location. A summary of the actual measurements or extrapolated results is given below: (that was also given in the Table). The actual measured strains: BARC1, BARC2, BARC4, BARC6 and BARC7. The extrapolated values due to strain gauge failure in between: BARC3, BARC5 and BARC8

The extrapolated values are provided due to early strain gauge failures. For example, in BARC8 tests, a ratcheting strain of about 5.5% was measured by the strain gauge before failure. However, by extrapolation this strain at a failure level of excitation was 8.3%. The details are provided in the IJPVP paper in reference [2].

C.2.3. References

Kiran, A.R., G.R. Reddy, M.K. Agrawal, M. Raj and S.D. Sajish (2019), "Ratcheting based seismic performance assessment of a pressurised piping system: Experiments and analysis", *International Journal of Pressure Vessels and Piping*, Volume 177.

Otani, A., I. Nakamura, H. Takada and M. Shiratori (2011), "Consideration on seismic design margin of elbow in Piping", *Pressure Vessels and Piping Conference*, Paper PVP2011-57146, Baltimore, United States.

Annex D. Damping values

D.1. Table of the damping values used in codes

**Table D.1. Table of the damping values used in codes**

Country	Document	Critical damping	Existing plants	New design	Applicable seismic Level	Frequency dependence	Additional dependence	Notes
US	ASME BPVC	0.05	+	+	OBE&SSE	NO	-	
US	ASME B31.E	0.05	+	+	"Design Earthquake"	NO	-	
US	SMA	0.05	+	-	RLE	NO	-	
US	RG 1.61 (NRC)	0.02 – 0.05	+	+	OBE: 0.03 SSE: 0.04	N-411	-	
Japan	JEAC	0.005 – 0.030	+	+	S_s/S_d	-	Type and number of supports and availability of thermal insulation	
Germany	KTA	0.04	+	+	DBE	NO	-	
Russia	NP-031	0.01 – 0.03	+	+	OBE&SSE	NO	Stress level and piping diameter	For practical purposes damping is taken as 0.02
	EUR	0.04 – 0.05	-	+	DBE	May be used		
	IAEA	0.05	+	-	RLE	-		
	EN 13480-3	0.04/0.03	+	+	SSE/OBE	N-411		OBE > SSE/3
France	RCC-M	-		+	-			Damping values are specified according to each project in corresponding RCC-P document
France	RCC-MRx	0.04		+	DBE	-		

D.2. Considerations about damping and support and interface loads

The damping values recommended in various national/international codes are summarised in Table D.1 for piping design. However, lower damping values may be used for estimating the design forces and moments for supports and the reasons for this suggestion are as follows.

1. Concerning the experiences of testing and observations of various experts on piping response, various country codes have specified damping values ranging from 0.5% to 5% (Table D.1). As per current understanding, higher damping values are recommended to reduce the margins in piping system (excluding supports), which increases thermal flexibility and reduces costs. These objectives shall be maintained if the support forces are evaluated with realistic damping. For this purpose, it is recommended to use earlier American Society of Mechanical Engineers (ASME) values or Japanese code values.

2. As given in Chapter 3, the damping values realised in the tests range from 0.6% to 4%. Similar damping values were evaluated by Hadjian et al., as shown in the Figures D.1-D.2. Shibata et al. also performed tests at various industries and published data in Pressure Vessels and Piping (PVP) conference proceedings and journals. The realised damping values were in line with the earlier ASME code values.

Figure D.1. Diameter of the piping varied from 25 mm to 450 mm
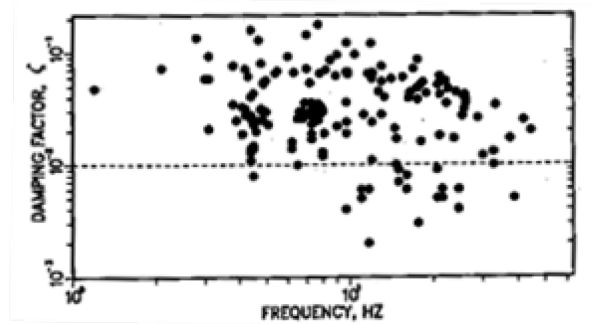
Source: EPRI, 1994.
Note:
Damping= 0.0053+0.0024D+0.0166R+0.009F-0.019L
Damping= 0.0924-0.0047D-0.022H+0.043S
D= diameter, R= response level, F= first mode, H= higher mode, S= snubbers, L= 0 for uniform piping and 1 for attaching massive valves, equipment attached. For example, for 1-inch diameter piping, it is 0.0167 in the first mode.

Figure D.2. Damping of multi span heat-exchanger tubing
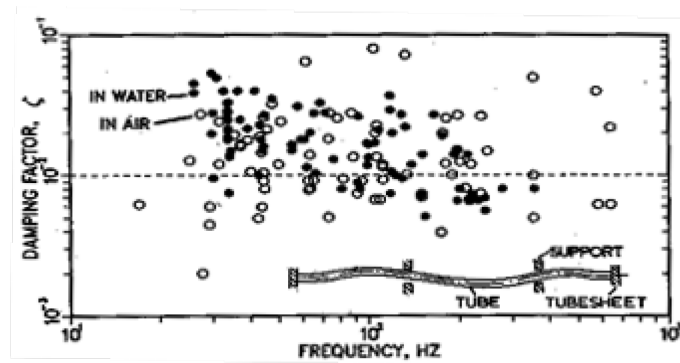
Source: EPRI, 1994.
Note:
Damping= 0.0053+0.0024D+0.0166R+0.009F-0.019L
Damping= 0.0924-0.0047D-0.022H+0.043S
D= diameter, R= response level, F= first mode, H= higher mode, S= snubbers; L= 0 for uniform piping and 1 for attaching massive valves, equipment attached. For example, for 1-inch diameter piping, it is 0.0167 in the first mode.

The above information justifies the recommendations given in (1).

1. Based on the earthquake experiences and tests, the margins in the piping supports are lower than the piping itself. There are failures of the piping supports due to a) foundations and b) loads generated in lieu of the large movement of attached equipment, etc. The forces and displacements generated in the piping also cause support failures. One example is snubber failure (Figure B.22) as reported. This justifies designing the supports with responses evaluated with realistic damping values, as given in (1).

2. As is evident from the information given in Annex B, it is also important have good piping supports that ensure flexibility and higher energy dissipation/absorption capabilities, resulting in high safety and lower cost, in order to generate a better performance of piping systems. As seen in Figure B.22, snubbers do not perform

well under dynamic loads and there is frequent locking and leakages in the case of hydraulic snubbers. In addition, maintenance man rem cost is very high in the nuclear industry. In view of this, it is highly recommended for supports to have the following good properties: energy absorbing and dissipation.

D.2.1. References

EPRI (1994), Reliability and Fitting Dynamic Reliability Program, Volume 3: System Tests EPRI report TR-102792-V3.

Annex E. Current practices

ASME III approach to evaluating ratcheting and fatigue in piping systems

E.1. Current ASME III stress intensity equations

The prevention of fatigue cracking of the pressure boundary of nuclear components is currently addressed in American Society of Mechanical Engineers (ASME) III Division 1, Sections NB-3200 and NB-3600. The analysis method and criteria of NB-3200 involves an elastic finite element analysis (FEA) and is applicable to all components (vessels, pumps, valves and piping). The analysis method and criteria of NB-3600 involve a heat transfer analysis to determine the temperature gradients (ΔT_1, ΔT_2, T_a and T_b), and classic pipe stress analysis (rather than a general purpose FEA) to determine the moments M_i at the various points along the pipe under thermal expansion, seismic and other applied loads. In this case, the seismic moments can be obtained by a classic modal analysis of the piping system.

The current NB-3600 method and criteria for piping systems will now be addressed and a discussion outlined on how they could be applied to explicitly evaluate ratcheting and fatigue from large seismic loads with a large pressure hoop stress. The full nomenclature of symbols is provided in NB-3650; a summary nomenclature, with some alterations for clarification, is provided here.

Equations (10) to (14) are applied to evaluate the extent of ratcheting (Equations [10], [12], and [13]) and the alternating stress intensity Salt is then calculated (Equations [11] and [14]) to obtain the fatigue usage factor. In the current ASME III code, these equations apply only to service levels A and B (normal and upset) conditions, which in the United States' regulation includes five operating basis earthquakes (OBE). The equations do not apply to service levels C and D (emergency and faulted), which therefore excludes the safe shutdown earthquake (SSE) in the United States' regulation.

$$B_1 \frac{P\, D_o}{2\, t} + B_2 \frac{D_o}{2\, I} M_{iDM} \leq 1.5 S_{mDM} \tag{9}$$

$$S_n = C_1 \frac{P_o\, D_o}{2\, t} + C_2 \frac{D_o}{2\, I} M_i + C_3 E_{ab} |\alpha_a T_a - \alpha_b T_b| \leq 3 S_m \tag{10}$$

$$S_p = K_1 C_1 \frac{P_o\, D_o}{2\, t} + K_2 C_2 \frac{D_o}{2\, I} M_i$$

$$+ K_3 C_3 E_{ab} |\alpha_a T_a - \alpha_b T_b| + \frac{1}{2(1-\nu)} K_3 E\alpha |\Delta T_1| + \frac{1}{1-\nu} E\alpha |\Delta T_2| \tag{11}$$

$$S_e = C_2 \frac{D_o}{2\, I} M_i^* \leq 3 S_m \qquad \text{(12) alternative to (10)}$$

$$C_1 \frac{P_o\, D_o}{2\, t} + C_2 \frac{D_o}{2\, I} M_i^{**} + C_3' \frac{E_{ab} |\alpha_a T_a - \alpha_b T_b|}{} \leq 3 S_m \quad \text{(13) alternative to (10)}$$

$$S_{alt} = K_e \frac{S_p}{2} \tag{14}$$

$$\Delta T_1 range \leq \frac{y' S_y}{0.7\, E\, \alpha}\, C_4$$

Table E.1. Nomenclature

B₁ and B₂	Primary stress indices of the pipe, component, or fitting.
C₁, C₂, and C₃	Secondary stress indices of the pipe, component, or fitting.
C₃'	Stress index of the pipe, component, or fitting.
C₄	Stress index which is a function of the material and the hoop stress.
E_ab	Average modulus of elasticity of the two sides of a gross structural discontinuity or material discontinuity at room temperature.
Eα	Modulus of elasticity, E, times the mean coefficient of thermal expansion, a, both at room temperature.
I	Moment of inertia of the pipe cross section.
K₁, K₂, and K₃	Local stress indices of the pipe, component, or fitting.
K_e	Ke is a plasticity correction factor which is a function of the material and the primary plus secondary stress intensity Sn.
M_iDM	Resultant moment amplitude due to the design mechanical loads.
M_i	Resultant range of moment which occurs when the system goes from one service load set to another. If a combination includes seismic loads, then Mi shall be either: (a) the resultant range of moment due to the combination of all loads considering one-half the range (i.e. the amplitude) of the seismic loads; or (b) the resultant range of moment due to the full range of the seismic loads alone, whichever is greater.
M_i*	Same as Mi for the pair of load sets under review, except it includes only moments due to thermal expansion and thermal anchor movements.
M_i**	Same as Mi for the pair of load sets under review, except it excludes the moments due to thermal expansion and thermal anchor movements.
P	Design pressure.
P_o	Range of service pressures.
S_alt	Alternating stress intensity.
S_e	Nominal value of expansion stress.
S_m	Average of the allowable stress intensity value for the highest and the lowest temperatures of the metal during the transient, when secondary stress is due to a temperature transient at the point at which the stresses are being analysed, or due to restraint of free-end deflection.
S_mDM	Allowable design stress intensity value at the temperature of the design mechanical loads.
S_n	Primary plus secondary stress intensity.
S_p	Peak stress intensity.
Ta(Tb)	Range of average temperature on side a(b) of a gross structural discontinuity or material discontinuity.
t	Nominal wall thickness of the pipe, component, or fitting.
αa (αb)	Coefficient of thermal expansion on side a(b) of a gross structural discontinuity or material discontinuity, at room temperature, 1/°F (1/°C).
|ΔT1|	Absolute value of the range of the temperature difference between the temperature of the outside surface To and the temperature of the inside surface Ti of the piping product assuming moment generating equivalent linear temperature distribution.
|ΔT2|	Absolute value of the range for that portion of the non-linear thermal gradient through the wall thickness not included in ΔT1.

E.2 Application to fatigue-ratcheting under seismic loads

The current ratcheting and fatigue equations (Equations 10 to 14) do not apply to the SSE because the number of cycles of a single SSE is considered to be small enough to not cause a fatigue crack, if the SSE stress is limited to the smaller of $2S_y$ or $3S_m$. It may be of interest to investigate the ratcheting and fatigue failures achieved during repeated seismic shake table tests at high pressure (large hoop stress) using the ASME III NB-3650 equations. In this case, the tests are conducted at ambient temperature, the thermal gradient terms (ΔT_1, ΔT_2, T_a and T_b) become zero and the thermal expansion moment ranges would also be zero. As a result, the equations to prevent fatigue failure would simplify to become:

$$B_1 \frac{P\,D_o}{2\,t} + B_2 \frac{D_o}{2\,I} M_{iDM} \leq min.\,(2S_y;\,3S_m) \qquad (9)$$

$$S_n = C_1 \frac{P_o\,D_o}{2\,t} + C_2 \frac{D_o}{2\,I} M_i \leq 3S_m \qquad (10)$$

$$S_p = K_1 C_1 \frac{P_o D_o}{2\,t} + K_2 C_2 \frac{D_o}{2\,I} M_i \qquad (11)$$

$$S_{alt} = K_e \frac{S_p}{2} \qquad (14)$$

If multiple sets of seismic shake table tests were run at different excitation levels (different g's), leading to ratcheting and fatigue cracking, each set of "n_j" runs "j" at a given g_j excitation would have their own seismic moment $M_{i \cdot j}$ and therefore their own peak stress intensity $S_{p \cdot j}$ (Equation 11) and alternating stress $S_{alt \cdot i}$ (Equation 14). The value $S_{alt \cdot j}$ would be used to enter the (S,N) fatigue curve and obtain the number of allowable cycles N_j. The cumulative usage factor (CUF) for the cumulative fatigue seismic damage caused by the series of nj shake table tests at different levels of seismic excitation g_j would be:

$$CUF = \sum_j \frac{n_j}{N_j}$$

In this case of a prediction of fatigue damage instead of design for fatigue, the experimentally-based mean (S,N) fatigue failure curves could be used in place of the ASME III Appendix I design fatigue curves.

Annex F. Peak factors of seismic responses

The seismic responses of piping systems appear as samples of narrow band signals due to their rather low damping ratio, such as signal x(t) presented in Figure F.1.

Figure F.1. Sample of the narrow band stochastic process and definition of the peak factor
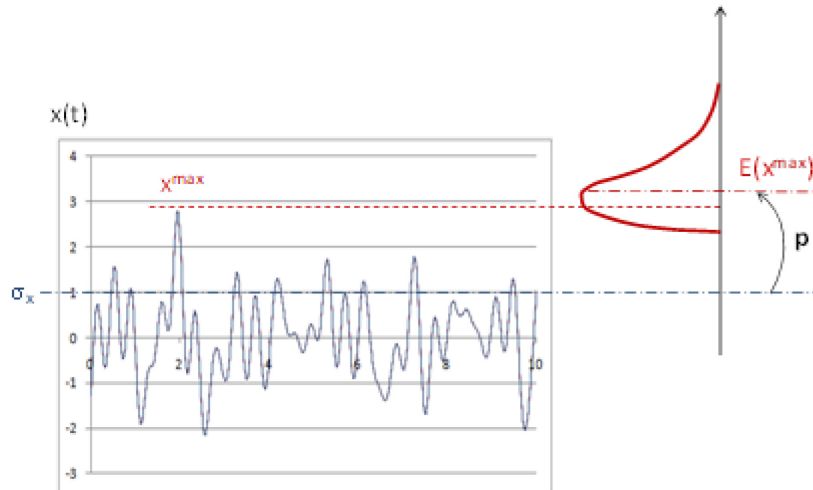
As usual for seismic input motions and seismic responses, this is a zero mean signal. The signal has a duration, T, which in practice is the duration of its strong phase and its maximum absolute value is noticed x^{max}. The response can be assumed to be stationary during the strong phase, with its frequency content being represented by its power spectral density (PSD), $G_x(\omega)$. A consequence of stationarity is that the standard deviation of x(t) is constant; it is noticed σ_x.

For the clarity of the reader, $G_x(\omega)$ and σ_x are linked by Formula (F-1), but this formula will not be used further.

$$\sigma_x = \int_0^\infty G_x(\omega)d\omega$$

Considering now another sample of the same PSD, it will theoretically have the same standard deviation, but another maximum value. This means that the maximum value of x(t) during the strong phase appears as a new random variable, as illustrated in Figure F.1. The peak factor of this process is by definition p, with (E[.] being the mean operator):

$$E[x^{max}] = p\ \sigma x.$$

The values of the peak factors of oscillator responses were extensively investigated by Der Kiureghian (1979) in view of establishing the complete quadratic combination of modal responses (1980). Der Kiureghian's outputs are presented in Figure F.2, where it appears that the peak factor is a function of the following:

- The product of the natural frequency, f, of the oscillator (of the mode in structural analysis) by the duration of the strong motion, T. This product is in abscissa in Figure F.2.

- The process bandwidth, which is controlled by the damping ratio of the system, corresponding to the different curves presented in Figure F.2.

The values of the equivalent number of cycles presented in Table 6.1 were obtained by catching the 5% damping curve in Figure F.2.

Annex Figure F.2. Peak factors of narrow band oscillator responses
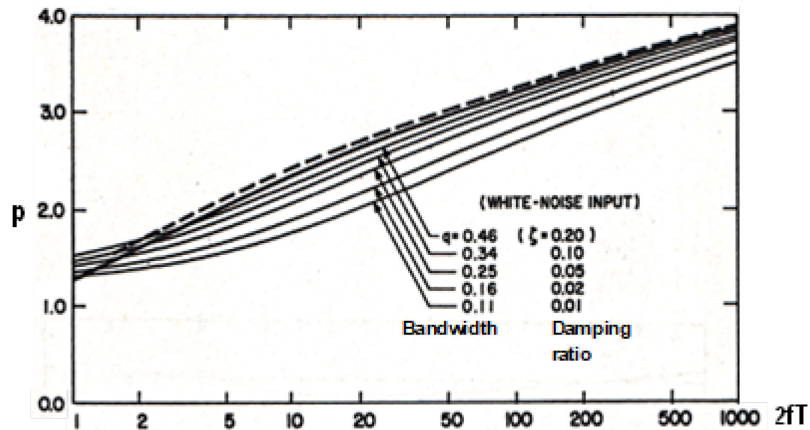
Source: Der Kiureghian, 1980.

Comments about Figure F.2:

- Considering the natural frequencies of structures and systems and the duration of strong motions, the range of interest of 2fT in earthquake engineering starts at 10 or more and goes up to around 100 for the vast majority of design situations. The possibility of very long input motions as are now being considered in Japan extends this range of interest.

- The figure was plotted for white noise input in acceleration. Der Kiureghian (1979) also studied the more realistic case of wide band filtered white noise input, such as the Kanai-Tajimi model of input motion. The outputs were not significantly affected.

Comments about stationarity assumption

Strong motion can seldom be regarded as samples of stationary processes. However, a consequence of non-stationarity is that actual peak factors have larger values than those resulting from the stationarity assumption. In this regard, it is clear that the equivalent number of cycles as calculated by Formula 6.2-17 is an overestimation.

References

Der Kiureghian, A. (1980), "A response spectrum method for random vibrations", Report No. UCB-EERC 80/15.

Der Kiureghian, A. (1979), "On response of structures to stationary excitations", Report No. UCB-EERC 79/32.

Annex G. Inputs for secondary index implementation

The primary part calculation introduced in Section 7.2.1.3 implies that the values of parameters λ and β are available for piping systems. These values can be derived from experimental observations as presented in Section G.1. The categorisation of higher modes and the associated code implementation for the analysis of multimodal systems, which are presented in Sections 7.2.1.4 and 7.1.1.5, require a spectral cut-off frequency to be identified. An example of such a cut-off frequency is presented in section G.2. The determination of this cut-off frequency is not necessary for the simplified code implementation presented in Section 7.2.1.6.

G.1. Evaluation of λ and β

An interpretation of the experimental outputs of piping systems enable an evaluation of the λ and β values that appear in the secondary index calculation.

The set of data from the Nuclear Power Engineering Centre (NUPEC) experimentation is presented in Table G.1 as per to DeGrassi et al. (2008). According to Labbé (2018), λ and β can be derived as per (G1) and (G2) where $k_{eq}/k_0 = (f_{eq}/f_0)^2$. The corresponding calculation is also presented in Table G.1.

$$\lambda = Ln(\mu\ k_{eq}/k_0)/Ln(\mu) \tag{G1}$$

$$\beta = Ln(\xi_{eq}/\xi)/Ln(\mu\ k_{eq}/k_0) \tag{G2}$$

Table G.1. Outputs of the NUPEC campaign and treatment

Experimental data					Treatment				
Elastic regime		Post-elastic regime							
Frequency	Damping	Ductility demand	Effective frequency	Effective damping					
f_0, Hz	ξ_0 %	μ	f_{eq}, Hz	ξ_{eq} %	f_{eq}/f_0	k_{eq}/k_0	λ	ξ_{eq}/ξ_0	β
3.8	0.9	24	3.6	4.5	0.947	0.898	0.966	5	0.52

The set of data presented in Table G.2 is from the BARC experimentation as per Ravikiran et al. (2015). Proceeding as above, the obtained λ and β values are presented in the same table.

Table G.2. Outputs of the BARC campaign and treatment

Experimental data					Treatment				
Elastic regime		Post-elastic regime							
Frequency	Damping	Ductility demand	Effective frequency	Effective damping					
f_0, Hz	ξ_0 %	μ	f_{eq}, Hz	ξ_{eq} %	f_{eq}/f_0	k_{eq}/k_0	λ	ξ_{eq}/ξ_0	β
4.1	0.6	1.89	4.014	1.1	0.979	0.958	0.933	1.83	1.02

G.2. Example of floor response spectrum and associated parameters

Figure G.1. Representative floor response spectrum
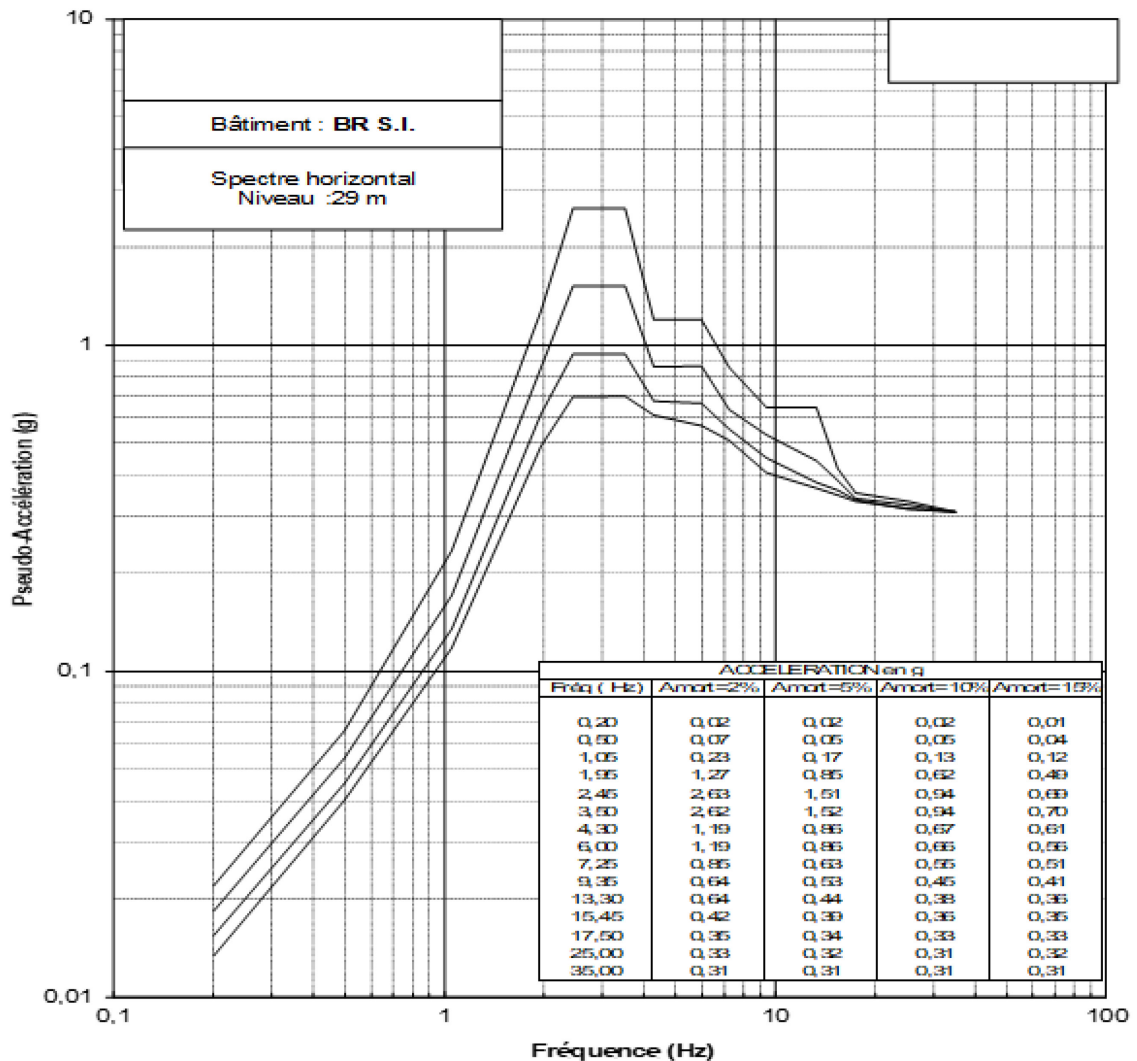
A typical floor response spectrum is presented in Figure G.1 as well as a determination of f_{peak} and f_{cut} of its 5% branch.

G.3. References

DeGrassi, G., J. Nie and C. Hofmayer (2008), "Seismic Analysis of Large-Scale Piping Systems for the JNES/NUPEC Ultimate Strength Piping Test Program", Report No. NUREG/CR-6983, Brookhaven National Laboratory, Upton, New York.

Labbé, P. (2018), "On categorization of seismic load as primary or secondary for piping systems with hardening capacity", *ASME 2018 PVP Conference*, 15-19 July, Prague.

Ravi Kiran, A., P.N. Dubey, M.K. Agrawal, G.R. Reddy, R.K. Singh and K.K. Vaze (2015a), "Experimental and Numerical Studies of Ratcheting in a Pressurised Piping System under Seismic Load", *Journal of Pressure Vessel Technology*, Volume 137, pp. 1-7.

Annex H. Roche method

H.1. General presentation of the method

Stresses and strain can significantly exceed the yield values under thermal loads and intense seismic or dynamic loads in piping systems and mechanical components in general. However, linear analyses are preferred for computational simplicity to keep the possibility of linear combination of loads and more simple input definition. It is therefore necessary to have some approaches aiming to estimate real strain-stress state from the strain-stress state obtained by linear analyses.

For the seismic design of piping systems, RCC-MRx is based on a method developed by R. Roche, from CEA Saclay (Roche, 1987). The method was first developed for thermal loads and creep evaluation for fast breeder reactors.

The basis of the method can be illustrated (Figure H.1) in the case of a straight variable section - A(x)- rod, which is clamped at one end and subjected to an imposed displacement, d, at the other end.

Figure H.1. Considered rod
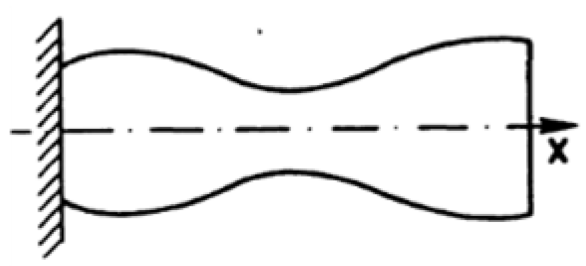
Source: Roche, 1993.

In the case of linear elastic material, it is easy to determine the stress-strain behaviour (unidirectional analysis is performed) anywhere along the rod:

R denotes the force applied to the free extremity of the rod in order to get the displacement d. The stress is then:

$$\sigma_0(x) = \frac{R}{A(x)}$$

and deformation is:

$$\epsilon_0(x) = \frac{R}{E.A(x)}$$

In this §H-1, the index 0 applies to the results of linear elastic analyses.

The total elongation of the rod is obtained by the following relation:

$$\int_0^L \epsilon_0(x)dx = d$$

from where we obtain:

$$R = \frac{E.d}{\int \frac{dx}{A(x)}}$$

From that expression, it is possible to determine stress and strain everywhere in the rod, using above equations.

If the behaviour of material is elastic no more, the situation is different. There are some complementary hypotheses:

- The displacement of the extremity of the rod is the same as the elastic rod, d.

- The deformation is no more proportional to stress, but can be written as:

  $\varepsilon = \varepsilon^e + \varepsilon^p$, where $\varepsilon^e = \frac{\sigma}{E}$ and ϵ^p is a non-linear function of stress. It is assumed that $\varepsilon^p(u.\sigma) = F(u).\varepsilon^p(\sigma)$, where u is a scalar, and $F(u)$, a non-linear function of u.

  This relation is obtained for a material verifying Ramberg-Osgood behaviour:

  $\varepsilon = \frac{\sigma}{E} + B.\sigma^n$, which will be assumed in the remaining paragraphs. In that case, it can be written: $\varepsilon^p(u.\sigma) = u^n.\varepsilon^p(\sigma)$.

- It is assumed that elasto-plastic stresses are proportional to the elastic one (the plastic behaviour does not modify the stress distribution). This is known as the Kachanov's condition and will be discussed further on in the report.

The axial force applied to the rod, in order to have a displacement, d, is still constant along the rod and is not equal to F, but is equal to another value, u.F.

The stress-strain state in the rod is now:

$$\sigma = u.\sigma_0$$

$$\varepsilon = u.\varepsilon_0 + F(u)\varepsilon_0^P \tag{A}$$

ε_0^P is the plastic strain corresponding to the stress σ_0 calculated elastically.

In these two equations, u is unknown. It can be determined by writing that the elongation of the rod is equal to the linear rod:

$$\int \varepsilon_0.u.dx + \int F(u).\varepsilon_0^P dx = \int \varepsilon_0 dx$$

The integration is along the length of the rod, from 0 to L.

This last equation can be written as:

$$(u-1)T + F(u) = 0 \tag{B}$$

where

$$T = \frac{\int \varepsilon_0\, dx}{\int \varepsilon_0^p\, dx}$$

T is fully deduced from the elastic analysis and called the global reversibility ratio. From Equation (B), *u* is determined and completely defines the elasto-plastic behaviour from Equation (A). This equation can be modified in order to introduce the ratio between elasto-plastic and elastic strains in the following way:

$$\frac{\varepsilon - \varepsilon_0}{(u-1).\varepsilon_0} = 1 + \frac{F(u)}{(u-1)} \cdot \frac{\varepsilon_0^p}{\varepsilon_0}$$

Introducing *T* from Equation (B) and denoting $t = \frac{\varepsilon_0}{\varepsilon_0^p}$ produces the relationship (linear) between the stress and strain obtained by linear analysis and those obtained by the non-linear analysis:

$$\sigma - \sigma_0 = -\frac{E}{r} \cdot (\varepsilon - \varepsilon_0) \tag{C}$$

where:

$r = \frac{T}{t} - 1$, is the follow-up factor,

t is the local reversibility ratio of the considered section. Such an evaluation is performed for each section of interest (*r* depends on *x*).

The Figure H.2 illustrates the different elements of the method. It makes it possible to determine the "true" stress-strain state (point N) from the elastically determined one (point L). A straight line of slope p (see below) from the point L, a result of linear analysis, intersects the "true" stress-strain curve in N.

Figure H.2. Illustration of results of application of the Roche method
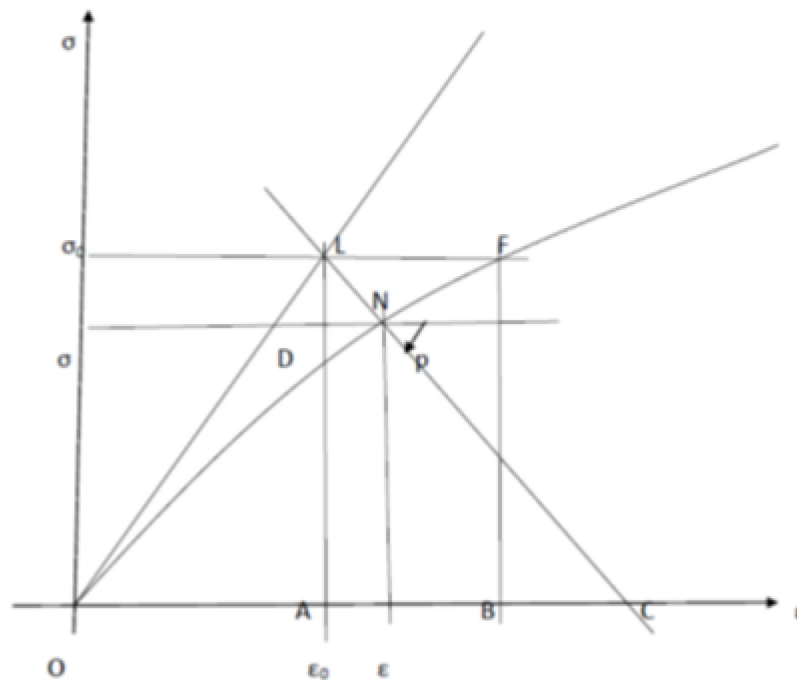
The slope, p, of this line is:

$$p = -\frac{E}{r}$$

r varies from -1 to $+\infty$. If r is very small (close to 0), the stress is almost secondary (the line is close to vertical). At the opposite when r is large, the stress is almost primary (the line is close to horizontal). If r=-1, the behaviour is elastic. Equation (C) shows that the value of r is independent of the amplitude of the applied loading. Different quantities introduced in the development above are presented graphically in Figure H.2:

$$\text{OA} = \varepsilon_0; \text{ AB} = \text{LF} = \varepsilon_0^p; \text{ OB} = \varepsilon_0 + \varepsilon_0^p = \text{OA/AB}; \text{ OC} = (\text{T/t}). \varepsilon_0$$

Applying the Ramberg-Osgood relation, Equation (B) can be rewritten as:

$$(u - 1).T + u^n = 0 \qquad\qquad (B')$$

The expression defining T can be rearranged by considering that A(x). ε_0 is a constant (independent of x), in the following way:

$$T = \frac{\int \varepsilon_0 dx}{\int \varepsilon_0^p dx} = \frac{\int \varepsilon_0 dx}{\int \frac{1}{t}\varepsilon_0 dx} = \frac{\int \varepsilon_0{}^2 A(x) dx}{\int \frac{1}{t}\varepsilon_0{}^2 A(x) dx} = \frac{\int \sigma_0{}^2 A(x) dx}{\int \frac{1}{t}\sigma_0{}^2 A(x) dx} \qquad\qquad (D)$$

These expressions will be used in the next paragraph.

H.2. Extension to a constant energy situation

The strong hypothesis is that the applied load is an imposed displacement. However, the method can also be developed with the assumption of an equality of energy between linear elastic and elasto-plastic case. This results from the equations giving the energy of internal deformation:

$$W = F.d = \int \sigma_0.\varepsilon_0.A(x).dx = \int \sigma.\varepsilon.A(x)dx$$

In the last equality, all the variables of strain and stress, elastic and elasto-plastic, as defined in the preceding paragraph, are introduced. Using the Equations (A), (C) and (D), the following equation can be produced instead of equation (B'):
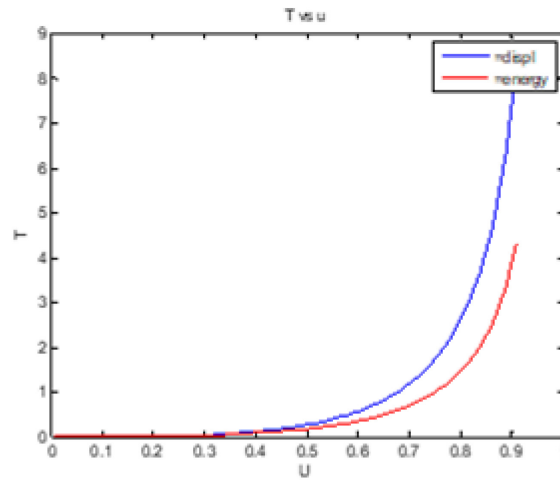
$$(u^2 - 1).T + u^n = 0 \qquad\qquad (B'')$$

and

$$r = \frac{T}{t}.\frac{1+u}{u} - 1 \qquad\qquad (C')$$

r is a function of x, as previously; but here, r depends of the amplitude of the loading.

Figure H.3 shows the graphical representation of Equations (B) and (B') for the case of a common stainless steel tabulated in the RCC-MRx for which n=0.343.

Figure H.3. Graphical representation of u vs. T

It can be observed that the two cases (equal displacement and equal energy) result in curves that are "rather close". The relevant values of T are limited, up to about five. Higher values correspond to small plastic strains compared to the elastic and to u values close to one.

H.3. Superposition of a primary load and general (with follow-up) load

Seismic load (and other similar loadings) are always superposed to primary loads, such as the weight of the piping and effect of pressure. There is no straightforward approach for this superposition. The RCC-MRx considers the approach illustrated by Figure H.4.

Figure H.4. Superposition of loads
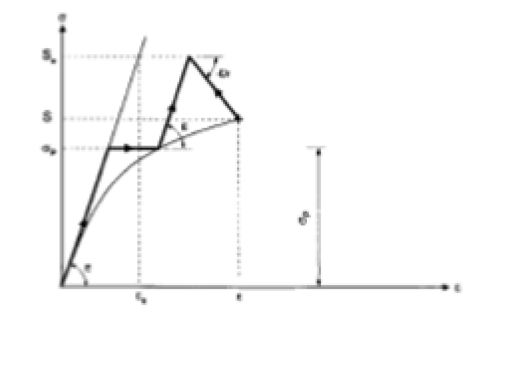
On this figure, σ_p is the stress due to primary load. The load is represented naturally on the elastic straight line. S is the allowable true stress (defined on the non-linear behaviour curve of the considered element - point T). S_e is the allowable stress for a linear analysis, considering follow-up. When the stress due to permanent loads plus seismic inertial ones, which is determined by a linear analysis, is equal to S_e, the "true stress" is equal to S. The figure shows how, for each section and considering σ_p, it is possible to determine S_e and consequently the factor G (knock down factor) by which the seismic stress will be reduced in order to get a maximum stress equal to S:

$$G = \frac{S - \sigma_p}{S_e - \sigma_p}$$

The expression for S_e is easily obtained by developing the equations of different lines on Figure H.4:

$$S_e = S + \frac{E.(F(S) - F(\sigma_p))}{1 + r}$$

Replacing this value in the expression of G, just above, produces:

$$G = \frac{(S - \sigma_p).(1 + r)}{(S - \sigma_p).(1 + r) + E(F(S) - F(\sigma_p))}$$

which is the formulation used in RCC-MRx.

It is important to note that in this case, the "real" stress is equal to S only if the elastically calculated one is equal to S_e, meaning only if the design is such that stresses are exactly equal to their limit. Another approach is to first apply the load with follow-up and to then in a second step apply the primary one. A different formulation results, which is more conservative. It also possible to derive the knockdown factor on true stress; but this construction necessitates the determination of the stress S, by solving non-linear equations. These formulations apply to any loading with follow-up, seismic inertial and anchor displacement. The determination of knock down factors for a combination of such loadings (primary part of inertial load and primary part of secondary load due to anchor movements) is not straightforward and necessary simplifications induce approximations in results.

The presentation of the Roche method was performed on a one-dimensional (1D) case on a rod in tension or compression. However, the approach can be generalised for a three-dimensional (3D) structure, with the same assumptions made as for the 1D rod: Kachanov's hypothesis, Ramberg-Osgood and equality of displacements (or energy) for elastic and elasto-plastic cases. In addition, the "relevant" stress for pipes is the combination of longitudinal stress due to pressure and stresses due to applied moments, with appropriate stress intensification factors. The Roche approach also applies to this case; the scalar stresses to be considered for the numerical application of the different formulas presented in this paragraph are the relevant stresses mentioned in the previous sentence. For a combination of the primary moment and the moment of a loading with follow-up, the considered moment is:

$$M_t = M + G.m$$

where M is the moment due to primary loads, m, the moment due to load with elastic follow-up and G the knock down factor mentioned above. M and m are calculated by linear analysis. This moment and the total stress to be considered in code evaluation are called the reference moment and reference stress respectively.

H.4. Extension to seismic analyses

In order to apply Roche method to seismic cases, it is important to bear in mind the fact that seismic load, as explained and illustrated in this document, is mainly a secondary type of loading. This is why the examples used for the qualification of the method for seismic cases was rather successful. Different lines with seismic excitation were considered. An application of the method was compared to analytical non-linear excitations or to test results, when available. Roche compared rather well to "exact" results.

It is important to recall that the Roche method and the way it is applied is an approached methodology. The first conditions of application presented in paragraph H.1 above introduce some uncertainties. Some of them are listed here:

- The Kachanov's hypothesis is verified in simple isostatic cases, but seems conservative in case of hyperstaticity.

- Ramberg-Osgood material behaviour is not always verified.

- The Roche equation derivation is based on reference stress and stress-strain curve. The real behaviour of a component (elbow, tee, straight pipe, etc.) accounts for other phenomena such as section deformation, local deformation, local buckling, etc. and is not specifically considered by the Roche approach.

- The equality of displacements linear/non-linear is globally verified in seismic behaviour, but some exceptions exist, for example in the case of piping in a base isolated structure, where the seismic load is globally primary.

- In a multimodal pipe (which is the great majority of cases) there are many different possibilities for calculating the knock down factor: either by determining it in each mode or in globally combined modes, or otherwise. The conservatism (or non-conservatism) of each approach is not easily demonstrated. A unique value of r can be used (how to define it "conservatively" but not too much…).

- Approximations due to the combination of primary loads with inertial and anchor motions seismic stresses.

Regardless, the Roche approach has the advantage of being rather simple to apply to the results of linear analysis. The approach gives results in any point of the considered pipeline and thus takes the structural detailed behaviour into account. The approach can identify elastic follow-up cases.

H.5. Reference

Roche, R.L. (1993), "Spring effect and primary stress", *SMIRT-12*, 15-20 August, Stuttgart, Germany.

Annex I. Draft analysis and design approach for class 2-3 piping

This appendix describes an alternate procedure for the seismic evaluation of class 2 and 3 piping.

I.1. Background for implementation

The proposed procedure is based on the following approaches and assumptions:

1. Imposed limitations for sustained loads that ensure the exclusion of the ratcheting (code limitations for reversing loads)

2. Low cycle fatigue is described by the Markl' equation for the best-fit fatigue curve:

$$S_{range} = 490 * N^{-0.2} \tag{I-1}$$

   where S_{range} – stress range; N – number of cycles.

3. The safety factor for stresses derived from the low cycle part of the Markl' fatigue curve is set to 1,67, which corresponds to the B31.1 and B31.3 American Society of Mechanical Engineers (ASME) codes. Considering this safety factor, the Equation (I-1) could be rewritten as:

$$S_{RANGE} = (490/1.67) * N^{-0.2} = 293 * N^{-0.2} \tag{I-2}$$

From the above equation, the cumulated usage factor for loads pertaining to levels A/B and safe shutdown earthquake (SSE) loads can be expressed as:

$$U_{A/B} + U_{SSE} = \frac{N_{A/B}}{\left(\dfrac{293}{S_{A/B}}\right)^5} + \frac{N_{SSE}}{\left(\dfrac{293}{S_{SSE}}\right)^5} \leq 1 \tag{I-3}$$

or:

$$S_{SSE} \leq \frac{293}{N_{SSE}{}^{0.2}}\,(1 - U_{AB})^{0.2} \tag{I-4}$$

According to NC-3611.2, the allowable stress range for expansion stresses is

$$S_A = f(1.25S_c + 0.25S_h) \tag{I-5}$$

where: $f = 1$, if N < 7 000;

   S_c = basic material allowable stress at minimum (cold) temperature;

   S_h = basic material allowable stress at maximum (hot) temperature;

Considering NC-3653.2 (c), the effects of pressure, weight, other sustained loads and thermal expansion shall meet the requirements of Equation (11):

$$S_{TE} \leq (S_h + S_A) \tag{I-6}$$

By introducing additional limitations for level A, B service loads, namely: $N_{A/B} \leq 1\,000$; S_c and $S_h \leq 20$ ksi, the following can be derived from (I-6):

$$S_{TE} = S_{A/B} \leq (S_h + S_A) = (S_h + 1.25S_c + 0.25S_h) = 1.25(S_h + S_c) = 1.25(20 + 20)$$
$$= 50 ksi$$

and

$$U_{A/B} = \frac{N_{A/B}}{\left(\frac{293}{S_{A/B}}\right)^5} = \frac{1000}{\left(\frac{293}{50}\right)^5} = \frac{1000}{6910} = 0.145$$

and consequently:

$$S_{SSE} \leq \frac{293}{N_{SSE}{}^{0.2}}\,(1 - U_{AB})^{0.2} = \frac{293}{N_{SSE}{}^{0.2}}\,(1 - 0.145)^{0.2} = \frac{293 * 0.97}{N_{SSE}{}^{0.2}} = \frac{284}{N_{SSE}{}^{0.2}}$$

I.2. Limitation of applicability

This procedure applies to above-ground carbon steel, low alloy steel, or stainless steel piping systems subjected to limitations for the reversing dynamic loads.

I.3. Evaluation criteria

I.3.1. Prevention of fatigue failure

I.3.1.1. General form

The stress range for service level D seismic loads shall meet the limit of Equation (1):

(United States customary units)

$$S_{SD} = i\frac{M_{SD}}{Z} \leq \frac{293}{N_{SD}{}^{0.2}}\,(1 - U_{AB})^{0.2} \qquad \text{Equation (1)}$$

(SI units)

$$S_{SD} = i\frac{M_{SD}}{Z} \leq \frac{2020}{N_{SD}{}^{0.2}}\,(1 - U_{AB})^{0.2}$$

Where

S_{SD} = stress range for service level D seismic loads, ksi (MPa)

i = stress intensification factor (NC-3673.2)

M_{SD} = range of resultant moments due to seismic loads specified for the level D service limits, in.-lb (N*mm)

Z = section modulus of pipe, in.^{3} (mm^3) (NC-3653.3)

N_{SD} = equivalent number of maximum stress cycles for service level D seismic loads

U_{AB} = usage factor from all service level A and B loads:

(United States customary units)

$$U_{AB} = \frac{N_{AB}}{\left(\frac{293}{S_{AB}}\right)^5} \qquad \text{Equation (2)}$$

(SI Units)

$$U_{AB} = \frac{N_{AB}}{\left(\frac{2020}{S_{AB}}\right)^5}$$

where

N_{AB} = total equivalent number of cycles for all service level A and B thermal cycles, calculated in accordance with NCD-3611.2

S_{AB} = maximum stress range for service level A and B thermal cycles, corresponding to N_E in NCD-3611.2, ksi (MPa).

I.3.1.2. Simplified form

If $N_{AB} \leq 1\,000$ cycles, and if S_c and S_h are below 20 ksi (140 MPa), then Equations (1) and (2) can be written as

(United States customary units)

$$S_{SD} = i\frac{M_{SD}}{Z} \leq \frac{284}{N_{SD}^{0.2}} \qquad\qquad \text{Equation (3)}$$

(SI Units)

$$S_{SD} = i\frac{M_{SD}}{Z} \leq \frac{1960}{N_{SD}^{0.2}}$$

I.3.2. Prevention of plastic instability

I.3.2.1. Plastic instability stress limits

In addition to the limits specified in Section 2.1 for the prevention of fatigue failure, the following primary stress limits apply to the prevention of plastic instability under the inertial effects of seismic loads.

The primary stress limits of NCD-3653 Equations (9a) or (9b) shall apply for the primary stress adjusted seismic response spectra.

I.3.2.2. Primary stress adjusted seismic response spectra

Adjusted seismic response spectra $S^*(f)$ may be obtained from the given seismic response spectra $S^*(f)$ in the following manner:
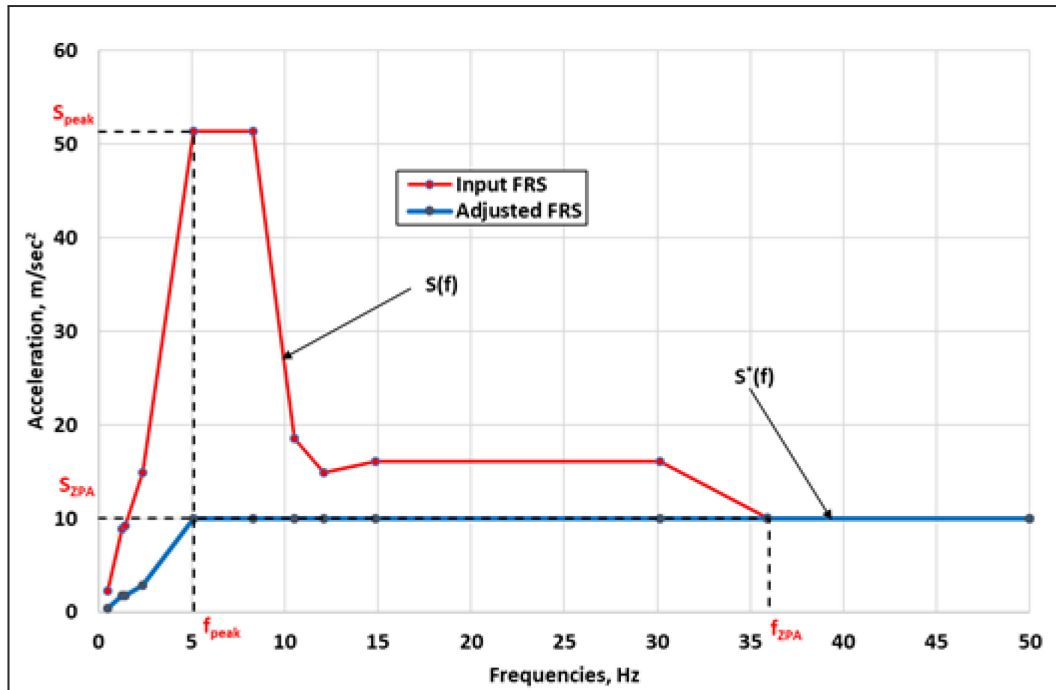
For frequencies in the range of $f \leq f_{peak}$:

$$S^*(f) = c^*S(f), \text{ where } c^* = (S_{peak}/S_{ZPA})$$

For frequencies above f_{peak}:

$$S^*(f) = S_{ZPA}$$

Figure I.1. Extraction of the floor response spectra (FRS) primary part

I.4. Reference

ASME (2019), "BPVC Section III, Rules for Construction of Nuclear Facility Components - Division 1 - Subsection NC, Class 2 Component", American Society of Mechanical Engineers, United States.

Annex J. Draft programme of a course on new approaches for piping seismic design

J.1. Objective of the course

Piping systems in nuclear plants are designed and qualified in accordance with codes, standards and regulations so as to withstand loads that occur or could occur during a plant's design life. The loads to be considered in the design encompass normal operating loads such as weight, operating pressures and temperatures, and anticipated hydraulic transients. In addition, piping systems in nuclear power plants must be designed for postulated accidental loads such as earthquakes. The postulated seismic loads are large and necessitate a number of seismic restraints in order to brace the pipe. These seismic restraints result in plant congestion, which limits access for inspection and maintenance. The seismic restraints also increase initial construction costs, as well as inspection and maintenance costs required during the plant lifetime. The seismic restraints could additionally provide an unnecessary constraint to the pipe, which could hinder its thermal expansion in normal operation and result in detrimental fatigue damage.

It is therefore essential for engineers to have the correct seismic design rules and criteria and thus install the necessary restraints while avoiding the installation of unnecessary hardware. This objective has guided the need to re-visit the current seismic design practices for piping systems in nuclear power plants in light of past and current experimental data, analytical and numerical studies, and observations of the damage caused by actual earthquakes, in order to optimise the seismic design, analysis and qualification rules and criteria.

J.2. Proposed list of topics to be presented

J.2.1. General subjects

- role and importance of piping systems in nuclear installations;
- conventional approach for seismic design;
  - existing codes;
  - consequences on design;
- other topics;
  - Leak-before-break (LBB);
  - rupture locations;
  - ...

J.2.2. Seismic behaviour of piping systems

- seismic feedback of experience;
- experimental feedback of experience, research and development (R&D) programmes;
  - in India;
  - in Japan;

- in the United States;

- other programmes;

- robustness and failure modes of piping systems.

J.2.3. Proposal of new approaches

- review of recent modifications of codes on seismic piping design;

  - illustration in Japan, Korea and the United States.

- primary part of seismic loading/seismically induced stresses with respect to plastic instability;

- seismically induced fatigue analysis;

- seismically accumulated plastic strain and ratchet analysis.

J.2.4. Applications, design examples and practical work appropriation of the analysis for oligocyclic fatigue failure on simple monomodal or bimodal piping systems;

- Interpretation of seismic tests performed in laboratories (in France, Japan, the United States, etc.) on scale 1 piping systems, up to failure. Numerical simulation exercises could be performed in order to capture the failure modes.

- Presentation of some industrial piping systems, in order to compare conventional seismic design approach and MECOS approach as defined in the document.